AD-783 390

FEASIBILITY INVESTIGATION OF ZERO-TORSIONAL-STIFFNESS COUPLINGS FOR SUPPRESSION OF RESONANCE AND INSTABILITY IN HELICOPTER DRIVE TRAINS

John M. Vance, et al

Florida University

Prepared for:

Army Mobility Research and Development Laboratory

June 1974

EUSTIS DIRECTORATE POSITION STATEMENT

The objective of this program was to conduct an analytical investigation of the feasibility of using a special type of transmission shaft coupling to achieve control by the designer over one helicopter drive train parameter - torsional stiffness - and possibly another - shaft damping.

A shaft coupling can be designed to meet the horsepower and speed requirement of modern helicopter drive trains with essentially zero torsional stiffness at the design speed and power. Two different types of zero torsional stiffness (ZTS) couplings were designed to transmit 5270 horsepower at 13,820 rpm. For one type of coupling, simple design equations were derived to size a coupling for any helicopter application. A ZTS coupling in a helicopter drive train acts as a torsional vibration isolator and can provide significant damping that is not otherwise available to the designer.

The technical monitor for this contract was Mr. James Gomez, Technology Applications Division.

Unclassified

SECURITY CLASSIFICATION OF THIS PAGE (When Data Entered)

AD-783390

REPORT DOCUMENTATION PAGE

READ INSTRUCTIONS BEFORE COMPLETING FORM

1. REPORT NUMBER: USAAMRDL-TR-73-103
2. GOVT ACCESSION NO.
3. RECIPIENT'S CATALOG NUMBER

4. TITLE (and Subtitle): FEASIBILITY INVESTIGATION OF ZERO-TORSIONAL-STIFFNESS COUPLINGS FOR SUPPRESSION OF RESONANCE AND INSTABILITY IN HELICOPTER DRIVE TRAINS
5. TYPE OF REPORT & PERIOD COVERED: Final Report
6. PERFORMING ORG. REPORT NUMBER

7. AUTHOR(s): John M. Vance, Mark S. Darlow, Roger A. Brown
8. CONTRACT OR GRANT NUMBER(s): DAAJ02-72-C-0076

9. PERFORMING ORGANIZATION NAME AND ADDRESS: Department of Mechanical Engineering, University of Florida, Gainsville, Fla. 32611
10. PROGRAM ELEMENT, PROJECT, TASK AREA & WORK UNIT NUMBERS: Project 1G162207AA72

11. CONTROLLING OFFICE NAME AND ADDRESS: Eustis Directorate, U.S. Army Air Mobility Research and Development Laboratory, Fort Eustis, Va. 23604
12. REPORT DATE: June 1974
13. NUMBER OF PAGES: 301

14. MONITORING AGENCY NAME & ADDRESS (if different from Controlling Office)
15. SECURITY CLASS. (of this report): Unclassified
15a. DECLASSIFICATION/DOWNGRADING SCHEDULE

16. DISTRIBUTION STATEMENT (of this Report)

Approved for public release; distribution unlimited.

17. DISTRIBUTION STATEMENT (of the abstract entered in Block 20, if different from Report)

18. SUPPLEMENTARY NOTES

19. KEY WORDS (Continue on reverse side if necessary and identify by block number)

Stiffness
Torsion
Feasibility Studies
Instability
Suppression
Resonance
Vibration

20. ABSTRACT (Continue on reverse side if necessary and identify by block number)

An investigation is made of the feasibility of designing a nonlinear shaft coupling, with zero or very low torsional stiffness at predetermined operating conditions, for helicopter drive trains. The purpose of such a coupling is to isolate torsional vibration and eliminate resonances.

It is found that a coupling can be designed to have zero torsional stiffness at high rotational speeds by using the centrifugal force field on connecting

DD FORM 1 JAN 73 1473 EDITION OF 1 NOV 65 IS OBSOLETE

Unclassified

SECURITY CLASSIFICATION OF THIS PAGE (When Data Entered)

Block 20. Abstract - Continued.

links from the driving to the driven flange of the coupling. Previous designs of such couplings for low-speed applications have been used successfully in marine diesel drives.

Design equations for two types of zero-stiffness couplings suitable for high speed turboshaft-powered helicopters are developed.

Computer simulations of the dynamic performance of drive trains, with and without a zero-torsional-stiffness coupling, are performed. Both open-loop and closed-loop (with automatic speed control) systems are simulated. The results indicate that a zero-torsional-stiffness coupling can produce three major advantages in a helicopter propulsion system:

1. The coupling can isolate the engine and fuel control from unavoidable torsional excitation at the rotor.

2. The coupling can make the achievement of closed-loop stability, through proper governor design, a less difficult task.

3. The coupling makes it possible to incorporate significant amounts of damping into a helicopter drive train, thereby improving torsional stability and further suppressing resonance.

PREFACE

This report presents the results of a study conducted by the University of Florida Engineering and Industrial Experiment Station for the Eustis Directorate, U.S. Army Air Mobility Research and Development Laboratory under Contract DAAJ02-72-C-0076, Project 1G162207AA72.

The study consisted of mathematical analyses of zero-torsional-stiffness shaft coupling designs described in the foreign literature, as well as of new design concepts generated in the Department of Mechanical Engineering at the University of Florida, for potential application in helicopter drive trains.

The principal investigator at the University of Florida was Dr. John M. Vance. Mr. Roger Brown and Mr. Mark Darlow were research assistants.

Part I of the report, which deals with design of the couplings and analysis of their effect on torsional vibration, was primarily authored by Mr. Brown. Part II, which describes stability analyses of closed-loop drive trains to determine the effect of ZTS couplings on torsional stability, was primarily authored by Mr. Darlow. The Introduction, Conclusions, and Recommendations were written by Dr. Vance, who also edited the entire report.

Dr. William H. Boykin of the Engineering Science and Mechanics Department at the University of Florida served as an invaluable consultant on questions of stability and control analysis.

TABLE OF CONTENTS

TABLE OF CONTENTS (Continued)

LIST OF ILLUSTRATIONS

LIST OF ILLUSTRATIONS (Continued)

LIST OF ILLUSTRATIONS (Continued)

LIST OF ILLUSTRATIONS (Continued)

LIST OF ILLUSTRATIONS (Continued)

LIST OF ILLUSTRATIONS (Continued)

LIST OF TABLES

INTRODUCTION

Torsional oscillation is a significant source of dynamic loads in helicopter drive trains, which must transmit ever-increasing amounts of horsepower with very high overall speed reduction ratios over significant distances between engines, transmissions, and rotors.

The automatic speed governor has been a significant development for helicopter flight control, as it relieves the pilot of the requirement to maintain constant rotor speed during changes of load and flight conditions. A special problem, which has been encountered in almost every recent helicopter development program, is that of maintaining torsional stability of the engine and drive train while at the same time providing a sufficiently rapid response to demand for power and speed changes. The helicopter drive train with closed-loop speed control is a system which is difficult to optimize without inducing torsional instability at or near a resonant frequency.

In the past, whenever the problem of torsional stability has been encountered, a typical solution has been to reduce the gain of the fuel control, thereby sacrificing desirable speed control properties of the governor.[1] However, there are other critical parameters of the system, such as drive train torsional stiffness and damping, drive train inertia, etc., which might be used as design variables to achieve torsional stability without sacrificing desirable control properties.

Torsional stiffness has always been a difficult design parameter to control, since it is effectively reduced by the square of the very high gear reduction ratio of the main transmission (see Appendix II). This very low resulting torsional stiffness produces a correspondingly low natural frequency of the drive train (typically 3-9 H_z), which makes it difficult to avoid resonant peaks in the closed-loop (governed) system.

Shaft damping is perhaps even more difficult to control in a drive train, since it requires large amounts of vibratory energy dissipation which usually involves friction, wear, or temperature dependence. As a result, typical values of shaft damping normally found in helicopter drive trains amount to only a few percent of the critical value, producing a vibratory system which is almost completely undamped between engine and rotor.

The major objective of this report is to document an analytical investigation of the feasibility of the use of a special type of shaft coupling to achieve control by the designer over one of these drive train parameters--torsional stiffness--and possibly another--shaft damping.

Shaft couplings have been developed independently in England and in Russia which use centrifugal force on link masses (see Figures 1 and 2) to produce torsional stiffnesses which are nonlinearly dependent on speed and transmitted torque. In particular, these couplings have been designed to have zero torsional stiffness at predetermined conditions of speed and torque.

The designs developed in England by Chapman[2] are being used to eliminate torsional resonances in marine drives with diesel propulsion. Very little information is available on the Russian designs, other than Reference 3, and the specific applications, if any, are unknown.

The marine drive applications with diesel propulsion involve low shaft speeds (100-2000 rpm), and consequently the couplings developed for such use are large and heavy to handle the high torques and to produce the required centrifugal force.

At the beginning of this study, it was postulated that a zero-torsional-stiffness (ZTS) coupling could be developed for high-speed application in a helicopter drive, and could eliminate instability at resonance by decoupling the inertias contributing to the resonance. Ideally, a ZTS coupling would not transmit any oscillatory deviations of torque because of its low stiffness, and would therefore reduce the natural frequency of the system to zero. It should be noted that this is opposite to recommendations[4] and efforts in the past toward stiffening the system and raising the natural frequency above the range of excitations, a procedure which has been found to be impractical because of the effect of the gear ratio noted above.

In practice, a ZTS coupling has zero stiffness only over a finite range of angular twist, and large excitations drive the coupling into nonlinear regions with some effective nonzero stiffness. Thus, one of the questions to be answered in Part I of this report is how a ZTS coupling actually affects the natural frequency and vibratory response of a helicopter drive train with realistic levels of excitation. Another, more basic question addressed in Part I is whether a ZTS coupling can be designed to meet modern helicopter requirements within the constraints of size, weight, and reliability. Finally, results of stability analyses are presented in Part II to indicate the predicted effect of a ZTS coupling on closed-loop torsional stability.

Before proceeding to Parts I and II of the report for the detailed answers to these and other questions, the reader may find it helpful to consider how zero torsional stiffness can be achieved in a shaft coupling, and thus gain some insight into the basic concept.

The pinned link design shown in Figure 1 lends itself well to a physical description of the principle of operation. Note that only one set of links is shown. A symmetric set of links with another counterweight would be required for high-speed balance.

At zero speed the coupling has no stiffness, since the driving flange can rotate freely with respect to the driven flange with no torque transfer (until the linkage straightens out).

At operating speed, centrifugal force holds the link mass (counterweight) out at some equilibrium value of α which is determined by the torque being transferred. Now when the driving flange is twisted with respect to the driven flange, two effects occur simultaneously. First, the link mass

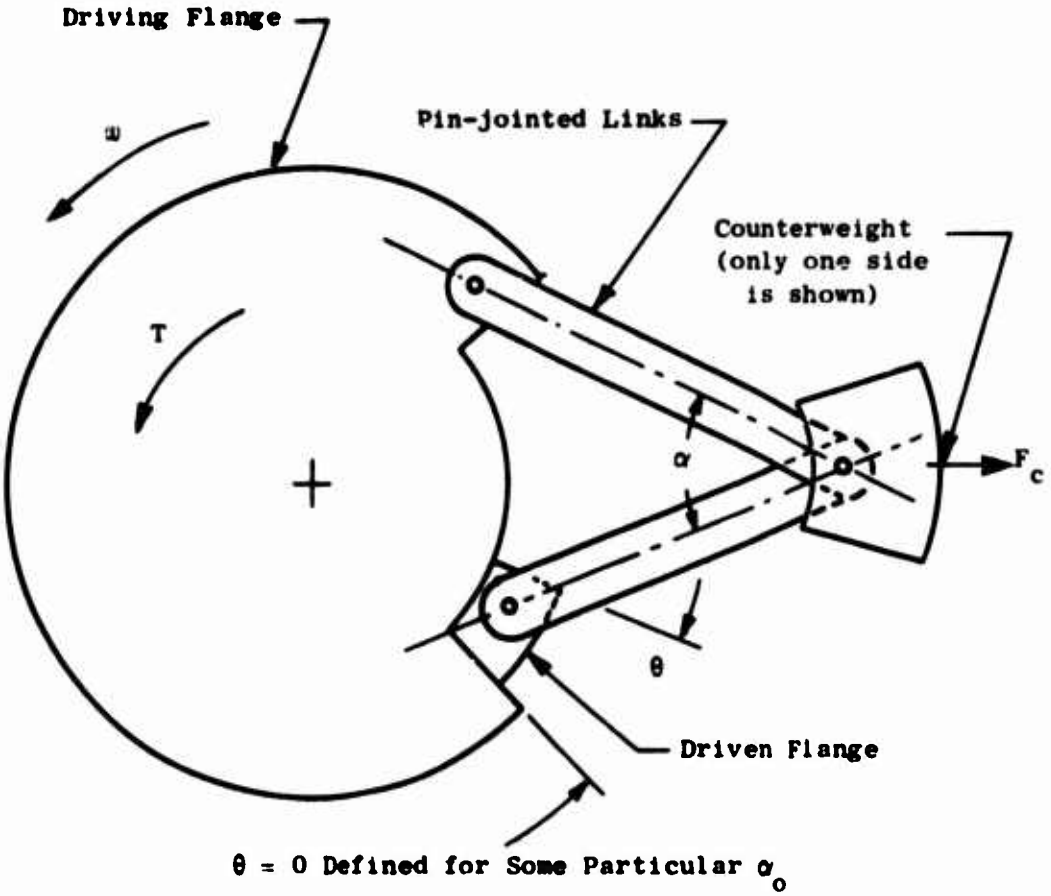

Figure 1. Zero-Torsional-Stiffness Coupling, Pinned Link Version.

moves inward to a reduced radius. This effect results in a reduced centrifugal force and therefore tends to reduce the transmitted torque. Second, the linkage geometry is changed (the angle α increases), which can either increase or decrease the transmitted torque, depending on the link lengths.

The first effect produces a negative torsional stiffness (positive twist produces a negative change in torque). The coupling can be designed so that the second effect produces a positive torsional stiffness which is equal and opposite to the negative stiffness from the first effect. The net result is zero torsional stiffness at a particular design speed and angle of twist. The link mass is sized to produce the desired torque under the design conditions.

In the design of Figure 2, centrifugal force is augmented by elasticity, so the coupling stiffness can be finite at zero speed.

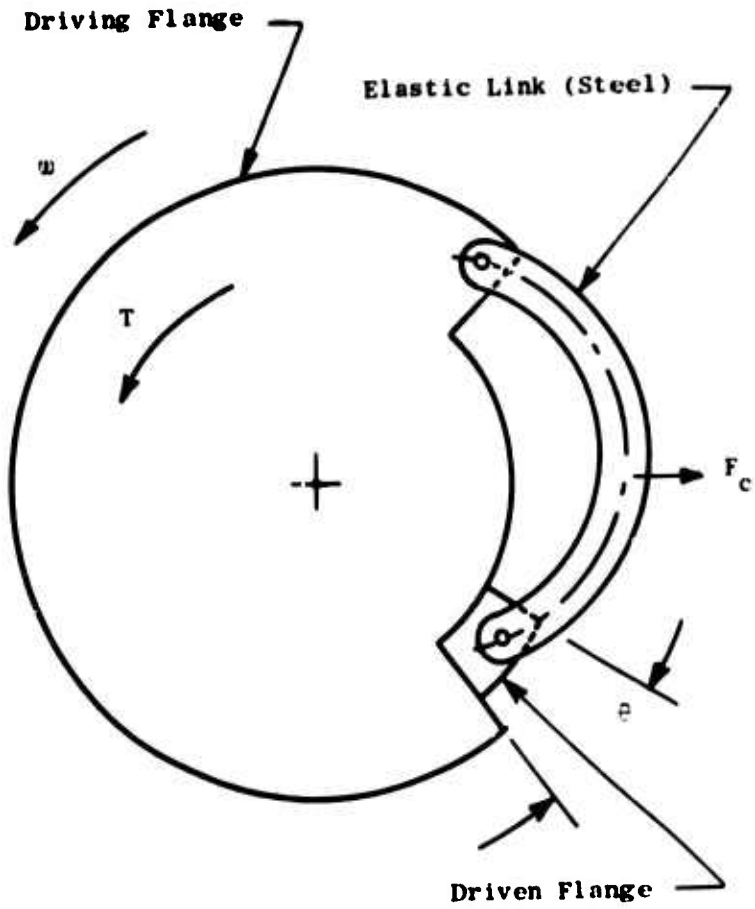

θ = 0 Defined for Zero Stress in the Elastic Link

Figure 2. Zero-Torsional-Stiffness Coupling, Elastic Link Version.

PART I: REDUCTION OF TORSIONAL VIBRATION THROUGH THE USE OF ZERO-TORSIONAL-STIFFNESS COUPLINGS

PRELIMINARY CONSIDERATIONS

Rotating machinery is inevitably subjected to exciting forces which set up torsional vibrations throughout the system. It is of utmost importance that the exciting frequency be different from the critical frequency of the system. If a system is excited at or near its critical frequency, the system energy will increase with each successive cycle. The limiting factor for the energy buildup is internal or external damping which dissipates energy in the form of heat.

Excitation at the critical frequency of a system normally designed to operate away from the critical can come about through

1. Start-up or shutdown
2. Operation at other than design speeds
3. Unexpected exciting forces
4. Unexpected critical frequencies.

Figure 3a is an example of an open-loop system where the torque input is independent of the system response. Open-loop systems of this type will not become torsionally divergent but can experience severe oscillation when externally excited at, or near, a critical frequency. For a closed-loop system (Figure 3b) where control action is dependent upon system response, instabilities can be caused by internal or external excitation. Turbo-powered machinery such as helicopters and electrical generators are closed-loop systems where the operating speed is controlled by a governor. The speed governor causes a dependence between driving torque and output speed. Swick and Akarvan,[5] Peczkowski,[4] Canale and MaCabe[6] and others describe governor systems for free turbine engines. Part I considers only the open-loop characteristics of torsional systems, such as free turbine helicopter systems, which are subjected to external excitation.

Removing critical speeds from the operating region in the open-loop system will generally improve closed-loop stability. In addition, fatigue failure due to cyclic torque variation from external excitation will be lessened.

Design Considerations

Critical design parameters such as strength, weight, material, and size often dictate the mass distribution of a system. It may be difficult to change the mass or inertia profile of a system without adversely affecting machine performance. Therefore, the designer may only be left with shaft stiffness and damping as free parameters with which to ensure safe operation at all expected operating speeds.

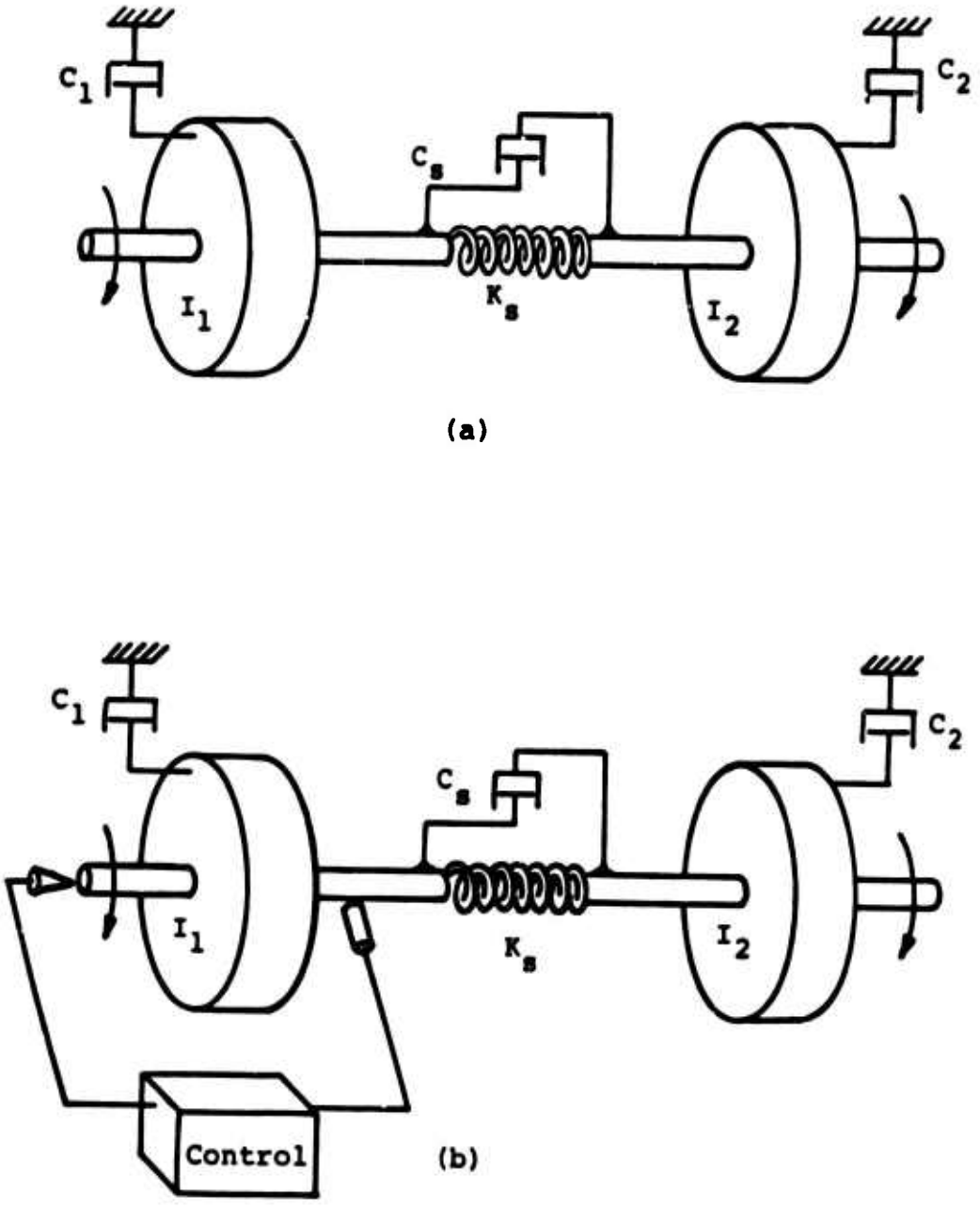

Figure 3. Torsional Systems.

With proper damping, passage through critical frequencies during start-up or shutdown is usually not a problem. This is due to the short time duration that the machine is driven at a critical speed. However, large amounts of damping are needed when there is continuous excitation at or near a critical frequency. The damping will prevent the system from becoming divergent and magnifying the exciting force out of safe bounds. Unfortunately, this type of damping is generally hard to achieve in mechanical drive trains In addition, a highly damped system will transmit more exciting force than a lesser damped system when operation is above critical speed.

If the exciting frequency is known, it may be possible to design a shaft that has a stiffness which gives the system a critical frequency much higher or lower than the frequency of excitation. However, it may often be difficult to design a shaft with the desired stiffness and still have acceptable strength, weight, and deflection characteristics.

Nonlinear Couplings

A low-stiffness shaft coupling may be used to solve the problem of excitation at a critical frequency. This is done by lowering the critical frequencies of a system to nearly zero, while at the same time transmitting the system torque requirements. Figures 4 and 5 show the characteristics of some linear and nonlinear couplings.* It is apparent from Figure 4 that a linear torsional spring with near zero stiffness would require large amounts of twist in order to transmit the design torque. The nonlinear spring, however, can transmit design torque with zero torsional stiffness at a small angle of twist. One of the objectives of this report is to determine if such a nonlinear "spring" (coupling) is a practical possibility for high torques and speeds. Present designs of nonlinear couplings which have zero or low stiffness for certain operating conditions are investigated in the following section.

For linear systems the resonant frequencies are inherent to the system and are not functions of the exciting forces. The resonant frequencies of nonlinear systems are functions of the amplitude and period of the exciting force, as well as the system state when excitation occurs. As can be seen in Figure 5, if the torque is varied over a large range, the nonlinear spring stiffness increases on either side of the low stiffness operating region. In order to obtain an "average" stiffness over a cycle, the time variation of the torque must be considered.

The Helicopter Problem

One objective of this report is to develop a procedure for the design and analysis of a zero-torsional-stiffness coupling, with particular emphasis

*Torsional stiffness is defined as the ratio of the change in coupling torque to the change in angle of twist across the coupling, i.e., the slope of the torque vs. twist angle curve.

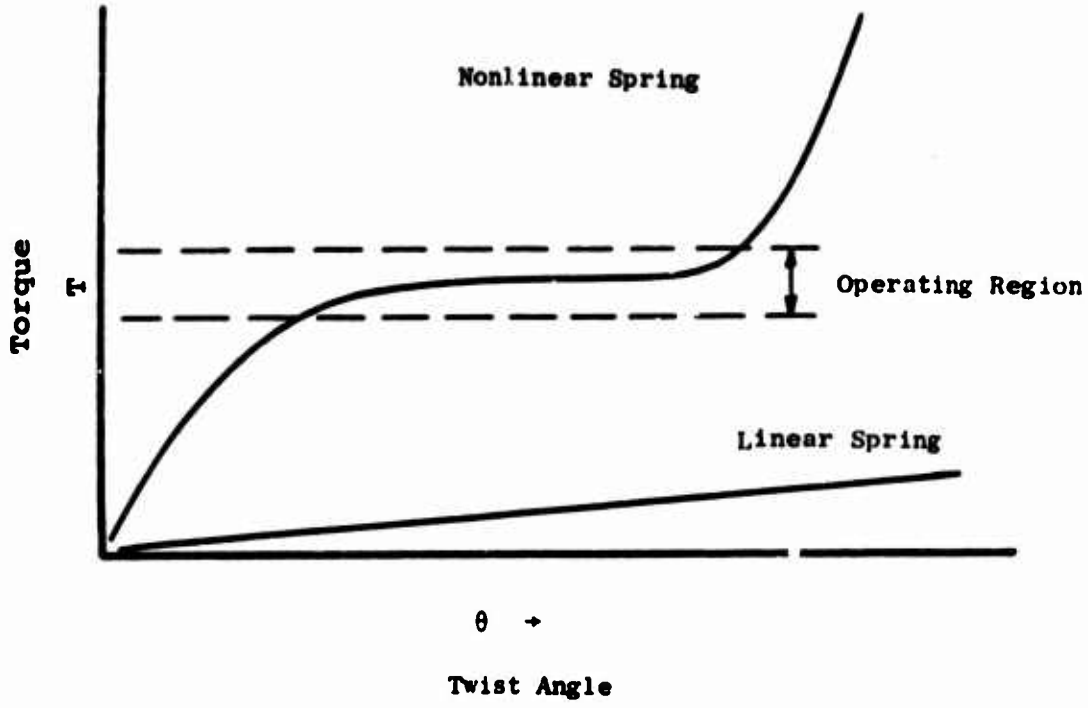

Figure 4. Coupling Characteristics

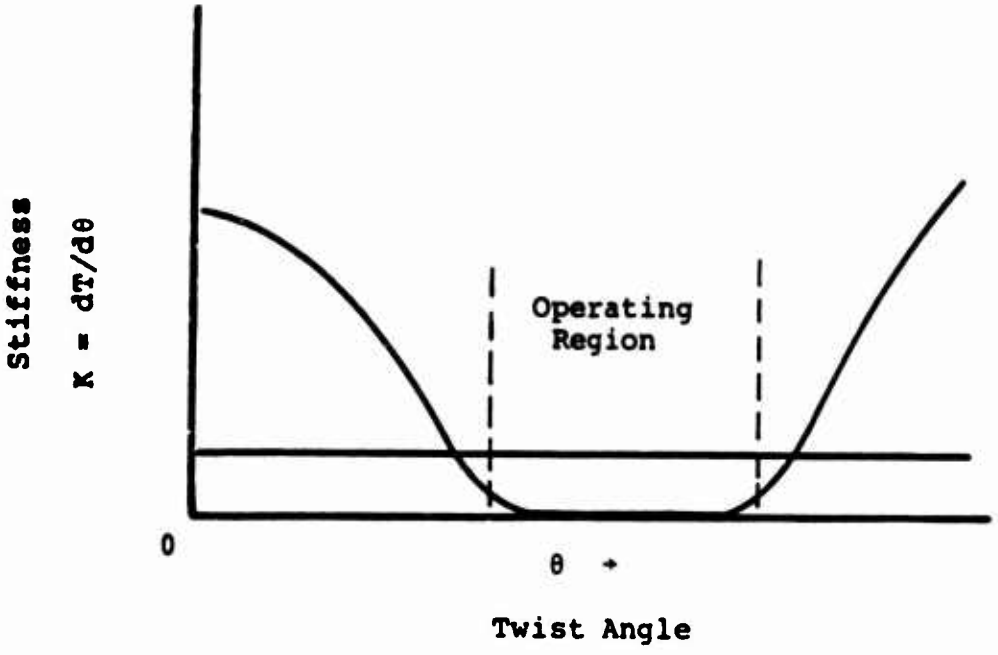

Figure 5. Coupling Stiffness.

on helicopter applications. The values used for the dynamic characteristics of the helicopter drive train were obtained from a helicopter stability analysis by Swick and Skarvan.[5] Figure 6 shows the basic helicopter drive system.

It has been found in past helicopter designs that the closed-loop system can become unstable under certain flight conditions. When this happens, self-excitation from a small perturbation can quickly cause destructive vibrations. It is hoped that by including a zero-torsional-stiffness coupling as part of the overall system, all torsional instabilities can be eliminated. The problem of fatigue failure of elastic members can also be reduced by lowering the amplitude and frequency of self-excited vibrations as well as the amplitude of vibration caused by external excitation. The major external sources of torsional excitation are:

1. Pilot excitation of control parameters
   a. collective pitch
   b. engine speed setting
2. Aerodynamic excitation of rotor blades.

As helicopter ground speeds increase, the whip effect caused by aerodynamic excitation of the rotor blades can be expected to increase. This is due to the changing relative air velocities the rotor blade sees as it enters and leaves the direction of flight. Figure 7 shows that the maximum velocity the rotor blades see during each revolution is

$$V_{max} = V_H + r\,\omega$$

and the minimum velocity is

$$V_{min} = V_H - r\,\omega.$$

This effect combined with the cylic variation of the rotor blades to achieve forward motion causes substantial torque variations on the rotor and drive train.

An added incentive for the development of a versatile coupling for helicopters comes from the nature of helicopter design and development. Nearly every major component of a helicopter drive train is made by a different company. It is usually the responsibility of the airframe manufacturer to couple all the drive train components together. Thus it is very possible, unless there is exceptional coordination during the component design phase, that the assembled system will have critical frequencies which are unacceptable.

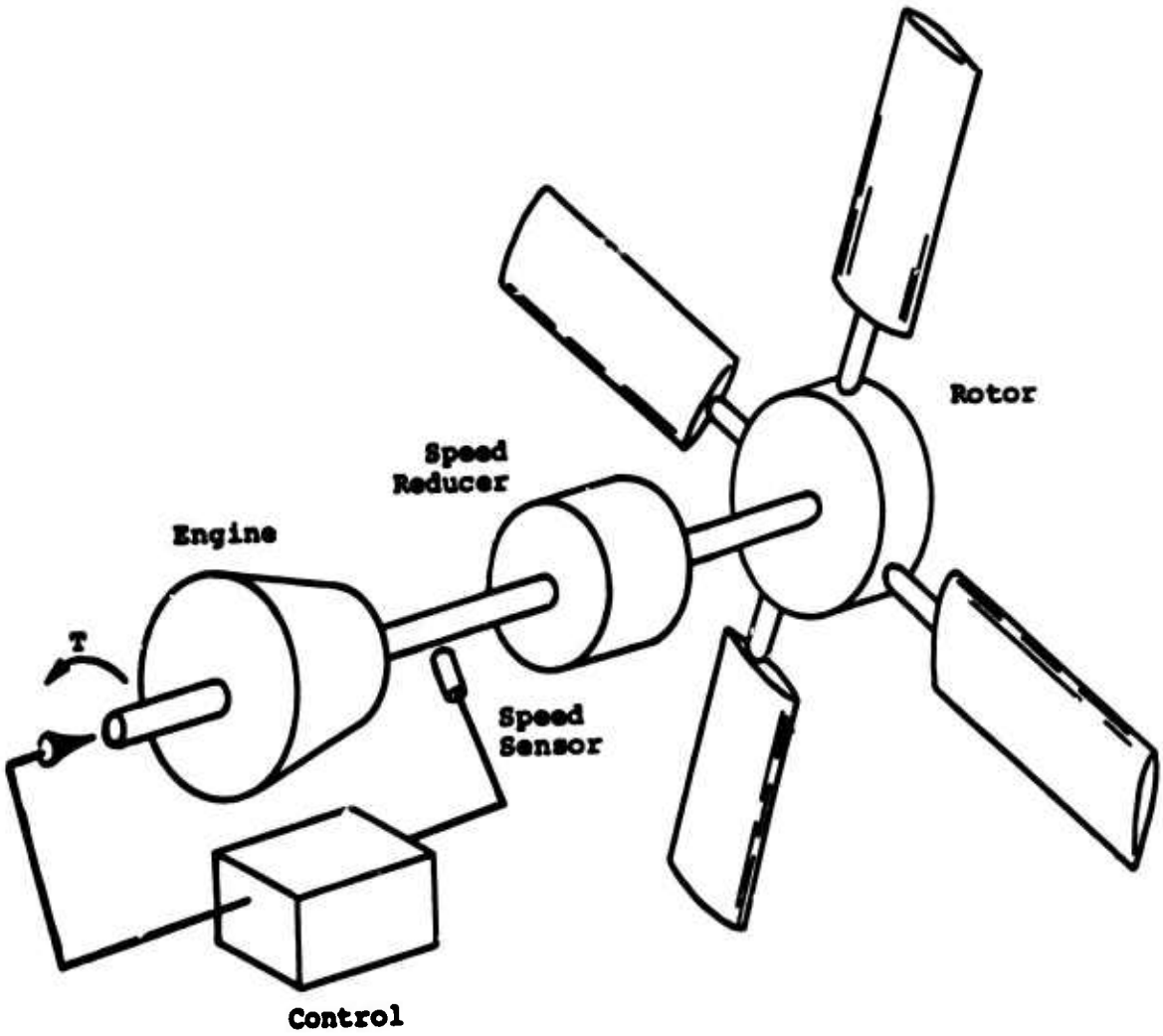

Figure 6. Closed-Loop Helicopter Drive Train.

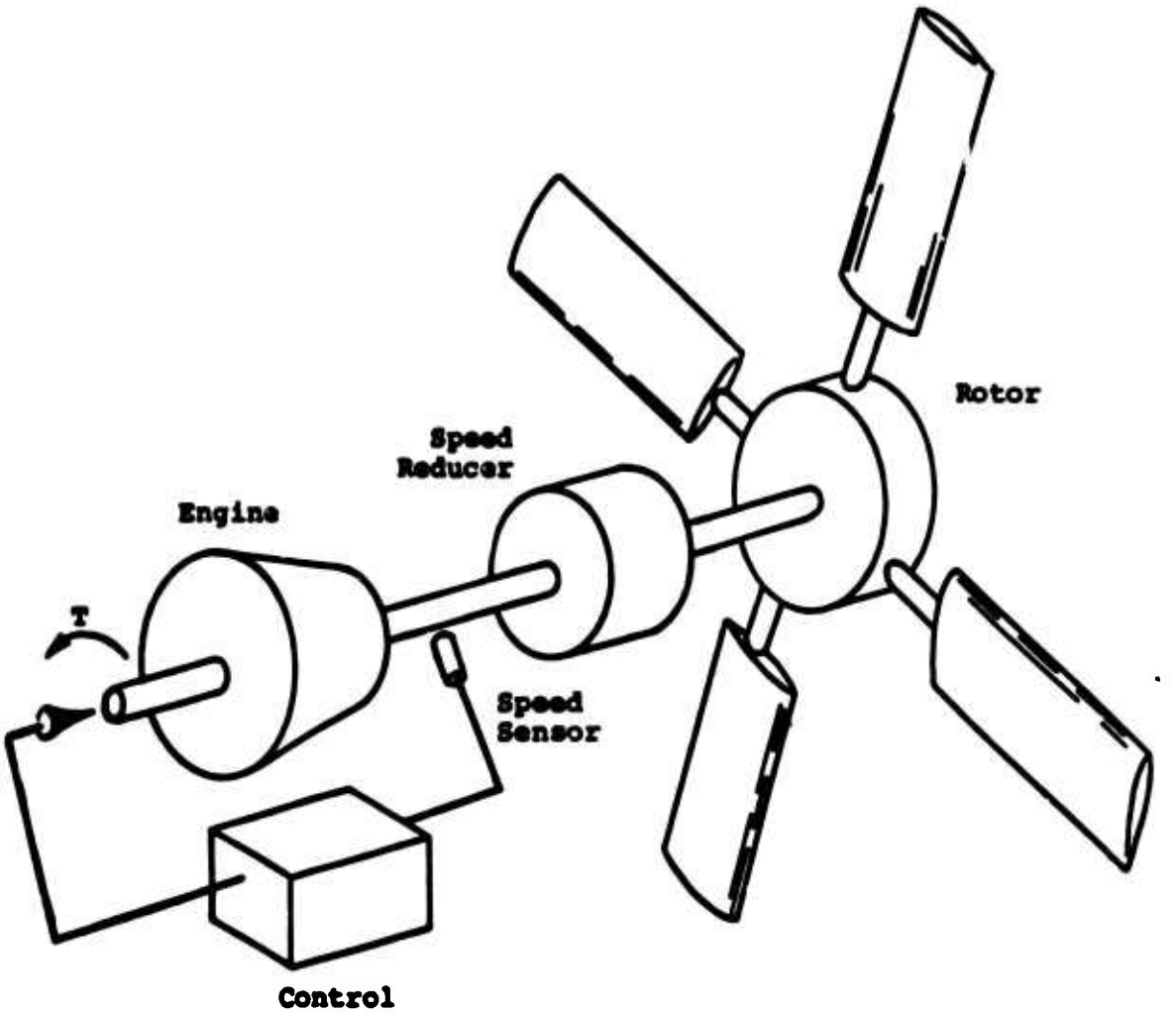

Figure 6. Closed-Loop Helicopter Drive Train.

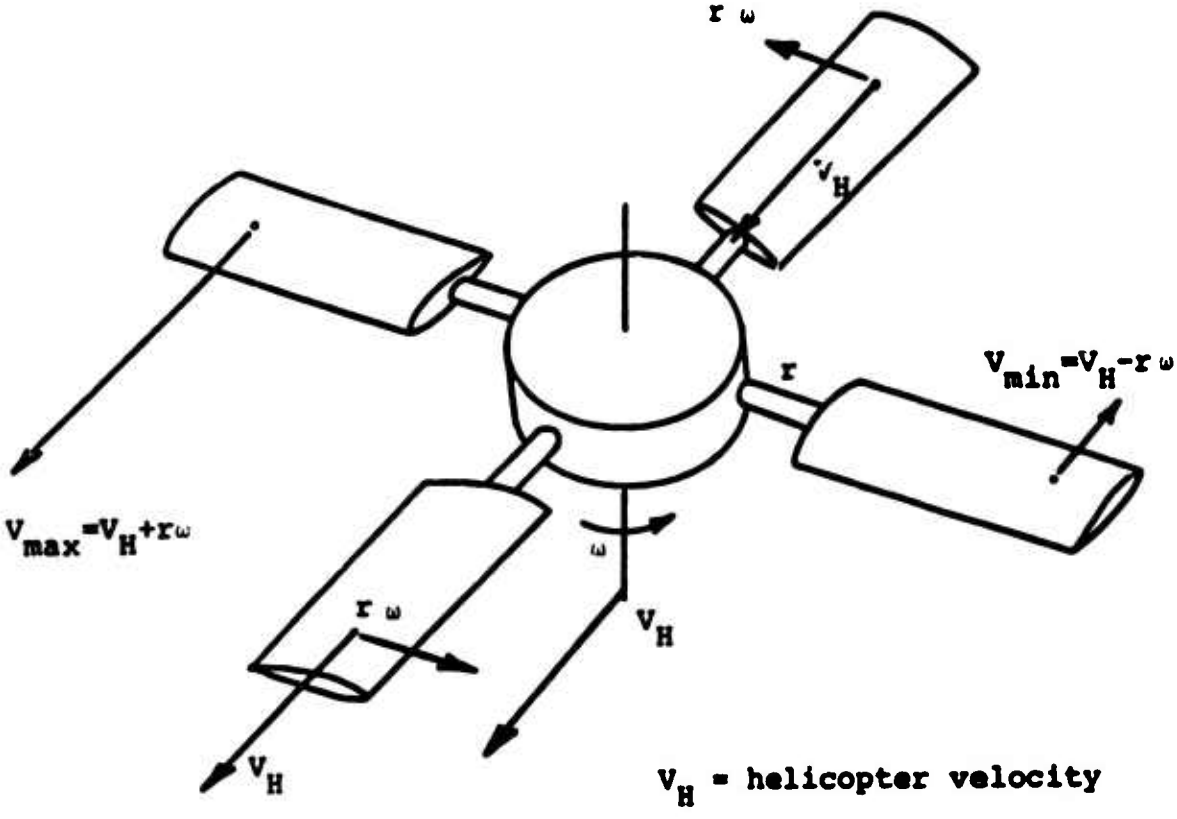

Figure 7. Rotor Blade Velocities.

Two concepts of zero-torsional-stiffness couplings for high-speed helicopter applications are analyzed later in this report. In addition, a Lagrangian formulation for a dynamic simulation of an open-loop helicopter drive train is included. The simulation is used to determine the effectiveness of a zero-torsional-stiffness coupling in reducing torsional vibrations. The procedure used for analyzing torsional vibrations of the open-loop system readily lends itself to the inclusion of governor dynamics for closed-loop analysis.

A synthesized design of a zero-torsional-stiffness coupling for helicopter applications, and the results and discussion of the drive train simulation study using the synthesized coupling are presented in subsequent sections.

SURVEY OF EXISTING LOW-TORSIONAL-STIFFNESS COUPLINGS

Low-torsional-stiffness couplings have been designed to place the critical frequency of a system below the excitation frequencies. The couplings can employ rigid and elastic linkages, as well as a variety of torsional and linear springs. Centrifugal force caused by the rotating links plays an important role in determining the stiffness characteristics of many of the couplings.

The geometry of the coupling (arrangement of components) is the dominant factor in determining the torque resulting from either the centrifugal force of the links or the force due to the elastic deformation of the links or springs.

This section describes various coupling designs which, for certain operating conditions, have low torsional stiffness and the capability of transmitting high torque.

Elastic Link Designs

The elastic materials used in coupling designs range from rubber to steel. For systems with low torque requirements, a rubber or elastomeric material may be used successfully to achieve low stiffness. For the more common high torque systems, steel links have been employed to achieve low torsional stiffness.

The most notable of the high torque elastic link designs is the half-moon (HM) coupling developed by C. W. Chapman.[2] Figure 8 is a diagram of the HM coupling showing the elastic (steel) links. Pins X_1 and X_2 are equally spaced about O and connected to the driving flange. Pins Y_1 and Y_2 are also equally spaced about O but are conected to the driven flange. When one flange is rotated relative to the other about point O, torque can be transmitted across the coupling through the mechanism of elastic deformation of the steel links. The zero-speed torque-deflection curve of the HM coupling is shown in Figure 9. At other than zero speed, the centrifugal force of the links enables additional torque to be transmitted across the coupling. The additional torque is proportional to the square of the

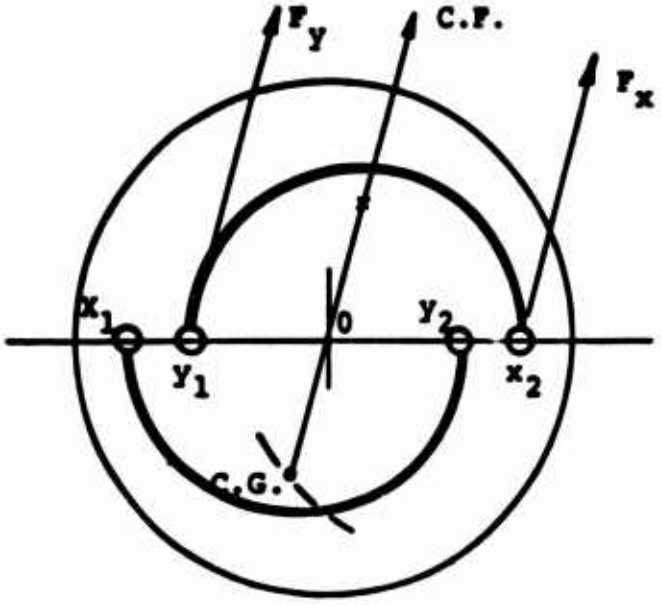

Figure 8. Half-Moon Coupling.[2]

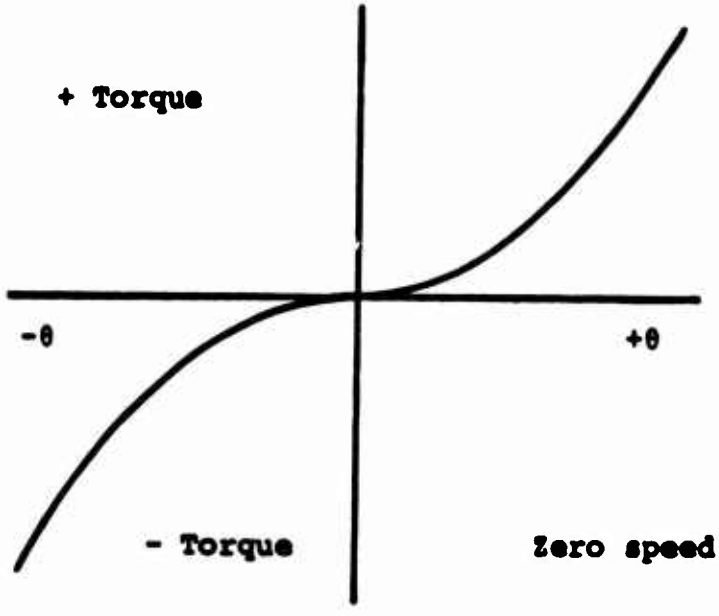

Figure 9. Stiffness Characteristic of HM Coupling.[2]

coupling speed. Figure 8 shows that the center of gravity of each link moves toward O as the twist of the coupling is increased. As a result of the path of the center of gravity, the amount of additional torque transmitted across the coupling resulting from centrifugal force is reduced with increasing twist angle. If, at a given speed, the decrease in torque resulting from centrifugal force is larger in magnitude than the increase in torque resulting from elastic link deformation, a negative torsional stiffness will result. Chapman overcomes the negative stiffness problem and the resulting instability for operation up to a maximum design speed, by including some torsional rigidity in the bushings at pins X_1, X_2, Y_1, and Y_2. The HM coupling has been quite successful in low speed/high power applications. Chapman has indicated through correspondence that he has been unable to design a steel elastic link coupling that can operate at the high speeds found in turbine engine helicopter drive trains.

A modified arrangement of the elastic links in the coupling is shown in Figure 10, where the pins X_1, X_2, Y_1, and Y_2 are not necessarily colinear in the unstrained position. The X and Y pins are the same distance from O, as opposed to Chapman's staggered pin design. The next section presents an analysis technique for the design of Figure 10 which will hopefully produce elastic link couplings with improved stability characteristics for high-speed applications.

Pinned Link Designs

Two pinned link coupling designs are known to have been developed. One is the toggle link (TL) coupling designed by C. W. Chapman.[2] The other is a design of Russian origin.[3] An illustration of the TL coupling is shown in Figure 11. The torsional stiffness of this coupling is effectively zero at zero speed but increases as the speed increases. Chapman has been able to produce TL couplings with torsional stiffness-to-mean torque ratios of 4 or less for low speed/high power applications. This ratio is a measure of relative stiffness which Chapman uses as criteria for effectively eliminating torsional vibrations. The TL coupling, like the HM coupling, has some torsional rigidity in the bushings to overcome negative stiffness at operating speed. The Russian pinned link design, shown in Figure 12, consists of a mass connected by two links, one to the driving flange and the other to the driven flange. The stiffness properties of this coupling are dependent upon the mass, weights of the links, speed of rotation, link length, and pin location on the flanges. Reference 3 gives very little analytical background which is of much use in designing a coupling of this type. There are no graphs given in this reference and, in addition, an equation intended to represent the torque-deflection characteristic of the coupling is dimensionally incorrect.

Low stiffness couplings up to now have been designed for low-speed operation (500-3000 rpm) as would be found in diesel engine systems. For turbine engine applications, such as found in many helicopter drive trains, drive shaft speeds of 10,000 to 20,000 rpm are not uncommon.

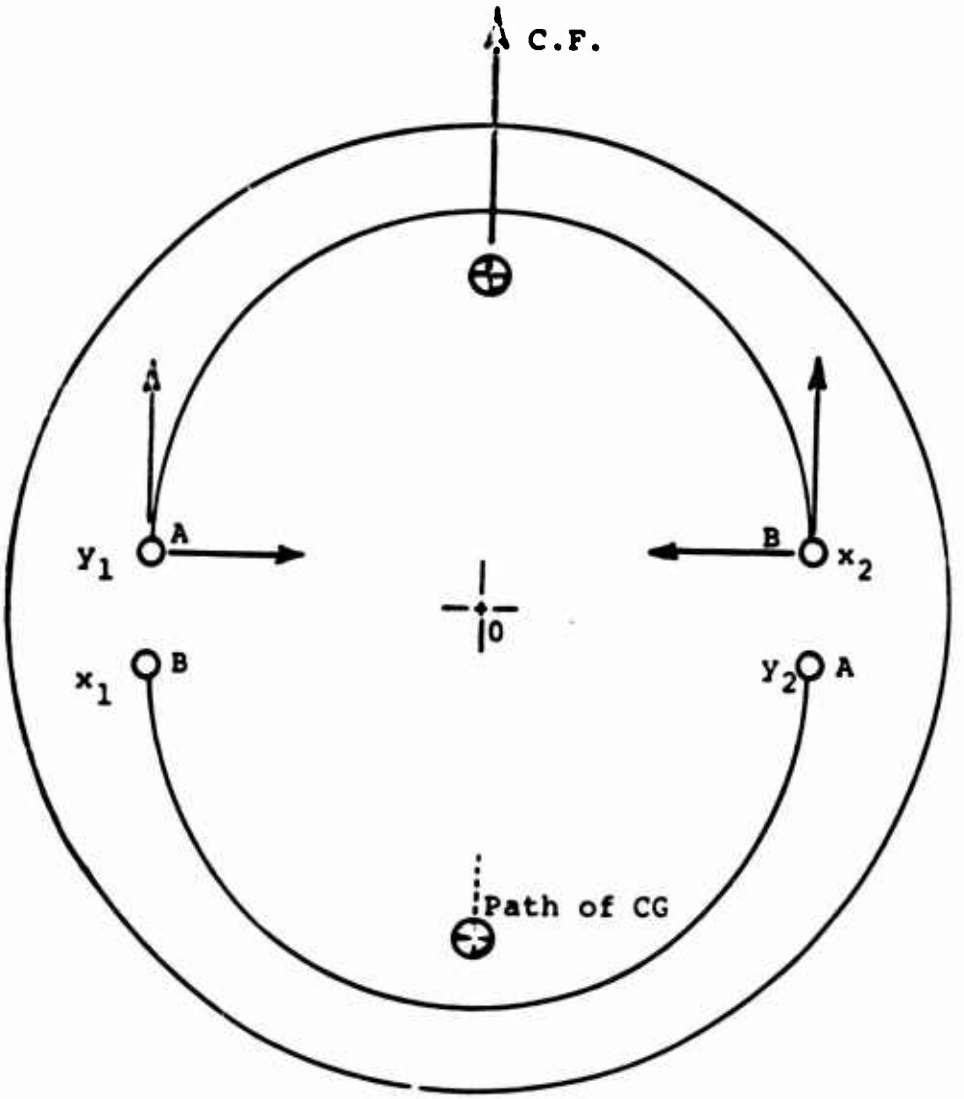

Figure 10. Elastic Link Coupling.

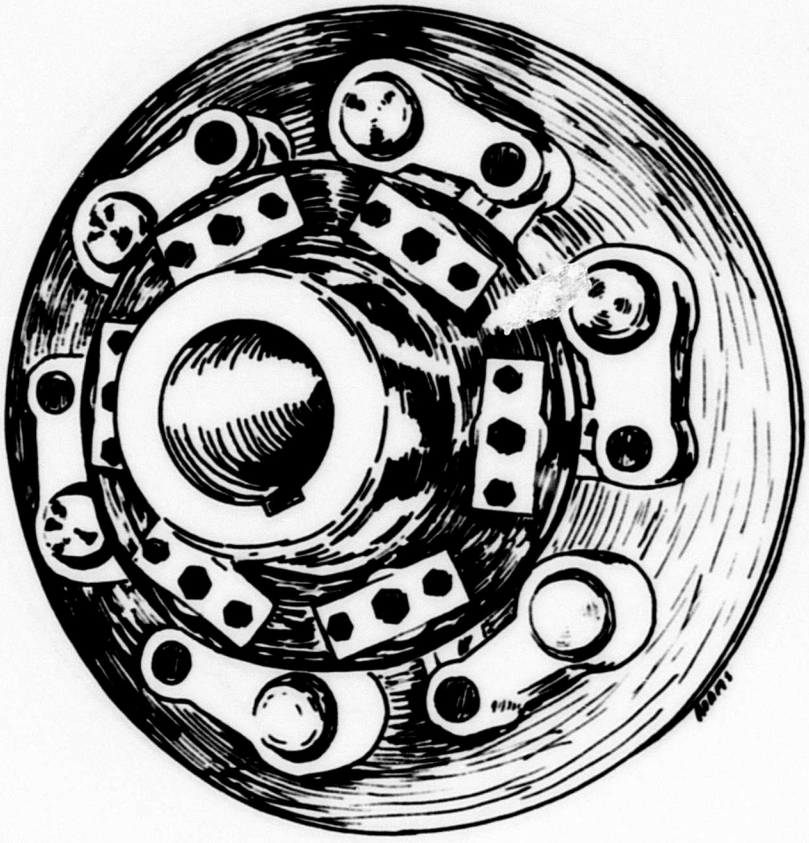

Figure 11. TL Coupling.[2]

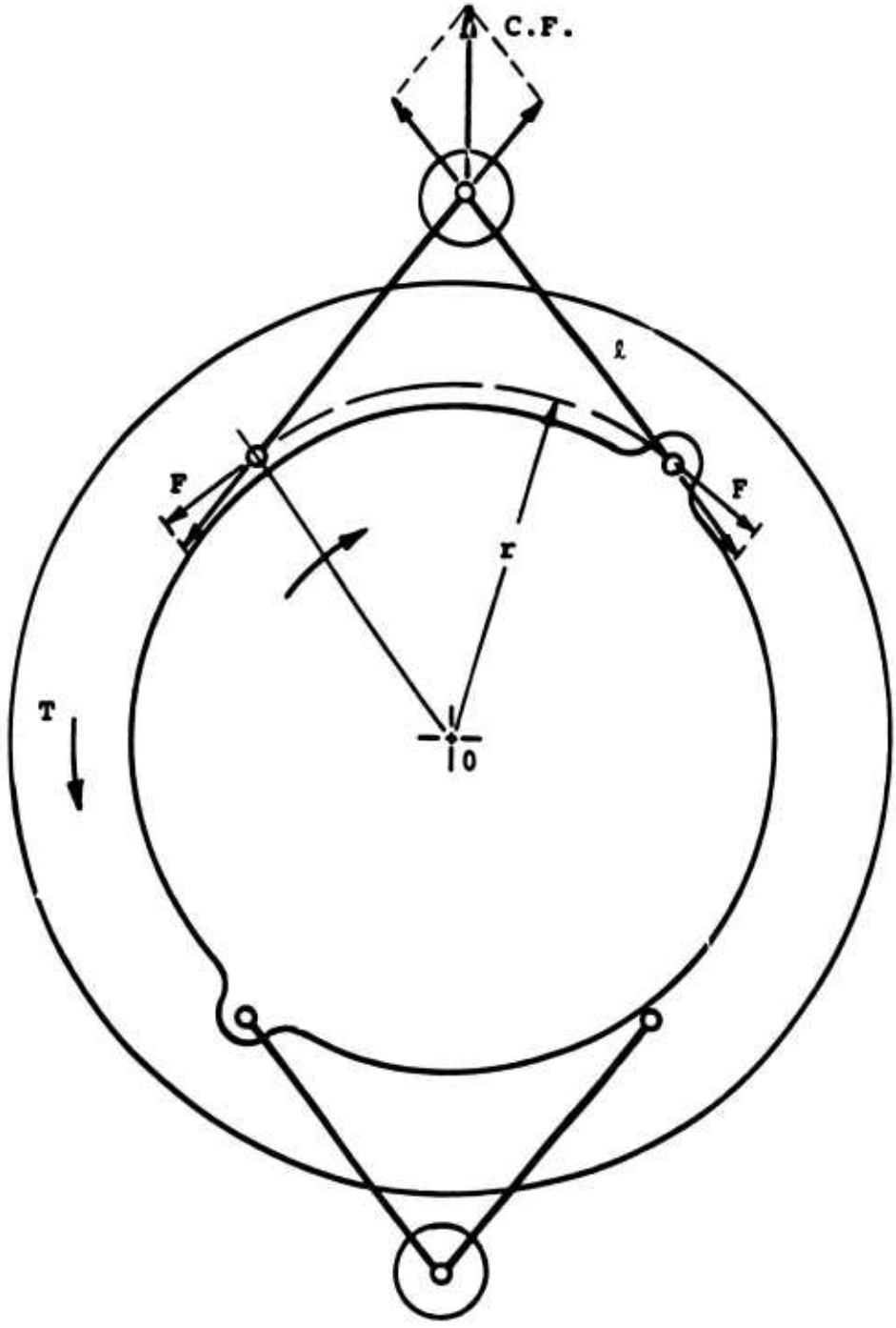

Figure 12. Russian Coupling (Pinned Link).

A new pinned link design is developed in the next section, "Design Analysis for Helicopter Applications." It is shown that a simple coupling can be synthesized which has zero-torsional stiffness at high speeds without the aid of bushing stiffness or other added torsional stiffness correctors which are used to avoid negative stiffness.

DESIGN ANALYSIS FOR HELICOPTER APPLICATIONS

Elastic Link Design Analysis

A procedure for analyzing the elastic link coupling shown in Figure 10 is developed in this section. The parameters involved in determining the stiffness properties and strength characteristics in this analysis (see Figure 13) are

Density of link ρ, lb-sec^2/in.^{4}

Dimensions of link a,b,d,t, in.

Initial position of link r, θ_o, rad.

Modulus of elasticity of link E, lb/in.^{2}

Speed of rotation ω, rad/sec

Yield strength σ_{max}, lb in.^{2}

Number of links N .

The location of the center of mass for the half-cylindrical link is

$$c = \frac{4}{3\pi} \cdot \frac{a^2 + ab + b^2}{a + b}$$

Due to the symmetrical distribution of pins A and B about the link center line, the force on the pins due to angular rotation, ω, of the coupling for a link of mass m is

$$F_y = \frac{F_c}{2} = \frac{m}{2} \omega^2 [c + r \cos(\theta + \theta_o)]$$

(assuming $c \neq c(\omega, F_c)$ (1)

where

$$m = \frac{1}{2} \pi d \rho (b^2 - a^2) \quad (2)$$

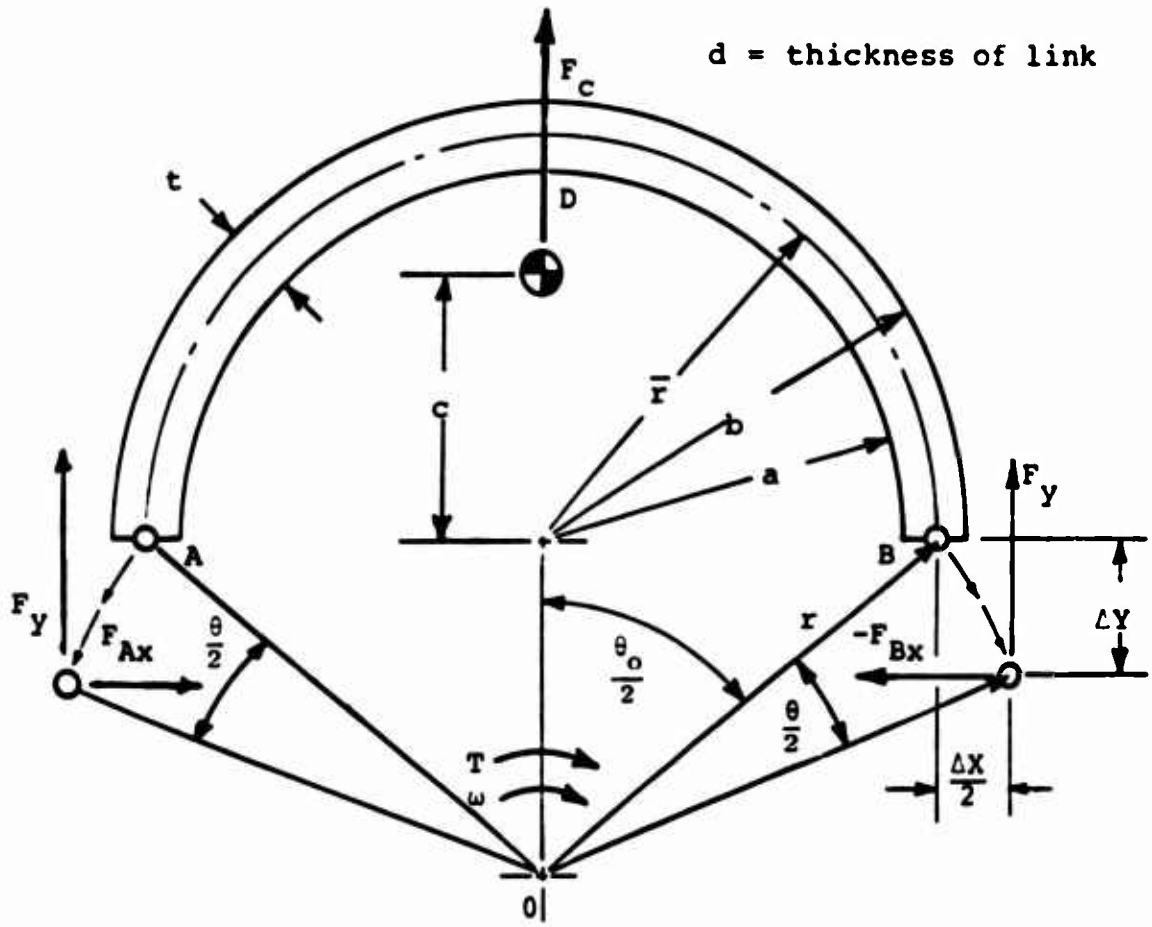

Figure 13. Elastic Link Coupling Parameters.

The force in the x direction on pins A and B is a function of the deflection, Δx. It is not a simple relationship and requires a Theory of Elasticity analysis for accurate results. An expression for the spring constant, K_p, due to elastic deformation of the link is developed from the Theory of Elasticity in Appendix I, the results of which are given below.

$$K_p = E\,d\,\frac{[(a^2 - b^2) + (a^2 + b^2)\,\log\frac{b}{a}]}{2\pi(a^2 + b^2)} \tag{3}$$

For a rotation of $\frac{\theta}{2}$ radians of each pin the change in relative displacement between A and B can be related to Δx by

$$\Delta X = 2r[\sin(\frac{\theta + \theta_o}{2}) - \sin\frac{\theta_o}{2}] \tag{4}$$

and, thus, the force directed between A and B is

$$F_{Ax} = -F_{Bx} = K_p \Delta X \tag{5}$$

The torque about O resulting from forces acting at A is equal and opposite to the torque about O resulting from forces acting at B. Since B is on the driving flange and A is on the driven flange, the torque transmitted by the coupling is

$$T = -F_{Bx}\,r\cos(\frac{\theta + \theta_o}{2}) + F_{By}\,r\sin(\frac{\theta + \theta_o}{2}) \tag{6}$$

Equations 1 and 5 are substituted into equation 6. The resulting equation is divided by d and the right side is multiplied by the number of links, N, giving

$$\frac{T}{d} = \frac{N\,E\,r}{\pi(a^2 + b^2)}[(a^2 - b^2) + (a^2 + b^2)\log\frac{b}{a}]$$

$$\cdot\,[\sin(\frac{\theta + \theta_o}{2}) - \sin\frac{\theta_o}{2}] + \frac{N\pi}{4}\,\omega^2(b^2 - a^2)$$

$$\cdot\,[\frac{4}{3\pi}\,\frac{(b^2 + ab + a^2)}{a + b} + r\cos(\frac{\theta + \theta_o}{2})]r\sin(\frac{\theta + \theta_o}{2}) \tag{7}$$

It is necessary to determine the coupling twist angle, $\frac{\theta}{2}$, which produces the maximum allowable stress in the link. At zero speed the stress at point D in Figure 13 will be

$$\sigma_D = \frac{Mt}{2I} + \frac{F_{Ax}}{td}$$

where

$$t = b - a, \quad M = F_{Ax}(a + \frac{t}{2}), \text{ and } I = \frac{dt^3}{12}$$

giving

$$\sigma_D \approx \frac{2F_{Ax}}{t^2 d} (3a + 2t) \tag{8}$$

At speeds other than zero, the stress at points A and B must be considered. However, the pins at these points can be made large to account for stress without affecting the stiffness properties of the coupling.

Finding a coupling with zero or low stiffness which can transmit the specified torque requirements at design speed is a formidable problem. Choosing a material such as steel for the links removes E, σ_{max}, and ρ from the list of free design parameters, leaving

θ_o	b
r	d
a	

Since d is factored out of the right side of equation 7, the ratio

$$\Omega = \frac{T}{d}$$

can be plotted against θ for various values of θ_o, r, a, and b.

The determination of a low stiffness coupling requires finding a Ω-θ curve, whose slope, $(1/d)(dT/d\theta)$, is zero or near zero but never negative. This can also be achieved by directly plotting the slope

$$K = \frac{d\Omega}{d\theta}$$

versus θ for various values of the design parameters. Using the value of Ω where low stiffness occurs, and the amount of torque which the coupling must transmit at design speed, the value of d can be evaluated from

$$d = \frac{T}{\Omega}$$

Equation 8 must be applied to see if the maximum allowable stress in the link is exceeded for the specified set of design parameters.

A slight change in the design speed or design torque would require one to start the search technique over again. The practicality of designing this

type of coupling for helicopter use by trial and error, where the design parameters are constantly changing, seems very low. On the other hand, if design charts were generated showing stiffness properties for various speeds and torques, this type of coupling might prove quite useful.

Under a set of simplifying assumptions, and with the design torque and speed known and invariant, a simplified set of design equations can be developed which renders a trial and error solution more tractable, as follows:

The assumptions are (see Figure 13)

1. $\theta = 0$ at design torque and speed. (All of the torque transmitted at design conditions will be due to centrifugal force.)

2. c/a = constant = 0.636 for small θ (the link is semicircular and t/a is small).

3. Elastic and centrifugal effects are independent.

4. Elastic effects are approximated by the bending solution, using the method of Castigliano.[17]

5. The pins are symmetrically placed at equal radii.

6. The material is steel.

The design speed and torque are calculated from the requirements of the Swick and Skarvan model as

$$\omega = 13{,}820 \text{ rpm} \times \frac{2\pi}{60} = 1447 \frac{\text{rad}}{\text{sec}} \tag{9}$$

$$T = \frac{(12)(550)}{(1447)} \times 5000 \text{ hp} = 22{,}850 \text{ in.-lb} \tag{10}$$

Thus the torque transmitted per link in a two-link coupling is 11,425 in.-lb.

The weight of a semicircular steel link is given by (see Figure 14 for link dimensions)

$$W = 0.89\ abt + 0.445\ bt^2 \tag{11}$$

The centrifugal load, concentrated at the cg of the link, is

$$F_c = m\omega^2 (h + c) \text{ , where } h = r \cos\left(\frac{\theta_o}{2}\right) \tag{12}$$

or

$$F_c = (h + .636a)(4810\ abt + 1405\ bt^2) \tag{13}$$

The resulting centrifugal tensile stress near the pin locations is set equal to the yield stress (with an appropriate factor of safety).

$$\sigma_y = \frac{F_c}{2bt} = (h + .636a)(2405a + 1202t) \tag{14}$$

The transmitted torque due to the centrifugal force is

$$T_c = \frac{F_c}{2} a = (h + .636a)(1202\ abt^2 + 2405\ a^2bt)$$

$$= 11{,}425\ \text{in.-lb} \tag{15}$$

By the method of Castigliano, the load-deflection relationship for the elastic link (assuming a diametrial load and deflection) is

$$\hat{P} = \frac{4Et^3}{3\pi(2a)^3}\,\delta = (1.59)(10^6)\,\frac{t^3}{a^3}\,\delta \tag{16}$$

where $\hat{P}$ is the value of the bending load for values of $\hat{\theta} \neq 0$.

The deflection δ is expressible in terms of θ as

$$\delta = 2(\hat{a}-a) = 2\left[r \sin\frac{(\theta_o+\theta)}{2} - r \sin\frac{(\theta_o)}{2}\right] \tag{17}$$

which for small θ reduces to

$$\delta = r\,\theta \cos\frac{\theta_o}{2} \tag{18}$$

The torque transmitted by elastic bending of the link is then

$$\hat{T}_e = \hat{P}h$$

$$= (1.59)(10^6)\frac{h^2t^3}{a^3}\,\theta \tag{19}$$

and the elastic stiffness is

$$k_e = \frac{\partial T_e}{\partial \hat{\theta}} = (1.59)(10^6)\,\frac{h^2t^3}{a^3} \tag{20}$$

When $\theta \neq 0$, the torque from centrifugal force is

$$\hat{T}_c = 2405\ \hat{a}^2bt\ (h + .636\ \hat{a}) \tag{21}$$

where

$$\hat{h} = r \cos \frac{(\theta_o+\theta)}{2} \tag{22}$$

$$\hat{a} = r \sin \frac{(\theta_o+\theta)}{2} \tag{23}$$

The centrifugal torque can now be written in terms of the twist angle θ as

$$\hat{T}_c = 2405\ bt\ (a^2+h^2)^{3/2} \sin^2 \frac{(\theta_o+\theta)}{2} \cos \frac{(\theta_o+\theta)}{2} + 0.63 \sin \frac{(\theta_o+\theta)}{2} \tag{24}$$

The centrifugal stiffness is

$$k_c = \frac{\partial T_c}{\partial \theta} = 2405\ bt\ (a^2+h^2)^{3/2}\ 1.9 \sin^2 \frac{(\theta_o+\theta)}{2} \cos \frac{(\theta_o+\theta)}{2} + \sin \frac{(\theta_o+\theta)}{2} \cos^2 \frac{(\theta_o+\theta)}{2} - \sin^3 \frac{(\theta_o+\theta)}{2} \tag{25}$$

At $\theta = 0$, the centrifugal stiffness reduces to

$$k_c(\theta = 0) = 2405\ bt\ (2ah^2 + 1.9\ a^2h - a^3) \tag{26}$$

The overall torsional stiffness of the coupling is the sum of the elastic and centrifugal stiffnesses, which is set equal to zero for $\theta = 0$ to give

$$k_o = (1.59)(10^6) \frac{h^2t^3}{a^3} + 2405\ bt\ (2ah^2 + 1.9\ a^2h - a^3) = 0 \tag{27}$$

A coupling can now be designed by trial and error, satisfying equations 27, 15, and 14, simultaneously.

In addition, it may be desired to introduce a size constraint equation. For the example being presented here with 5000 hp, and 13,800 rpm, a reasonable constraint on the diameter of the coupling might be taken as

$$a + h = 4\ \text{in.} \tag{28}$$

A solution which satisfies equations 27, 15, 14, and 28, simultaneously, is found to be

$a = 3$ in. $\qquad b = 0.57$ in.

$h = 1$ in. $\qquad t = 0.302$ in.

A similar procedure would be required in order to design a coupling for another set of horsepower, speed, and size requirements.

As will be shown immediately below, an advantage of the pinned link coupling over the elastic link coupling described above is that a very simple design equation can be developed for the pinned link coupling, which eliminates the necessity for the method of solution just described.

Pinned Link Design Analysis

The investigation of pinned link couplings which have zero- or low-torsional stiffness begins with the analysis of the Russian coupling shown in Figure 12. Its reduction to a basic kinematic model with one degree of freedom, θ, is shown in Figure 14. From the principles of virtual work and conservation of energy (assuming no friction), the following equations result:

$$\delta W_F = F\,\delta R$$

$$\delta W_\theta = T\,\delta\theta$$

$$\delta W_F = -\delta W_\theta$$

$$T = -F\left(\frac{\delta R}{\delta\theta}\right) \tag{29}$$

Since the system in Figure 14 has one degree of freedom, then $R = f(\theta)$ where

$$f(\theta) = r\cos\frac{\theta}{2} + \sqrt{\ell^2 - r^2\sin^2\frac{\theta}{2}} \tag{30}$$

Taking the variation of $f(\theta)$ with respect to θ gives

$$\frac{\delta R}{\delta\theta} = -\frac{1}{2}\left(r\sin\frac{\theta}{2} + \frac{r^2\sin\theta}{2\sqrt{\ell^2 - r^2\sin\frac{\theta}{2}}}\right) \tag{31}$$

The force F caused by the rotation of the coupling about O is

$$F = m R \omega^2 \tag{32}$$

Substituting equations 30 through 32 into equation 29 and letting

$$Z = \sqrt{\frac{\ell^2}{r^2} - \sin^2\frac{\theta}{2}} \tag{33}$$

gives

$$\frac{T}{Nmr^2\omega^2} = \frac{1}{2}\left[\sin\theta + Z(\sin\theta/2) + \frac{\sin\theta(\cos\theta/2)}{2Z}\right] \tag{34}$$

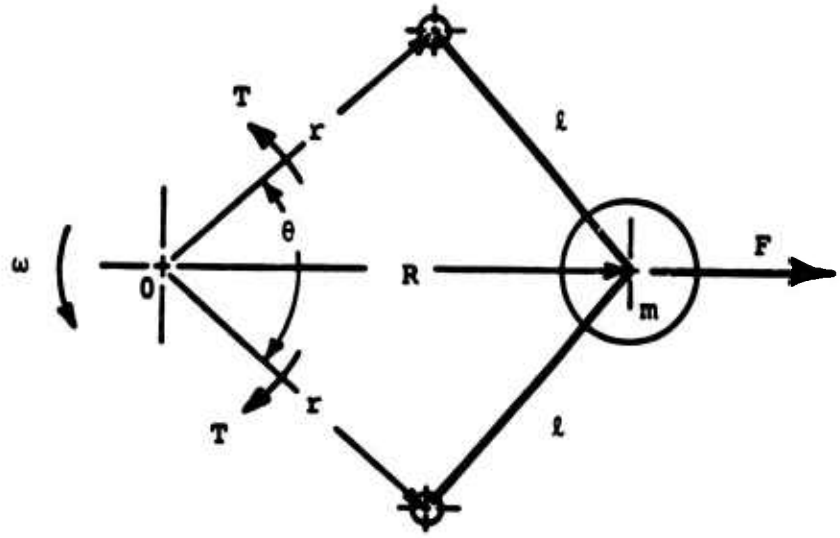

Figure 14. Kinematic Model of Russian Coupling.

where N is the number of linkages.

Values must be determined for r, ℓ, and m which will give the coupling zero stiffness at operating torque and speed. If the ratio ℓ/r is defined as a new parameter β, equation 34 becomes

$$\frac{T}{Nmr^2\omega^2} = f(\beta,\theta) \tag{35}$$

which results in a one-parameter family of curves.

The function, $f(\beta,\theta)$, plotted against θ for various values of β is shown in Figure 15. As can be seen from the graph, values of $\beta = .87$ and $\theta = 100°$ give nearly zero stiffness over several degrees of coupling rotation.

Since the operating torque and speed are given for the helicopter problem, the value of either m or r can be chosen. The other value can be calculated from equation 35 where $\beta = .87$ and $\theta = 100°$.

Design Equation I

$$\frac{T}{Nmr^2\omega^2} = f(.87,100) = 2.445 \times 10^{-6} \tag{36}$$

Design Equation II

$$\beta = \frac{\ell}{r} = .87 \tag{37}$$

where

T	ft-lb	ω	rpm
r	in.	N	1
m	lb_m	ℓ	in.

Equations 36 and 37 are now general design equations for a zero-torsional-stiffness coupling for any speed and torque. It is necessary to see if values for m, r, and ℓ can be found which are physically realizable for the helicopter coupling design.

For high-speed applications, it is very likely that the mass of the links which has been ignored up to now will have a significant effect on the stiffness characteristics of the coupling. Fortunately the mass, m_ℓ, of each link, and the mass, m_B, at point B in Figure 16 can be combined for steady-state analysis (ω = constant). Figure 17a shows the centrifugal force F resulting from the distributed mass m_ℓ of a link. If mass m_ℓ is equally redistributed to points A and B (Figure 17b), the center of

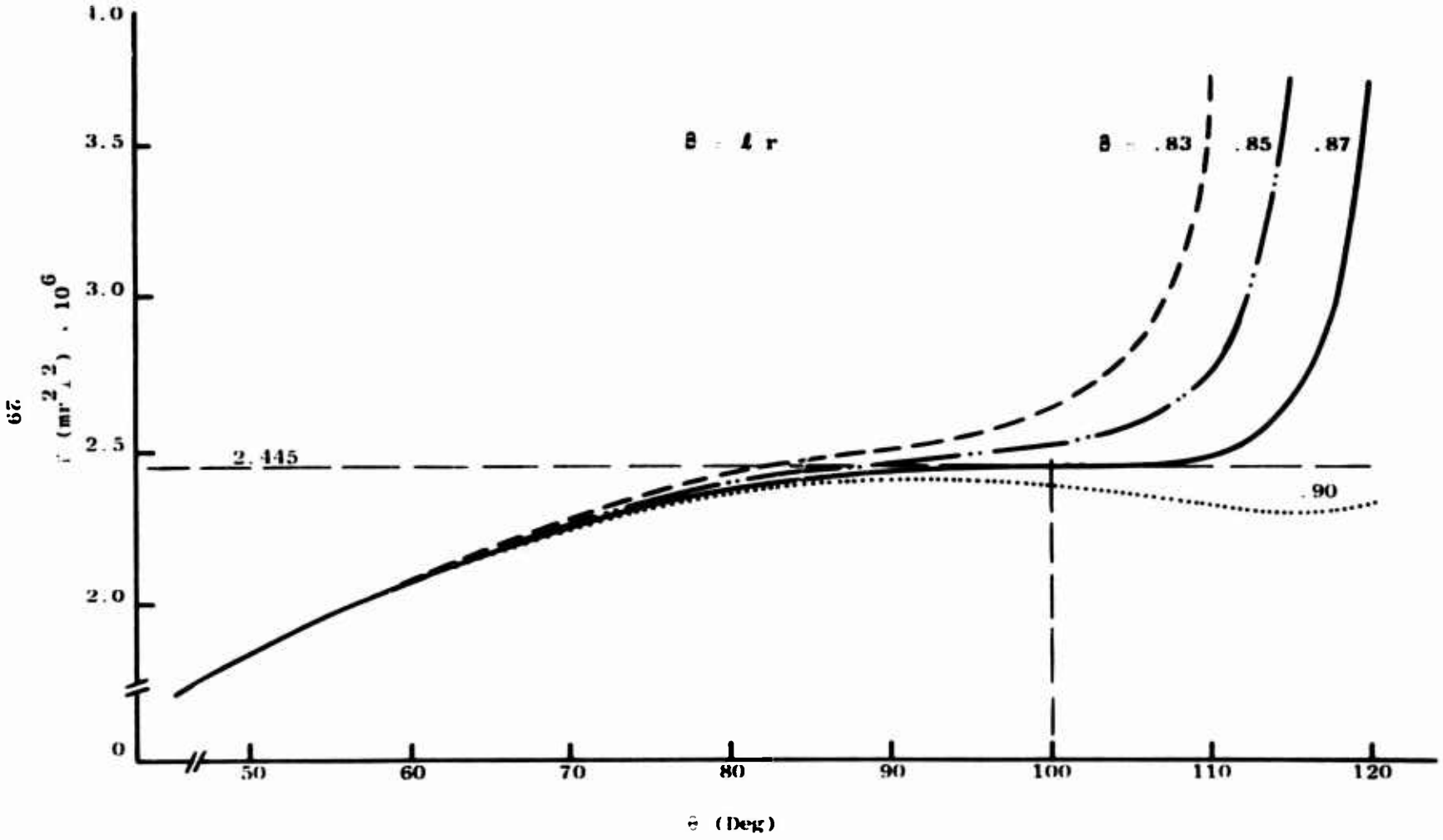

Figure 15. Characteristic Curves of Pinned Link Coupling.

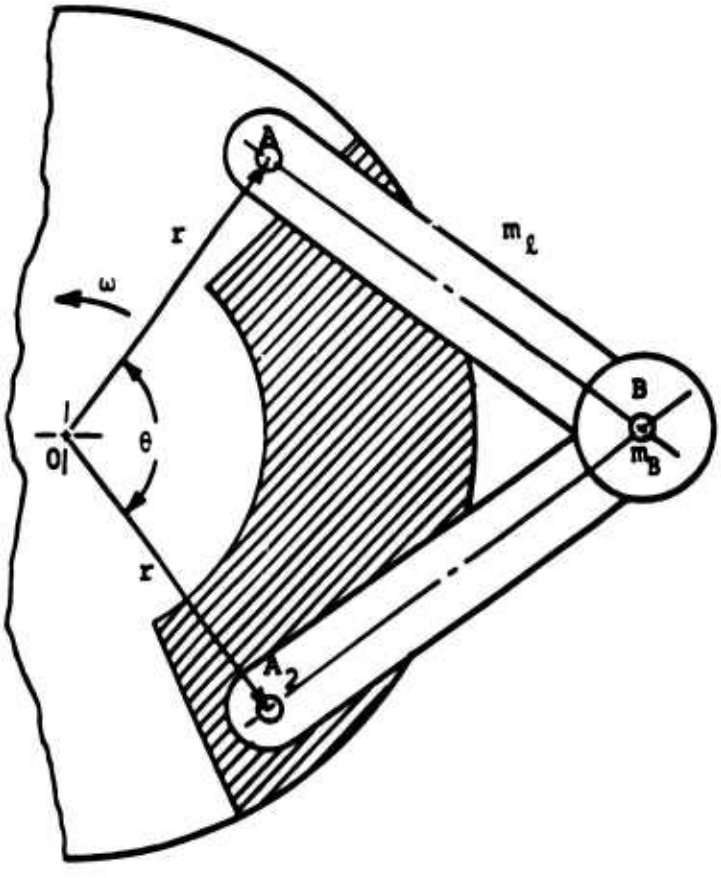

Figure 16. Coupling Mass.

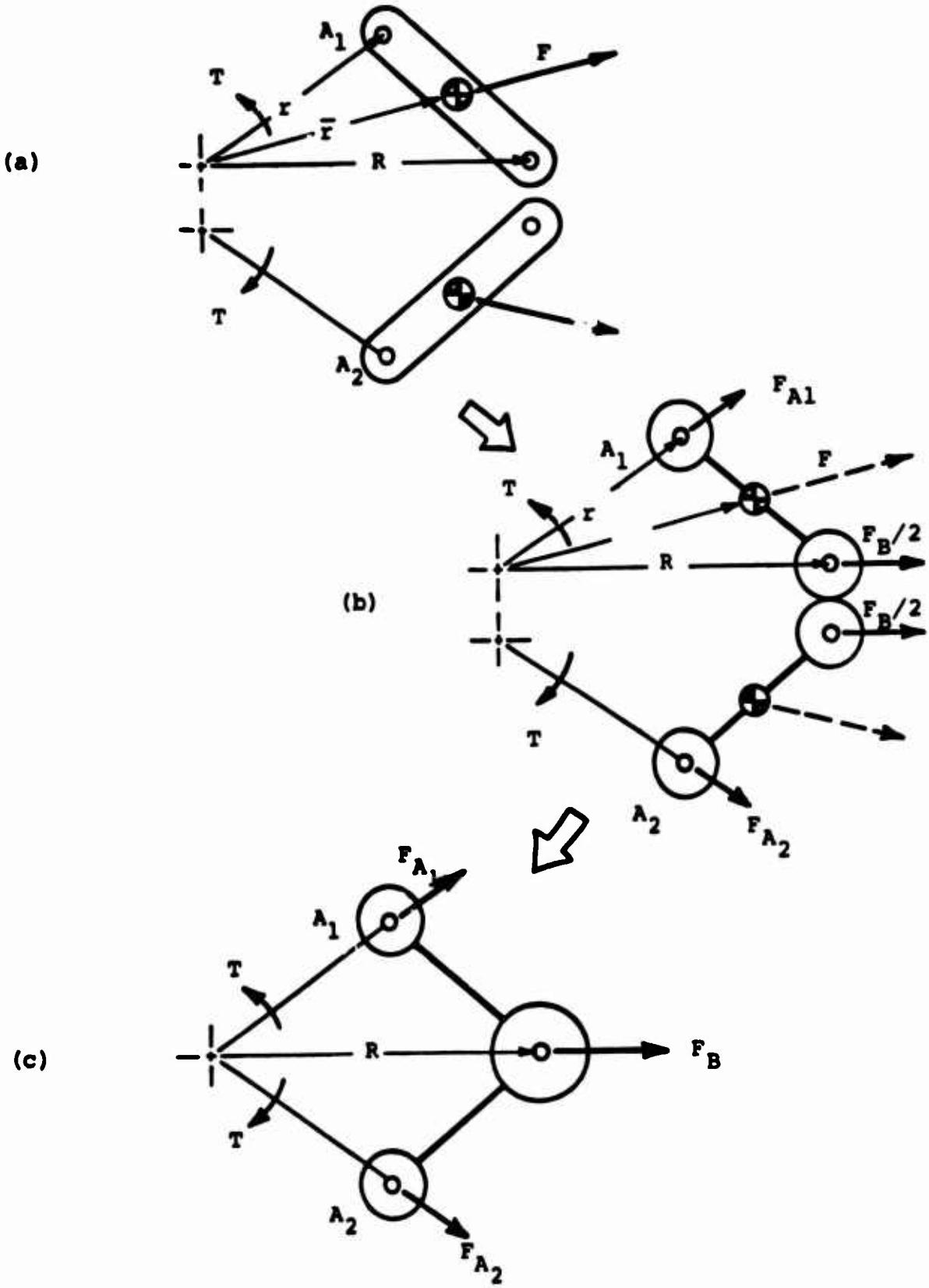

Figure 17. Equivalent Mass.

gravity of the link does not change; thus the force F does not change. The force vector can, however, be resolved into the two components shown in Figure 17b.

$$F_A = F_{A1} = F_{A2} = \frac{1}{2} m_{\ell} r_{\ell}^2$$

$$\frac{F_B}{2} = \frac{1}{2} m_{\ell} R_{\ell}^2$$

Figure 17c shows the two links combined, giving

$$F_B = m_{\ell} R_{\ell}^2$$

$$F_A = \frac{1}{2} m_{\ell} r_{\ell}^2$$

Including m_{ℓ} with m_B gives

$$F_B = F_B + m_B R_{\ell}^2 = (m_{\ell} + m_B) R_{\ell}^2$$

The forces F_{A1} and F_{A2} cannot contribute to the torque T since they are directed radially outward from point 0 and have no moment about 0. This leaves only force F_B to produce torque T. Thus, the relationship between torque and twist angle can be determined from design equation 1 by setting $m = m_{\ell} + m_B$. The proof of this statement, given below, comes from the principle of virtual work.

$$\delta W_e = \delta W_A + \delta W_B$$

where

$$\delta W_e = T \delta \theta$$

$$\delta W_A = F_A \delta r$$

$$\delta W_B = F_B \delta R$$

thus

$$T = F_A \frac{\delta r}{\delta \theta} + F_B \frac{\delta R}{\delta \theta}$$

$$T = F_B \frac{\delta R}{\delta \theta} = (m_{\ell} + m_B) R_{\ell}^2 \frac{\delta R}{\delta \theta}$$

Substituting equations 31 through 35 into the above equation gives

$$\frac{T}{N(m_{\ell}+m_B)r^2\omega^2} = f(\beta,\delta)$$

which is the same as design equation I, with $m = m_{\ell} + m_B$.

Therefore, to include the mass of the links, m_{ℓ}, with mass m_B, simply add m_{ℓ} to m_B. It should be noted that adding the mass of one link, m_{ℓ}, at point B will represent the total effect of both links.

Due to strength considerations, it may be required to make the links more massive than called for in the design equations 36 and 37. This may very likely be the case in high-speed turbine applications. Through the use of a form of counterbalancing, the links can be made as massive as desired, without altering the prescribed stiffness properties of the coupling. After mass m has been determined from design equation I, it is necessary to counterbalance any extra mass, m_e, where

Design Equation III

$$m_e = m_{\ell} + m_B - m \tag{38}$$

A negative value for m_e means the link is too light and $+m_e$ must be added at point B or to the cg of each link. If m_e is positive in equation 38, then mass m_c must be added at point E to each link at a distance r_e as shown in Figure 18, such that

Design Equation IV

$$m_c r_e = \frac{1}{2} m_e \ell$$

or

$$m_c = \frac{\ell m_e}{2r_e} \tag{39}$$

Coupling Parameters for Helicopter Analysis

Representative values of turbine power and speed from Swick and Skarvan[5] are

Normal operating power = 5270 hp

Normal operating speed = 13,820 rpm

Equation 40 shows that a zero-torsional-stiffness coupling must be designed to transmit a torque of 2004 ft-lb at 13,820 rpm (1447 rad sec).

$$T_{(ft-lb)} = \frac{hp(33,000)}{2\pi\omega_{(rpm)}} = \frac{5270(33,000)}{2\pi(13,820)} = 2004 \tag{40}$$

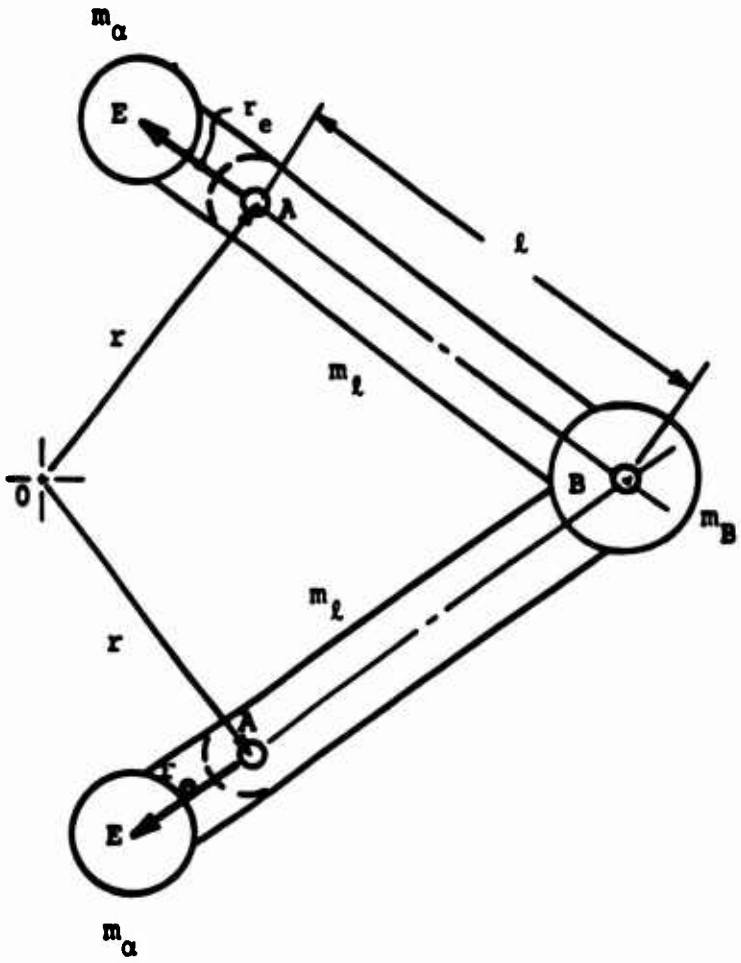

Figure 18. Counterweight m_α.

The size and weight of the coupling can diminish the helicopter payload; therefore the value of r, which has a direct bearing on the coupling flange size, will be kept to a minimum. A reasonable choice for r which should allow sufficient clearance of various existing helicopter hardware is 3 inches.

For design equation I (36) with

$$r = 3 \text{ in.}$$

$$\omega = 13{,}820 \text{ rpm}$$

$$T = 2004 \text{ ft-lb}$$

$$N = 2 \text{(symmetric coupling)}$$

$$\beta = .87 \text{(zero stiffness)}$$

a value of $m = .2385\ lb_m$ is obtained. The value of ℓ from design equation II (37) is 2.61 in. All kinematic design parameters for a zero-torsional stiffness have been determined and are shown in Figure 19.

Helicopter Drive Train Parameters

The helicopter drive train shown in Figure 20 can be modeled with the following parameters:

Rotor inertia	I_R
Engine inertia	I_e
Speed reducer inertia	I_G
Mast shaft stiffness	K_s
Drive shaft stiffness	K_t
Rotor damping	C_L
Engine damping	C_e
Mast shaft damping	C_s

(see Figure 20)

For systems with speed reducers, it is common practice to reference all springs and inertias to one side of the gearbox (see Appendix II). For this helicopter analysis the engine input side will be used.

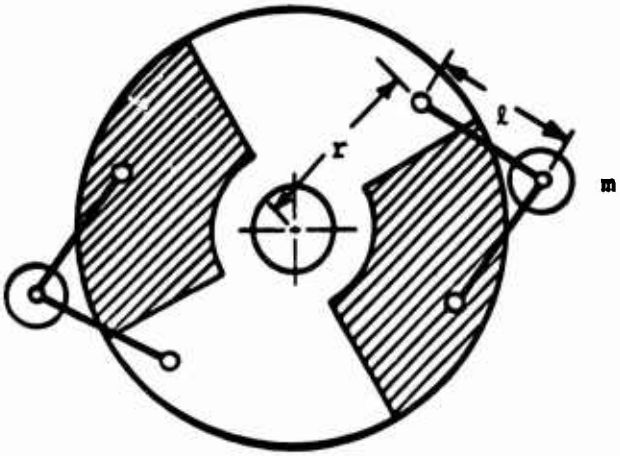

r = 3 in.

ℓ = 2.61 in.

m = .2385

Figure 19. Kinematic Design Parameters.

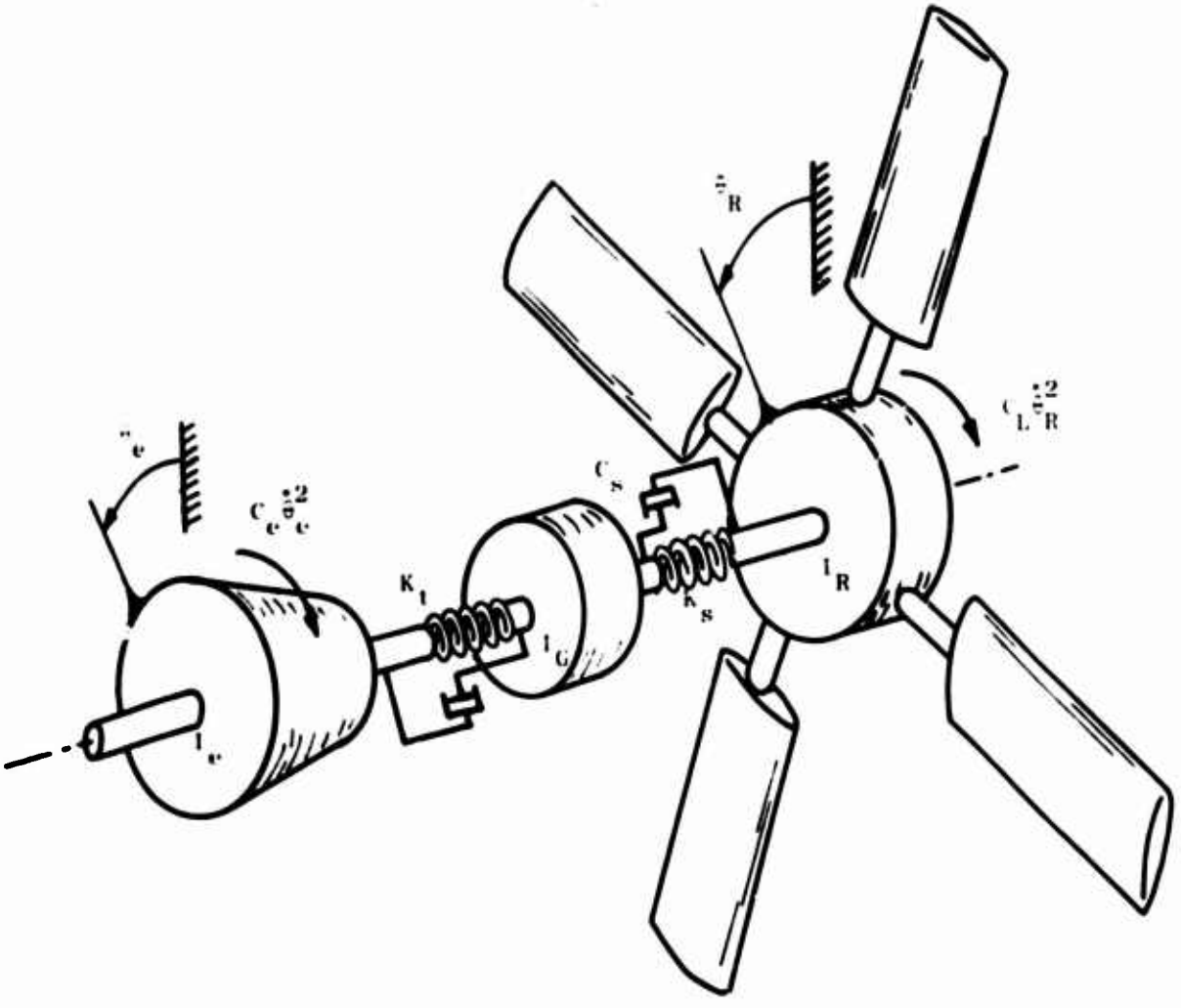

Figure 20. Helicopter Drive Train Parameters.

Numerical values for the above inertias and spring constants taken from Swick and Skarvan[5] are

$$I_R = 3.888 \quad \text{slug-ft}^2$$

$$I_e = 0.500 \quad \text{slug-ft}^2$$

$$I_G = 0.144 \quad \text{slug-ft}^2$$

$$K_s = 212.1 \quad \text{ft-lb/rad}$$

$$K_t = 21,417 \quad \text{ft-lb/rad}$$

(all values referenced to engine input side of gearbox)

It will be assumed that the aerodynamic rotor drag and engine drag are proportional to angular velocity squared.[3] Nearly all of the shaft horsepower of the engine is dissipated in the aerodynamic drag of the rotor, where

$$T_{DRAG} = C_L \dot{\theta}_R^2$$

For steady-state operation with T = 2004 ft-lb and $\dot{\theta}_R = \dot{\theta}_e = 1447$ rad/sec,

$$C_L = 9.564 \times 10^{-4} \text{ ft-lb-sec}^2$$

A value for the engine damping coefficient C_e is determined by assuming a 25-30 percent total power loss due to turbine drag; thus, total hp $\approx$ 7400.

From equation 40 an engine drag torque of about 800 ft-lb is obtained, giving

$$C_e \dot{\theta}_e^2 = 800 \text{ ft-lb}$$

or

$$C_e = 3.82 \times 10^{-4} \text{ ft-lb-sec}^2$$

The speed reducer inertia is small compared to the engine inertia, and the drive shaft stiffness is much larger than the mast shaft stiffness which is effectively reduced by the speed reduction ratio.

Since the investigation of torsional vibrations is not directly concerned with vibrations of very high frequency, the drive shaft can be assumed to be rigid, allowing the speed reducer inertia to be combined with the engine inertia giving a new value I_e':

$$I_e' = I_e + I_G$$

The model for the helicopter drive train with $K_t \rightarrow \infty$ and $I'_e = I_e + I_G$ reduces to the two-degree-of-freedom system shown in Figure 21 (System 1).

The mast shaft damping is assumed to be 10 percent of critical damping.

$$C_s = \frac{1}{10}\left(2\sqrt{K_s I_{eff}}\right) = 2.24$$

where

$$I_{eff} = \frac{I'_e I_R}{I'_e + I_R}$$

The drive train model in Figure 21, with the zero torsional stiffness coupling developed in the previous section inserted along the drive shaft, has an additional degree of freedom. The inertia of the driving flange of the coupling is combined with the engine inertia, since K_t is assumed to be infinite, giving $I'_e = I_e + I_{fe}$. The driven flange of the coupling is combined with the speed reducer inertia to give $I'_{fr} = I_G + I_{fr}$.

Figure 22 shows the three-degree-of-freedom system incorporating the coupling (System 2).

System Simulation

The open-loop helicopter drive train model without a zero-torsional-stiffness coupling can be dynamically described by the following two differential equations of motion:

$$\Sigma T_e = I'_e \ddot{\theta}_e \qquad\qquad \Sigma T_R = I_R \ddot{\theta}_R$$

or by inspection

$$I_e \ddot{\theta}_e = -K_s(\theta_e - \theta_R) - C_e \dot{\theta}_e^2 - C_s(\dot{\theta}_e - \dot{\theta}_R) + T(t)$$

$$I_R \ddot{\theta}_R = K_s(\theta_e - \theta_R) - C_L(t)\dot{\theta}_R^2 + C_s(\dot{\theta}_e - \dot{\theta}_R) \qquad (41)$$

The most common procedure for numerically solving these equations is to first use two dummy variables λ_e and λ_R where

$$\lambda_e = \dot{\theta}_e \qquad\qquad \dot{\lambda}_e = \ddot{\theta}_e$$

$$\lambda_R = \dot{\theta}_R \qquad\qquad \dot{\lambda}_R = \ddot{\theta}_R$$

and transform equations 41 into the following set of first-order differential equations.

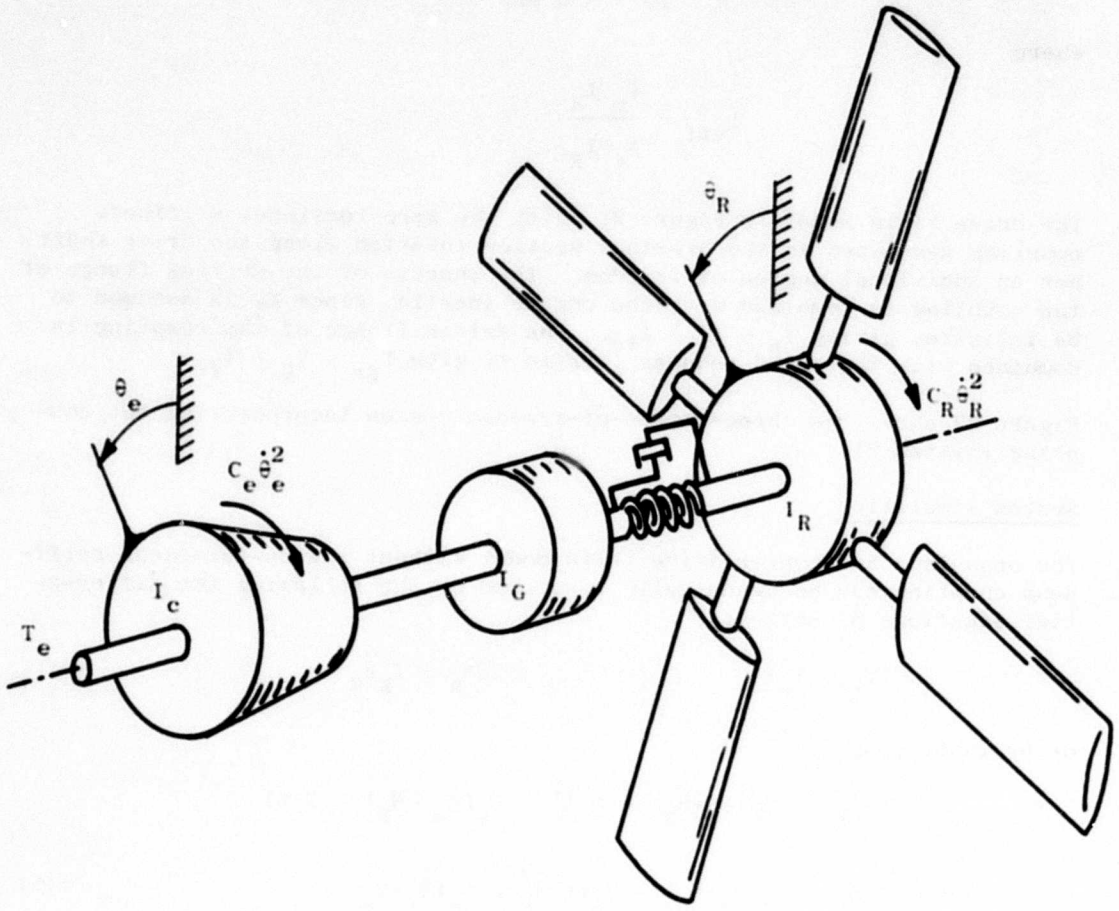

Figure 21. System 1--Helicopter Drive Train (Without Coupling).

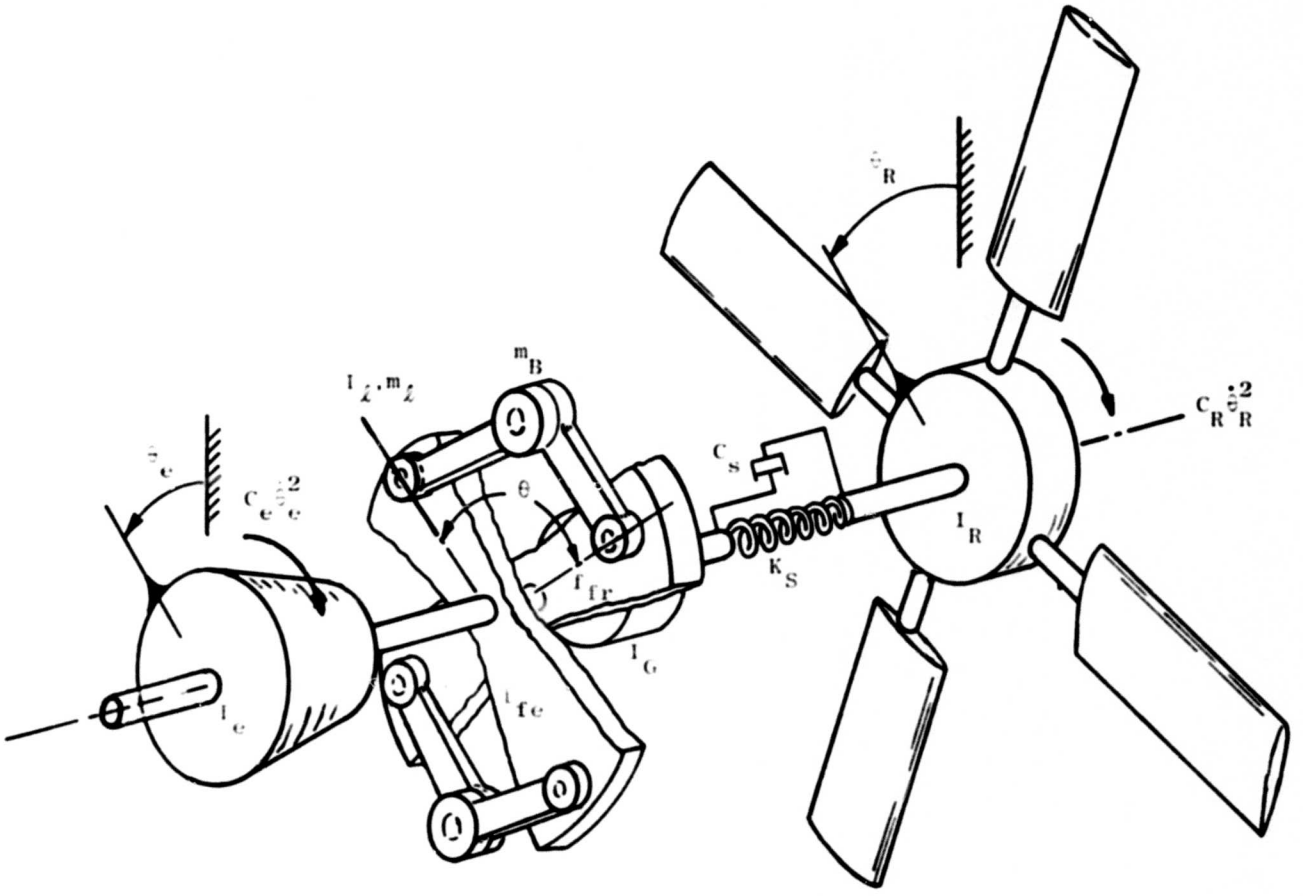

Figure 22. System 2--Helicopter Drive Train (With Coupling).

$$\dot{\lambda}_e = \frac{1}{I'_e}\left[K_s(\theta_e-\theta_R) - C_e\lambda_e^2 - C_s(\lambda_e-\lambda_R) + T(t)\right]$$

$$\dot{\lambda}_R = \frac{1}{I_R}\left[K_s(\theta_e-\theta_R) - C_L(t)\lambda_R^2 + C_s(\lambda_e-\lambda_R)\right]$$

$$\dot{\theta}_e = \lambda_e$$

$$\dot{\theta}_R = \lambda_R \qquad (42)$$

The equations of motion for the helicopter drive train with a zero torsional stiffness coupling are much more complex than the above. The most effective form of solution is through the use of analytical dynamics, more specifically the method of Vance and Sitchin[7] for directly obtaining first-order difference equations from Hamilton's principle.

The method will first be used with the two-degree-of-freedom system. The resulting equations will be used for the actual numerical integration due to its generally improved accuracy over other methods.[7]

Hamilton's principle for nonconservative systems is

$$\delta I = \delta \int_{t_1}^{t_2} L\, dt + \int_{t_1}^{t_2} \left(\sum_{i=1}^{K} F_i\, \delta_{qi}\right) dt = 0$$

where

$L = T-V$ = the Lagrangian

T = the kinetic energy

V = the potential energy

F_i = the nonconservative forces

Hamilton's principle is satisfied by the set of k second-order Lagrange's equations

$$\frac{d}{dt}\left(\frac{\partial L}{\partial \dot{q}_i}\right) - \frac{\partial L}{\partial q_i} = F_i \qquad (43)$$

The generalized coordinates q_i for the two-degree-of-freedom system (Figure 21) are

$$\theta_e,\ \theta_R \qquad K = 2$$

For the three-degree-of-freedom system (Figure 22), the generalized coordinates are

$$\theta_e,\ \theta,\ \theta_R \qquad K = 3$$

Equations of Motion for System 1

The Lagrangian is

$$L = \frac{1}{2} I'_e \dot{\theta}_e^2 + \frac{1}{2} I_R \dot{\theta}_R^2 - \frac{1}{2} K_s(\theta_e - \theta_R)^2$$

The elements of Lagrange's equations 43 are

$$\frac{\partial L}{\partial \dot{\theta}_e} = I'_e \dot{\theta}_e$$

$$\frac{\partial L}{\partial \dot{\theta}_R} = I_R \dot{\theta}_R \tag{44}$$

$$\frac{\partial L}{\partial \theta_e} = K_s(\theta_e - \theta_R)$$

$$\frac{\partial L}{\partial \theta_R} = -K_s(\theta_e - \theta_R) \tag{45}$$

Momentum is defined as

$$P_i = \frac{\partial L}{\partial \dot{q}_i} \tag{45}$$

For the two generalized coordinates θ_e and θ_R, the momenta and their respective time derivaties are

$$P_e = \frac{\partial L}{\partial \dot{\theta}_e} = I'_e \dot{\theta}_e$$

$$P_R = \frac{\partial L}{\partial \dot{\theta}_R} = I_R \dot{\theta}_R \tag{46}$$

$$\dot{P}_e = \frac{d}{dt}\left(\frac{\partial L}{\partial \dot{\theta}_e}\right)$$

$$\dot{P}_R = \frac{d}{dt}\left(\frac{\partial L}{\partial \dot{\theta}_R}\right) \tag{47}$$

The generalized forces F_i can be determined from the principle of virtual work:

$$\delta W_i = F_i \, \delta q_i$$

for θ_e

$$\delta W_e = F_e \, \delta \theta_e$$

$$F_e = -C_e \dot{\theta}_e^2 - C_s(\dot{\theta}_e - \dot{\theta}_R) + T_e(t)$$

and for θ_R

$$\delta W_R = F_R \, \delta \theta_R$$

$$F_R = -C_L \dot{\theta}_R^2 + C_s(\dot{\theta}_e - \dot{\theta}_R) \tag{48}$$

Using equations 45, 47, and 48, Lagrange's equations 43 can be written in the canonical form:

$$\dot{P}_e = K_s(\theta_e - \theta_R) - C_e \dot{\theta}_e^2 - C_s(\dot{\theta}_e - \dot{\theta}_R) + T_e(t) \tag{49}$$

$$\dot{P}_R = -K_s(\theta_e - \theta_R) - C_L \dot{\theta}_R^2 + C_s(\dot{\theta}_e - \dot{\theta}_R)$$

For dynamical systems the P_i's are always linear in the $\dot{q}_i$'s; therefore, from linear algebra

$$\{P_i\} = [A]\{\dot{q}i\} \tag{50}$$

or

$$\{\dot{q}i\} = [A^{-1}]\{P_i\} \quad \text{(assuming A is nonsingular)} \tag{51}$$

From equations 44 and 50 the remaining canonical equations are formed.

$$\begin{bmatrix} \dot{\theta}_e \\ \\ \dot{\theta}_e \end{bmatrix} = \begin{bmatrix} 1/I_e' & 0 \\ \\ 0 & 1/I_R \end{bmatrix} \cdot \begin{bmatrix} P_e \\ \\ P_R \end{bmatrix} \tag{52}$$

Equations 49 and 52 form a set of four first-order differential equations in coordinates:

$$P_e \qquad \theta_e$$

$$P_R \qquad \theta_R$$

These equations can be numerically solved by

1. Specifying initial conditions for P_{e_0}, P_{R_0}, θ_{e_0}, and θ_{R_0}
2. Finding values for $\dot{\theta}_e$ and $\dot{\theta}_R$ from equation 52
3. Finding values for $\dot{P}_e$ and $\dot{P}_R$ from equation 49
4. Numerically integrating $\dot{P}_e$, $\dot{P}_R$, $\dot{\theta}_e$ and $\dot{\theta}_R$ using routines such as Euler or Runge-Kutta

Using Euler integration,

$$\begin{aligned}
\theta_{e_{n+1}} &= \theta_{e_n} + \dot{\theta}_{e_n} \Delta t \\
\theta_{R_{n+1}} &= \theta_{R_n} + \dot{\theta}_{R_n} \Delta t \\
P_{e_{n+1}} &= P_{e_n} + \dot{P}_{e_n} \Delta t \\
P_{R_{n+1}} &= P_{R_n} + \dot{P}_{R_n} \Delta t \\
t_{n+1} &= t_n + \Delta t
\end{aligned} \tag{53}$$

5. Using the n+1 values, return to step 2 and repeat procedure for desired length of time.

Equation of Motion for System 2

In order to find an expression for the Lagrangian of the three-degree-of-freedom system, the linear and angular velocities of each mass and inertia must be determined. For the engine and rotor inertias I_e and I_R, the angular velocities are $\dot{\theta}_e$ and $\dot{\theta}_R$ respectively. The velocities of the coupling links are functions of $\dot{\theta}_e$ and $\dot{\theta}$ as well as θ_e and θ. Referring to Figures 22 and 23, the kinetic and potential energies are

$$\begin{aligned}
T &= \frac{1}{2} I_e \dot{\theta}_e^2 + \frac{1}{2} I_R \dot{\theta}_R^2 + \frac{1}{2} I'_{fR} (\dot{\theta}_e - \dot{\theta})^2 + \frac{1}{2} Nm_B v_B^2 + \frac{1}{2} Nm_\ell (v_{\ell_1}^2 + v_{\ell_2}^2) \\
&\quad + \frac{1}{2} NI_\ell (\omega_{\ell_1}^2 + \omega_{\ell_2}^2) \\
V &= \frac{1}{2} K_s (\theta_e - \theta - \theta_R)^2
\end{aligned} \tag{54}$$

where

v_{ℓ_1} = linear velocity of cg of link 1

ω_{ℓ_1} = angular velocity of link 1

v_{ℓ_2} = linear velocity of cg of link 2

ω_{ℓ_2} = angular velocity of link 2

(see Figure 23)

For the static analysis of the coupling, it was shown that m_ℓ and m_B can be combined, but when $\dot{\theta}$ is not constant the mass distribution of the links will have some effect on the system response. A significant effect would only be expected when the links are massive (low speed/high power) but will be left in the analysis for generality.

The expressions for the v's and ω's in the kinetic energy equation 53 are developed in Appendix III and are given below.

$$v_B^2 = \dot{R}^2 + R^2(\dot{\theta}_e - \dot{\theta}/2)^2$$

$$v_\ell^2 = v_{\ell_1}^2 + v_{\ell_2}^2 = \frac{1}{2}\{r^2(\dot{\theta}_e^2 - \dot{\theta}_e\dot{\theta} + \dot{\theta}^2/2) - r\,\dot{R}\,\dot{\theta}(\sin\theta/2)$$

$$+ \dot{R}^2 + 2rR(\dot{\theta}_e - \dot{\theta}/2)^2\cos\theta/2 + R^2(\dot{\theta}_e - \dot{\theta}/2)^2\} \qquad (55)$$

$$\omega_\ell^2 = \omega_{\ell_1}^2 + \omega_{\ell_2}^2 = \frac{2}{\ell^2}\{r^2(\theta_e^2 - \dot{\theta}_e\dot{\theta} + \dot{\theta}^2/2) + r\,\dot{R}\,\dot{\theta}(\sin\theta/2)$$

$$+ \dot{R}^2 - 2rR(\dot{\theta}_e - \dot{\theta}/2)^2\cos\theta/2 + R^2(\dot{\theta}_e - \dot{\theta}/2)^2\}$$

where $\dot{R}$ is the time derivative of R in equation 30

$$\dot{R} = -\frac{1}{2}\dot{\theta}\left[r(\sin\theta/2) + \frac{r^2\sin\theta}{2\sqrt{\ell^2 - r^2(\sin\theta/2)}}\right] \qquad (56)$$

The Lagrangian can now be written in terms of the generalized coordinates as

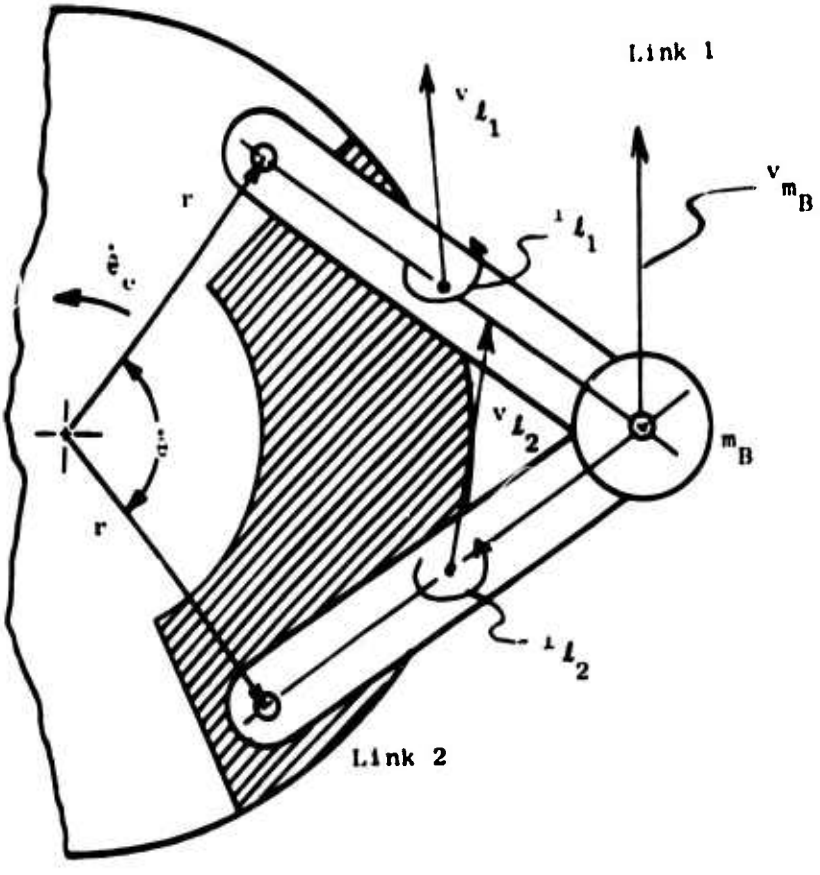

Figure 23. Coupling Velocities.

$$L = \frac{1}{2} I_R \dot{\theta}_R^2 + \frac{1}{2} I_e'' \dot{\theta}_e^2 + \frac{1}{2} I'_{fR}(\dot{\theta}_e - \dot{\theta})^2$$

$$+ \frac{1}{2} N M_1[\dot{R}^2 + R^2(\dot{\theta}_e - \dot{\theta}/2)^2]$$

$$- \frac{1}{2} N M_2[r \dot{R} \dot{\theta}(\sin \theta/2) - 2rR(\dot{\theta}_e - \dot{\theta}/2)^2 \cos \theta/2]$$

$$+ \frac{1}{2} N M_3[r^2(\dot{\theta}_e^2 - \dot{\theta}_e \dot{\theta} + \dot{\theta}^2/2)]$$

$$- K_s(\theta_e - \theta - \theta_R)^2 \qquad (57)$$

where

$$M_1 = m_B + m_\ell/2 + 2I_\ell/\ell^2$$

$$M_2 = m_\ell/2 - 2I_\ell/\ell^2$$

$$M_3 = m_\ell/2 + 2I_\ell/\ell^2$$

The potential forces, $\partial L/\partial q_i$, in Lagrange's equations are

$$\frac{\partial L}{\partial \theta} = \frac{1}{2} NM_1[2\dot{R} \frac{\partial \dot{R}}{\partial \theta} + 2R \frac{\partial R}{\partial \theta}(\dot{\theta}_e - \dot{\theta}/2)^2]$$

$$- \frac{1}{2} NM_2[r\dot{\theta} \frac{\partial \dot{R}}{\partial \theta}(\sin \theta/2) + \frac{1}{2} r \dot{R} \dot{\theta}(\cos \theta/2)$$

$$- 2r \frac{\partial R}{\partial \theta}(\dot{\theta}_e - \dot{\theta}/2)^2 \cos \theta/2$$

$$+ r R(\dot{\theta}_e - \dot{\theta}/2)^2 \sin \theta/2] + K_2(\theta_e - \theta - \theta_R) \text{ for } \theta$$

$$\frac{\partial L}{\partial \theta_e} = - K_s(\theta_e - \theta - \theta_R) \quad \text{for } \theta_e$$

$$\frac{\partial L}{\partial \theta_R} = K_s(\theta_e - \theta - \theta_R) \quad \text{for } \theta_R \qquad (58)$$

The momenta, P_i, in Lagrange's equations are

$$P_T = \frac{\partial L}{\partial \dot{\theta}} = - I_{fR}(\dot{\theta}_e - \dot{\theta})$$

$$+ \frac{1}{2} NM_1[2\dot{R} \frac{\partial \dot{R}}{\partial \dot{\theta}} - R^2(\dot{\theta}_e - \dot{\theta}/2)]$$

$$- \frac{1}{2} NM_2[r\dot{\theta} \frac{\partial \dot{R}}{\partial \dot{\theta}} (\sin \theta/2) + r \dot{R}(\sin \theta/2)$$

$$+ 2 r R(\dot{\theta}_e - \dot{\theta}/2) \cos \theta/2] + \frac{1}{2} NM_3 r^2(\dot{\theta} - \dot{\theta}_e) \quad \text{for } \theta$$

$$P_e = \frac{\partial L}{\partial \dot{\theta}_e} = I_e'' + I_{fR}(\dot{\theta}_e - \dot{\theta})$$

$$+ \frac{1}{2} NM_1[2R^2(\dot{\theta}_e - \dot{\theta}/2)]$$

$$+ \frac{1}{2} NM_2[4rR(\dot{\theta}_e - \dot{\theta}/2) \cos \theta/2]$$

$$+ \frac{1}{2} NM_3[2r^2(\dot{\theta}_e - \dot{\theta}/2)] \quad \text{for } \theta_e$$

$$P_R = \frac{\partial L}{\partial \dot{\theta}_R} = I_R \dot{\theta}_R \quad \text{for } \theta_R \tag{59}$$

The expressions for the partial derivatives of R and $\dot{R}$ used in equations 58 in terms of the generalized coordinate θ are

$$\frac{\partial R}{\partial \theta} = -\frac{1}{2}\left[r (\sin \theta/2) + \frac{r^2 \sin \theta}{2\sqrt{l^2 - r^2(\sin^2 \theta/2)}}\right]$$

$$\frac{\partial \dot{R}}{\partial \dot{\theta}} = -\frac{1}{4} \dot{\theta} \left[r(\cos \theta/2) + \frac{r^2 \cos \theta}{\sqrt{l^2 - r^2(\sin^2 \theta/2)}}\right.$$

$$\left. + \frac{r^4 \sin^2 \theta}{4[l^2 - r^2(\sin^2 \theta/2)]^{3/2}}\right]$$

$$\frac{\partial \dot{R}}{\partial \dot{\theta}} = \frac{\partial R}{\partial \theta}$$

The time derivatives of the momenta, $\dot{P}_i$'s, need not be taken.

$$\left.\begin{aligned} \dot{P}_T &= \frac{d}{dt}\left(\frac{\partial L}{\partial \dot{\theta}}\right) \quad \text{for } \theta \qquad \dot{P}_e = \frac{d}{dt}\left(\frac{\partial L}{\partial \dot{\theta}_e}\right) \quad \text{for } \theta_e \\ \dot{P}_R &= \frac{d}{dt}\left(\frac{\partial L}{\partial \dot{\theta}_R}\right) \quad \text{for } \theta_R \end{aligned}\right\} \tag{60}$$

The generalized forces F_i determined from the principle of virtual work are

$$\delta W_e = F_e \delta\theta_e$$

$$F_e = T_e(t) - C_s(\dot{\theta}_e - \dot{\theta} - \dot{\theta}_R) - C_e\dot{\theta}_e|\dot{\theta}_e| \qquad \text{for } \theta_e$$

where $T_e(t)$ is any time function of the input torque.

$$\delta W_R = F_R \delta\theta_R$$

$$F_R = C_s(\dot{\theta}_e - \dot{\theta} - \dot{\theta}_R) - C_L(\cdot)\dot{\theta}_R|\dot{\theta}_R| \qquad \text{for } \theta_R$$

where $C_L(t)$ is any time function of the rotor lift coefficient.

$$\delta W_T = F_T \delta\theta$$

$$F_T = C_s(\dot{\theta}_e - \dot{\theta} - \dot{\theta}_R) - C_D\dot{\theta} - K_{fK}(\theta) \qquad \text{for } \theta \tag{61}$$

where C_D is viscous hinge friction in the coupling and $K_{fK}(\theta)$ represents any additional springs that might be added to the coupling. C_s and C_e are the shaft and engine damping coefficients respectively.

Using equations 58, 60, and 61, 'Lagrange's equations' can be written in canonical form:

$$\dot{P}_e = \frac{\partial L}{\partial \theta_e} + F_e$$

$$\dot{P}_T = \frac{\partial L}{\partial \theta} + F_T \tag{62}$$

$$\dot{P}_R = \frac{\partial L}{\partial \theta_R} + F_R$$

From equations 50 and 58,

$$\begin{Bmatrix} P_T \\ P_e \end{Bmatrix} = [A] \cdot \begin{bmatrix} \dot{\alpha} \\ \dot{\theta}_e \end{bmatrix} \tag{63}$$

$$P_R = I_R\dot{\theta}_R$$

where the elements of the A matrix are

$$a_{11} = \frac{1}{2} N \left[M_1 \left(2\bar{\dot{R}} \frac{\partial \dot{R}}{\partial \dot{\theta}} + \frac{1}{2} R^2 \right) \right.$$

$$\left. + M_2 \left(-r \frac{\partial \dot{R}}{\partial \dot{\theta}} (\sin \theta/2) - r\bar{\dot{R}}(\sin \theta/2) + rR(\cos \theta/2) + M_3 r^2 \right\} + I'_{fR} \right.$$

$$a_{12} = -\frac{1}{2} N(M_1 R^2 + 2M_2 rR(\cos \theta/2) + M_3 r^2) - I'_{fR}$$

$$a_{21} = a_{12}$$

$$a_{22} = I''_e - I'_{fR} - 2a_{12}$$

and

$$\bar{\dot{R}} = \dot{R}/\dot{\theta} = \frac{\partial R}{\partial \theta}$$

Upon inversion of equations 63, the following expressions for the three generalized velocities result:

$$\dot{\theta} = (a_{22} P_R - a_{12} P_e)/(a_{11} a_{22} - a_{21} a_{12})$$

$$\dot{\theta}_e = (a_{11} P_R - a_{21} P_e)/(a_{11} a_{22} - a_{21} a_{12})$$

$$\dot{\theta}_R = P_R / I_R \qquad (64)$$

Equations 62 and 64 form a set of six first-order differential equations in coordinates:

P_e	θ_e
P_T	θ
P_R	θ_R

These equations can be numerically solved by

1. Specifying initial conditions for P_{T_0}, P_{e_0}, P_{R_0}, θ_{e_0}, θ_0 and θ_{R_0} (initial conditions for $\dot{\theta}_{e_0}$, $\dot{\theta}_0$, and $\dot{\theta}_{R_0}$ can be used with equations 63 to produce P_{e_0}, P_{T_0}, and P_{R_0})

2. Finding values for $\dot{\theta}_e$, $\dot{\theta}$ and $\dot{\theta}_R$ from equations 64

3. Finding values for $\dot{P}_e$, $\dot{P}_T$ and $\dot{P}_R$ from equations 62

4. Numerically integrating $\dot{P}_e$, $\dot{P}_T$, $\dot{P}_R$, $\dot{\theta}_e$, $\dot{\theta}$, $\dot{\theta}_R$

Using Euler integration,

$$\theta_{e_{n+1}} = \theta_{e_n} + \dot{\theta}_{e_n} \Delta t$$

$$\theta_{n+1} = \theta_n + \dot{\theta}_n \Delta t$$

$$\theta_{R_{n+1}} = \theta_{R_n} + \dot{\theta}_{R_n} \Delta t$$

$$P_{e_{n+1}} = P_{e_n} + \dot{P}_{e_n} \Delta t$$

$$P_{T_{n+1}} = P_{T_n} + \dot{P}_{T_n} \Delta t$$

$$P_{R_{n+1}} = P_{R_n} + \dot{P}_{R_n} \Delta t$$

$$t_{n+1} = t_n + \Delta t$$

5. Using the n+1 values from step 4, return to step 2 and repeat procedure for desired length of time.

THE SYNTHESIZED COUPLING DESIGNS

Description of Pinned Link Coupling

Three views of the synthesized zero torsional stiffness (ZTS) pinned link coupling for helicopter application are shown in Figures 24, 25, and 26. The various components of the coupling are

A driving flange	F connecting tubes
B driven flange	G deformable stops
C link	H link pin and fastener
D connecting pin	I torsion bar (not shown)
E alignment shaft	

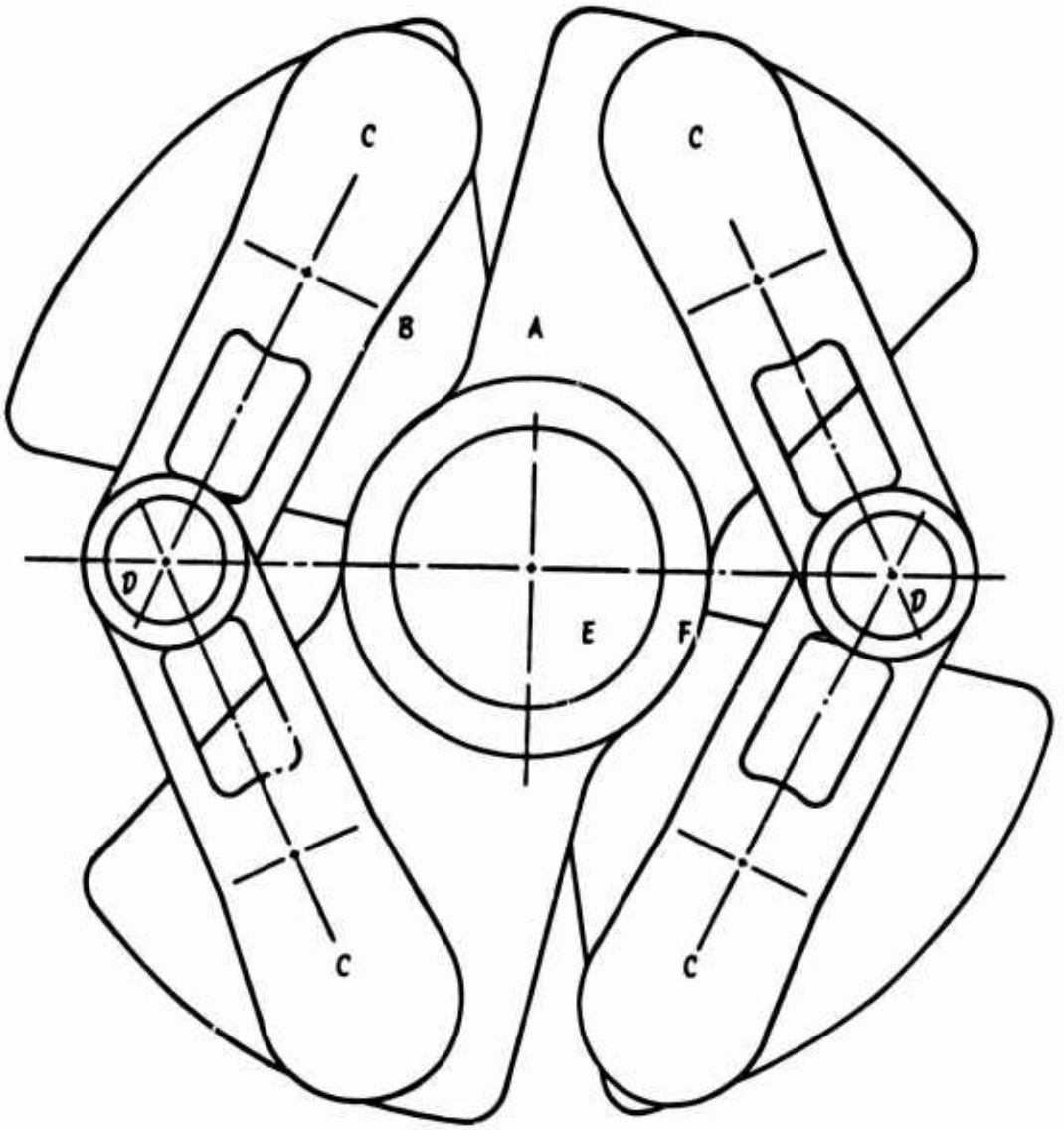

Figure 24. ZTS Coupling (Front).

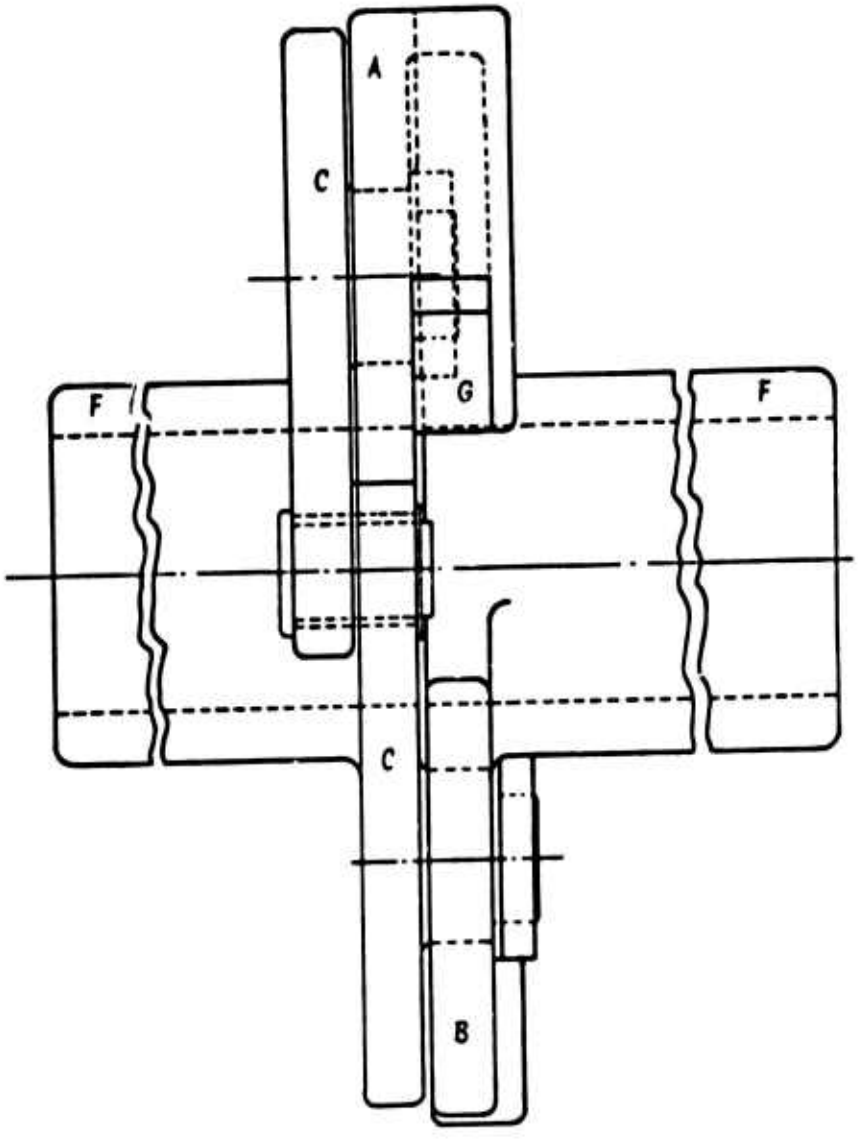

Figure 25. ZTS Coupling (Side).

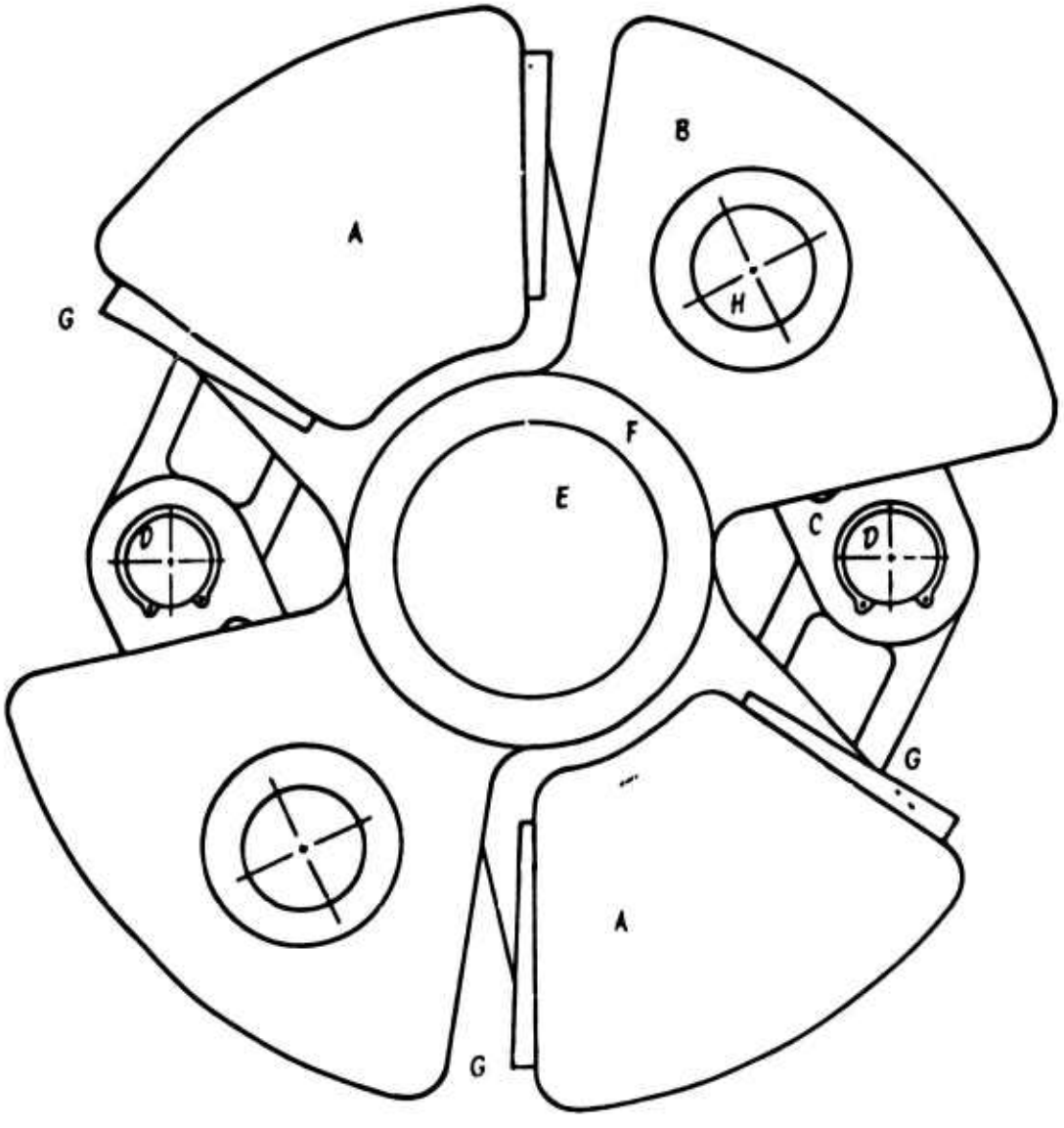

Figure 26. ZTS Coupling (Back).

The connecting tubes are part of the flanges and are designed to fit inside the drive shaft of the helicopter. A free running alignment shaft may be used to prevent lateral motion of the flanges. A soft torsion bar can be inserted through the center of the alignment shaft which will close the coupling when the system is at rest. This will prevent banging of the coupling against the stops during initial start-up. The ends of the torsion bar can be attached at any point inside the drive shaft.

Figure 27 shows the type of link used in the ZTS coupling. The dimensions of the link are

ℓ = 2.61 in. t = .5 in.

r_p = .375 in. H = 1.375 in.

r_1 = .625 in. h = .625 in.

r_2 = .6875 in. r_c = 1.3 in.

The areas shown in Figure 27 are

$A_1 = 2(H-h)t = .375 \text{ in.}^2$

A_2 = projected bearing surface = $2tr_2$

$= .6875 \text{ in.}^2$

$A_3 = 2(r_2-r_1)t = .25 \text{ in.}^2$ $A_4 = \pi r_p^2 = .4418 \text{ in.}^2$

The bending moment caused by the links being in different planes can be eliminated by replacing each link connected to flange B with two similar links of thickness t/2. The new links go on either side of the link connected to flange A.

Determining Counterweight m_c

The link, before counterweighting, is divided into three sections. Section 1 is all mass symmetrically distributed about point B, which for each link is $m_B/2$. Assuming that the pin, bearing, and link all have the density of steel ($\rho = .28 \text{ lb}_m/\text{in.}^3$) gives

$$m_1 = \frac{m_B}{2} = \rho \pi r_2^2 t = 0.208 \text{ lb}_m$$

Section 2 is the portion of the link which has the cross section shown in Figure 27c. The center of mass for this section is located at $\ell/2$; thus it can be treated simply as m_ℓ.

$$m_2 = m_\ell = \rho(H-h)(\ell-2r_2)(t) = 0.130 \text{ lb}_m$$

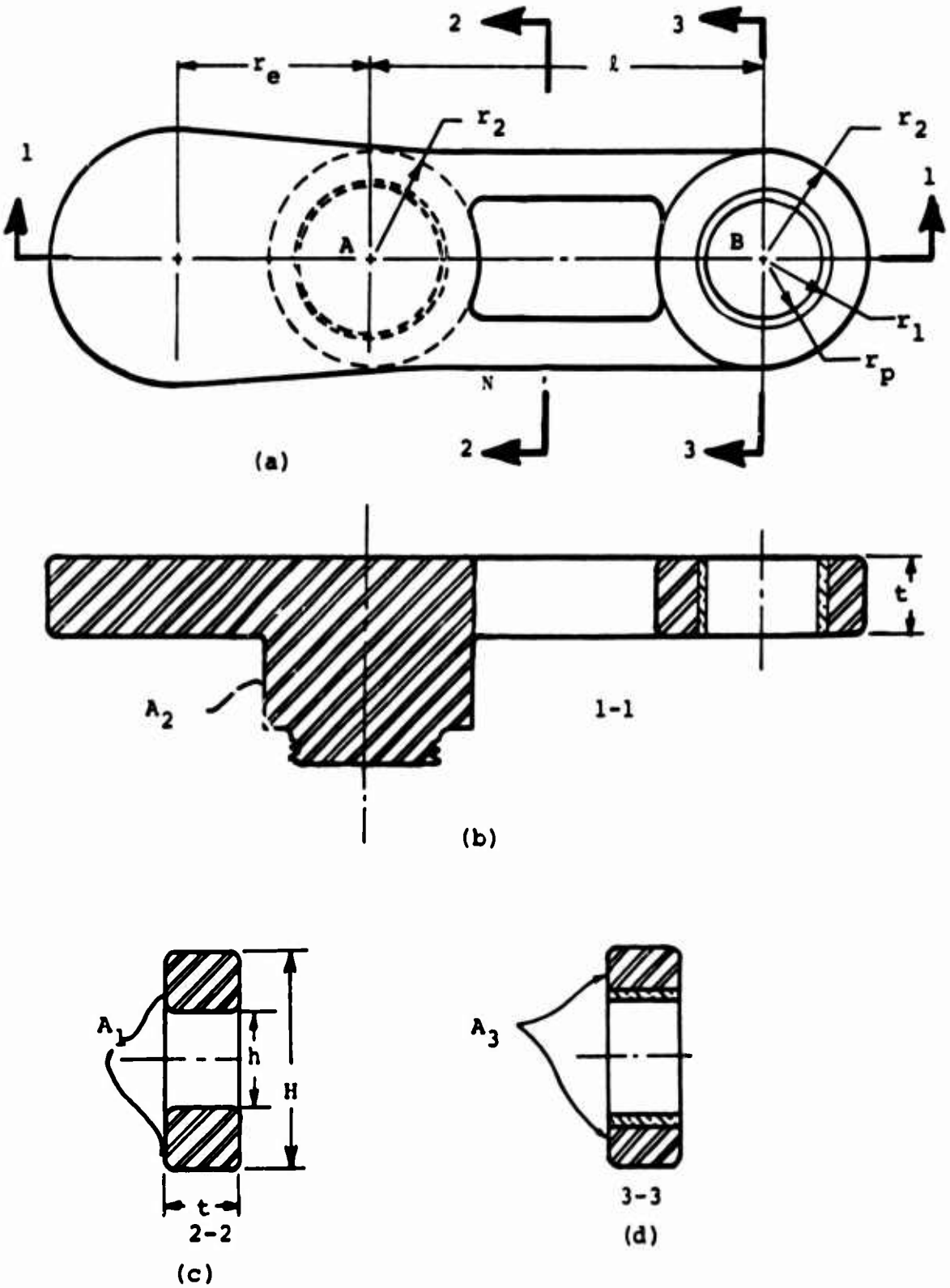

Figure 27. Coupling Link.

Section 3 is all mass symmetrically distributed about point A.

$$m_3 \approx \rho \pi r_2^2 (2t) = .416 \text{ lb}_m$$

This mass does not affect the torque characteristics of the coupling and can be neglected when determining m_α. From design equation (38),

$$m_e = m_\ell + m_B - m$$

The value of m has previously been determined on page 35 to be .2385 lb_m. The value for m_e from equation 38 is therefore

$$m_e = .307 \text{ lb}_m$$

Design equation IV (39) with $r_c = \ell/2$ gives

$$m_\alpha = .307 \text{ lb}_m$$

Stress Analysis

The coupling geometry used for the stress analysis is shown in Figure 28a where

$$R = r(\cos \theta/2) + \sqrt{\ell^2 - r^2(\sin^2\theta/2)}$$

$$\bar{h} = r(\sin \theta/2)$$

$$\alpha = \sin^{-1} h/\ell$$

Figure 28b shows the forces acting on each link and pin.

Mass m_α was determined so that m_e would not contribute to the torque characteristics of the coupling. This was done by making $(m_e/2) + m_\alpha$ for each link have a resulting center of gravity at point A. Figure 17 shows that the link mass, m_ℓ, can be equally distributed to points A and B. The force acting at point A caused by m_ℓ, m_e, and m_α is

$$F_1 = (m_\alpha + \frac{m_e}{2} + \frac{m_\ell}{2}) r\omega^2$$

The force at point A caused by all mass located in section 3 is

$$F_2 = m_3 r\omega^2$$

where

$$m_3 \approx 2\rho \pi r_2^2 t$$

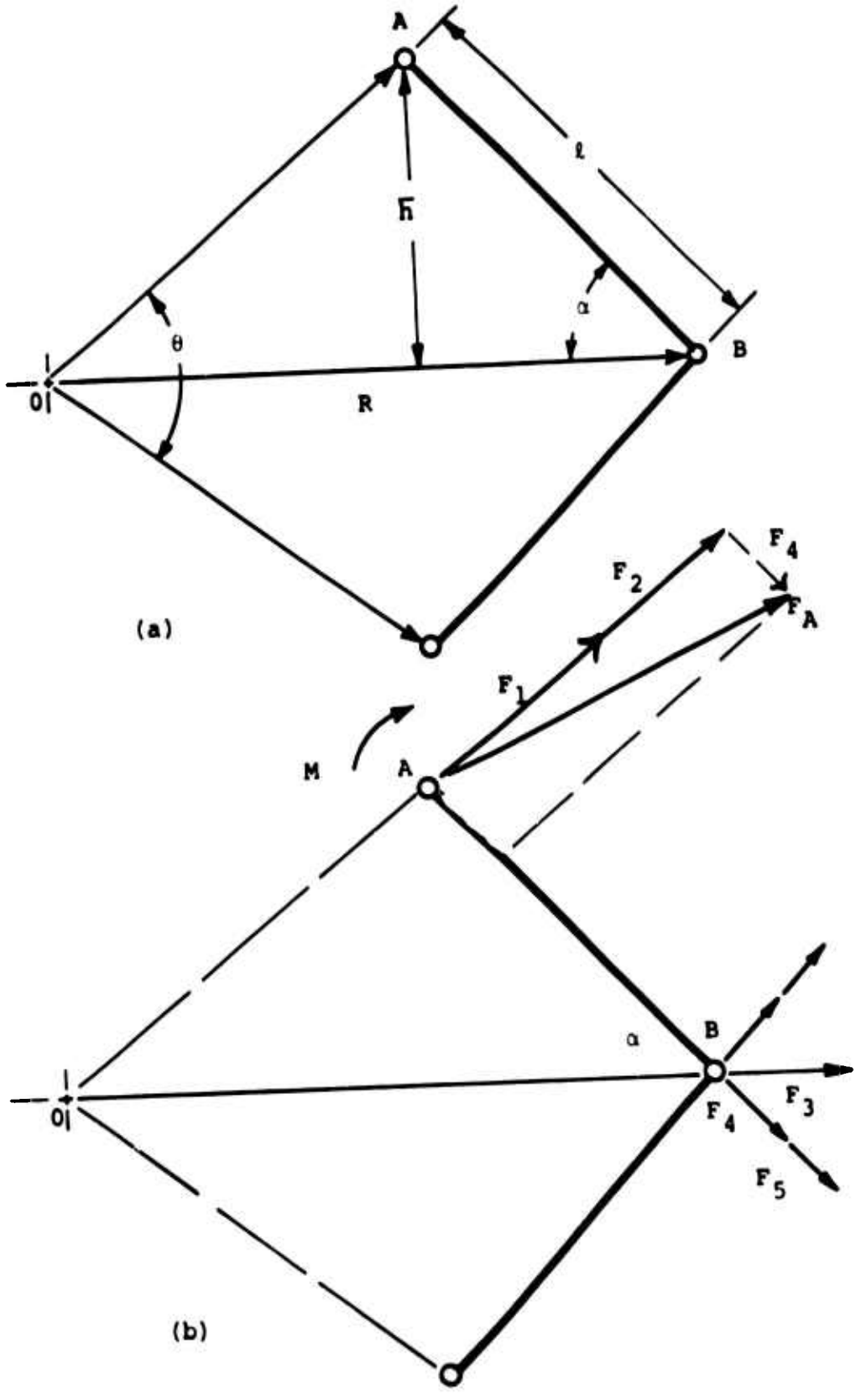

Figure 28. Link and Pin Forces.

The noncounterbalanced mass m produces a force at point B with magnitude

$$F_3 = mR\omega^2$$

which causes each link to have a tension force

$$F_4 = \frac{1}{2} m R(\omega^2 \cos \alpha)$$

The total force F_A acting on the bearing at point A is the vector sum of F_1, F_2, and F_4:

$$F_A = \{[(F_1+F_2)(\cos \theta/2)+F_4 \cos \alpha]^2 + [(F_1+F_2)(\sin \theta/2) - F_4 \sin \alpha]^2\}^{1/2}$$

The shear force on the pin at B caused by the force acting between the links is

$$F_B = F_4 \sin \alpha$$

(due to symmetry, only normal force between the links exists).

Equation 39 shows that the moment caused by m_a on one side of Point A is equal to the moment caused by $m_c/2$ on the other side of A. The value for the moment where the open section of the link begins (point N) is

$$M = \left(\frac{\ell - r_2}{\ell} \bar{h}\right) \cdot \left(\frac{m_c}{2} R\omega^2\right)$$

projected moment arm — force

The mass $m_B + m_\ell$ causes a tension force F_5 in each link where

$$F_5 = \frac{1}{2} (m_B + m_\ell) R(\omega^2 \cos \alpha)$$

The normal stress in the link at point N is

$$\sigma_N = \frac{Mc}{I} + \frac{F_5}{A_1}$$

The stress on the bearing at pin A is

$$\sigma_A = \frac{F_A}{A_2}$$

The normal stress in the link at the section shown in Figure 27d is

$$\sigma_B \approx \frac{F_4}{A_3}$$

and the shear stress acting on the pin at B is

$$\tau_B = \frac{F_B}{A_4}$$

The value of each stress and force is a function of θ. The maximum values are computed by the stress program in Appendix IV and are given below.

Maximum Stress

$\sigma_N \approx 60{,}000$ psi	$F_A \approx 17{,}200$ lb
$\sigma_A \approx 25{,}000$ psi	$F_B \approx 5{,}700$ lb
$\sigma_B \approx 23{,}000$ psi	$F_4 \approx 5{,}800$ lb
$\tau_B \approx 13{,}000$ psi	$F_5 \approx 13{,}200$ lb

$M \approx 4{,}800$ in.-lb

The stress distribution about pin A is very complex and depends on the rigidity of the bearing, flange, and link as well as the moment caused by m_σ and the normal stress caused by m. The pin has been made large to help account for these effects and to increase rigidity. An experimental analysis is required in order to determine the exact mode of failure. This region is not critical in the design other than for stress, since the mass in the region contributes nothing to the torque characteristics of the coupling.

The steel links and pins should be as strong or rigid as possible to avoid link deflection and prevent damage due to extreme overloading if system failure occurs. AISI 2330 steel drawn at 400°F has a yield strength of 195 ksi and a Brinell hardness of 425. The bearing surfaces are subjected to high stress and are difficult to lubricate. Self-lubricating bearings made with woven Teflon have been designed to withstand loads to 80 ksi.[8]

Design of Deformable Stops

Stops have been included in the coupling design to limit θ between 1 and 2 radians. The stops can come in contact during

1. Start-up
2. Shutdown
3. High speed/low torque conditions
4. Low speed/high torque conditions
5. Low frequency/high magnitude excitation

An elastomeric material is used for the stops to reduce impact. The total contact area of each set of stops is 2 $in.^2$. The spring constant of the stops is designed so that the operating torque (2004 ft-lb) at zero speed can be transmitted with a .03 radian coupling rotation from initial stop contact.

The center of the contact region is 3.25 in. from the center of the coupling; thus the force on the stop is

$$F = (2004 \text{ ft-lb})(12 \text{ in./ft})/3.25 \text{ in.} = 7,400 \text{ lb}$$

The linear spring constant is

$$K_L = (7,400 \text{ lb}) \ (.03 \text{ rad} \cdot 3.25 \text{ in. rad})$$

$$= 75,900 \text{ lb/in.}$$

The torsional spring constant is

$$K_T = (2004 \text{ ft-lb})/(.03 \text{ rad}) = 66,800 \text{ ft-lb/rad}$$

An expression for the approximate value for the deflection of the elastomeric material is

$$\delta = \frac{PL}{AE}$$

where

$$K_L = \frac{P}{\delta} = \frac{AE}{L}$$

Letting L (the initial length of the material) be equal to .75 in. gives

$$E = \frac{(75,900 \text{ lb/in.})(.75 \text{ in.})}{2 \text{ in.}^2} = 28,500 \text{ psi}$$

Low density polyethylene has an elastic modulus range of 14,000-38,000 psi.[9]

Description of Elastic Link Coupling

Two views of the synthesized zero torsional stiffness elastic link coupling for helicopter application are shown in Figures 29 and 30. The only two major differences from the pinned link coupling are:

1. Substitution of semicircular elastic links for the straight pinned links.

2. Reduction of the angle of twist (from stop to stop) to 10 degrees.

As shown in the section on design analysis, the determination of elastic link dimensions is an indirect and time-consuming process. Link dimensions are given on page 25 for the example taken from Swick and Skarvan.

The different angles of twist between stops for the pinned link design and for the elastic link design represent two different philosophies of design, rather than special requirements of each type of coupling, although the small twist angle in the elastic link coupling eliminates the necessity to avoid negative stiffness at large angles of twist. The small twist angle also eliminates the possibility of a bending failure load in the elastic link.

With its small (10°) angle of twist between stops, the elastic link coupling acts as if it were solid (no compliance) during acceleration or deceleration and exhibits zero stiffness only at the steady-state design conditions. Thus the elastic link coupling, as designed here, is best suited to providing zero stiffness to improve closed-loop stability, without the capability to absorb large excitations or dissipate vibration energy through damping.

The two designs presented here (pinned link and elastic link) can be regarded as representing the two extremes of design philosophy which contain the zero stiffness concept. The questions of whether pinned links or elastic links are superior, or how much angle of twist between stops is optimum, must finally be answered by testing for a specific application.

Provision for Damping

The large angle of twist between stops incorporated in the pinned link design, along with the available space represented by the alignment shaft, provides an excellent opportunity to introduce significant amounts of shaft damping into the helicopter system.

Figure 31 shows a design concept developed at the University of Florida to accomplish this. The alignment shaft consists of a hollow steel sleeve containing an annulus of elastomeric material. A steel rod is a sliding fit into the elastomeric material. The rod is fixed to one flange of the coupling and the steel sleeve is attached to the other flange. The only bonds between steel and elastomer are at areas "A" and "B." The system

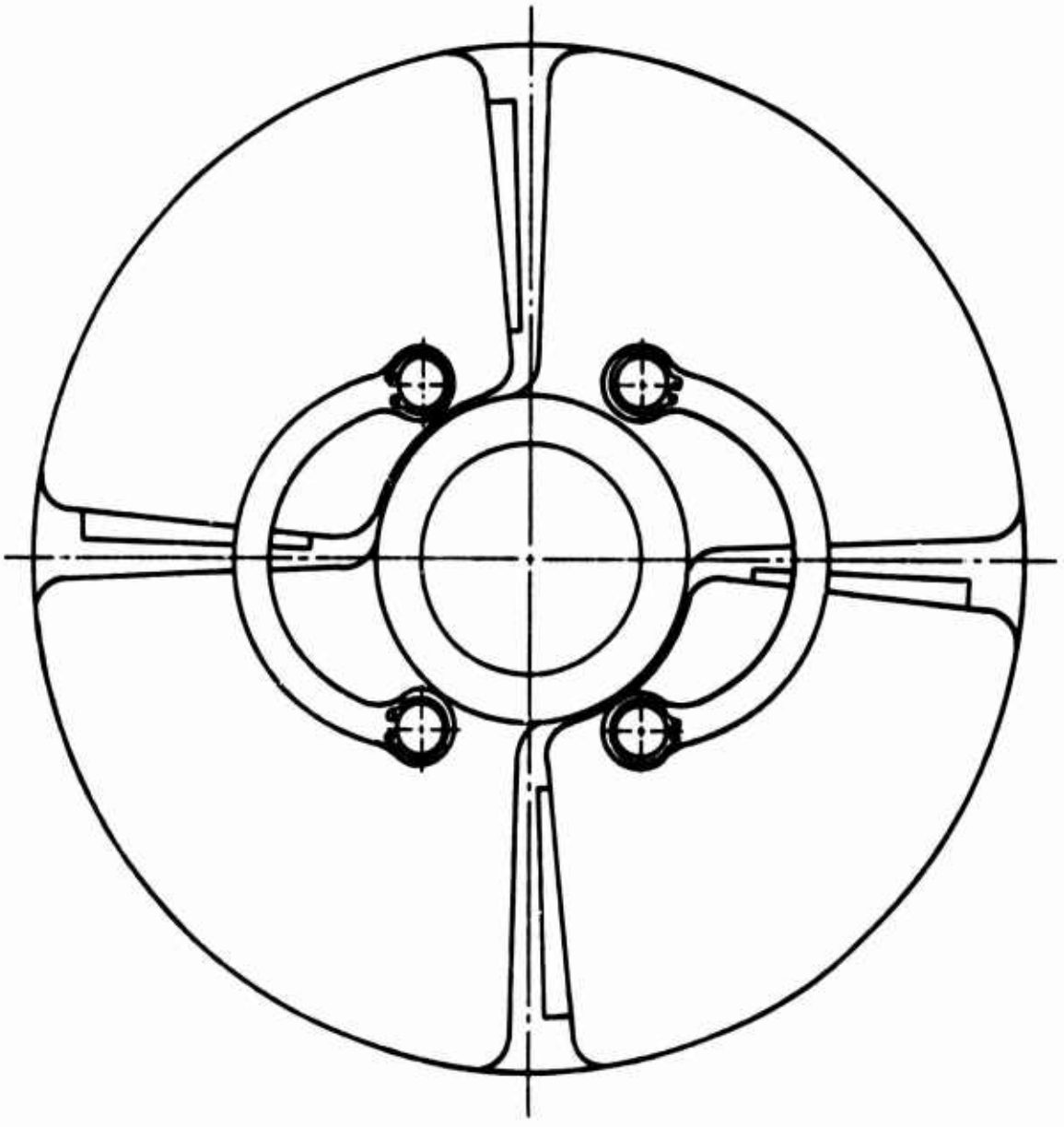

Figure 29. Elastic Link Coupling, Front View.

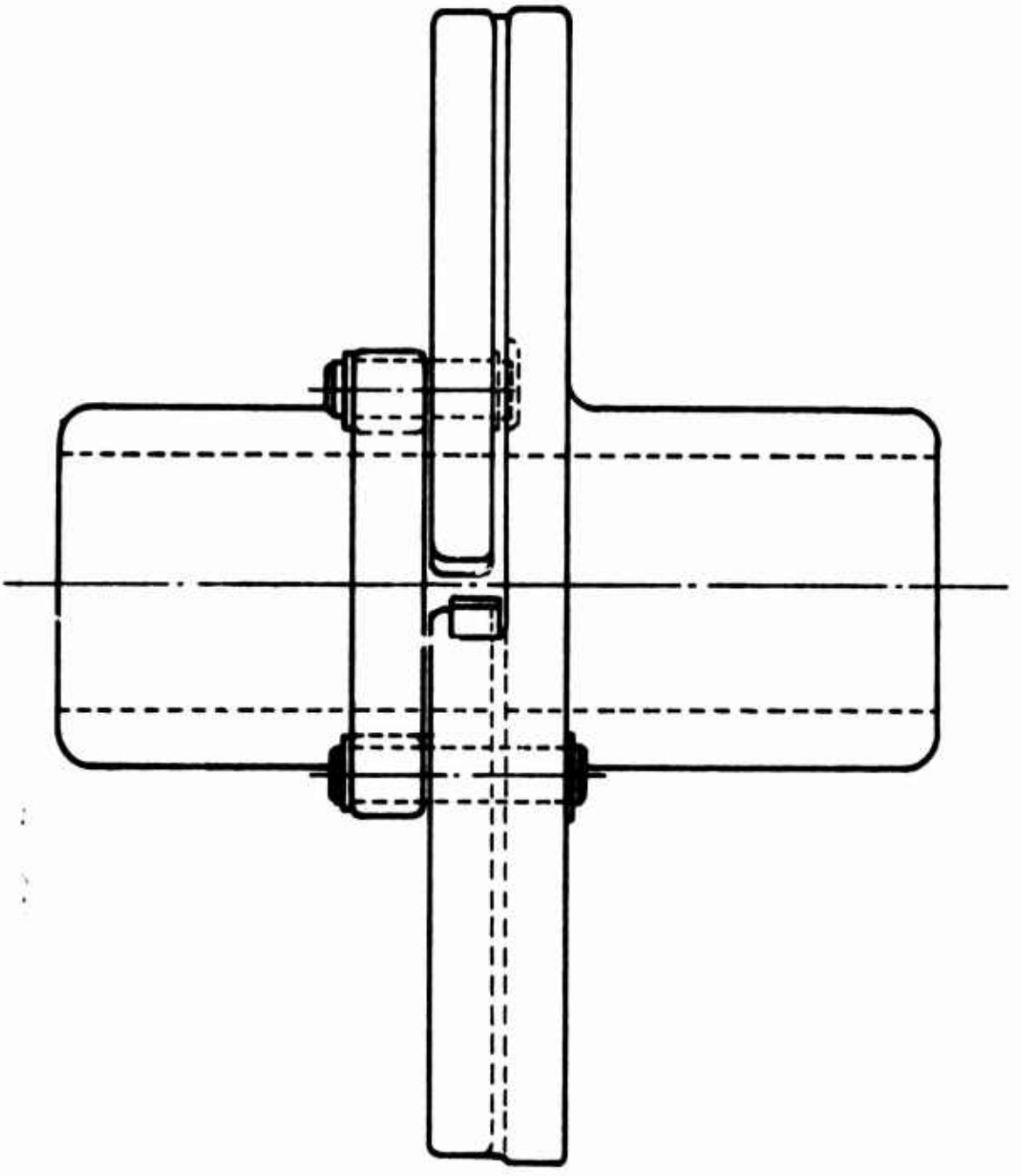

Figure 30. Elastic Link Coupling, Side View.

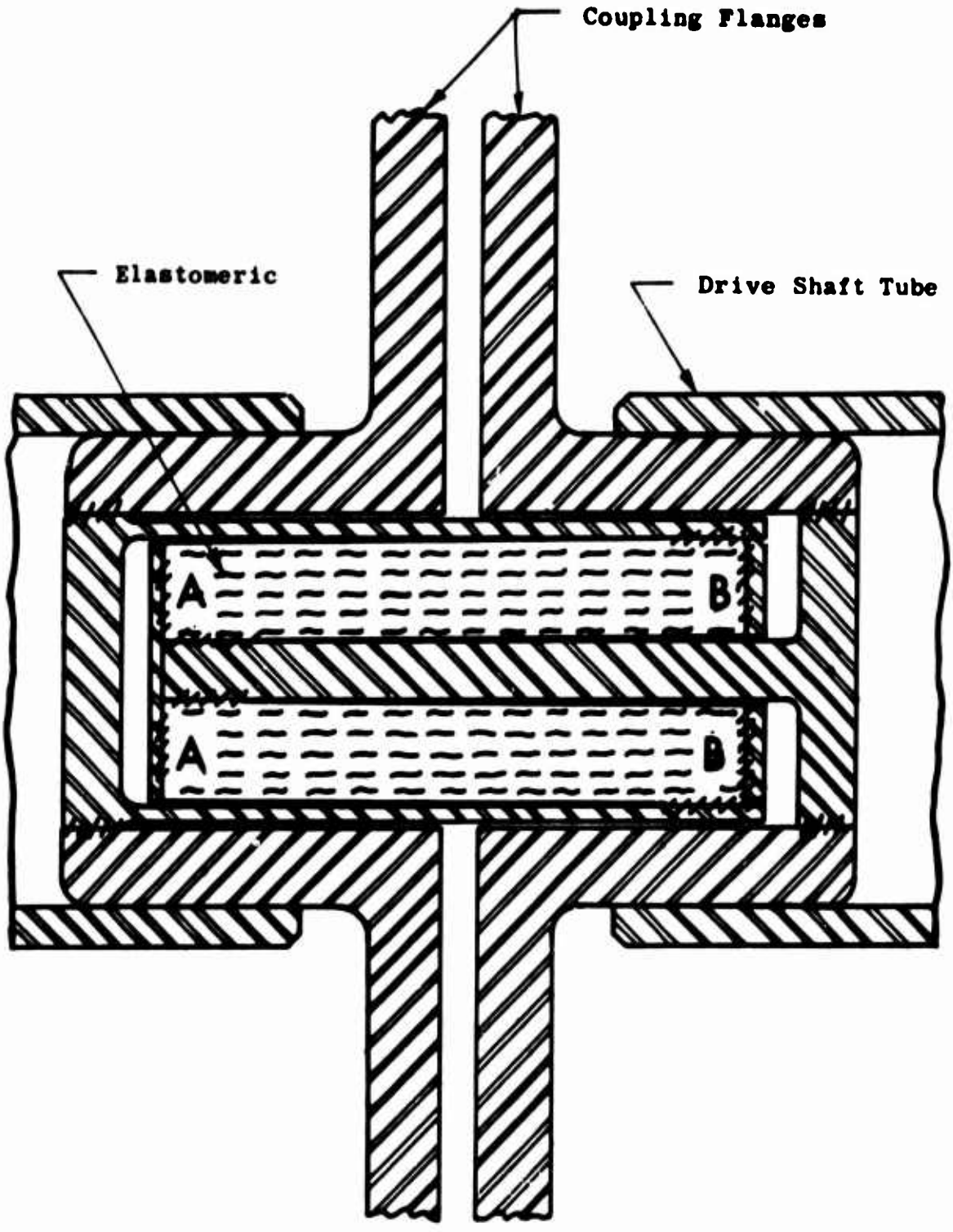

Figure 31. View of Proposed ZTS Coupling Dampener Configuration.

is pretwisted on assembly to provide an elastic closing torque which keeps the coupling against its stops until centrifugal force from rotation pulls it open. Thus, "banging" or impact of stops during start-up is eliminated. Figure 32 shows a section view.

It can be seen that torsional oscillation of the coupling produces the following effects, all of which dissipate energy:

1. Twisting (sliding) of the steel rod with respect to the elastomeric annulus.

2. Twisting (deformation) of the elastomeric material.

3. Twisting (sliding) of the elastomeric annulus with respect to the hollow steel sleeve.

It is shown in Part II that shaft damping is an extremely sensitive and influential parameter in improving closed-loop torsional stability.

RESULTS OF SYSTEM SIMULATION WITH A SYNTHESIZED DESIGN--OPEN-LOOP VIBRATION ISOLATION

The results of the computer simulations described previously are presented in this section. Appendix IV contains the computer programs and numerical data used for the simulation of the drive train. All of the simulations reported in Part I were done with the pinned link coupling without damping in the system taken from Swick and Skarvan.

Modes of Excitation

System 1 (Figure 21) and System 2 (Figure 22) are subjected to the following external excitations:

Test 1--Variation of C_L

This test models the cyclic change of the aerodynamic rotor drag caused by the rotor blades entering and leaving the direction of flight as well as cyclic variations caused by pilot excitation of collective pitch. The lift coefficient of the rotor, C_L, is sinusoidally varied ±10 percent about its average value.

$$C_L(t) = C_L(1 + 0.1 \sin \omega t)$$

$$\omega = 2.5 \rightarrow 10 \text{ Hz}$$

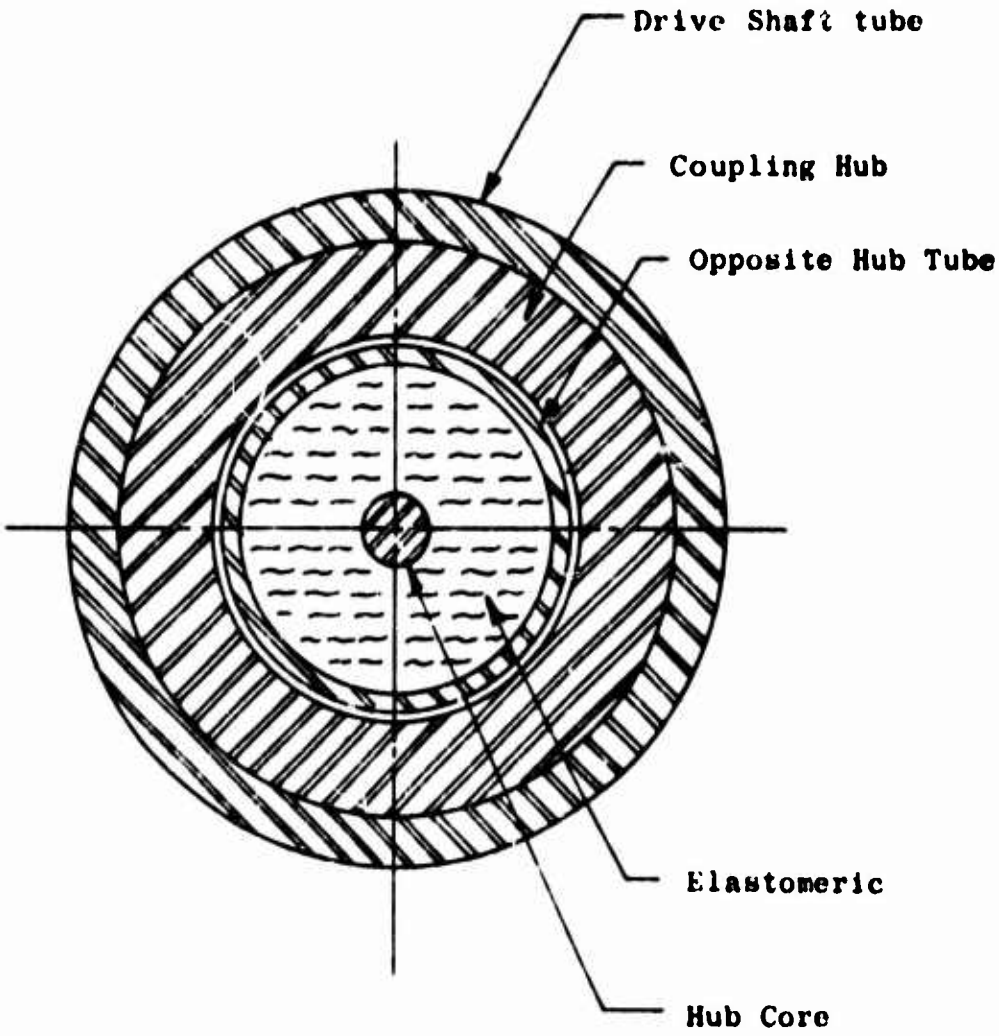

Figure 32. Section View of Proposed ZTS Coupling Dampener Configuration.

Test 2--Variation of T_e

Pilot adjustment of engine speed as well as possible feedback instability is represented by sinusoidally varying the engine torque ±10 percent about normal operating input torque, T_e (2804 ft-lb).

$$T_e(t) = T_e(1+0.1 \sin \omega t)$$

$$\omega = 2.5 - 10\text{Hz}$$

Test 3--$T_e(t)$

System start-up is modeled by increasing engine torque parabolically from 0 to 2800 ft-lb in 3 seconds. System shutdown is modeled by cutting the engine torque to zero when system is operating at steady state.

$$T_e(t) = \frac{1}{3}\, t\, T_e(2-t\ 3) \qquad 0 < t < 3 \text{ sec}$$

$$T_e(t) = T_e \qquad 3 \leq t < 20 \text{ sec}$$

$$T_e(t) = 0 \qquad t \geq 20 \text{ sec}$$

Measuring System Response

A helicopter control system compares the engine speed with a desired speed and alters the various engine torque producing parameters accordingly. If external excitations cause large variations of the engine speed, controlling system stability may prove to be difficult. A beneficial effect of the ZTS coupling is to effectively isolate the engine inertia from the rest of the system, resulting in a reduction of the engine speed variation due to external excitation. The first measure of system response is $\Delta\dot{\theta}_e$, the engine speed variation about the normal operating speed (1447 rad/sec). The second measure of system response is ΔT_s, the variation of the torque transmitted by the mast shaft about the normal operating torque (2004 ft-lb). The quantity ΔT_s indicates the torque overload experienced by the mast shaft, gearbox, engine turbine, and rotor.

The speed variation, $\Delta\dot{\theta}_e$, has units of rad/sec and the torque overload, ΔT_s, is in percentage of operating torque.

System Response

The results of Test 1 given in Figure 33a show the engine speed variation, $\Delta\dot{\theta}_e$, and mast torque variation, ΔT_s, as a function of the exciting frequency ω. Above 5 Hz, $\Delta\dot{\theta}_e$ and ΔT_s are virtually unaffected by the exciting force. At slightly above 3 Hz, System 1 experiences a critical frequency.

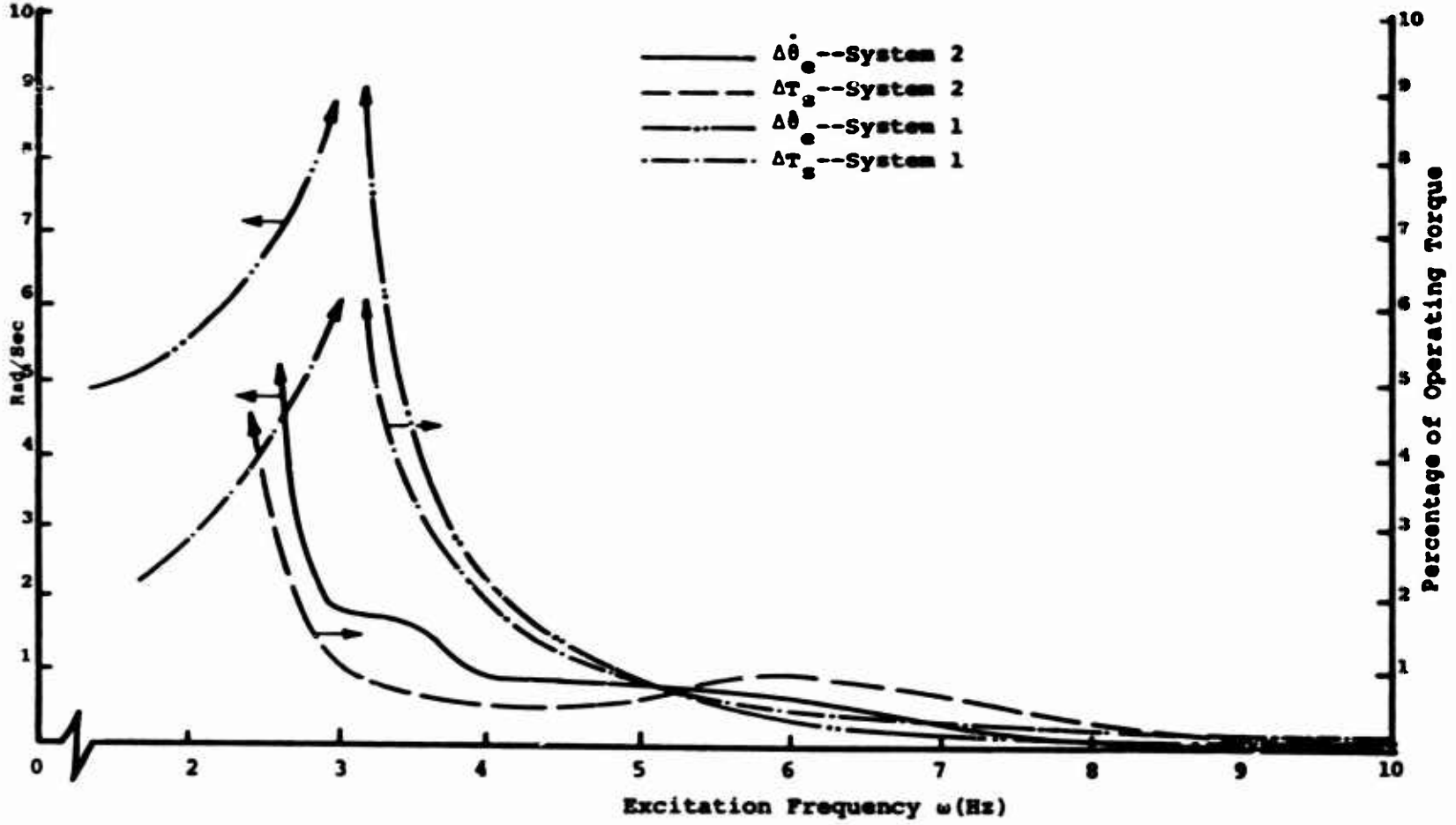

Figure 33a. Variation of C_L (K_s = 212.1).

System 2 has a critical region below 2.5 Hz where the coupling hits against the stops during each cycle of excitation.

Due to the nonlinearity of the coupling in System 2, the values of $\Delta\dot{\theta}_e$ and ΔT_s depend not only on the exciting frequency but on the state (position and velocity) the system is in when excitation occurs. If either System 1 or 2 is excited at very low frequencies $\omega < .5$ Hz, then the values of $\dot{\theta}_e$ and $\dot{\theta}_R$ will be nearly the same. For this type of excitation the coupling in System 2 may close against the stops, causing the system to assume the stiffness of the mast shaft, K_s.

Figure 33b shows the results from Test 2. The engine inertia is directly excited in this test, causing severe oscillations of engine speed and mast shaft torque when excitation occurs at or near the critical frequency.

A time response curve of $\dot{\theta}_e$ and $\dot{\theta}_R$ during start-up and shutdown is shown in Figure 34. $\dot{\theta}_e$ and $\dot{\theta}_R$ of System 1 and System 2 closely follow curve 1 for the first 20 seconds (start-up and steady state). During initial start-up, $\dot{\theta}_e$ leads $\dot{\theta}_R$ while the mast shaft "winds up" and then small oscillations of $\dot{\theta}_e$ and $\dot{\theta}_R$ about curve 1 slowly dampen out. After 20 seconds, when T_e is set to zero, $\dot{\theta}_e$ and $\dot{\theta}_R$ of System 1 closely follow curve 2. Small oscillations again occur as the mast shaft unwinds. $\dot{\theta}_R$ in System 2 closely follows curve 2 but $\dot{\theta}_e$ experiences severe oscillations for the first 1/2 second when the system is shut down. This is due to the coupling mass traveling radially outward, causing the coupling to quickly close against the reverse stops.

Other Systems

Swick and Skarvan[5] point out that the difference in the natural frequencies of helicopter drive trains depends primarily on mast shaft stiffness. A common range for the natural frequencies is 2-6 Hz. The basic helicopter design presented thus far has a critical frequency slightly above 3 Hz. Increasing the mast shaft stiffness of the helicopter design by a factor of four gives the system a natural frequency of approximately 6 Hz. Figure 35 shows the response of Systems 1 and 2 with increased mast shaft stiffness to the excitation of Test 1. At the critical frequency of System 1 (6 Hz) the torque variation is over 22 percent while the speed variation is over 11 rad/sec. With the use of a ZTS coupling (System 2), the critical frequency of the system is shifted below 4 Hz.

The time response of $\dot{\theta}_e$, $\dot{\theta}_R$ and mast shaft torque to a 6 Hz excitation of the systems in Figure 35 is shown in Figure 36. The zero reference speed in Figure 36 is 1447 rad/sec and the zero reference torque is 2004 ft-lb.

The rotor speed varies ±2.2 rad/sec for System 1 and ±1.3 rad/sec for System 2. The engine varies ±12 rad/sec for System 1 while the engine variation for System 2 is less than ±.5 rad/sec. Variation of the mast shaft torque is ±23 percent for System 1 and less than 1 percent for System 2.

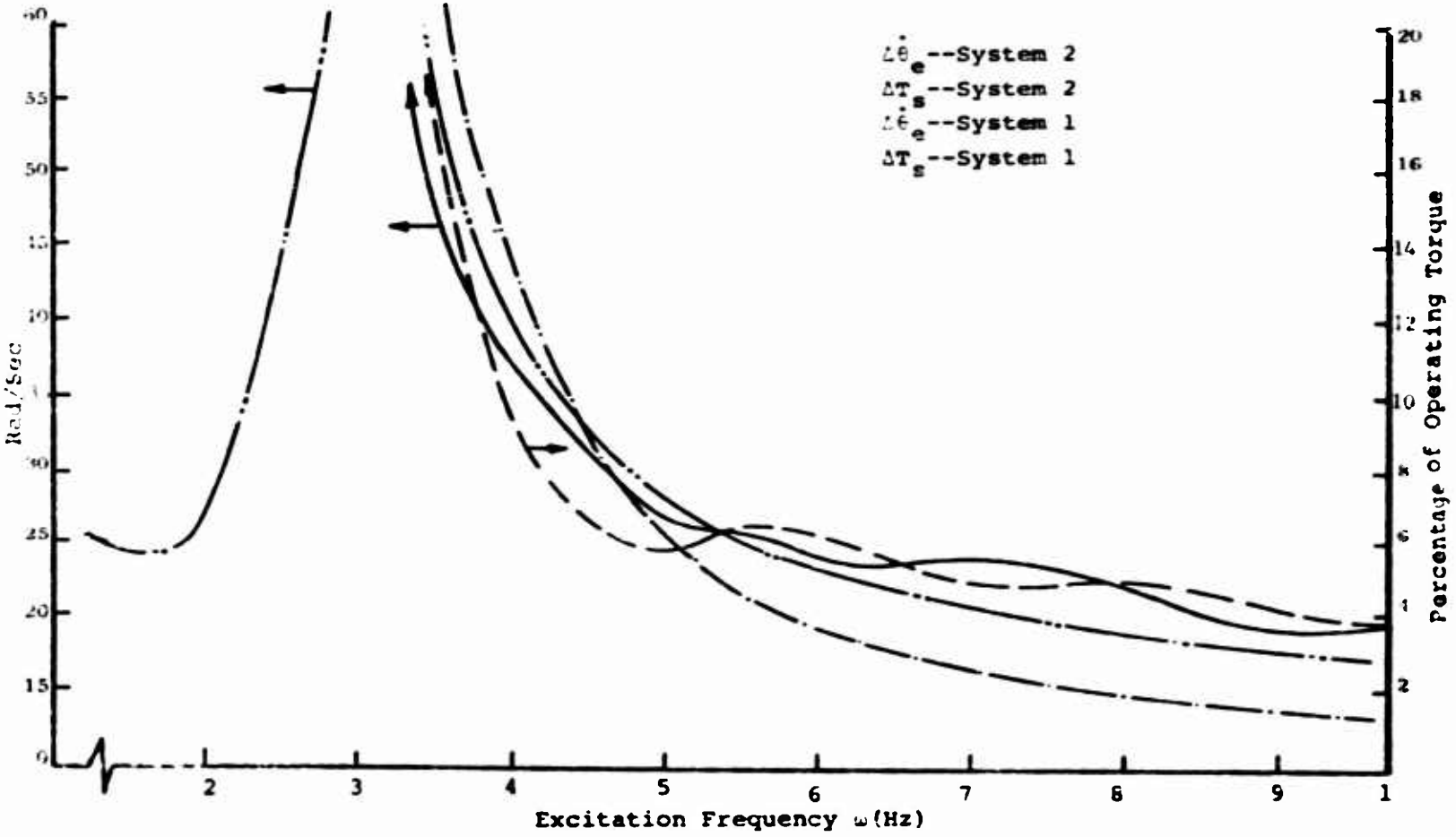

Figure 33b. Variation of T_e.

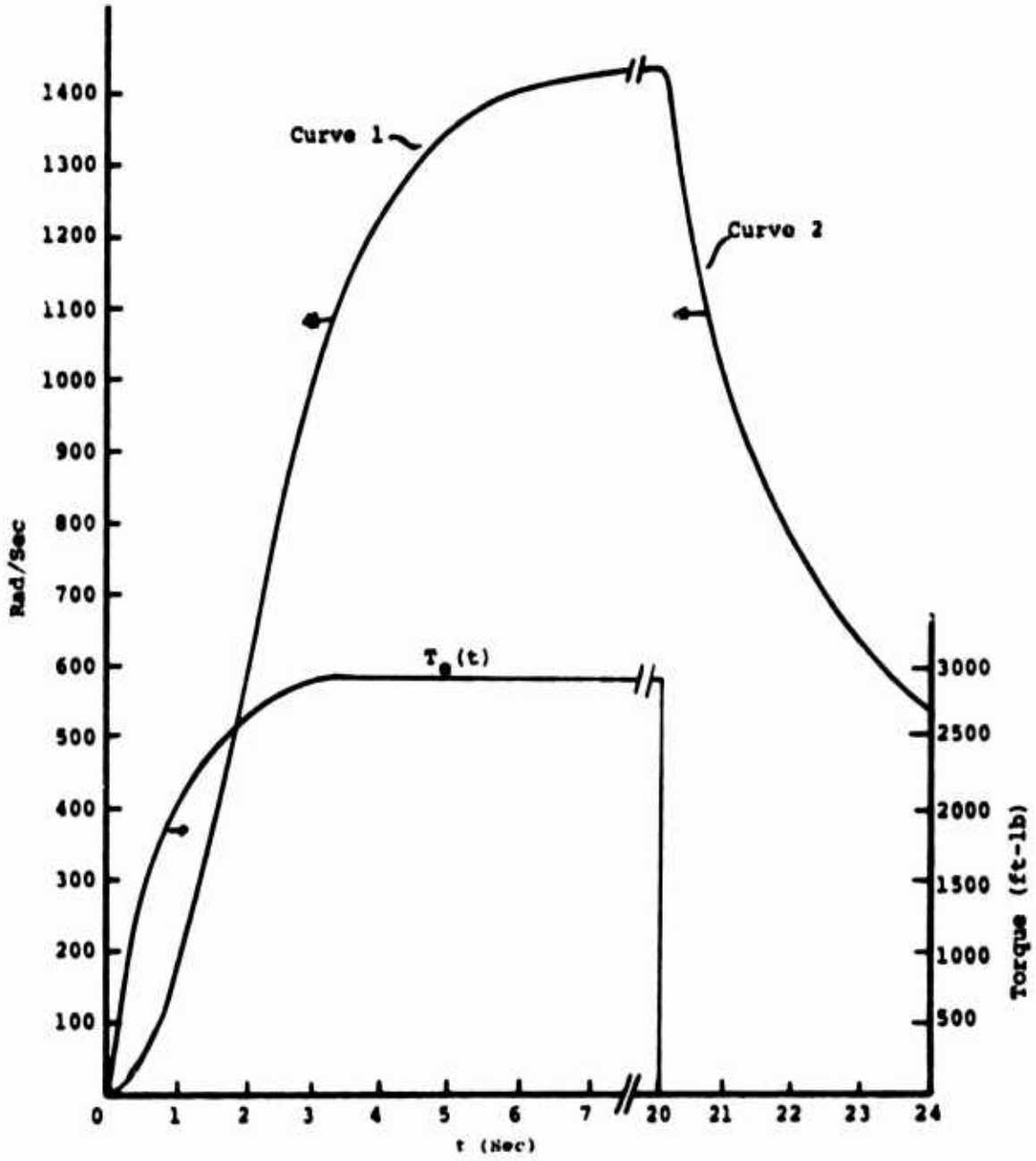

Figure 34. Time Response of Helicopter Drive Train.

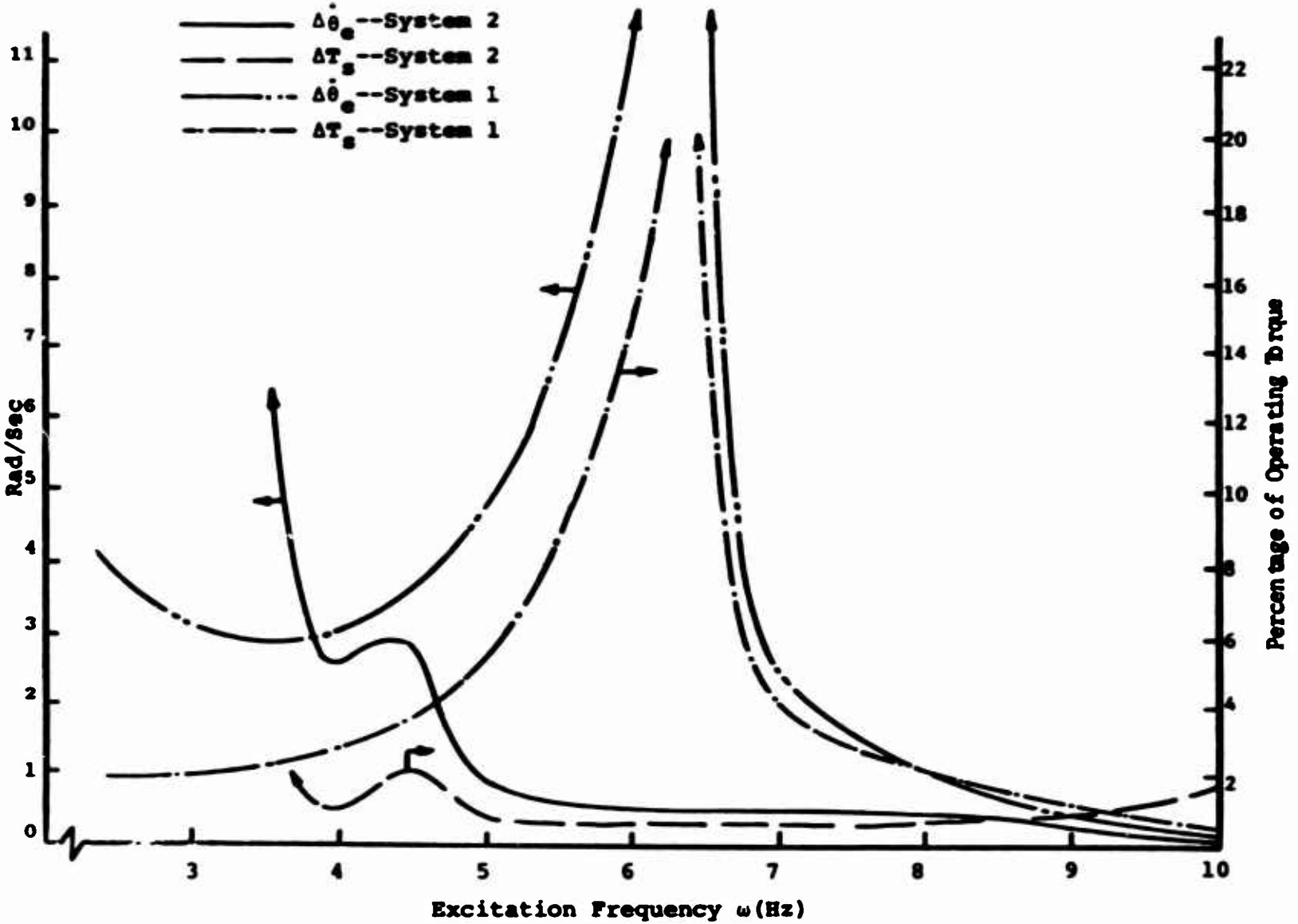

Figure 35. Variation of C_L (K_s = 848.4).

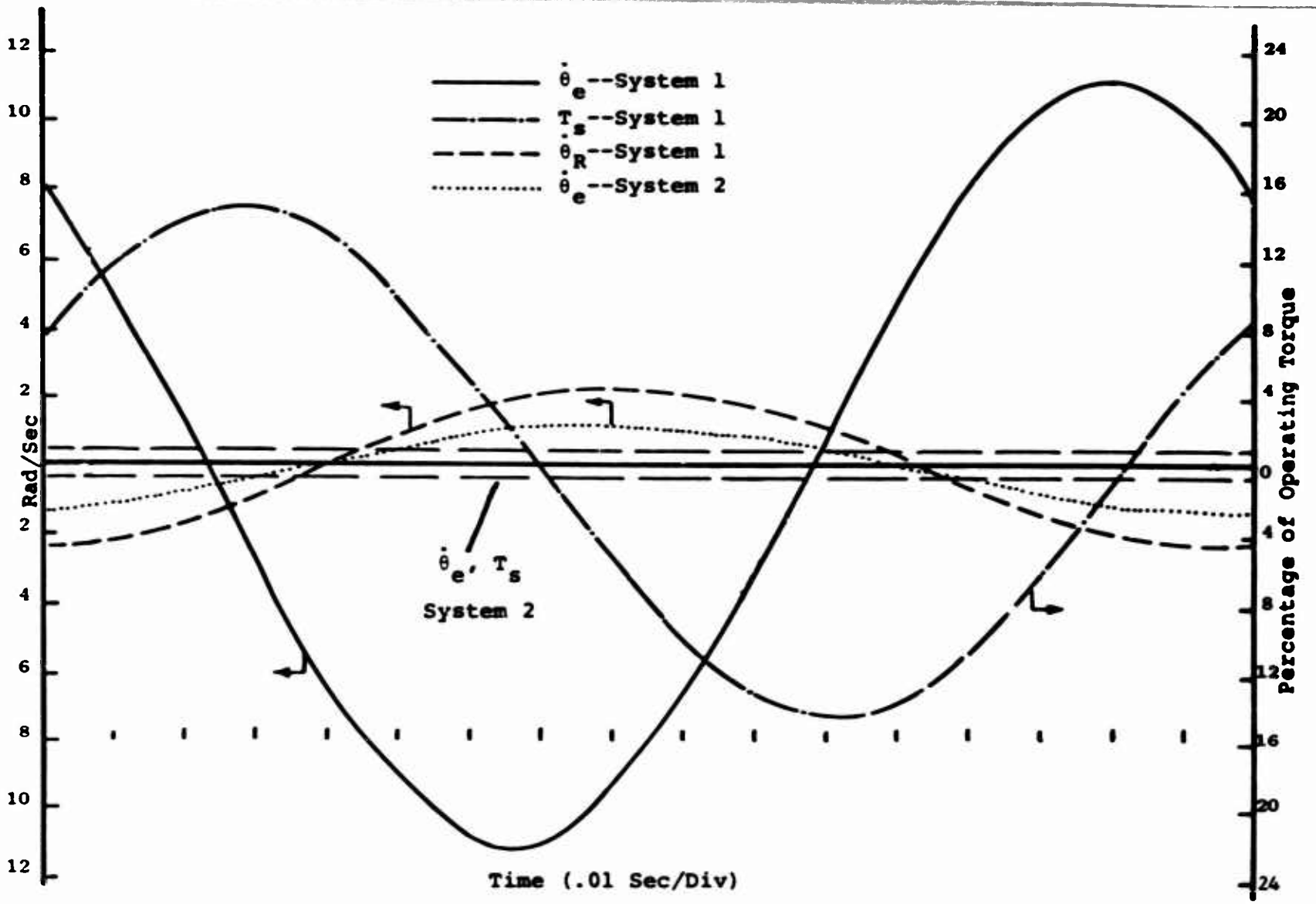

Figure 36. System Time Response to Excitation.

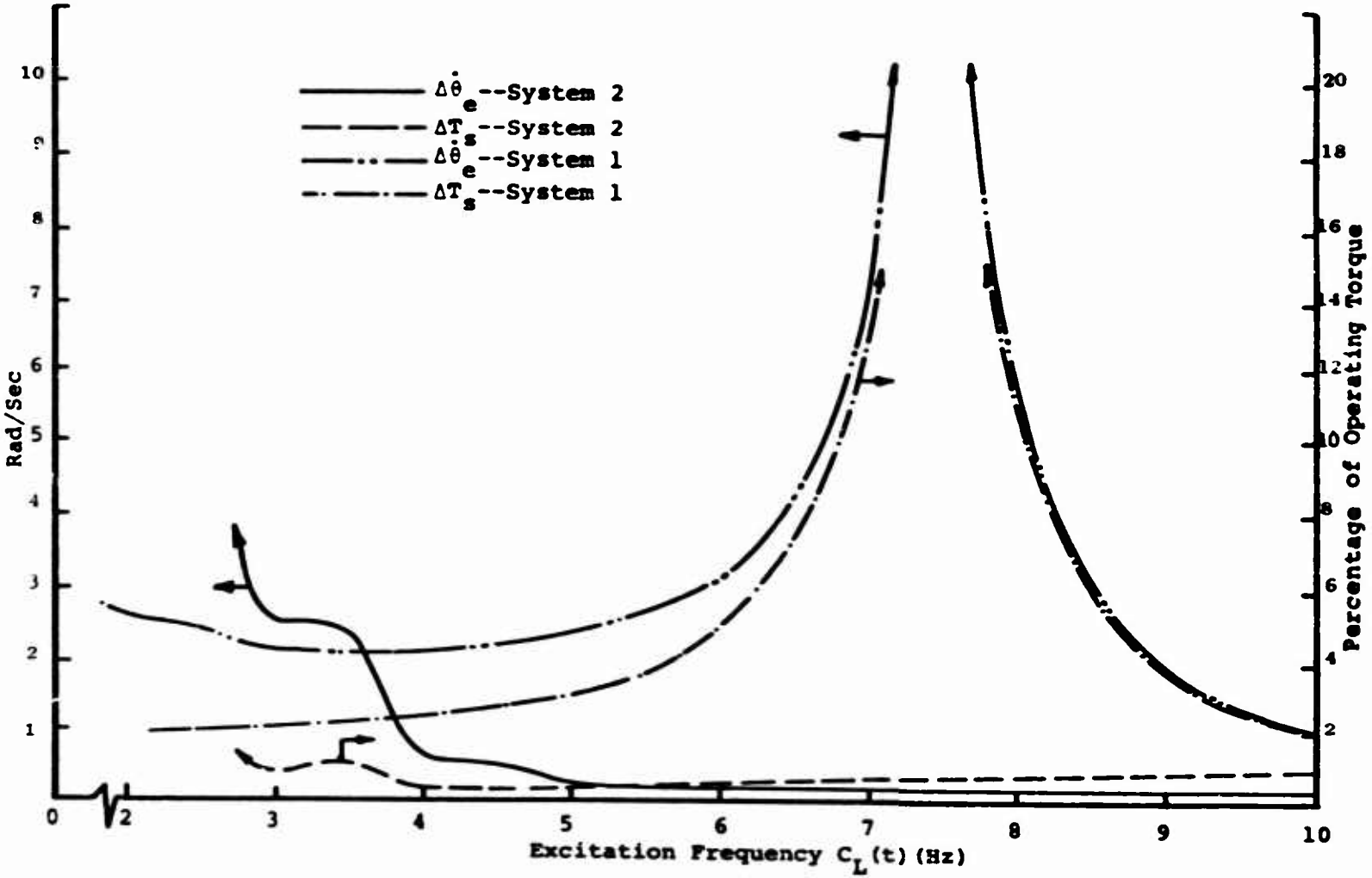

Figure 37. Variation of C_L (K_s = 1696.8).

Systems which have higher shaft stiffness may represent other turbine applications such as pump or generator systems. The final investigation of system response to external excitation is with mast shaft stiffness eight times that of the original helicopter design. Figure 37 shows the system response from Test 1. The critical frequency of System 1 is slightly under 7.5 Hz. Using a ZTS coupling shifts the critical frequency of the system below 4 Hz.

SUMMARY OF RESULTS

1. Torsional vibrations can be reduced or eliminated with a ZTS coupling. The factors limiting coupling effectiveness are

   a. Very low frequency excitation

   b. Very large torque variations

   c. New critical frequencies in range of excitation

2. Through link counterbalancing, the ZTS pinned link coupling can enter the domain of high-speed turbo-powered machinery.

3. For systems where the drag torque is proportional to the angular velocity squared (helicopter system), the ZTS coupling becomes speed independent (see design equation I with $T = \omega^2$).

4. Low stiffness pinned link couplings which can handle large torque variations can easily be designed. If a lower value of θ or β is chosen for $f(\beta,\theta)$ in equation 36, then a low stiffness coupling will result. Higher torque fluctuations across the coupling will be possible without causing impact of the coupling's stops (see Figure 15).

5. Zero or low stiffness pinned link couplings can be designed with four basic equations, 36 - 39.

6. The two advantages of link counterbalancing and ease of design analysis make the pinned link design apparently superior to the elastic link design for very high speed applications.

PART II: EFFECT OF ZTS COUPLINGS ON CLOSED-LOOP TORSIONAL STABILITY

PRELIMINARY CONSIDERATIONS

When designing a dynamic system, it is essential to be certain that the system will not become unstable. This is especially true of the closed-loop system, in which a small perturbation can build into a destructive instability through self-excitation. A closed-loop system is one in which the output is compared with a desired output, and the resulting error is used as an input to the system. This is sometimes called a feedback loop.[10]

The complete dynamics of a modern helicopter is an example of such a closed-loop system. The elements of the system are the turbine engine, drive train, and speed governor. These are shown in block diagram form in Figure 38. It has been shown that to make this system stable, either special features must be provided in the design of the governor or the gain of the system must be reduced which will increase the steady-state droop.[5] The steady-state droop of a closed-loop system is the difference between the desired output and the actual output obtained. Equation 65 gives the steady-state speed droop for the closed-loop helicopter system, where SSD is the steady-state speed droop in percent, $\bar{\omega}_e$ is the steady-state engine speed, and Ω is the design speed at which the governor is set. Hereafter, any equation nomenclature not defined in context will be given in the List of Symbols at the beginning of this report.

$$SSD = \frac{\Omega - \bar{\omega}_e}{\Omega} \times 100 \qquad (65)$$

The governor modifications mentioned above, introduced to ensure stability, will decrease efficiency or increase expense, neither of which is desirable.

A major objective of Part II is to determine if system stability can be achieved by means of effectively modifying the drive train without having to complicate the design of the governor. The proposed method of modifying the drive train is to place a zero-torsional-stiffness-coupling in the drive shaft, to effectively decouple the rotor inertia from the engine inertia. A particular coupling has been designed in Part I for the operating conditions of a helicopter. It will be attempted in Part II to determine and compare the stability of the closed-loop helicopter system with and without a zero torsional stiffness coupling in the drive shaft. In this way, it will be determined if the use of a ZTS coupling is an effective way of maintaining stability while retaining the desirable properties of a fast, simple governor.

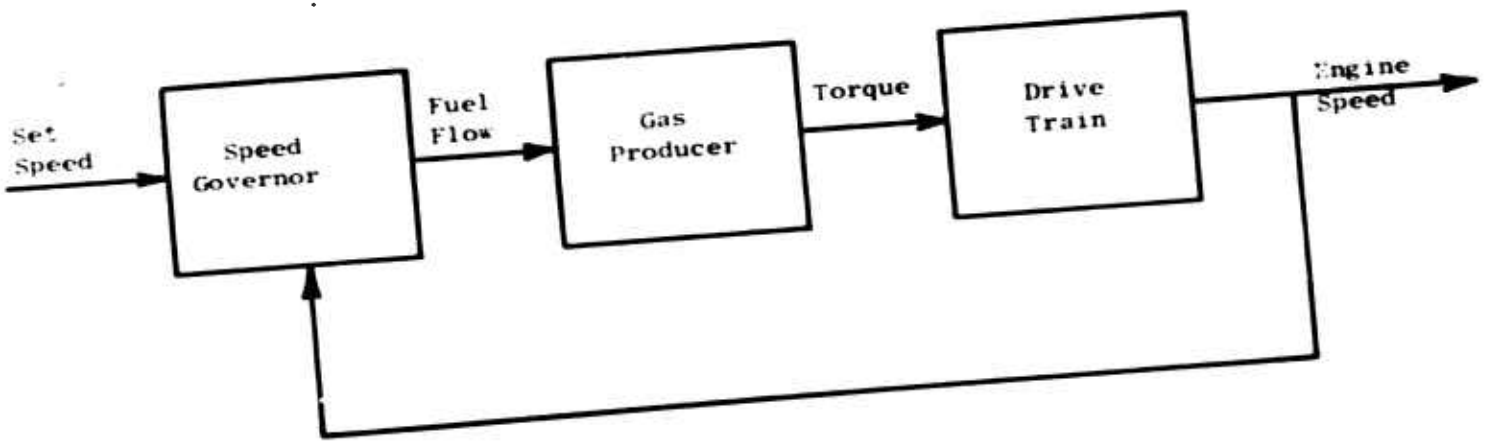

Figure 38. Flow Chart of Helicopter Drive System.

In the discussion of speed governors, the major emphasis will be placed on the direct fuel flow speed governor. It is the simplest and least expensive speed governor available for use in helicopter applications. Unfortunately, the ordinary helicopter system is unstable with a direct fuel flow speed governor.[5] If it can be shown that the helicopter system with the ZTS coupling is stable with a direct fuel flow speed governor, the effectiveness of the coupling will have been demonstrated.

THE LINEARIZED SYSTEM WITH AN IDEAL GOVERNOR

The helicopter system is inherently nonlinear. However, the governing equations may be linearized, which greatly simplifies the problem of evaluating system stability. These equations are made linear by assuming that the physical parameters of the system remain within some small, well defined, operating region. Linearization of equations will be discussed in more detail later, and the system governing equations will be derived. The results obtained for the linearized equations are directly applicable to the case of small perturbations about an operating point. They can also be helpful in getting an intuitive "feel" for the more realistic case of large perturbations about an operating point. More specifically, it will be seen that perturbations of the gas producer and speed governor system parameters are of a sufficiently small magnitude for realistic perturbations of the drive train system parameters, that the linearized governing equations for the gas producer and speed governor are fairly accurate even for the "large perturbation" case. However, this is unfortunately not the case for the linearized drive train equations, especially when the ZTS coupling is included.

A reasonably accurate open-loop model of the helicopter drive train is shown in Figure 39. This system can be represented by equations 66 and 67.

$$I_{eg}\ddot{\theta}_e + C_e\dot{\theta}_e^2 + C_s(\dot{\theta}_e-\dot{\theta}_R) + K(\theta_e-\theta_R) = T_e \qquad (66)$$

$$I_R\ddot{\theta}_R + C_L\dot{\theta}_R^2 + C_s(\dot{\theta}_R-\dot{\theta}_e) + K_s(\theta_R-\theta_e) = 0 \qquad (67)$$

The inertia I_{eg} is the sum of the power turbine inertia, I_e, and the gearbox inertia, I_{gb}. The only nonlinear terms in the two equations are the turbine drag and rotor drag. Actually, the engine torque is also nonlinear for the closed-loop system, but that will be dealt with as one of the gas producer system parameters. Under the assumption of small changes in the system parameters from some steady-state operating conditions, equations 66 and 67 can be linearized. This is made less difficult by first applying a coordinate transformation. A new coordinate, θ_S, is introduced and the coordinate θ_R is eliminated. θ_S is defined as the angle of twist in the shaft and is given by

$$\theta_S = \theta_e - \theta_R$$

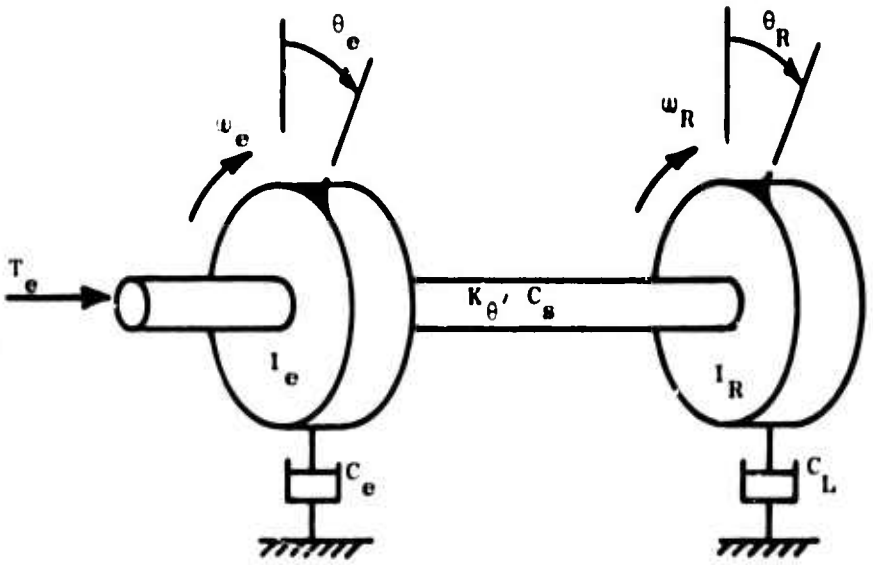

Figure 39. Schematic of Helicopter Drive Train.

for this model. Using this substitution in equations 66 and 67 yields

$$I_{eg}\ddot{\theta}_e + C_e\dot{\theta}_e^2 + C_s\dot{\theta}_s + K_\theta\theta_s = T_e$$

$$I_R(\ddot{\theta}_e - \ddot{\theta}_s) + C_L(\dot{\theta}_e - \dot{\theta}_s)^2 - C_s\dot{\theta}_s - K_\theta\theta_s = 0$$

Since θ_e is now a cyclic coordinate (i.e., does not appear explicitly in the equations), these equations can be rewritten with the following substitutions:

$$\dot{\theta}_e = \omega_e \qquad\qquad \ddot{\theta}_e = \dot{\omega}_e$$

where ω_e is the engine speed, to give

$$I_{eg}\dot{\omega}_e + C_e\omega_e^2 + C_s\dot{\theta}_s + K_\theta\theta_s = T_e \tag{68}$$

$$I_R(\dot{\omega}_e - \ddot{\theta}_s) + C_L(\omega_e - \dot{\theta}_s)^2 - C_s\dot{\theta}_s - K_\theta\theta_s = 0 \tag{69}$$

These equations are linearized about a steady-state operating point, by replacing the generalized coordinates as follows:

$$\omega_e = \bar{\omega}_e + \hat{\omega}_e \qquad \theta_s = \bar{\theta}_s + \hat{\theta}_s \qquad T_e = \bar{T}_e + \hat{T}_e$$

where $\bar{\omega}_e$ is the steady-state engine speed, and $\hat{\omega}_e$ is the difference between the engine speed and its steady-state value, or the engine speed perturbation. Making these substitutions gives

$$I_{eg}\dot{\omega}_e + C_e(\bar{\omega}_e^2 + 2\bar{\omega}_e\hat{\omega}_e + \hat{\omega}_e^2) + C_s\dot{\theta}_s + K_\theta(\bar{\theta}_s + \hat{\theta}_s) = \bar{T}_e + \hat{T}_e$$

$$I_R(\dot{\omega}_e - \ddot{\theta}_s) + C_L(\bar{\omega}_e^2 + \hat{\omega}_e^2 + \dot{\theta}_s^2 + 2\bar{\omega}_e\hat{\omega}_e - 2\bar{\omega}_e\dot{\theta}_s$$

$$- 2\hat{\omega}_e\dot{\theta}_s) - C_s\dot{\theta}_s - K_\theta(\bar{\theta}_s + \hat{\theta}_s) = 0$$

Since all system variables are now small, any above first degree can be ignored as being negligible, resulting in

$$I_{eg}\dot{\omega}_e + C_e\bar{\omega}_e^2 + 2C_e\bar{\omega}_e\hat{\omega}_e + C_s\dot{\theta}_s + K_\theta\bar{\theta}_s + K_\theta\hat{\theta}_s = \bar{T}_e + \hat{T}_e$$

$$I_R(\dot{\omega}_e - \ddot{\theta}_s) + C_L\bar{\omega}_e^2 + 2C_L\bar{\omega}_e(\hat{\omega}_e - \dot{\theta}_s) - C_s\dot{\theta}_s - K_\theta\bar{\theta}_s - K_\theta\hat{\theta}_s = 0$$

By letting the system perturbations and their time derivatives go to zero, the above equations can be made to yield the steady-state operating conditions, which also represent the particular solutions to the differential equations. When the system perturbations and their time derivatives are set equal to zero, the resulting equations are

$$C_e\bar{\omega}_e^2 + K_\theta\bar{\theta}_s = \bar{T}_e$$

$$C_L\bar{\omega}_e^2 - K_\theta\bar{\theta}_s = 0$$

These equations can be solved for the steady-state operating conditions. Meanwhile, the particular solution can now be removed from the differential equations, leaving

$$I_{eg}\dot{\omega}_e + 2C_e\bar{\omega}_e\omega_e + C_s\dot{\theta}_s + K_\theta\hat{\theta}_s = \hat{T}_e$$

$$I_R(\dot{\omega}_e - \ddot{\theta}_s) + 2C_L\bar{\omega}_e(\omega_e - \dot{\theta}_s) - C_s\dot{\theta}_s - K_\theta\hat{\theta}_s = 0$$

From these equations it can be seen that the linearized engine and rotor damping coefficients are represented by equations 70 and 71.

$$C_T = 2C_e\bar{\omega}_e \tag{70}$$

$$C_D = 2C_L\bar{\omega}_e \tag{71}$$

Substituting these linearized damping coefficients into the differential equations yields equations 72 and 73 which represent the linearized helicopter drive train.

$$I_{eg}\dot{\omega}_e + C_T\omega_e + C_s\dot{\theta}_s + K_\theta\hat{\theta}_s = \hat{T}_e \tag{72}$$

$$I_R(\dot{\omega}_e - \ddot{\theta}_s) + C_D(\omega_e - \dot{\theta}_s) - C_s\dot{\theta}_s - K_\theta\hat{\theta}_s = 0 \tag{73}$$

Figure 40 is a plot of the torque on the engine due to turbine damping as a function of the engine speed. It is of interest to note that the linearized engine damping coefficient given by equation 70 is the same as the slope of the curve at the steady-state engine speed. This is reasonable since, in considering small changes of torque and engine speed, it is the slope of this curve at the operating point, rather than the average slope, which gives the linearized damping coefficient of interest. It is also of interest that these linearized damping coefficients are equal to, precisely, twice the average linearized damping coefficient (average slope of the curve).

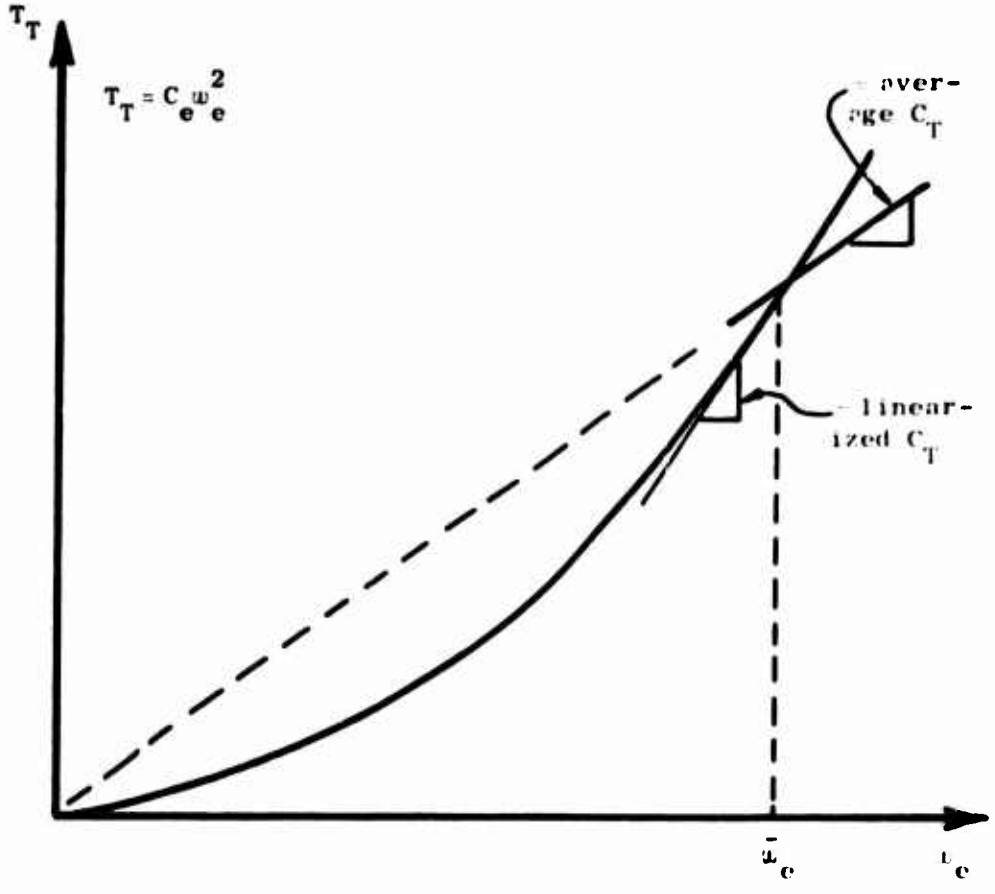

Figure 40. Turbine Damping Torque Versus Engine Speed.

Again assuming small changes in the system variables, the use of a ZTS coupling would reduce the shaft stiffness and shaft damping to zero, effectively decoupling the rotor inertia from the engine inertia. This is represented schematically in Figure 41. The differential equations representing this system are given by

$$I_e\ddot{\theta}_e + C_e\dot{\theta}_e^2 = T_e - T_c$$

$$I_R\ddot{\theta}_R + C_L\dot{\theta}_R^2 = T_c$$

where T_c is the torque that the ZTS coupling is designed to transmit at speed ω_e. These equations are cyclic in both θ_e and θ_R. Therefore, by substituting in

$$\dot{\theta}_e = \omega_e \qquad \ddot{\theta}_e = \dot{\omega}_e$$

$$\dot{\theta}_R = \omega_R \qquad \ddot{\theta}_R = \dot{\omega}_R$$

they can be rewritten as

$$I_e\dot{\omega}_e + C_e\omega_e^2 = T_e - T_c \tag{74}$$

$$I_R\dot{\omega}_R + C_L\omega_R^2 = T_c \tag{75}$$

Linearizing these equations and eliminating the particular solutions, using the same method as used above, yields equations 76 and 77.

$$I_e\dot{\hat{\omega}}_e + C_T\hat{\omega}_e = \hat{T}_e \tag{76}$$

$$I_R\dot{\hat{\omega}}_R + C_D\hat{\omega}_R = 0 \tag{77}$$

It is noted that the equations representing the system without a ZTS coupling include the gearbox inertia in with the engine inertia, while the equations representing the system with a ZTS coupling do not. This is because it is assumed that the shaft connecting the engine to the gearbox is completely rigid (a reasonable assumption, in comparison with the mast shaft stiffness), and that the ZTS coupling will be located in this shaft. Therefore, the ZTS coupling will also decouple the gearbox inertia from the engine inertia.

To obtain a feel for the effect of the various components on the stability of the drive train system, the preceding equations will be coupled with an ideal speed governor, while the gas producer dynamics are ignored. In effect, this system represents a single-spool turbine engine with an ideal governor. Figure 42 shows the system of Figure 39 coupled with an

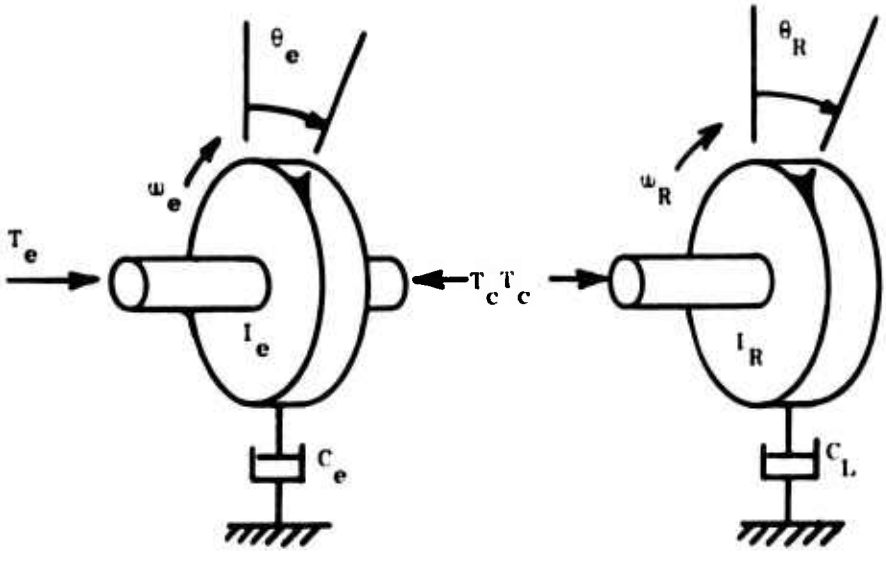

Figure 41. Schematic of Helicopter Drive Train With ZTS Coupling.

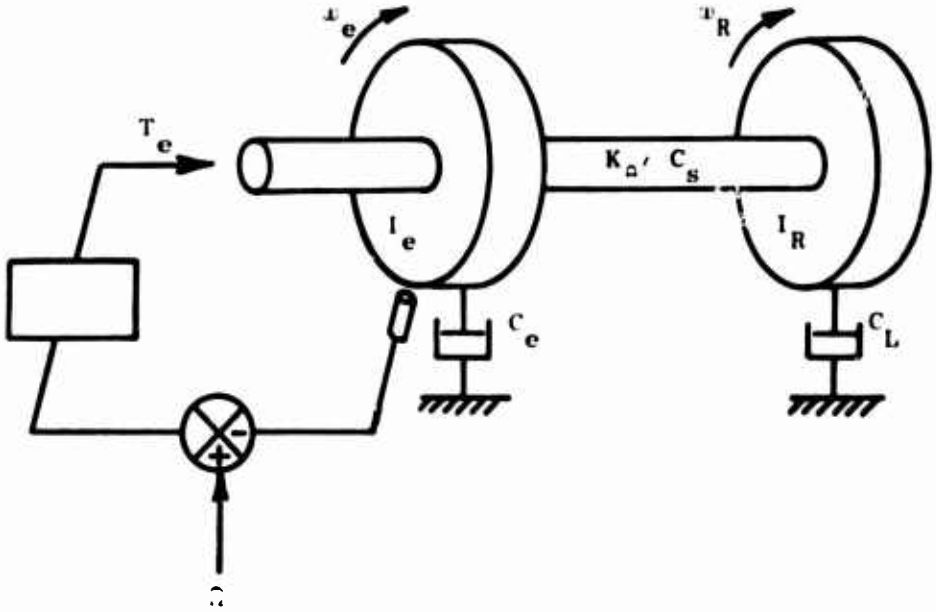

Figure 42. Schematic of Helicopter Drive Train With Ideal Speed Governor.

ideal governor. An ideal speed governor is one in which there are no lags or other dynamics and the output signal is directly proportional to the input signal.

For the problem presently being considered, the input signal is the engine speed error and the output signal is the engine torque. The engine speed error is the difference between the actual engine speed and the desired engine speed to which the speed governor has been set. The speed governor can be represented by equation 78.

$$T_e = G(\Omega - \omega_e) \tag{78}$$

Making the same small change substitutions as before yields

$$\bar{T}_e + \hat{T}_e = G(\Omega - \bar{\omega}_e - \hat{\omega}_e)$$

From equation 78 the steady-state engine torque is given by

$$\bar{T}_e = G(\Omega - \bar{\omega}_e)$$

Subtracting this from the previous equation gives equation 79.

$$\hat{T}_e = -G\hat{\omega}_e \tag{79}$$

Substituting this into equations 72 and 73 and regrouping terms gives equations 80 and 81.

$$I_{eg}\dot{\omega}_e + (C_T+G)\hat{\omega}_e + C_s\dot{\theta}_s + K_\theta\hat{\theta}_s = 0 \tag{80}$$

$$I_R(\dot{\omega}_e-\ddot{\theta}_s) + C_D\hat{\omega}_e - (C_D+C_s)\dot{\theta}_s - K_\theta\dot{\theta}_s = 0 \tag{81}$$

Equation 80 is a first-order differential equation, and equation 81 is a second-order differential equation. They are converted into three first-order differential equations by making the substitutions of equation 82.

$$\hat{\omega}_e = X_1 \qquad \dot{\omega}_e = \dot{X}_1$$

$$\hat{\theta}_s = X_2 \qquad \dot{\theta}_s = X_3 \qquad \ddot{\theta}_s = \dot{X}_3 \tag{82}$$

The three first-order differential equations are

$$I_{eg}\dot{X}_1 + (C_T+G)X_1 + C_sX_3 + K_\theta X_2 = 0$$

$$I_R(\dot{X}_1-\dot{X}_3) + C_DX_1 - (C_D+C_s)X_3 - K_\theta X_2 = 0$$

$$\dot{X}_2 = X_3$$

Solving these equations for $\dot{X}_1$, $\dot{X}_2$ and $\dot{X}_3$ produces equations 83 through 85.

$$\dot{X}_1 = -\frac{(C_T+G)}{I_{eg}} X_1 - \frac{K_\theta}{I_{eg}} X_2 - \frac{C_s}{I_{eg}} X_3 \tag{83}$$

$$\dot{X}_2 = X_3 \tag{84}$$

$$\dot{X}_3 = \left[\frac{C_D}{I_R} - \frac{(C_T+G)}{I_{eg}}\right] X_1 - \left(\frac{K_\theta}{I_{eg}} + \frac{K_\theta}{I_R}\right) X_2 - \left[\frac{C_s}{I_{eg}} + \frac{C_D+C_s)}{I_R}\right] X_3 \tag{85}$$

This can be written in matrix form as shown in equation 86.

$$\begin{bmatrix} \dot{X}_1 \\ \dot{X}_2 \\ \dot{X}_3 \end{bmatrix} = \begin{bmatrix} -\frac{(C_T+G)}{I_{eg}} & -\frac{K_\theta}{I_{eg}} & -\frac{C_s}{I_{eg}} \\ 0 & 0 & 1 \\ \left[\frac{C_D}{I_R} - \frac{(C_T+G)}{I_{eg}}\right] & -\left(\frac{K_\theta}{I_{eg}} + \frac{K_\theta}{I_R}\right) & -\left[\frac{C_s}{I_{eg}} + \frac{(C_D+C_s)}{I_R}\right] \end{bmatrix} \cdot \begin{bmatrix} X_1 \\ X_2 \\ X_3 \end{bmatrix} \tag{86}$$

In this form the system equations easily lend themselves to the evaluation of stability by the first method of Lyapunov. When using this method of stability analysis, it is necessary to have the differential equations in the form of equation 87, where $\underline{x}$ and $\dot{\underline{x}}$ are vectors and $\underline{\underline{A}}$ is a matrix.

$$\dot{\underline{x}} = \underline{\underline{A}}\,\underline{x} \tag{87}$$

This is the form of equation 86. The procedure is to subtract λ from each element along the main diagonal of the matrix $\underline{\underline{A}}$ from equation 87. Following this procedure for the matrix $\underline{\underline{A}}$ of equation (86) results in the matrix given by equation 88.

$$\begin{bmatrix} -\lambda - \frac{(C_T+G)}{I_{eg}} & -\frac{K_\theta}{I_{eg}} & -\frac{C_s}{I_{eg}} \\ 0 & -\lambda & 1 \\ \left[\frac{C_D}{I_R} - \frac{(C_T+G)}{I_{eg}}\right] & -\left(\frac{K_\theta}{I_{eg}} + \frac{K_\theta}{I_R}\right) & -\lambda - \left[\frac{C_s}{I_{eg}} + \frac{(C_D+C_s)}{I_R}\right] \end{bmatrix} \tag{88}$$

The result will be a polynomial in λ that is the same order as the matrix $\underline{\underline{A}}$. If this polynomial is set equal to zero, the roots of λ, or eigenvalues of the dynamic system, can be solved for. If all of the roots have negative real parts, the system is stable, since the system solution will converge to a steady-state value. If any of the roots have positive real parts, the system will be unstable, since the system solution will grow toward infinity. If one, or more, of the roots has no real part and the rest of the roots have negative real parts, the stability of the system is uncertain. If the above-mentioned polynomial, known as the characteristic equation, is higher than second order, finding its roots may be difficult. In such a case it may be advantageous to use the "Routh-Hurwitz Criteria," a method for testing the coefficients of the characteristic equation for the existence of roots with nonnegative real parts without having to actually solve it.

The characteristic equation derived from equation 88 is given in equation 89.

$$\lambda^3 + \left(\frac{C_T+G+C_s}{I_{eg}} + \frac{C_D+C_s}{I_R}\right)\lambda^2 + \left[\frac{(C_T+G)(C_D+C_s)+C_DC_s}{I_{eg}I_R} + \frac{K_\theta}{I_{eg}} + \frac{K_\theta}{I_R}\right]\lambda + \left[\frac{K_\theta(C_D+C_T+G)}{I_{eg}I_R}\right] = 0 \qquad (89)$$

It appears that the three eigenvalues would be very difficult to solve for. Since the actual values of the eigenvalues are unimportant for the stability problem, it is much more efficient to use the "Routh-Hurwitz Criteria" to determine the signs of the real parts of the eigenvalues.

In order for all of the roots of a real polynomial, of the form of equation 90 to have negative real parts, all of the coefficients of the polynomial must be positive.

$$\lambda^3 + a\lambda^2 + b\lambda + c = 0 \qquad (90)$$

In addition, the coefficients of equation 90 must satisfy equation 91.[11]

$$ab - c > 0 \qquad (91)$$

From equation 89 the coefficients of equation 90 for this problem are given by equations 92 through 94.

$$a = \frac{C_T+G+C_s}{I_{eg}} + \frac{C_D+C_s}{I_R} \qquad (92)$$

$$b = \frac{(C_T+G)(C_D+C_s)+C_DC_s}{I_{eg}I_R} + \frac{K_\theta}{I_{eg}} + \frac{K_\theta}{I_R} \qquad (93)$$

$$c = \frac{K_\theta (C_D + C_T + G)}{I_{eg} I_R} \tag{94}$$

Since all of the physical system parameters, including the gain of the speed governor, must be positive, then all of the coefficients must also be positive. Therefore, the first test for roots with negative real parts is satisfied. Substituting equations 92 through 94 into equation 91 results in equation 95, which can be rearranged to produce equation 96.

$$\left[\frac{C_T + G + C_s}{I_{eg}} \cdot \frac{C_D + C_s}{I_R}\right]\left[-\frac{(C_T + G)(C_D + C_s) + C_D C_s}{I_{eg} I_R} + \frac{K_\theta}{I_{eg}} + \frac{K_\theta}{I_R}\right]$$

$$- \frac{K_\theta (C_D + C_T + G)}{I_{eg} I_R} > 0 \tag{95}$$

$$\frac{[I_R (C_T + G + C_s) + I_{eg} (C_D + C_s)](C_T C_D + G C_D + C_T C_s + G C_s + C_D C_s)}{I_{eg}^2 I_R^2}$$

$$+ \frac{[(C_T + G + C_s) I_R^2 + (C_D + C_s) I_{eg}^2 + 2 C_s I_{eg} I_R] K_\theta}{I_{eg}^2 I_R^2} > 0 \tag{96}$$

Since all of the physical system parameters are positive, then equation 96 is satisfied. Therefore, the previously described linearized model of the helicopter drive system with an ideal governor and no gas producer dynamics is stable.

By the same method as that just used, the stability of the reduced system represented by equations 76 and 77 is evaluated. It can be seen that equations 76 and 77 are decoupled, and, since it is the dynamics of the engine speed, ω_e, that is of primary interest, equation 77 can be ignored. As in the unreduced problem, the system will include an ideal speed governor represented by equation 78. This system is illustrated in Figure 43. Substituting equation 79 into equation 76 results in equation 97.

$$I_e \dot{\hat{\omega}}_e + C_T \hat{\omega}_e = -Q\hat{\omega}_e \tag{97}$$

Using the same method of substitution shown previously, equation 97 can be converted into the matrix form of equation 87 shown in equation 100, using the substitutions of equations 98 and 99.

$$X_1 = \omega_e \tag{98}$$

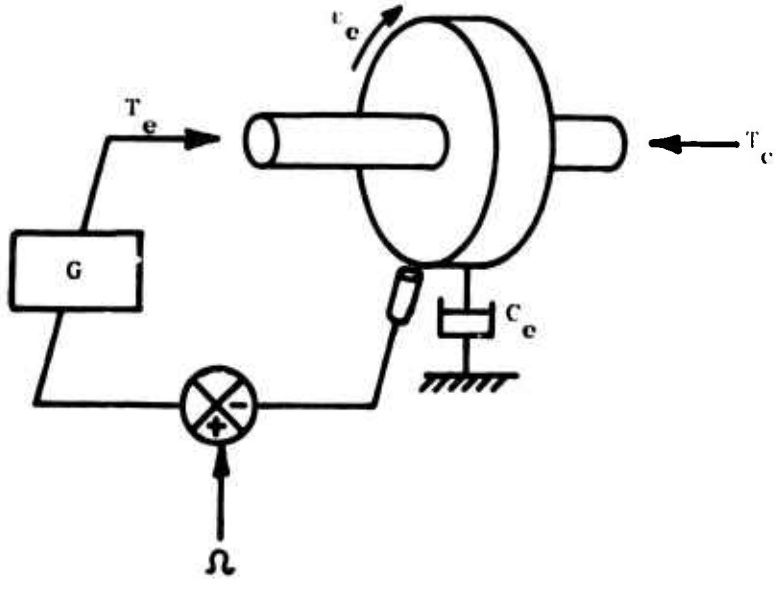

Figure 43. Schematic of Helicopter Drive Train With ZTS Coupling and Ideal Governor.

$$\dot{X}_1 = \dot{\omega}_e \tag{99}$$

$$\dot{X}_1 = \frac{(C_T+G)}{I_e} X_1 \tag{100}$$

The characteristic equation for the system can be found easily and is given by equation 101.

$$\lambda + \frac{(C_T+G)}{I_e} = 0 \tag{101}$$

Since the engine damping and speed governor gain are both positive, the one eigenvalue of this system of equations is definitely negative. Therefore, the linearized model of a helicopter drive system with an ideal speed governor and no gas producer dynamics is stable whether or not it has a ZTS coupling. However, in the design and operation of realistic helicopter drive systems, stability problems are often encountered. Therefore, it must be assumed that these instabilities are due to, or at least aided by, either the dynamics of realistic speed governors or realistic gas producer dynamics, or both. Consequently, it is necessary to go to a more sophisticated and realistic model of the helicopter drive system, including speed governor and gas producer dynamics, in order to determine the cause of these system instabilities and the effectiveness of a ZTS coupling in eliminating them.

THE LINEARIZED SYSTEM WITH A DIRECT FUEL FLOW GOVERNOR

The equations for more realistic models of the speed governor and gas producer are derived in this section. These models are then combined with the previously described linearized model of the drive train to form a more realistic model for the helicopter drive system under discussion.

The speed governor of interest is a direct fuel flow speed governor, and the conceptual model is shown, schematically in Figure 44.[12] Conceptually, the speed governor operates in the following manner. The speed stick is set to a desired engine speed, Ω, thereby determining the value of the coordinate S. The pressure, p, on the piston of mass, M_g, is produced by a mechanical or electrical transducer from the actual engine speed, ω_e. This pressure is assumed to be directly proportional to the actual engine speed. This is represented, analytically, in equation 102.

$$p = K_1 \omega_e \tag{102}$$

When operating at steady state, the piston will be in the position to allow the correct amount of fuel flow, such that the engine speed resulting

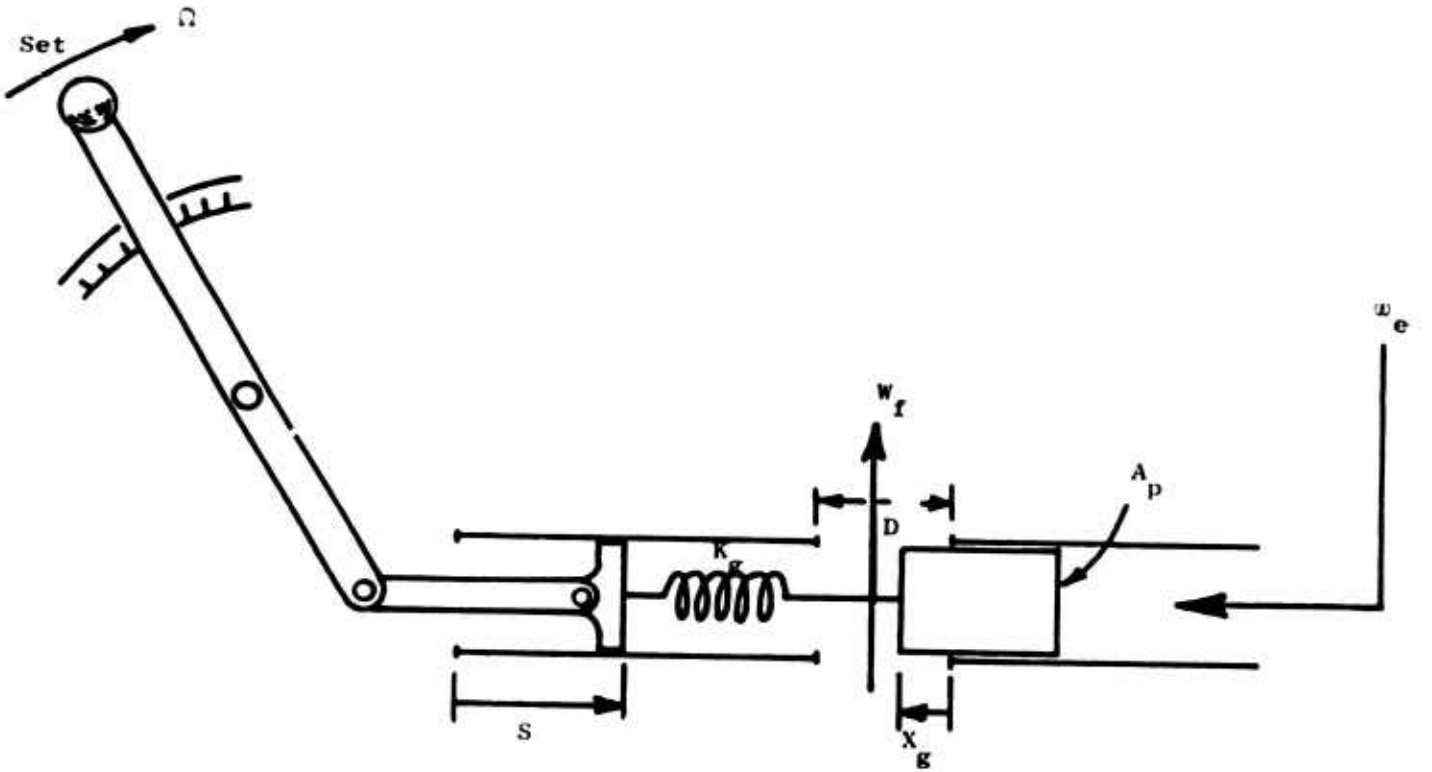

Figure 4-1. Direct Fuel Flow Speed Governor.

from that fuel flow will create a pressure, p, which will result in a force on the piston equal in magnitude to the force exerted on the piston by the spring of stiffness, K_g. If the engine speed suddenly decreases, possibly due to an increased load, then the force on the piston due to the pressure, p, will become less than the spring force on the piston. The piston will move to the right, decreasing the spring force, until the forces on the piston are balanced. This will result in an increased fuel flow, increasing the engine speed, and subsequently forcing the piston to move back to the left. This damped oscillation of the piston will continue for a short time until the piston settles down into a new steady-state position. The damping of the piston is assumed to be purely viscous. This appears to be an accurate assumption.[12] Also, an increase in the engine speed or a pilot-induced change in the set speed will produce dynamics of the piston similar to those described above.

The differential equation of motion for the piston is derived by means of Newton's law, represented by equation 103.

$$\Sigma F_x = M\ddot{X} \tag{103}$$

Under the assumptions that the damping is viscous and the spring is linear, the equation of motion, 104, will be linear.

$$M_g\ddot{X}_g + C_g\dot{X}_g + K_gX_g = K_\omega A_p x_e - K_g a\Omega + K_g D \tag{104}$$

The speed governor can be physically designed so that equation 105 is satisfied.

$$K_g a = K_I A_p \tag{105}$$

If this is done, then equation (104) will reduce to equation 106.

$$M_g\ddot{X}_g + C_g\dot{X}_g + K_gX_g = K_g\,[a(x_e-\Omega) + D] \tag{106}$$

When relating parts of the helicopter drive system, it is much more convenient to use the fuel flow, W_f, as a system parameter, than to use the piston displacement, X_g. Assuming that the fuel flow orifice is rectangular, that the fuel flow reduction near the boundary of the orifice is negligible, and that the fuel supply pressure is constant, the fuel flow can be related to the piston displacement by equation 107. Under the above-listed assumptions, the partial derivative of the fuel flow with respect to the piston displacement is a constant.

$$W_f = -\frac{\partial W_f}{\partial X_g}(D-X_g) \tag{107}$$

This constant is negative, since an increase in X_g will cause a decrease in the fuel flow. Making the substitution of equation 108 into equation 107, noting that Q is positive, and solving the resulting equation for X_g will give equation 109.

$$Q = - \frac{\partial W_f}{\partial X_g} \tag{108}$$

$$X_g = D - \frac{W_f}{Q} \tag{109}$$

The first two time derivatives of X_g are taken as shown in equations 110 and 111.

$$\dot{X}_g = - \frac{\dot{W}_f}{Q} \tag{110}$$

$$\ddot{X}_g = - \frac{\ddot{W}_f}{Q} \tag{111}$$

Equations 109 through 111 are substituted into equation 106, resulting in equation 112. This equation is in terms of the fuel flow rather than the piston displacement.

$$M_g \ddot{W}_f + C_g \dot{W}_f + K_g W_f = K_g Q a (\Omega - \omega_e) \tag{112}$$

A schematic representation of the gas producer and power turbine is given in Figure 45.[13] This is known as a two-spool or free turbine engine. The fuel flow is delivered from the speed governor to the combustor. The fuel is burned in the combustor, which creates a driving torque on the gas producer, as well as on the power turbine. The gas producer creates a driving torque on the power turbine as well as on the compressor. Therefore, when the rate of fuel flow is suddenly changed it has a direct, rapid effect on the engine torque. However, it also has an indirect, delayed effect through the speed of the gas producer. That is, a change in fuel flow causes a change in the gas producer speed that is not immediate, due to the inertia of the gas producer. This change in gas producer speed then causes a change in the engine torque created by the gas producer. This delayed reaction of engine torque to fuel flow is significant in considerations of helicopter drive system instability.

The differential equation of motion for the gas producer is derived by means of Newton's law, as given in equation 113.

$$\Sigma \tau_g = I_g \dot{\omega}_g \tag{113}$$

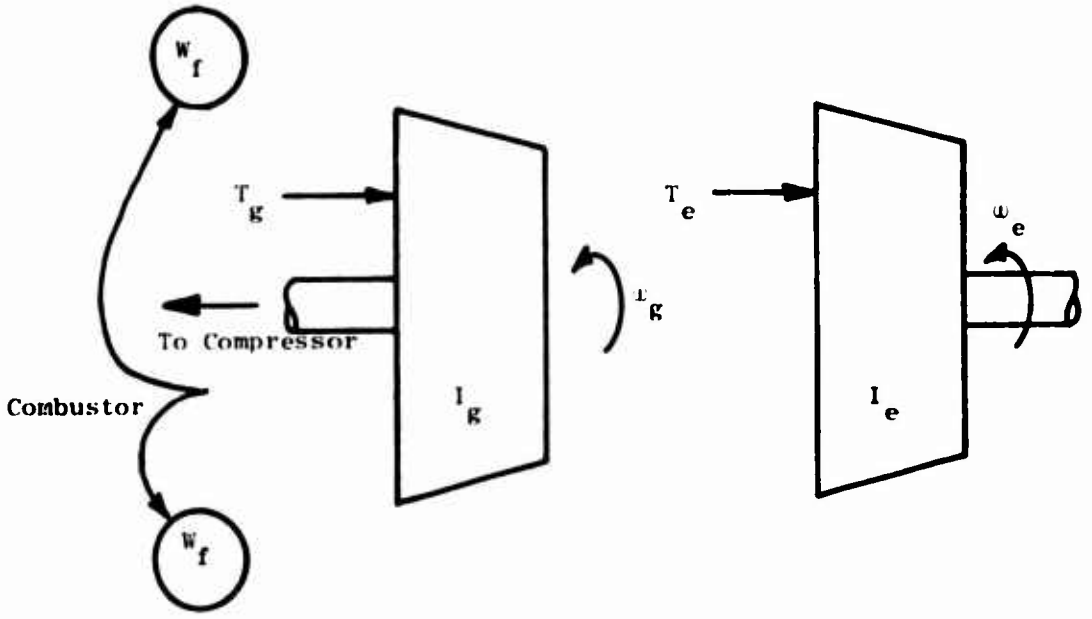

Figure 45. Two-Spool Turbine Engine.

Under the assumption that the relative changes in fuel flow, gas producer speed, and engine torque are fairly small, equation 114 is derived from equation 113.

$$I_g \dot{\omega}_g = \hat{W}_f \frac{\partial T_g}{\partial W_f} - \hat{\omega}_g \frac{\partial T_g}{\partial \omega_g} \tag{114}$$

Each of the partial derivatives actually represents a set of curves such as those shown in Figure 46.[4] For example, equation 115 represents the graph of Figure 46. If the region of operation is relatively small, the curves can be assumed to approximate straight lines through the operating point, thereby making the partial derivatives constant values for that operating point.

$$\hat{T}_e = \frac{\partial T_e}{\partial W_f} \hat{W}_f + \frac{\partial T_e}{\partial \omega_g} \hat{\omega}_g \tag{115}$$

The same argument can be used to find constants to replace the partial derivatives in equation 114. It is likely that these linearized equations are sufficiently accurate to give reliable results for realistic perturbations about the steady-state operating conditions.

Figure 47 is an illustration of a single-spool or fixed turbine engine. The two-spool engine has the advantage of allowing the gas producer spool to spin free of the power turbine if a large enough load is suddenly applied to the power turbine to stop it, or at least slow it down significantly very quickly. If such a load were applied to a single spool engine, the compressor would also be forced to slow down or stop, and the potential for damage to the turbine engine would be much greater. However, a single-spool engine has the advantage of being less dynamically complex and more inherently stable. A curve representing the relationship between engine torque and fuel flow for a fixed turbine engine would look like one member of the family of curves shown in Figure 46. Under the small perturbation assumption, the engine torque for a one-spool turbine engine would be given by

$$\hat{T}_e = \frac{\partial T_e}{\partial W_f} \hat{W}_f \tag{116}$$

where the partial derivative can be considered a constant.

In order to carry out a Bode plot stability analysis of a helicopter drive system, it is necessary to convert the system differential equations into Laplace transfer functions. The transfer function for the speed governor is derived from equation 112. Equation 117 is substituted into equation 112 and the Laplace transform is taken of the resulting equation, giving equation 118.

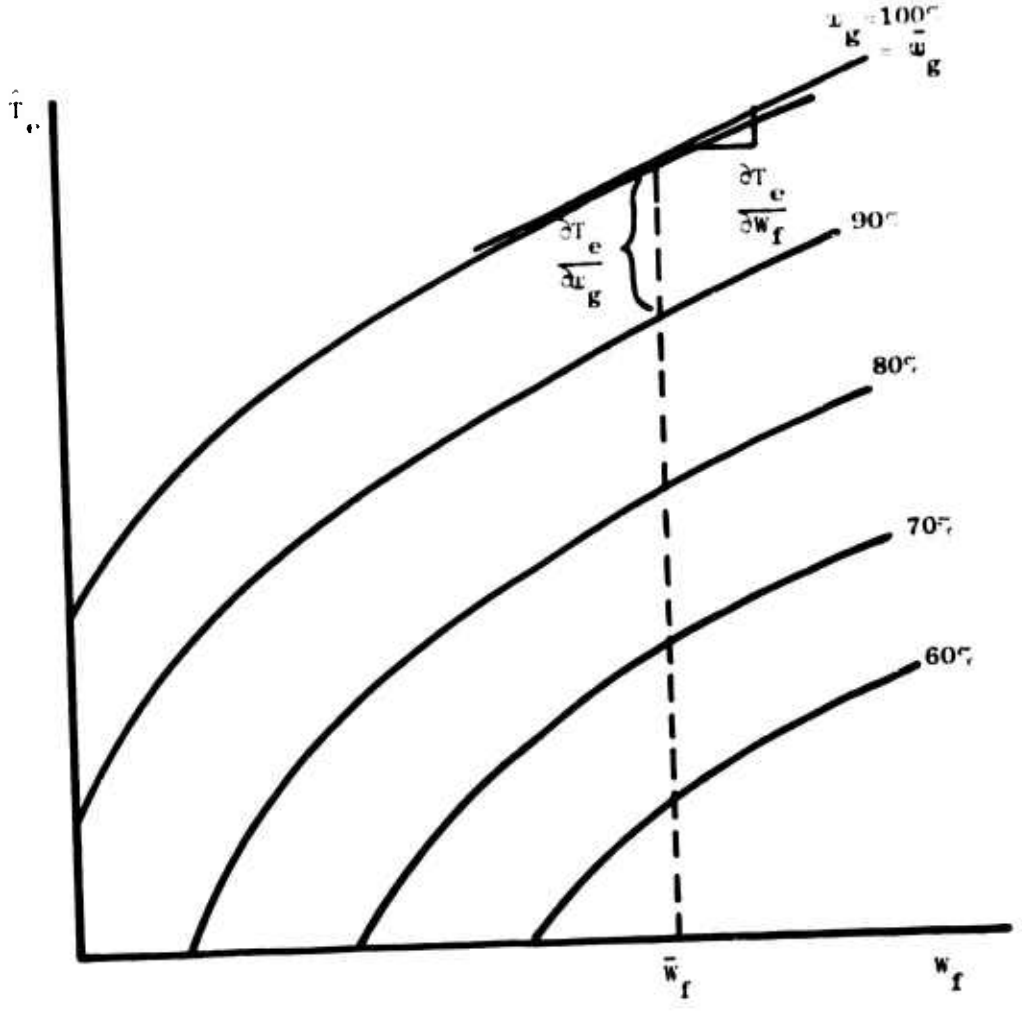

Figure 46. Engine Torque Versus Fuel Flow.

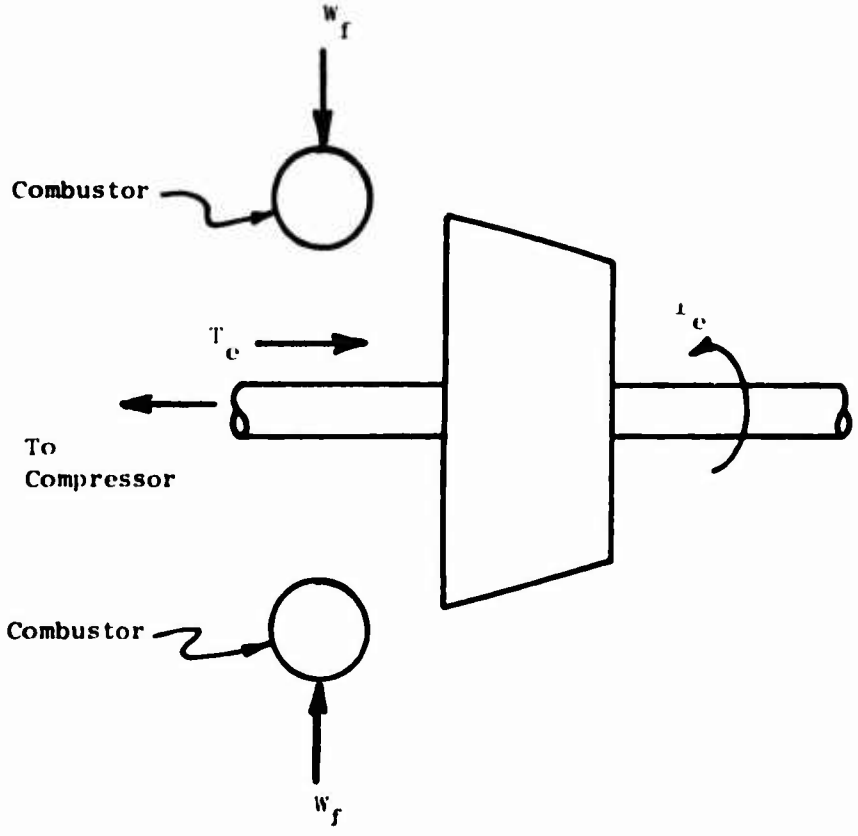

Figure 47. One-Spool Turbine Engine.

$$(\Omega - \omega_e) = \epsilon \tag{117}$$

$$M_g W_f(s) S^2 + C_g W_f(s) S + K_g W_f(s) = K_g Qa E(s) \tag{118}$$

The speed error, ϵ, is a variable rather than a constant, and therefore its Laplace transform is the Laplace function E(s). Equation 118 is rearranged to form equation (119). Also, since the system model is based on the assumption of small changes, the transfer function is written in terms of small changes in the system parameters.

$$\frac{\Delta W_f(s)}{\Delta E(s)} = \frac{K_g Qa}{m_g S^2 + C_g S + K_g} \tag{119}$$

Dividing the numerator and denominator of the transfer function by K_g results in equation 120.

$$\frac{\Delta W_f(s)}{\Delta E(s)} = \frac{Qa}{\frac{m_g}{k_g} S^2 + \frac{C_g}{K_g} S + 1} \tag{120}$$

The denominator of this transfer function can be factored, and with the substitutions of equations 121 through 123, equation 124 will be the resulting speed governor transfer function.

$$K_p = Qa \tag{121}$$

$$\tau_1 = \frac{C_g}{2K_g} - \sqrt{\frac{C_g^2}{4K_g^2} - \frac{M}{K_g}} \tag{122}$$

$$\tau_2 = \frac{C_g}{2K_g} + \sqrt{\frac{C_g^2}{4K_g^2} - \frac{M}{K_g}} \tag{123}$$

$$\frac{\Delta W_f(s)}{\Delta E(s)} = \frac{K_p}{(\tau_1 s + 1)(\tau_2 s + 1)} = Y_1(s) \tag{124}$$

Equation 124 is the same transfer function as given in Reference 5.

The transfer function for the complete turbine engine is derived from equations 114 and 115. The Laplace transform of those two equations is taken after the substitutions of equations 125 through 128 are made. Equations 129 and 130 result from equations 114 and 115 respectively.

$$\frac{\partial T_g}{\partial \omega_g} = C_1 \tag{125}$$

$$\frac{\partial T_g}{\partial W_f} = K_1 \tag{126}$$

$$\frac{\partial T_e}{\partial W_f} = K_2 \tag{127}$$

$$\frac{\partial T_e}{\partial \omega_g} = K_3 \tag{128}$$

$$I_g \Delta W_g(s) S = \Delta W_f(s) K_1 - \Delta W_g(s) C_1 \tag{129}$$

$$\Delta T_e(s) = \Delta W_f(s) K_2 + \Delta W_g(s) K_3 \tag{130}$$

It is advantageous to eliminate the gas producer speed Laplace function, $W_g(s)$, from the equations. This is accomplished by solving equation 129 for $W_g(s)$ and substituting the result into equation 130 to give equation 131.

$$\Delta T_e(s) = \Delta W_f(s) K_2 + \Delta W_f(s) \frac{K_1 K_3}{I_g s + C_1} \tag{131}$$

Both sides of the equation are divided by $\Delta W_f(s)$ and the terms on the right side of the equation are regrouped to form equation 132. Also, since the equation is based on the assumption of small changes, the system variables are written as small changes in system parameters.

$$\frac{\Delta T_e(s)}{\Delta W_f(s)} = \frac{I_q K_2 S + C_1 K_2 + K_1 K_3}{I_g s + C_1} \tag{132}$$

The transfer function is further rearranged and the substitutions of equations 133 through 135 are made in order to derive equation 136.

$$K_B = K_2 + \frac{K_1 K_3}{C_1} \tag{133}$$

$$\tau_e = \frac{I_g}{C_1} \tag{134}$$

$$\tau_B = \frac{I_g}{C_1 + \frac{K_1 K_3}{K_2}} \tag{135}$$

$$\frac{\Delta T_e(s)}{\Delta W_f(s)} = \frac{K_B(\tau_B S+1)}{(\tau_e s+1)} = Y_2(s) \tag{136}$$

This equation is the Laplace transfer function representing the two-spool turbine engine and gas producer. It is the same as the gas producer transfer function given in References 5 and 4.

The transfer function for the one-spool turbine engine is derived from equation 116. The Laplace transform is taken of this equation, and equation 127 is substituted in to give equation 137.

$$\Delta T_e(s) = K_2 \Delta W_f(s) \tag{137}$$

This leads to the transfer function given by equation 138, where K_2 is not numerically equal to the K_2 found in equation 133), since they are found from different curves.

$$\frac{\Delta T_e(s)}{\Delta W_f(s)} = K_2 = Y_2'(s) \tag{138}$$

K_2 from equation 137 is assumed to be of the order of magnitude of K_B from equation 136. That is, the steady-state gain of a one-spool turbine engine is assumed to be about the same as that for a two-spool turbine engine.

Equations 72 and 73 are used to derive the transfer function for the linearized drive train without a ZTS coupling. The Laplace transform of both equations is taken, resulting in equations 139 and 140 with the Δ's representing small changes in the system parameters, from their steady-state values, the same as the $\hat{}$'s in time domain.

$$I_{eg}\Delta W_e(s)S + C_T\Delta W_e(s) + C_s\Delta\theta_s(s)S + K_\theta\Delta\theta_s(s) = \Delta T_e(s) \tag{139}$$

$$I_r(\Delta W_e(s)S - \Delta\theta_s(s)S^2) + C_D(\Delta W_e(s) - \Delta\theta_s(s)S)$$

$$- C_s\Delta\theta_s(s)S - K_\theta\Delta\theta_s(s) = 0 \tag{140}$$

Equation 140 is solved for $\Delta\theta_s(s)$ to give equation 141.

$$\Delta\theta_s(s) = \Delta W_e(s)\ \frac{(I_R S + C_D)}{[I_R S^2 + (C_D + C_s)S + K_\theta]} \tag{141}$$

This is substituted into equation 139 in order to eliminate $\Delta\theta_s(s)$ from the transfer function, resulting in equation 142. This equation is consolidated to give equation 143.

$$I_{eg}\Delta W_e(s)S + C_T\Delta W_e(s) + \frac{(I_R S + C_D)(C_s S + K_\theta)\Delta W_e(S)}{[I_R S^2 + (C_D + C_s)S + K_\theta]}$$

$$= \Delta T_e(s) \tag{142}$$

$$\Delta W_e(s)\left\{\frac{I_{eg} I_R S^3 + (C_T I_R + C_s I_R + C_s I_{eg} + C_D I_{eg})S^2}{[I_R s^2 + (C_D + C_s)S + K_\theta]}\right.$$

$$\left. + \frac{[K_\theta(I_{eg} + I_R) + C_T(C_D + C_s) + C_D C_s]S + (C_T + C_D)K_\theta}{[I_R s^2 + (C_D + C_s)s + K_\theta]}\right\}$$

$$= \Delta T_e(s) \tag{143}$$

This equation is divided by $\Delta W_e(s)$ and inverted. Then, the substitutions of equations 144 through 149 are made in order to get the transfer function into the more tractable form of equation 150.

$$K_L = \frac{1}{C_D + C_T} \tag{144}$$

$$A_1 = \frac{I_R}{K_\theta} \tag{145}$$

$$A_2 = \frac{C_D + C_s}{K_\theta} \tag{146}$$

$$B_1 = \frac{I_{eg} I_R}{K_\theta(C_D + C_T)} \tag{147}$$

$$B_2 = \frac{I_{eg} C_D + I_R C_T + (I_{eg} + I_R)C_s}{K_\theta(C_D + C_T)} \tag{148}$$

$$B_3 = \frac{(I_{eg}+I_R)K_\theta + C_D C_T + C_D C_s + C_T C_s}{K_\theta (C_D + C_T)} \tag{149}$$

$$\frac{\Delta W_e(s)}{\Delta T_e(s)} = \frac{K_L (A_1 S^2 + A_2 S + 1)}{(B_1 S^3 + B_2 S^2 + B_3 S + 1)} = Y_3(s) \tag{150}$$

Equation 150 is the Laplace transfer function which represents a linearized helicopter drive train without a ZTS coupling.

The only Laplace transfer function left to derive for the Bode plot stability analysis is the one representing the linearized helicopter drive train with a ZTS coupling; that is, the system with the decoupled rotor represented by equations 76 and 77. Again, equation 77 has no effect on the engine speed and is therefore of no interest. This leaves just equation 76, which is reproduced as equation 151.

$$I_e \dot{\hat{\omega}}_e + C_T \hat{\omega}_e = \hat{T}_e \tag{151}$$

The Laplace transform of this equation is given by equation 152

$$I_e S \Delta W_e(s) + C_T \Delta W_e(s) = \Delta T_e(s) \tag{152}$$

Solving this equation for $\frac{\Delta W_e(s)}{\Delta T_e(s)}$ gives equation 153.

$$\frac{\Delta W_e(s)}{\Delta T_e(s)} = \frac{1}{I_e s + C_T} \tag{153}$$

The substitutions of equations 154 and 155 into equation 153 result in equation 156, which is the Laplace transfer function which represents a linearized helicopter drive train with a ZTS coupling.

$$K_{LC} = \frac{1}{C_T} \tag{154}$$

$$B_4 = \frac{I_e}{C_T} \tag{155}$$

$$\frac{\Delta W_e(s)}{\Delta T_e(s)} = \frac{K_{LC}}{B_4 S + 1} = Y_3'(s) \tag{156}$$

Equation 153 may also be derived by allowing the torsional stiffness, K_θ, and torsional damping, C_s, of the mast shaft to go to zero and replacing I_{eg} with I_e in equation 143, which is, in effect, what the ZTS coupling is supposed to do.

The total open-loop transfer function for a helicopter drive system without a ZTS coupling is given by the product of equations 124, 136, and 150, as shown in equation 157.

$$Y_0(s) = Y_1(s)Y_2(s)Y_3(s) = \frac{\Delta W_e(s)}{\Delta E(s)} = \frac{\Delta W_f(s)}{\Delta E(s)} \frac{\Delta T_e(s)}{\Delta W_f(s)}$$

$$\cdot \frac{\Delta W_e(s)}{\Delta T_e(s)} = \frac{K_p K_B K_L (\tau_B s+1)(A_1 s^2 + \quad_2 s+1)}{(\tau_1 s+1)(\tau_2 s+1)(\tau_e s+1)(B_1 s^3 + B_2 s^2 + B_3 s+1)} \tag{157}$$

The total open-loop transfer function for the system with a ZTS coupling, the product of equations 124, 136, and 156, is given in equation 158.

$$Y_0(s) = Y_1(s)Y_2(s)Y_3(s) = \frac{\Delta W_e(s)}{\Delta E(s)}$$

$$= \frac{K_p K_B K_{LC} (\tau_B s+1)}{(\tau_1 s+1)(\tau_2 s+1)(\tau_e s+1)(B_4 s+1)} \tag{158}$$

A flow chart of the closed-loop helicopter drive system is shown in Figure 48. Since it has unity feedback, the closed-loop transfer function can be found from the open-loop transfer function using equation 159.

$$Y_c(s) = \frac{Y_0(s)}{1 + Y_0(s)} \tag{159}$$

The open-loop transfer function represents the ratio of the engine speed to the speed error. This is substituted into equation 159 to form equation 160.

$$Y_c(s) = \frac{\dfrac{\Delta W_e(s)}{\Delta E(s)}}{1 + \dfrac{\Delta W_e(s)}{\Delta E(s)}} = \frac{\Delta W_e(s)}{\Delta W_e(s) + \Delta E(s)} \tag{160}$$

The Laplace transform of equation 117 is given in equation 161, which is substituted into equation 160, resulting in equation 162,

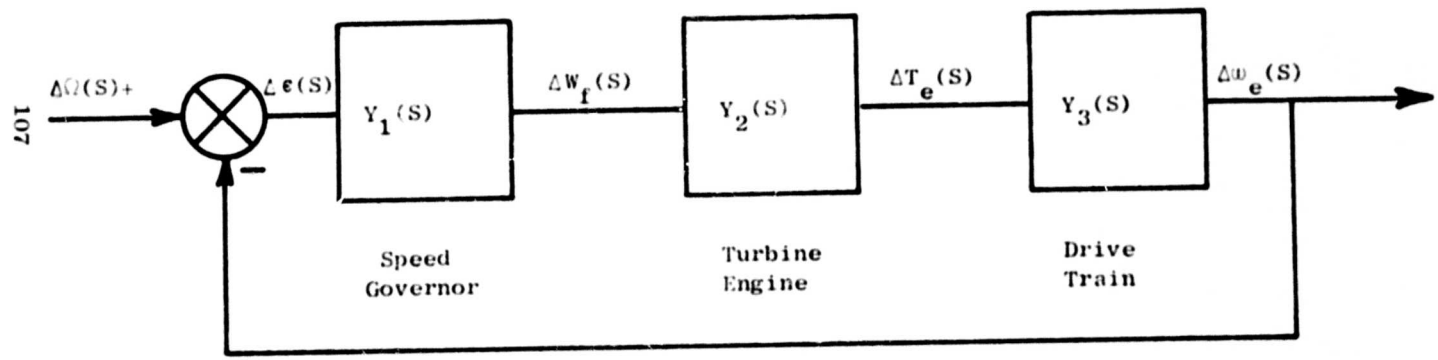

Figure 48. Block Diagram of Helicopter Drive System.

$$\Delta E(s) = \Delta\Omega(s) - \Delta W_e(s) \tag{161}$$

$$Y_c(s) = \frac{\Delta W_e(s)}{\Delta\Omega(s)} \tag{162}$$

To find the steady-state speed droop of the system, it is necessary to find the steady-state value for the engine speed. The transfer functions $Y_1(s)$ $Y_2(s)$, and $Y_2'(s)$ can be used in their present form. However, the engine and rotor damping coefficients of $Y_3(s)$ and $Y_3'(s)$ were derived for the purpose of giving a change in damping torques. In order to give the actual damping torques at steady-state operating conditions, it is necessary to use the average damping coefficients, which are equal to exactly half of the linearized damping coefficients. With this substitution in $Y_3(s)$, the Δ's are removed from equation 162. To find the steady-state droop, the set speed is considered to be a step input, and then the engine speed can be represented by equation 163.

$$W_e(s) = \bar{Y}_c(s)\,\frac{\Omega}{s} \tag{163}$$

In this equation, $\bar{Y}_c(s)$ is the closed-loop transfer function which will give the actual system parameters, with the intent of finding the steady-state system parameters.

The steady-state value of a Laplace transfer function can be found by using the final value theorem, given in equation 164.

$$\lim_{t\to\infty} Y(t) = \lim_{s\to 0} sY(s) \tag{164}$$

Using the final value theorem, the steady-state value of the engine speed is found in equation 165.

$$\bar{W}_e = \Omega\bar{Y}_c(0) \tag{165}$$

Substituting this equation into equation 65 for the steady-state speed droop results in equation 166.

$$SSD = (1 - \bar{Y}_c(0)) \times 100 \tag{166}$$

For the helicopter drive system without the ZTS coupling, $\bar{Y}_c(0)$ is given by equation 167.

$$\bar{Y}_c(0) = \frac{2K_pK_BK_2}{1 + 2K_pK_BK_L} \tag{167}$$

Therefore, the steady-state speed droop of the system without the ZTS coupling is given by equation 168.

$$SSD = \left(\frac{1}{1 + 2K_p K_B K_L}\right) \times 100 \tag{168}$$

For the system with a ZTS coupling, the transfer function $Y_3(s)$ was determined for small changes such that a constant torque, Tc, was dropped from the governing equations. Consequently, that transfer function cannot be used to determine the steady-state system parameters, since they would all be off by some factor of that constant torque. Therefore, the above procedure cannot be used to find the steady-state speed droop for a helicopter drive system with a ZTS coupling.

The steady-state speed droop can also be derived directly from the differential equations of motion. This method of derivation is applicable whether the system has a ZTS coupling or not. An attempt is made to find the stationary values, or steady-state solutions, of the system parameters. This is done by setting the highest time derivatives in the system differential equations equal to zero, and solving for the system parameters. For a helicopter drive system without a ZTS coupling, equations 68, 69, 112, 114, and 115, at steady state, become equations 169 through 173 respectively. The engine and rotor damping terms are replaced by the average linearized damping terms.

$$\frac{C_T}{2}\bar{\omega}_e + C_s\bar{\dot{\theta}}_s + K_\theta\theta_s = \bar{T}_e \tag{169}$$

$$\frac{C_D}{2}(\bar{\omega}_e - \bar{\dot{\theta}}_s) - C_s\bar{\dot{\theta}}_s - K_\theta\theta_s = 0 \tag{170}$$

$$\bar{W}_f = Oa(\Omega - \bar{\omega}_e) \tag{171}$$

$$\bar{W}_f \frac{\partial T_g}{\partial W_f} = \bar{\omega}_g \frac{\partial T_g}{\partial \omega_g} \tag{172}$$

$$\bar{T}_e = \bar{W}_f \frac{\partial T_e}{\partial W_f} + \bar{\omega}_g \frac{\partial T_e}{\partial \omega_g} \tag{173}$$

Also, the values of the partial derivatives of equations 172 and 173 are assumed to be constant all the way from zero to steady-state engine speed, for the purpose of determining the steady-state system parameters only. Since $\bar{\dot{\theta}}_s$ is equal to zero at steady state, equations 169 and 170 reduce to equations 174 and 175.

$$\frac{C_T}{2}\bar{\omega}_e + K_\theta\bar{\theta}_s = \bar{T}_e \tag{174}$$

$$\frac{C_D}{2}\bar{\omega}_e - K_\theta\bar{\theta}_s = 0 \tag{175}$$

Equations 171 through 173 are manipulated in order to get equations for the steady-state values for the system parameters as functions of the steady-state engine speed. This results in equations 176 through 178.

$$\bar{W}_f = Qa(\Omega - \bar{\omega}_e) \tag{176}$$

$$\bar{\omega}_g = Qa(\Omega - \bar{\omega}_e)\frac{(\frac{\partial T_g}{\partial W_f})}{(\frac{\partial T_g}{\partial \omega_g})} \tag{177}$$

$$\bar{T}_e = Qa(\Omega - \bar{\omega}_e)\left[\frac{\partial T_e}{\partial W_f} + \frac{\partial T_e}{\partial \omega_g}\frac{(\frac{\partial T_g}{\partial W_f})}{(\frac{\partial T_g}{\partial \omega_g})}\right] \tag{178}$$

Using the substitutions of equations 117, 121, 125 through 128, and 133), these reduce to equations 179 through 181.

$$\bar{W}_f = K_p\bar{\epsilon} \tag{179}$$

$$\bar{\omega}_g = K_p\bar{\epsilon}\frac{K_1}{C_1} \tag{180}$$

$$\bar{T}_e = K_pK_B\bar{\epsilon} \tag{181}$$

Equations 174 and 175 are added together and equation 181 is used to substitute for $\bar{T}_e$, giving equation 182.

$$1/2(C_T + C_D)\bar{\omega}_e = K_pK_B\bar{\epsilon} \tag{182}$$

Using equation 144 and resubstituting for the speed error from equation 117 results in equation 183.

$$\bar{\omega}_e = 2K_pK_BK_L(\Omega - \bar{T}_e) \tag{183}$$

Solving for the steady-state engine speed gives equation 184, and inserting this into equation 65 gives equation 185.

$$\bar{\epsilon}_e = \left(\frac{2K_p K_B K_L}{1 + 2K_p K_B K_L}\right)\Omega \tag{184}$$

$$SSD = \left(\frac{1}{1 + 2K_p K_B K_L}\right) \times 100 \tag{185}$$

Equations 168 and 185 are identical.

The above procedure is repeated for a helicopter drive system with a ZTS coupling. Equations 74 and 75 with the average linearized engine and rotor damping terms become equations 186 and 187 at steady state.

$$\frac{1}{2} C_T \bar{\epsilon}_e = \bar{T}_e - T_c \tag{186}$$

$$\frac{1}{2} C_D \bar{\epsilon}_R = T_c \tag{187}$$

Equations 186 and 187 are added and equation 181 is used to substitute for $\bar{T}_e$, giving equation 188, considering that the steady-state engine speed is equal to the steady-state rotor speed.

$$\frac{1}{2} (C_T + C_D)\bar{\epsilon}_e = K_p K_B \bar{\epsilon} \tag{188}$$

Using equation 144 and resubstituting for the speed error from equation 117 results in equation 189.

$$\epsilon_e = 2K_p K_B K_L (\Omega - \bar{\epsilon}_e) \tag{189}$$

Solving this equation for the steady-state engine speed gives equation 190, and inserting this into equation 65 gives equation 191.

$$\bar{\epsilon}_e = \left[\frac{2K_p K_B K_L}{1 + 2K_p K_B K_L}\right]\Omega \tag{190}$$

$$SSD = \left[\frac{1}{1 + 2K_p K_B K_L}\right] \times 100 \tag{191}$$

It can be seen from equations 185 and 191 that the steady-state speed droop for this helicopter drive system is the same whether or not it has a ZTS coupling.

BODE ANALYSIS OF THE LINEAR SYSTEM

A Bode plot of a frequency transfer function is a plot of the gain and phase of the transfer function versus frequency. The frequency transfer functions of interest are derived by taking the open-loop transfer functions of equations 157 and 158 and making the substitution of equation 192.

$$s = j\omega \tag{192}$$

This results in equations 193 and 194.

$$F_1(j\omega) = \frac{K_p K_B K_L (\tau_B j\omega+1)[A_1(j\omega)^2+A_2 j\omega+1]}{(\tau_1 j\omega+1)(\tau_2 j\omega+1)(\tau_e j\omega+1)[B_1(j\omega)^3+B_2(j\omega)^2+B_3 j\omega+1]} \tag{193}$$

$$F_2(j\omega) = \frac{K_p K_B K_{LC} (\tau_B j\omega+1)}{(\tau_1 j\omega+1)(\tau_2 j\omega+1)(\tau_e j\omega+1)(B_1 j\omega+1)} \tag{194}$$

The gain of the frequency transfer function $F(j\omega)$, given by equation 195, is expressed in decibels.

$$\text{GAIN}(\omega) = 20 \log |F(j\omega)| \tag{195}$$

The phase of the same frequency transfer function is given by equation 196 and is expressed in degrees.

$$\text{PHASE}(\omega) = \angle F(j\omega)$$

where

$$-180 \text{ degrees} \leq \angle F(j\omega) \leq 180 \text{ degrees} \tag{196}$$

A Bode plot is actually comprised of two plots. One plot is of the gain of the frequency transfer function versus ω and the other plot is of the phase of the frequency transfer function, versus ω. The gain margin for a frequency transfer function is defined as the gain increase needed to drive the system unstable.[14] The gain margin is calculated as the negative of the gain at the point of phase crossover. The phase crossover is where the phase plot crosses over 180 degrees, or minus 180 degrees. The phase margin is equal to the phase shifted 180 degrees at the point of gain crossover. The gain crossover is where the gain plot crosses over zero decibels. If the gain or phase margin of a system is negative, then that system is unstable. If the gain and phase margins of a system are both positive, then that system will converge to some steady-state operating condition following a perturbation. However, the lower the gain or phase margin, the longer the system will take to stabilize.

For the type of helicopter drive system under discussion, a minimum gain margin of 4 to 6 decibels and phase margin of 20 to 30 degrees is necessary to achieve an acceptable transient response.[5]

The helicopter drive system of interest is the helicopter analyzed in Reference 5 with a normal operating engine power output of 5270 horsepower at a speed of 13,820 revolutions per minute or 1447 radians per second. It is assumed that at steady-state operating conditions, all of this power is dissipated as aerodynamic rotor damping. Torsional aerodynamic damping is generally assumed to be of the form of equation 197.

$$T_L = C_L \omega_R^{-2} \tag{197}$$

The relationship of torque to horsepower and speed is given in equation 198, with speed in radians per second and torque in foot-pounds.

$$T_L = \frac{550 \text{ hp}}{\bar{\omega}_e} \tag{198}$$

The value for C_L can be found by substituting the torque from equation 198 into equation 197 and solving for the damping coefficient. The result is given as equation 199.

$$C_L = 9.564 \times 10^{-4} \text{ ft-lb (rad per sec)}^2 \tag{199}$$

From equation 71 the linearized rotor damping coefficient is calculated and given in equation 200.

$$C_D = 2.768 \text{ ft-lb rad sec} \tag{200}$$

Since the model for the helicopter power plant is borrowed from Reference 5, then it is reasonable to use the helicopter drive train and speed governor models from the same reference. The system parameters for the direct fuel flow speed governor of Reference 5 are given as follows:

$$\tau_1 = 0.02 \text{ sec}$$

$$\tau_2 = 0.03 \text{ sec}$$

The gas producer and turbine engine from the same reference have the following system parameters:

$$K_b = 0.914 \frac{\text{ft-lb}}{\text{lb/hr}}$$

$$\tau_B = 0.1869 \text{ sec}$$

$$\tau_e = 0.3 \text{ sec}$$

$$K_2 = 0.57 \frac{\text{ft-lb}}{\text{lb/hr}}$$

$$K_3 = 3.2563 \frac{\text{ft-lb}}{\text{rad/sec}}$$

The drive train system parameters, as referenced to the engine design speed, from Reference 5 are as follows:

$$I_e = 0.5 \frac{\text{ft-lb}}{\text{rad/sec}^2}$$

$$I_{gb} = 0.1944 \frac{\text{ft-lb}}{\text{rad/sec}^2}$$

$$I_R = 3.888 \frac{\text{ft-lb}}{\text{rad/sec}^2}$$

$$K_{TM} = 21,417 \frac{\text{ft-lb}}{\text{rad}}$$

$$K_\theta = 93.0 \text{ to } 837.3 \frac{\text{ft-lb}}{\text{rad}}$$

The torquemeter stiffness, K_{TM}, is at least 25 times the mast stiffness, K_θ. Therefore, the torquemeter can be assumed to be rigid as compared to the mast. The range of mast stiffness listed will give the required critical frequencies of the model of 2 to 6 cycles per second. In order to reproduce the stability results reported in Reference 5 for the direct fuel flow speed governor, it is necessary to use a mast stiffness of about 800 foot-pounds per radian, corresponding to a critical frequency of about 5.86 cycles per second.

The shaft damping, C_s, is assumed to be about 5 percent of the critical shaft damping for the torsional two-degree-of-freedom system. The critical shaft damping for such a system is represented by equation 201.

$$C_{SCR} = 2 \sqrt{K_\theta \frac{I_{eg} I_R}{I_{eg} + I_R}} \tag{201}$$

Using the system parameter values given above, the critical shaft damping is found. Five percent of that value gives the shaft damping used; see equation 202.

$$C_s = 2.24 \text{ ft-lb/rad/sec} \tag{202}$$

The torque necessary to overcome the turbine damping is assumed to be about 40 percent of the load torque of equation 198. The turbine damping is assumed to be aerodynamic, as shown in equation 203.

$$T_T = C_e \omega_e^{-2} \tag{203}$$

Using T_T, equal to 40 percent of T_L, and equation 203, C_e is calculated and given in equation 204.

$$C_e = 3.82 \times 10^{-4} \text{ ft-lb (rad sec)}^2 \tag{204}$$

The linearized turbine damping coefficient is calculated from equation 70 and is given in equation 205.

$$C_T = 1.106 \text{ ft-lb/rad/sec} \tag{205}$$

The gain of the drive train, K_L, is a function of the linearized turbine and rotor damping, and is found in equation 206.

$$K_L = \frac{1}{C_T + C_D} = 0.258 \text{ rad/sec/ft-lb} \tag{206}$$

The only system parameter of this helicopter drive system model which is not yet specified is the governor gain, K_p. Equation 168, for the steady-state speed droop, can be solved for the governor gain resulting in equation 207.

$$K_p = \frac{100\text{-SSD}}{2K_B K_L (\text{SSD})} \tag{207}$$

With a 5-percent steady-state speed droop (standard for this type of helicopter drive system[5]) and values of K_B and K_L from above, K_p is calculated and given in equation 208.

$$K_p = 40.27 \text{ lb/hr/(rad/sec)} \tag{208}$$

The transfer functions used in Reference 5 for the direct fuel flow speed governor and the gas producer and turbine engine are identical to those derived in this report. However, the transfer function for the drive train used in Reference 5, given by equation 209, is a simplification of the one derived in this report, given by equation 150.

$$\frac{\Delta W_e(s)}{\Delta T_e(s)} = K_L \frac{\left[\left(\frac{S}{\omega_r}\right)^2 + \left(\frac{2\xi_r}{\omega_r}\right)S+1\right]}{(\tau_L S+1)\left[\left(\frac{S}{\omega_n}\right)^2 + \left(\frac{2\xi_n}{\omega_n}\right)S+1\right]} = Y_3(s) \qquad (209)$$

This transfer function is derived in Appendix V. To obtain equation 209 from equation 150, first shaft damping is set equal to zero. Then, the denominator is approximately factored and the following substitutions are made:

$$K_L = \frac{1}{C_T + C_D}$$

$$\tau_L = \frac{I_{eg} + I_R}{C_T + C_D}$$

$$\omega_r = \sqrt{\frac{K_\theta}{I_R}}$$

$$\omega_n = \sqrt{\frac{K_\theta (I_{eg}+I_R)}{I_{eg} I_R}}$$

$$\xi_r = \frac{C_D}{2\sqrt{K_\theta I_R}}$$

$$\xi_n = \frac{C_D I_{eg}^2 + C_T I_R^2}{2\sqrt{K_\theta I_R I_{eg}}(I_{eg}+I_R)^{3/2}}$$

The error introduced by the approximate factoring is negligible. However, the error introduced by ignoring the shaft damping can be significant. In fact, for the value of damping given by equation 202, the error of stability margin for the helicopter drive system of Reference 5 is considerable. This will be demonstrated by a comparison of the gain and phase margins of the helicopter drive system model of Reference 5 with zero shaft damping and with the value of shaft damping calculated above. The gain and phase margins are found from Bode plots which are made by inserting incremental values of 0.01 to 10.0 cycles per second into the frequency transfer functions representing the helicopter drive system model with

1. Zero shaft damping--from equation 193

2. Nonzero shaft damping--from equation 193

3. A ZTS coupling in the drive shaft--from equation 194

The resulting Bode plots are given in Figures 49, 50, and 51 respectively. The gain and phase margins are given in Table I. It can be seen that the addition of shaft damping makes the unstable system of Reference 5 stable. However, it still does not meet the minimum phase margin criteria, in order to give an acceptable transient response. It can also be seen that the addition of a ZTS coupling gives a system stability which is better than the zero shaft damping case, but is not significantly better than the case with shaft damping. Furthermore, the system with the ZTS coupling does not meet the minimum phase margin criteria. Therefore, it appears, at least for the linearized model, that the addition of a ZTS coupling to the helicopter drive system of Reference 5 does not increase the stability of that system enough to be acceptable.

The points for the Bode plots are calculated and plotted by the computer program listed in Appendix VI. The same computer program also makes Bode plots for the two helicopter drive systems using two, other, more sophisticated, speed governors. These two speed governors are typical examples of the results of adding additional dynamics to a direct fuel flow speed governor in order to achieve stability. Unfortunately, they also add additional cost and complexity to the direct fuel flow speed governor. One of these other speed governors is a direct fuel flow speed governor with lagged gain reset. It is basically similar to a direct fuel flow speed governor with the addition of a feedback loop from the speed governor output to vary its speed setting. This feedback loop acts as a reset function through a time lag.[5] Block diagrams for a direct fuel flow speed governor and a direct fuel flow speed governor with lagged gain reset are reproduced from Reference 5 in Figures 52 and 53, respectively. A transfer function for the second type of speed governor is found from Figure 53 and is given in equation 210.

$$\frac{\Delta W_f(s)}{\Delta E(s)} = \frac{\dfrac{K_t}{(1-K_r)}(\tau_r S+1)}{(\tau_1 S+1)\left|\dfrac{\tau_r}{1-K_r} S+1\right|(\tau_2 S+1)} = Y_1(s) \qquad (210)$$

Bode plots of the helicopter system without a ZTS coupling, using a direct fuel flow speed governor with lagged gain reset, are given in Figure 54 for zero shaft damping and in Figure 55 for nonzero shaft damping. To get these Bode plots, values of 0.2 second for the reset time constant, τ_r, and 0.5 (dimensionless) for the reset gain, K_r, are used.[5] Also, a value of 20.14 pounds per hour, per radian per second, is used for the speed

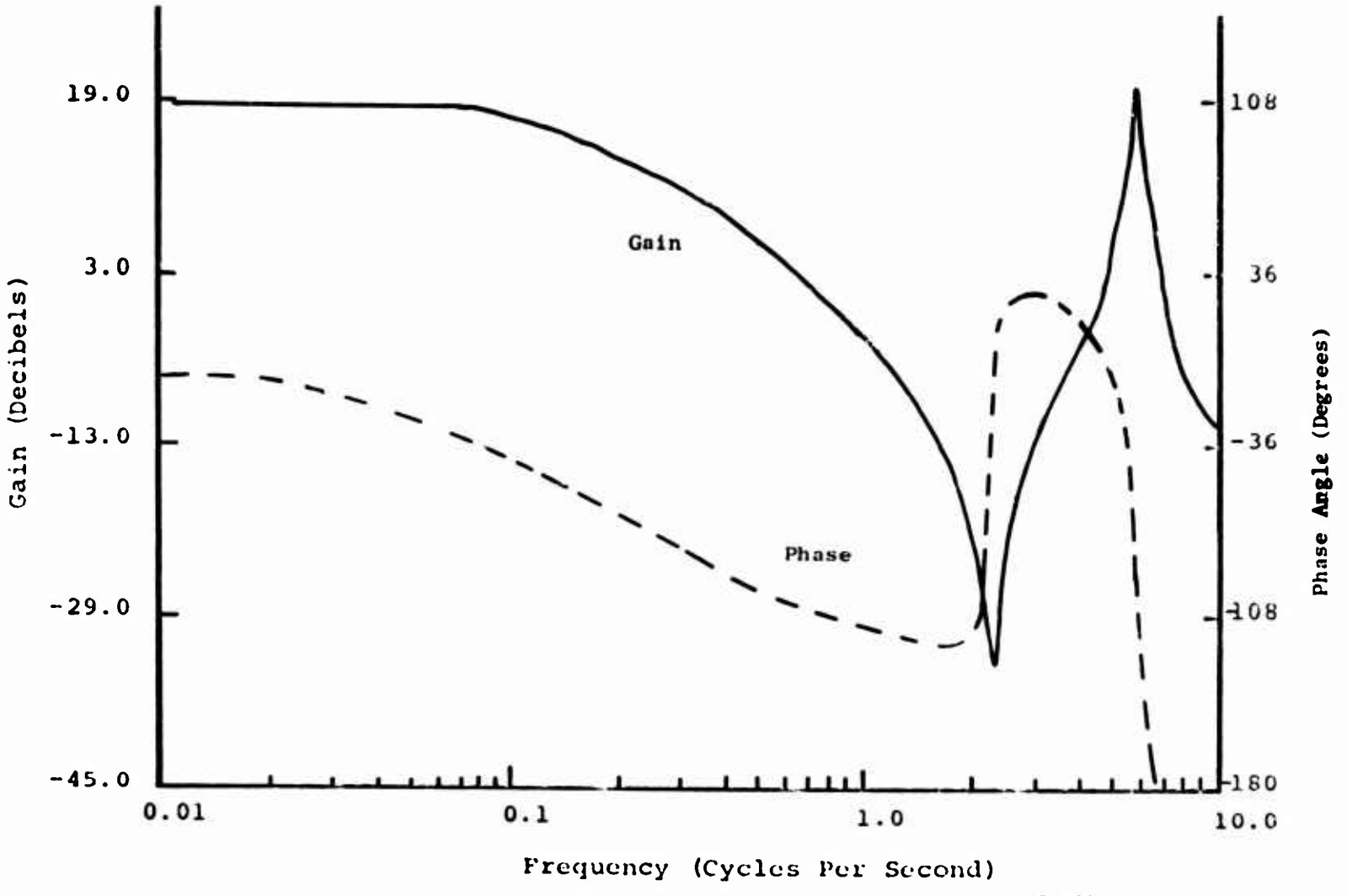

Figure 49. Bode Plots--Direct Fuel Flow Governor, $C_s = 0.0 \frac{ft\text{-}lb}{rad/sec}$.

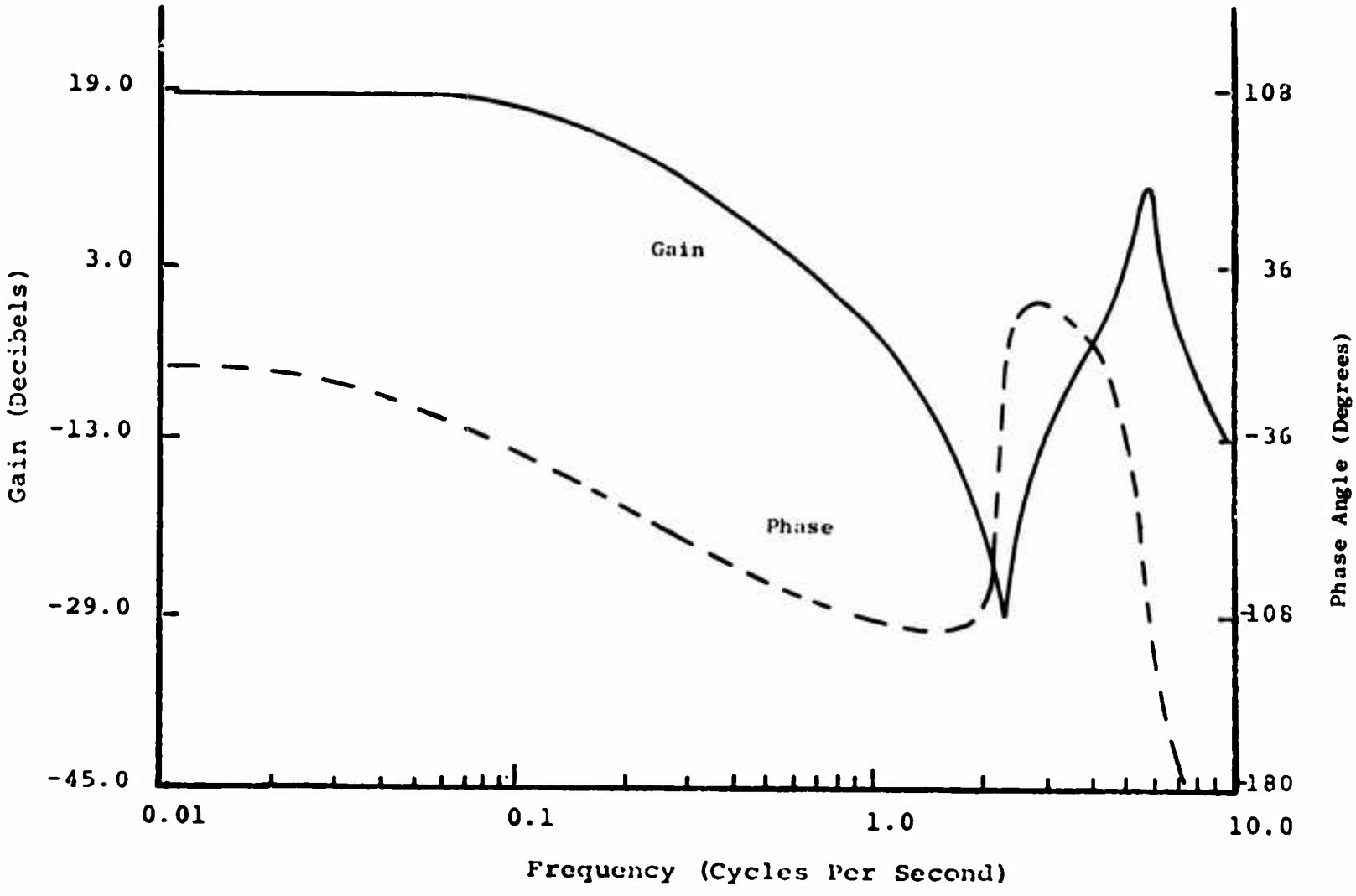

Figure 50. Bode Plots--Direct Fuel Flow Governor, $C_s = 2.24 \frac{\text{ft-lb}}{\text{rad/sec}}$.

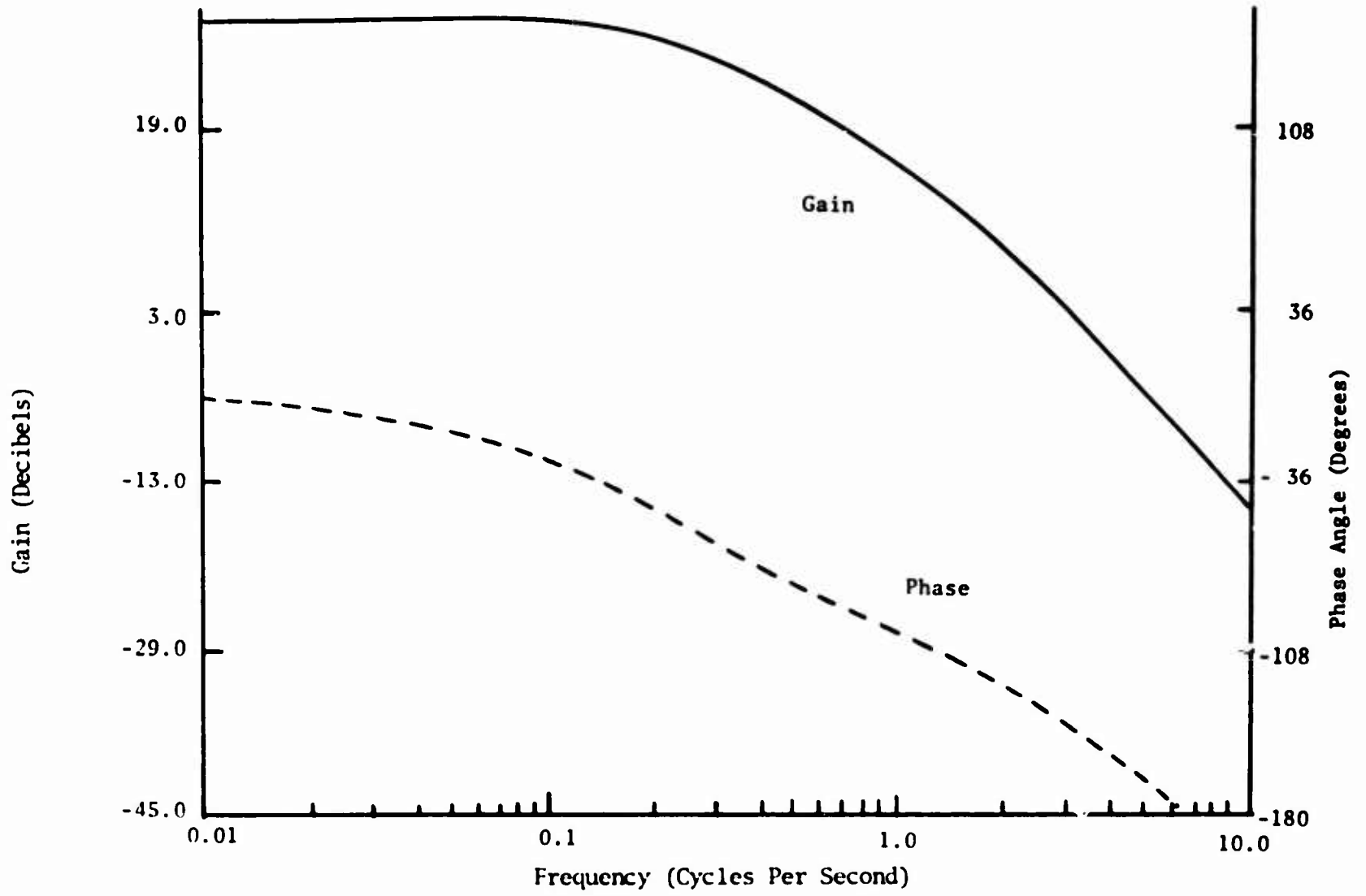

Figure 51. Bode Plots--Direct Fuel Flow Governor With ZTS Coupling (Decoupled Rotor Model).

TABLE I. RESULTS OF BODE ANALYSIS

Type of Speed Governor	Type of Turbine Engine	ZTS Coupling	C_s (ft-lb/rad per sec)	Gain Margin (db)	Phase Margin (deg)
Direct fuel flow	Two-spool	Without	0.0	-0.44	-0.7
Direct fuel flow	Two-spool	Without	2.24	5.4	15.7
Direct fuel flow	Two-spool	With	0.0	5.25	18.1
Direct fuel flow with lagged gain reset	Two-spool	Without	0.0	0.9	2.1
Direct fuel flow with lagged gain reset	Two-spool	Without	2.24	10.2	53.6
Direct fuel flow/compressor discharge pressure with lagged gain reset	Two-spool	Without	0.0	9.9	25.0
Direct fuel flow/compressor discharge pressure with lagged gain reset	Two-spool	Without	2.24	17.5	43.3

TABLE I - Continued

Type of Speed Governor	Type of Turbine Engine	ZTS Coupling	C_s (ft-lb/rad per sec)	Gain Margin (db)	Phase Margin (deg)
Direct fuel flow	One-spool	Without	0.0	-2.9	-4.8
Direct fuel flow	One-spool	Without	2.24	2.2	5.9
Direct fuel flow	One-spool	With	0.0	2.0	6.9

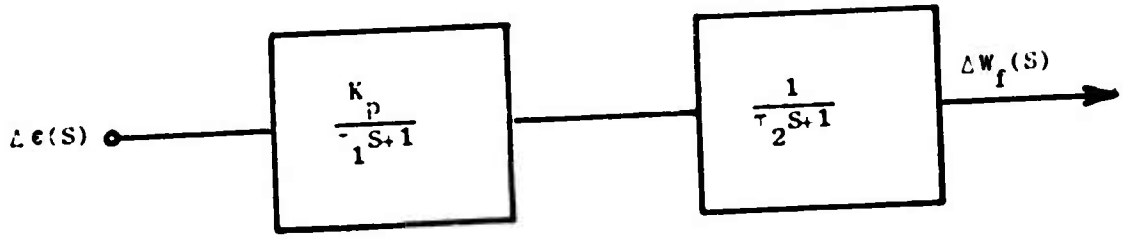

Figure 52. Direct Fuel Flow Speed Governor Block Diagram.

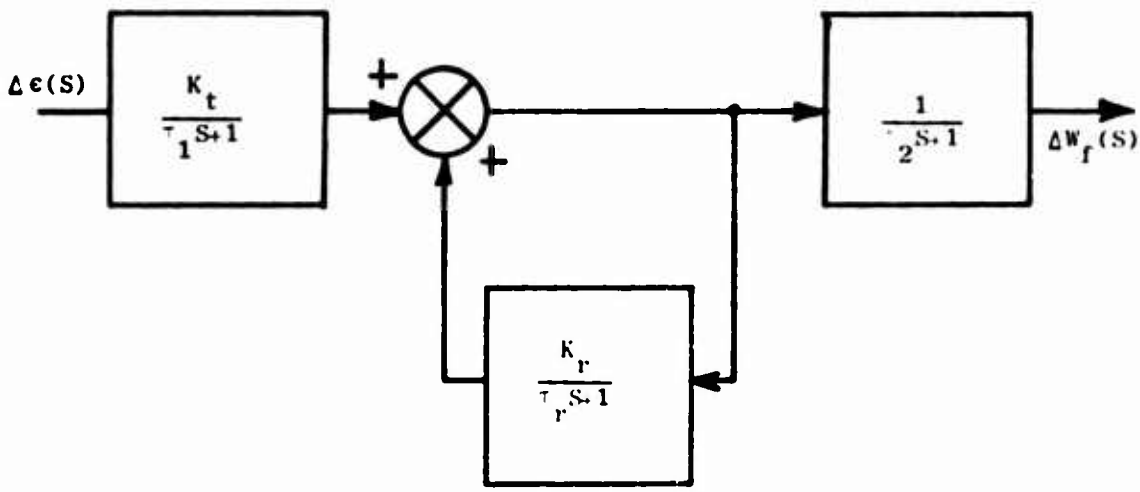

Figure 53. Direct Fuel Flow Speed Governor With Lagged Gain Reset Block Diagram.

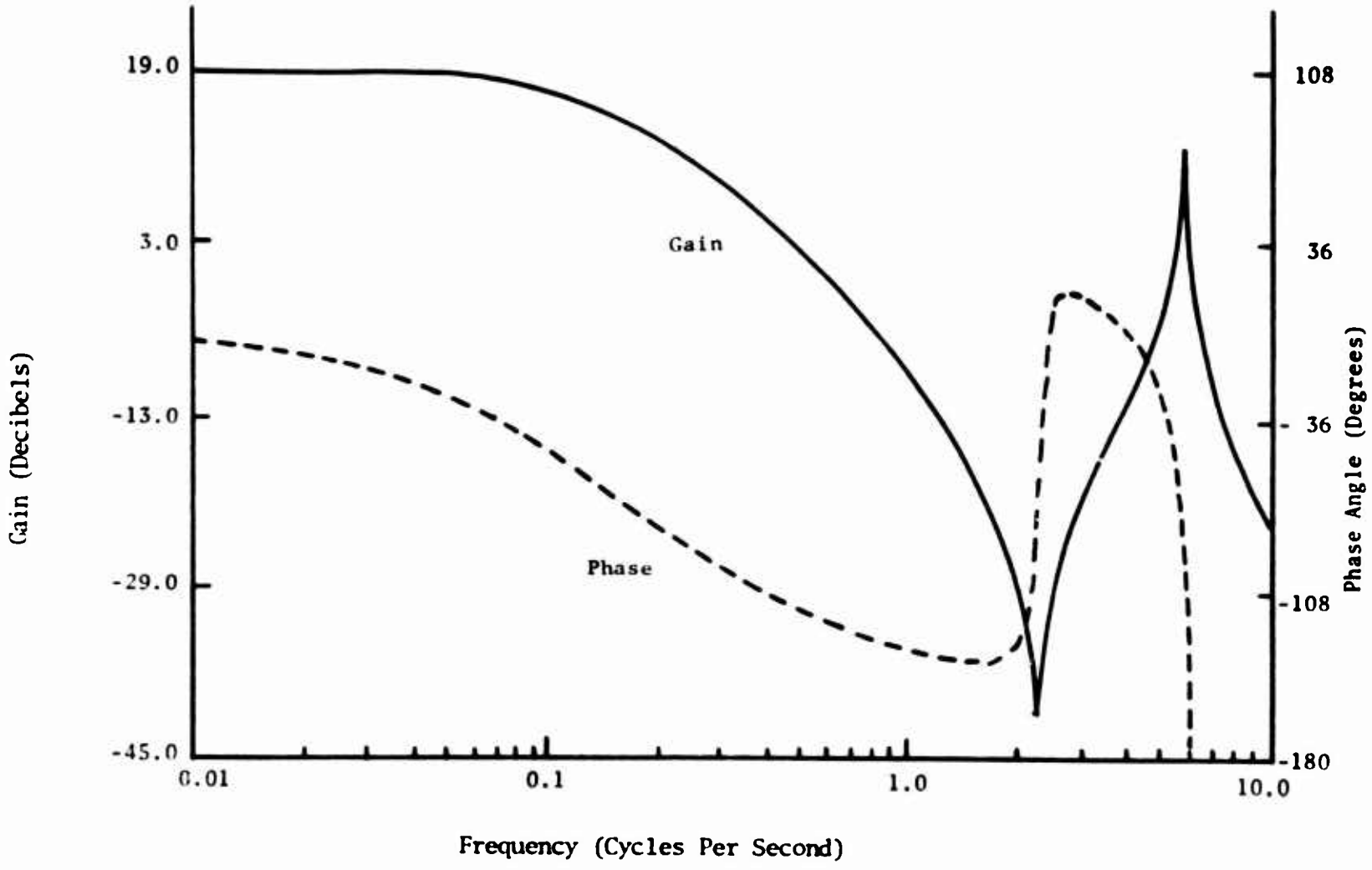

Figure 54. Bode Plots--Direct Fuel Flow/Lagged Gain Reset, $C_s = 0.0 \frac{\text{ft-lb}}{\text{rad/sec}}$.

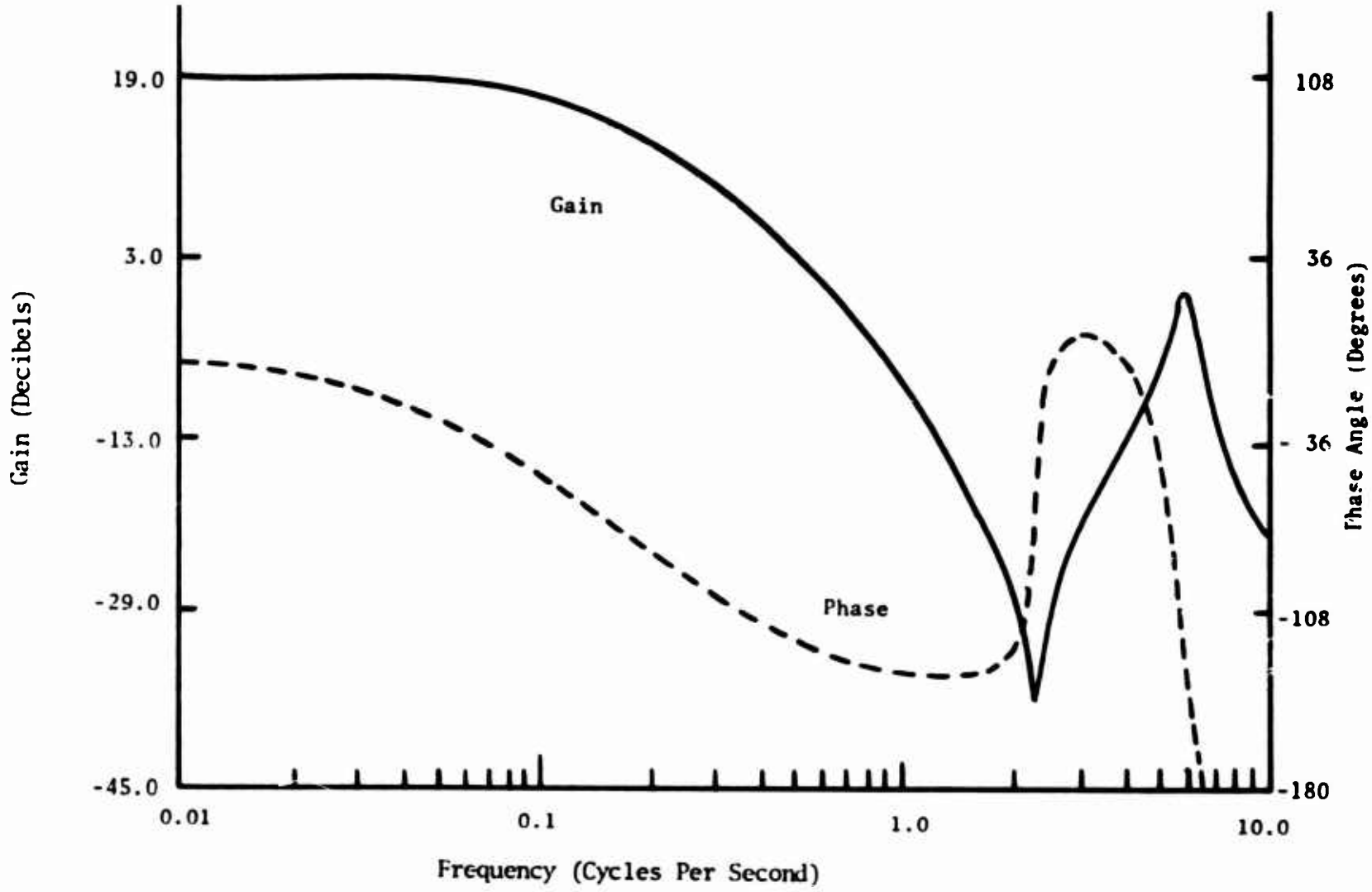

Figure 55. Bode Plots--Direct Fuel Flow/Lagged Gain Reset, $C_s = 2.24 \frac{\text{ft-lb}}{\text{rad/sec}}$.

governor proportional gain, K_t, to retain a 5-percent steady-state speed droop. Then equation 210 is used in place of equation 124 in finding the open-loop transfer function of the helicopter drive system, used to get the frequency transfer function, which subsequently yields the Bode plots for the system, using the computer program in Appendix VI. The gain and phase margins determined from all of these Bode plots are given in Table II. It can be seen that this system is stable even with zero shaft damping, although it does not meet the minimum gain or phase margin criteria for a practical system. However, with the nonzero value of shaft damping used, this system is not only stable, but it easily meets and exceeds those minimum gain and phase margin criteria. This demonstrates the value of adding complexity to the speed governor.

The other, even more complex, type of speed governor presented is a direct fuel flow compressor discharge pressure speed governor with lagged gain reset. This type of speed governor is very similar to a direct fuel flow speed governor with lagged gain reset, with the further addition of a feedback signal from the compressor discharge pressure to be used as an additional criterion for determining the fuel flow.[5]

A block diagram for a direct fuel flow compressor discharge pressure speed governor with lagged gain reset is reproduced from Reference 5 in Figure 56. A transfer function for this type of governor is found in the same reference and is given by equation 211.

$$\frac{\Delta W_f(s)}{\Delta E(s)} = \frac{\dfrac{K_t}{(1-K_r)}(\tau_r S+1)(\tau_e S+1)}{(\tau_I S+1)\left[\left(\dfrac{\tau_r}{1-K_r}\right)S+1\right](\tau_1 S+1)(\tau_2 S+1)}$$

$$= Y_1(s) \qquad (211)$$

Bode plots are made of the helicopter drive system without a ZTS coupling, with a direct fuel flow compressor discharge pressure speed governor with lagged gain reset, with zero and nonzero shaft damping, using the same method as outlined above, and are given in Figures 57 and 58 respectively. To get this Bode plot, in addition to the values given above, a value of 0.773 second is used for τ_I.[5] The gain and phase margins from these Bode plots are given in Table II. It can be seen from the positive gain and phase margins that this system is not only stable, but it meets the minimum gain and phase margin criteria, with either zero or nonzero shaft damping. Also, it is more stable than either of the speed governors previously presented, but is also much more complex.

It was previously shown that the helicopter drive system with an ideal speed governor and no gas producer dynamics (one-spool turbine engine) is stable, whether or not it includes a ZTS coupling. This is substantiated

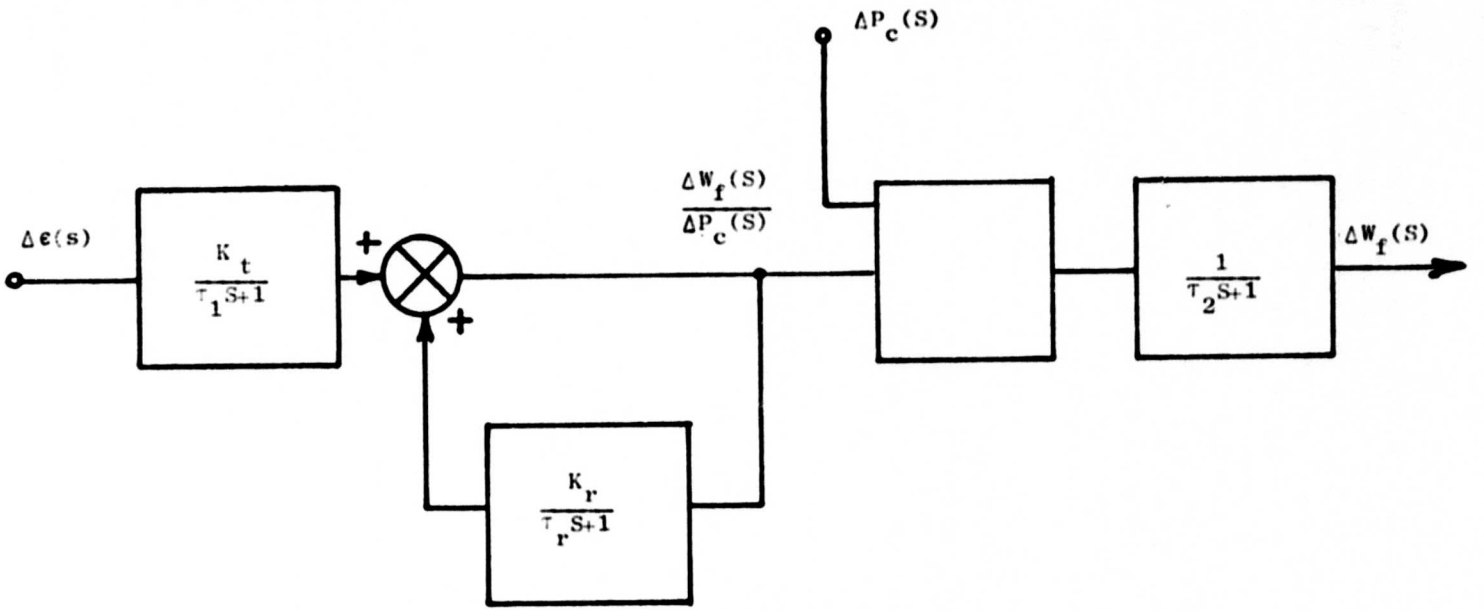

Figure 56. Direct Fuel Flow/Compressor Discharge Pressure Speed Governor With Lagged Gain Reset.

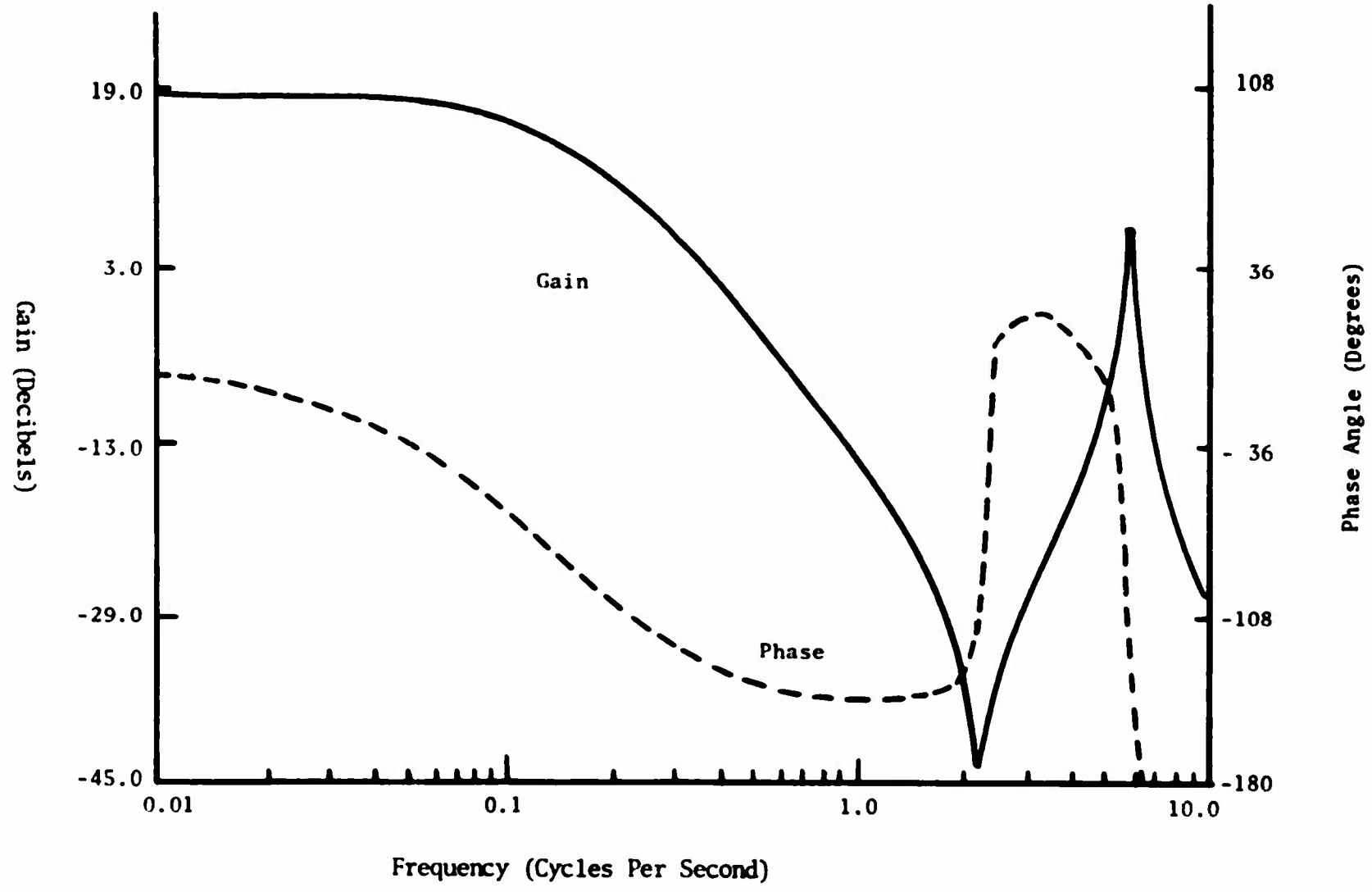

Figure 57. Bode Plots--Fuel Flow/Compressor Discharge Pressure/Lagged Gain Reset, $C_s = 0.0 \frac{\text{ft-lb}}{\text{rad/sec}}$.

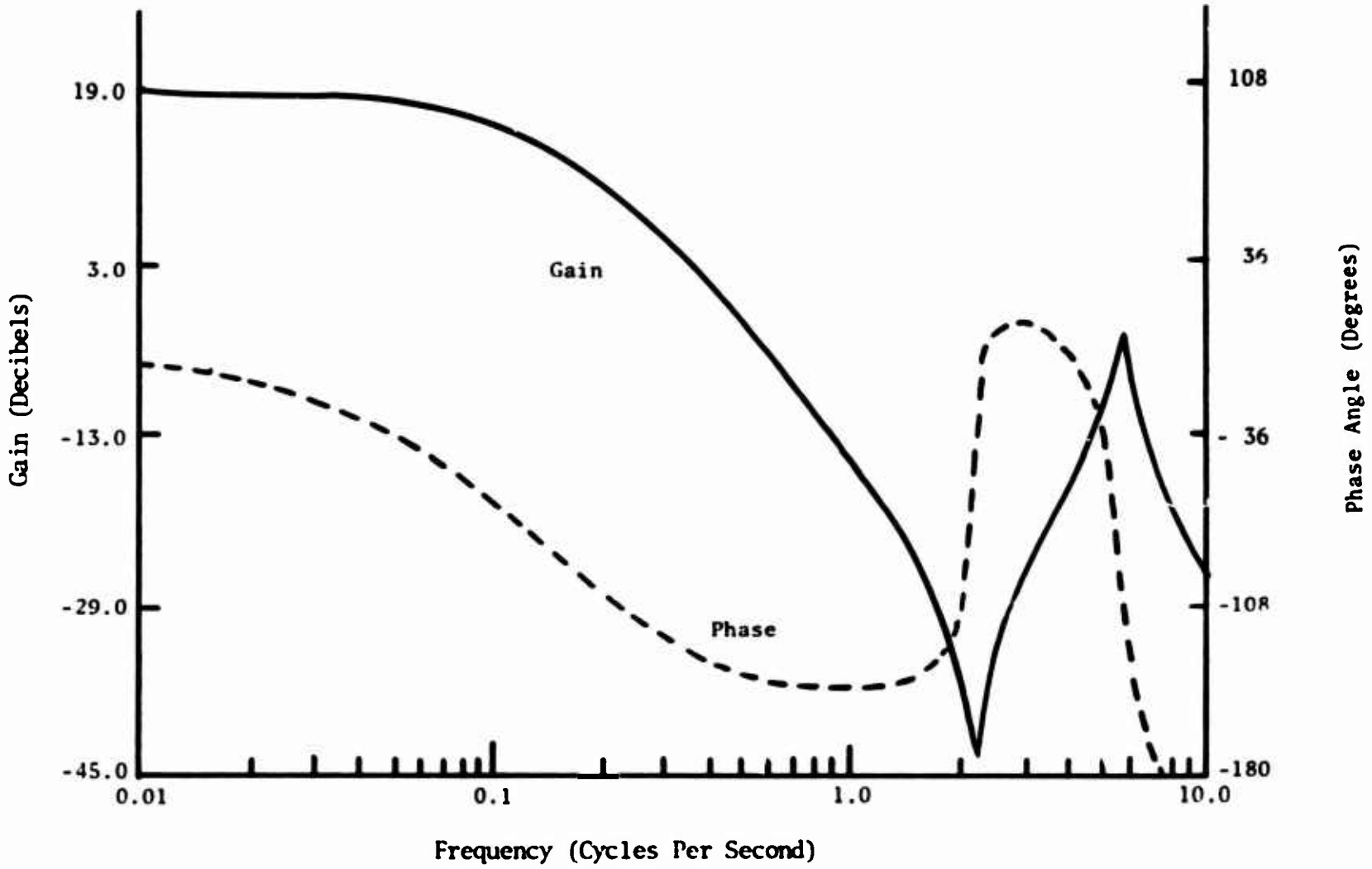

Figure 58. Bode Plots--Fuel Flow/Compressor Discharge Pressure/Lagged Gain Reset, $C_s = 2.24 \frac{\text{ft-lb}}{\text{rad/sec}}$.

by a Bode analysis. Replacing the direct fuel flow speed governor with an ideal governor and using a one-spool turbine engine, whose transfer function is given by equation 138, equations 193 and 194 become equations 212 and 213.

$$F_1(j\omega) = \frac{K_p K_2 K_L [A_1(j\omega)^2 + A_2(j\omega) + 1]}{[B_1(j\omega)^3 + B_2(j\omega)^2 + B_3(j\omega) + 1]} \tag{212}$$

$$F_2(j\omega) = \frac{K_p K_2 K_{LC}}{[B_1(j\omega) + 1]} \tag{213}$$

Assuming that the value of K_2 for a one-spool turbine engine is the same as the value of K_B for a two-spool turbine engine, these equations can be derived from equations 193 and 194 by setting all governor and gas producer time constants equal to zero. Bode plots are constructed for this system for the following cases:

1. Zero shaft damping--from equation 212
2. Nonzero shaft damping--from equation 212
3. ZTS coupling in drive shaft--from equation 213.

The resulting Bode plots are shown in Figures 59, 60, and 61, respectively. It can be seen that there is no phase crossover. Therefore, this system is stable for any positive value of speed governor gain. This agrees with the previous characteristic equation analysis results. Therefore, it appears that the principal cause of the closed-loop instability is not in the drive train, but is rather in the governor dynamics or in the gas producer dynamics or in a combination of both. However, if the drive train is not the principal cause of the system instability, it does not necessarily follow that it is not a contributing factor.

In an attempt to determine the relative effect of the speed governor and gas producer dynamics on the system stability, a Bode analysis is done on the helicopter drive system with an ideal speed governor and a two-spool turbine engine. That is, the speed governor dynamics are eliminated, but the gas producer dynamics are included. The frequency transfer functions for this system, corresponding to equations 193 and 194, are given by equations 213 and 215 respectively.

$$F_1(j\omega) = \frac{K_p K_B K_L [\tau_B(j\omega)+1][A_1(j\omega)^2 + A_2(j\omega)+1]}{[\tau_e(j\omega)+1][B_1(j\omega)^3 + B_2(j\omega)^2 + B_3(j\omega)+1]} \tag{214}$$

$$F_2(j\omega) = \frac{K_p K_B K_{LC} [\tau_B(j\omega)+1]}{[\tau_e(j\omega)+1][B_1(j\omega)+1]} \tag{215}$$

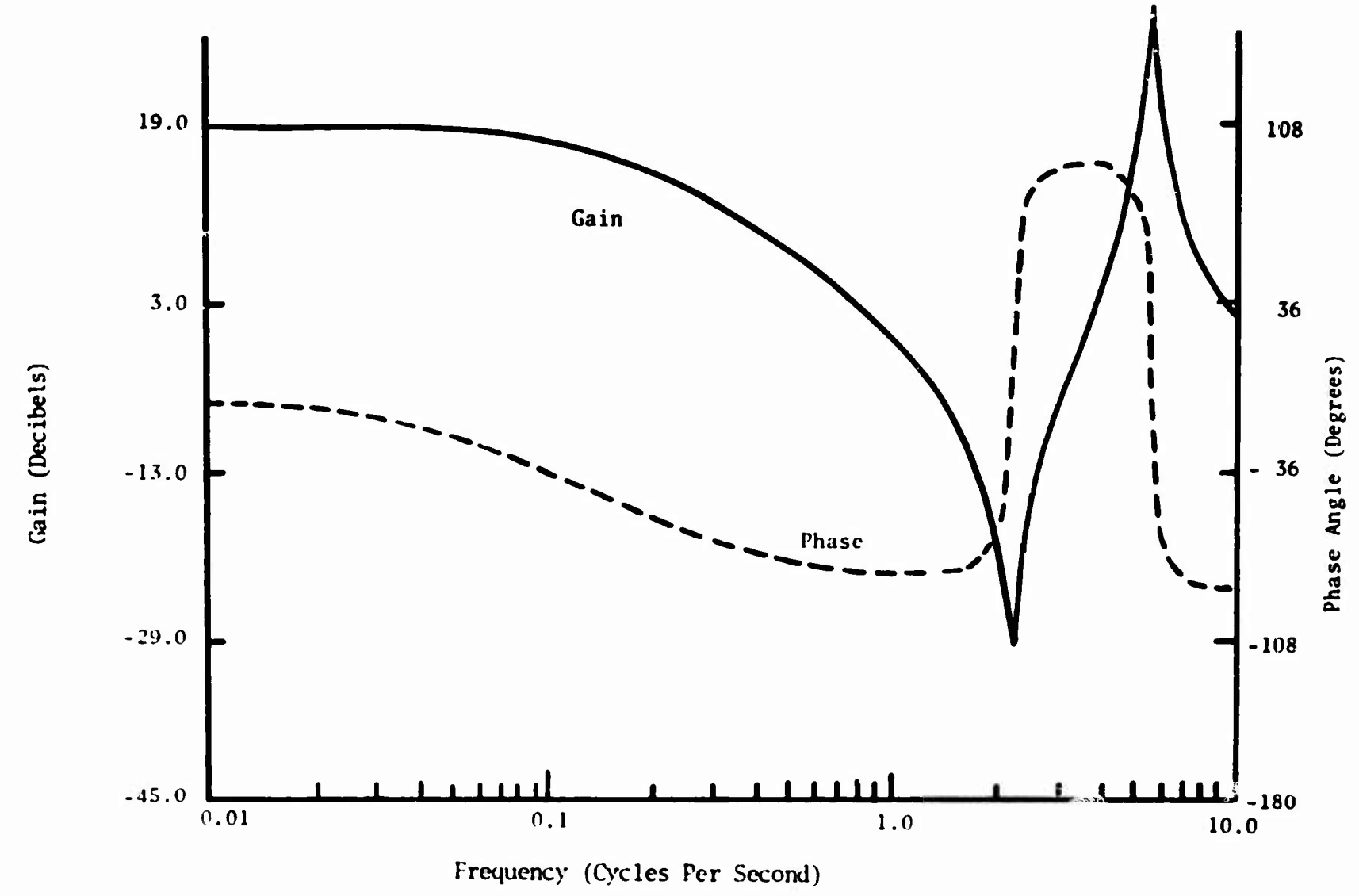

Figure 59. Bode Plots--Ideal Governor, One-Spool Turbine Engine, $C_s = 0.0 \frac{ft\text{-}lb}{rad/sec}$.

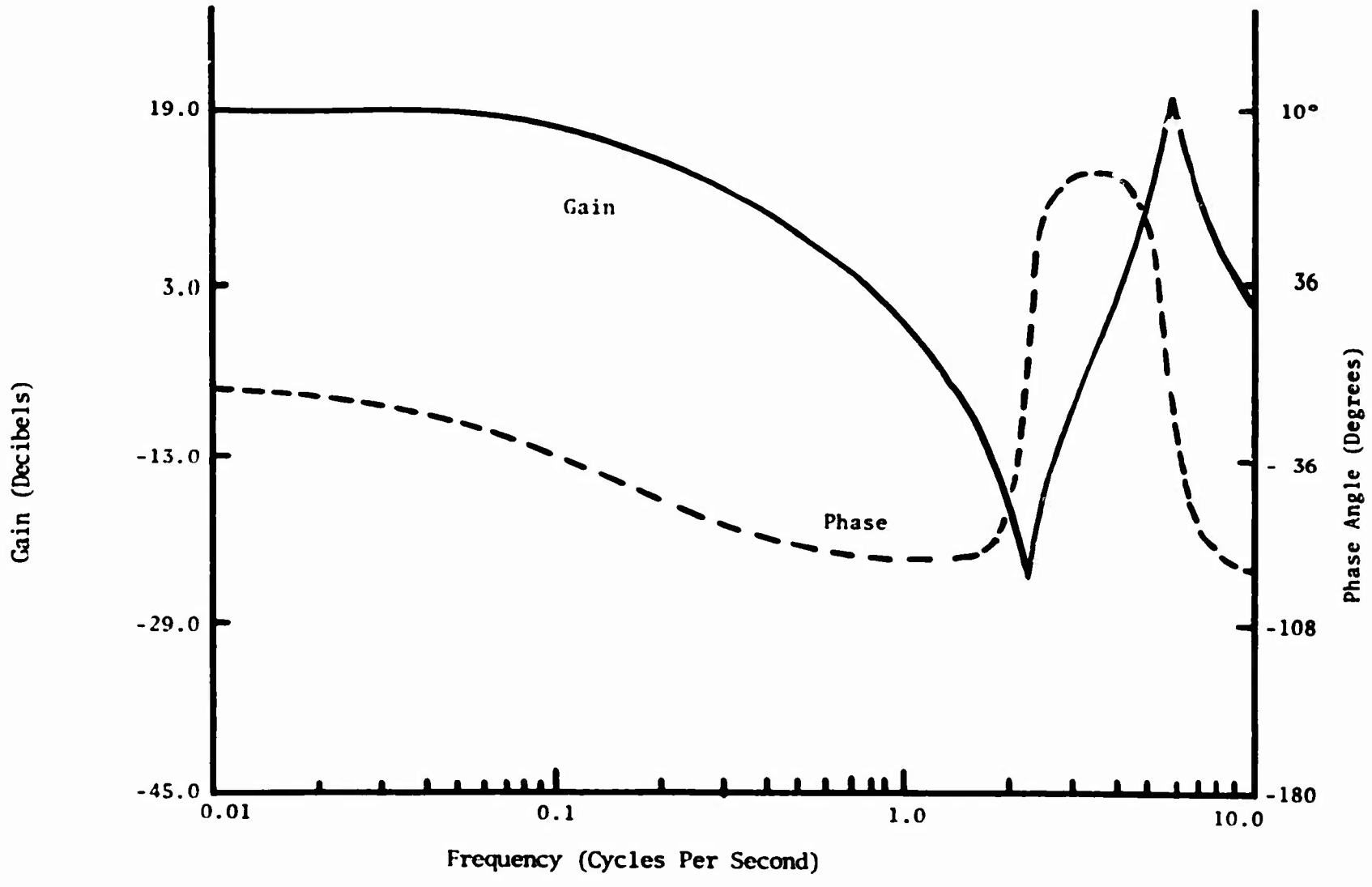

Figure 60. Bode Plots--Ideal Governor, Single-Spool Turbine, Engine, $C_s = 2.24 \frac{\text{ft-lb}}{\text{rad/sec}}$.

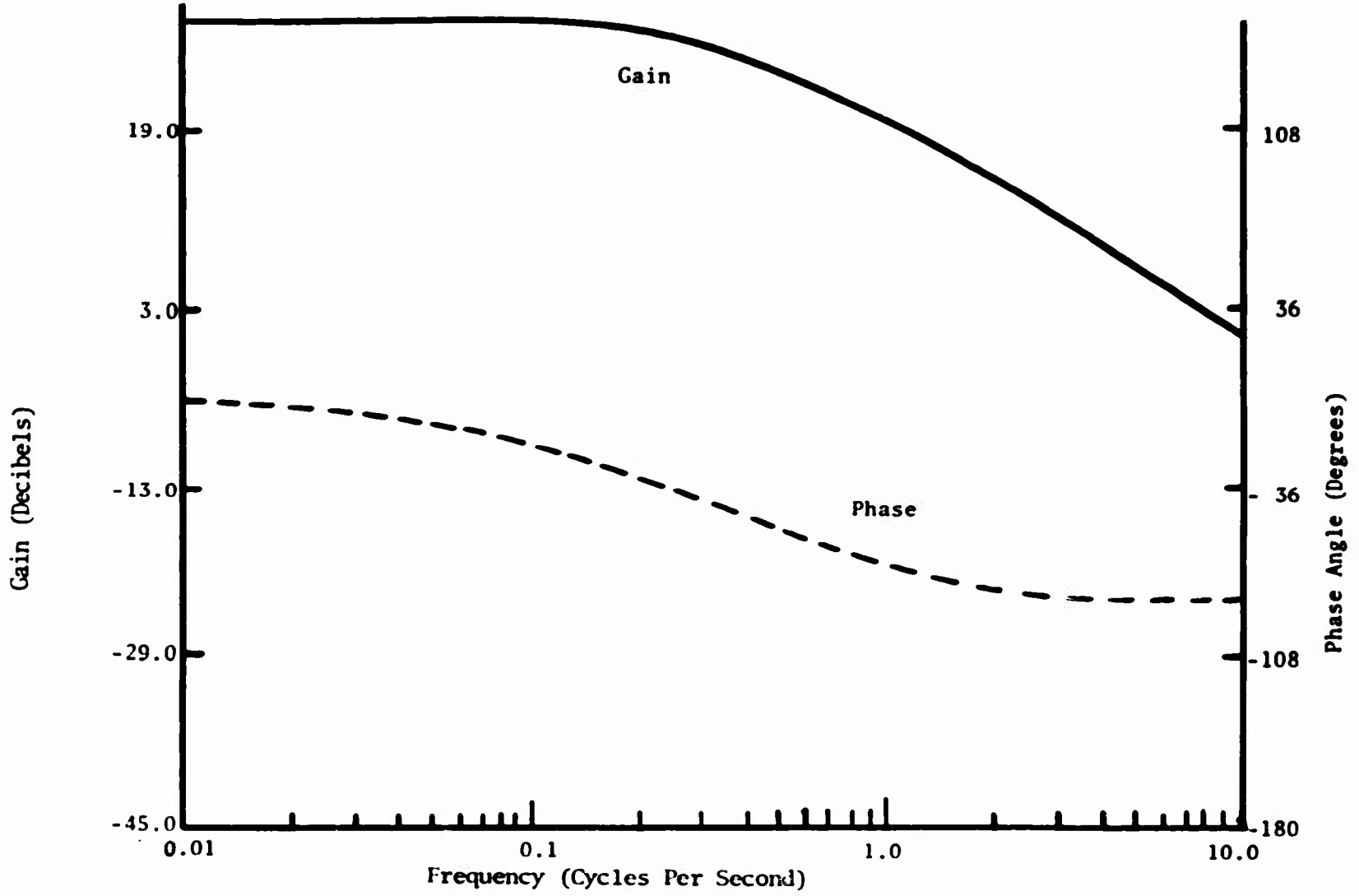

Figure 61. Bode Plots--Ideal Governor, Single Spool Turbine Engine With ZTS Coupling (Decoupled Rotor Model).

Bode plots are made for the same three cases as listed above, except that the frequency transfer functions given by equations 214 and 215 are used instead of those given by equations 212 and 213. The resulting Bode plots are given in Figures 62, 63, and 64. Once again there is no phase crossover; therefore, this system is stable for any positive gain of the ideal speed governor.

For comparison, the gas producer dynamics can be eliminated by using a one-spool turbine engine in the model, whose transfer function is given by equation 138, while the dynamics of the speed governor are included. Bode plots are made for the helicopter drive system model with a direct fuel flow speed governor and a one-spool turbine engine for the same three cases as were considered above. The necessary frequency transfer functions are derived by substituting equation 138 for equation 136 in the derivation of equations 193 and 194 in order to obtain equations 216 and 217.

$$F_1(j\omega) = \frac{K_p K_2 K_L [A_1(j\omega)^2 + A_2 j\omega + 1]}{[\tau_1(j\omega)+1][\tau_2(j\omega)+1][B_1(j\omega)^3 + B_2(j\omega)^2 + B_3(j\omega)+1]} \tag{216}$$

$$F_2(j\omega) = \frac{K_p K_2 K_{LC}}{[\tau_1(j\omega)+1][\tau_2(j\omega)+1][B_1(j\omega)+1]} \tag{217}$$

Using the value for K_2 as the same as the value for K_B of the two-spool turbine engine, the Bode plots resulting for those three cases are given in Figures 65, 66, and 67 and the gain and phase margins are given in Table II. It appears that this system is even less stable then the system with both speed governor and gas producer dynamics. Therefore, it seems that the speed governor lags are the principal causes of the closed-loop system instability.

In general, the addition of a ZTS coupling to all of these systems greatly simplifies the Bode plots of the systems. That is, it reduces the number of gain crossovers and eliminates the peak in the gain plot, which represents a critical frequency of the system. These are definite advantages to the use of a ZTS coupling. However, from the Bode analysis, it also appears to be generally true that the addition of an undamped ZTS coupling to an unstable, or insufficiently stable, system does not, in itself, improve the stability of the system enough to be practically useful.

TRANSIENT SOLUTION FOR THE LINEAR SYSTEM

The transient solution of the engine speed, in time domain, is calculated from the linear Laplace transfer functions. Equation 162 is solved for the variation in the engine speed from a steady-state value to give equation 218.

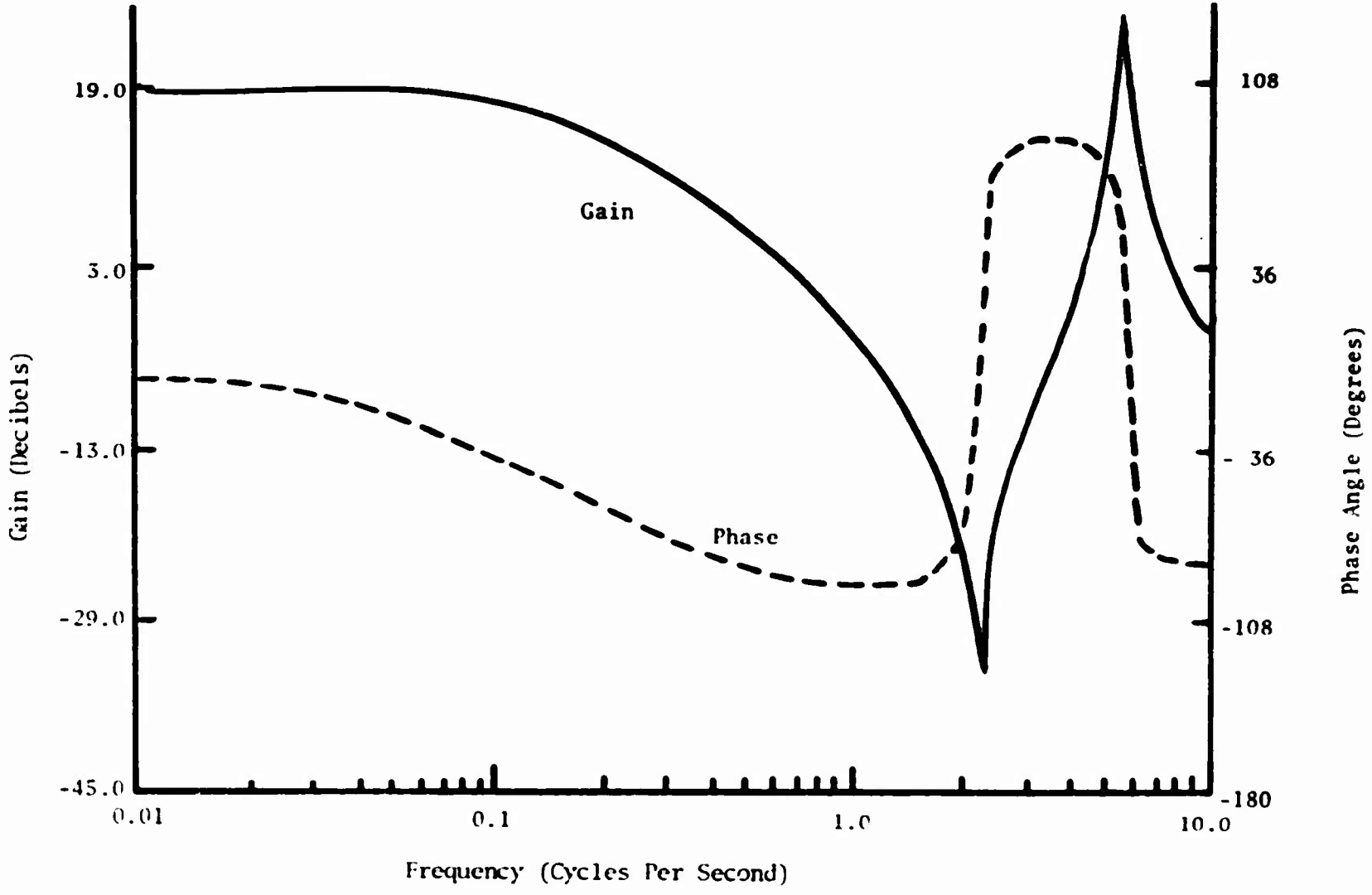

Figure 62. Bode Plots--Ideal Governor, Two-Spool Turbine Engine, $C_s = 0.0 \frac{\text{ft-lb}}{\text{rad/sec}}$.

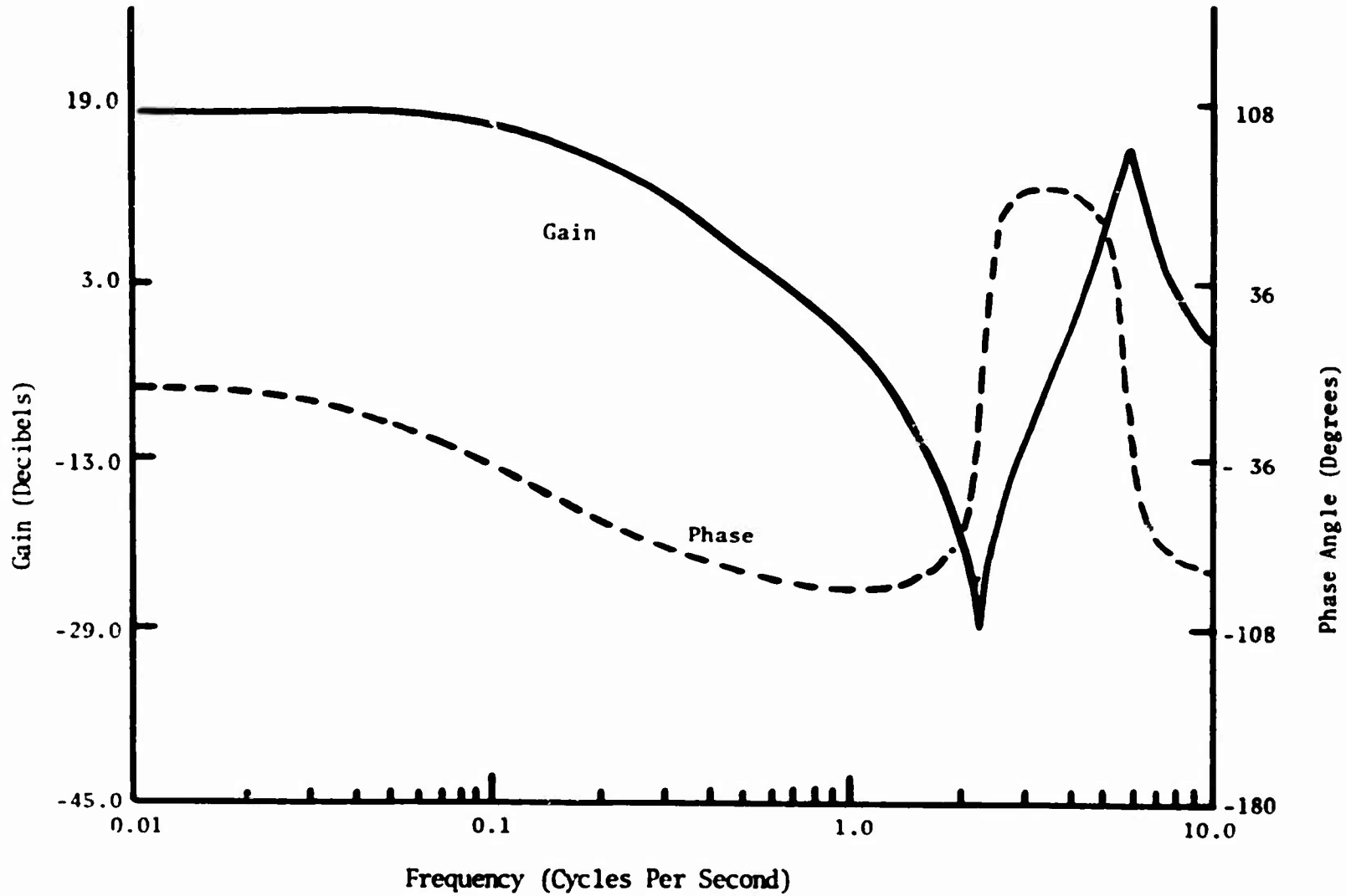

Figure 63. Bode Plots--Ideal Governor, Two-Spool Turbine Engine, $C_s = 2.24 \frac{\text{ft-lb}}{\text{rad/sec}}$.

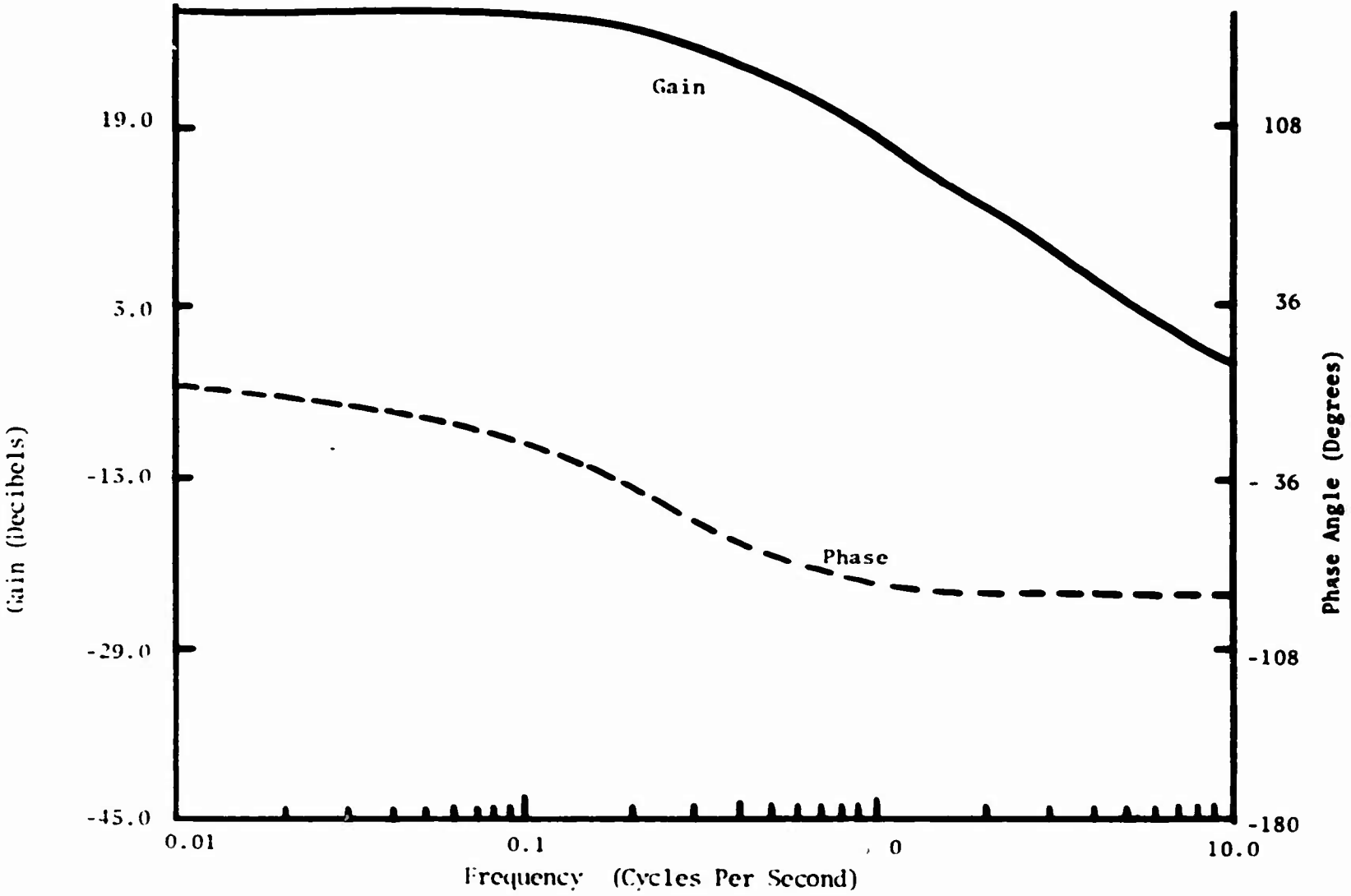

Figure 64. Bode Plots--Ideal Governor, Two-Spool Turbine Engine With ZTS Coupling (Decoupled Rotor Model).

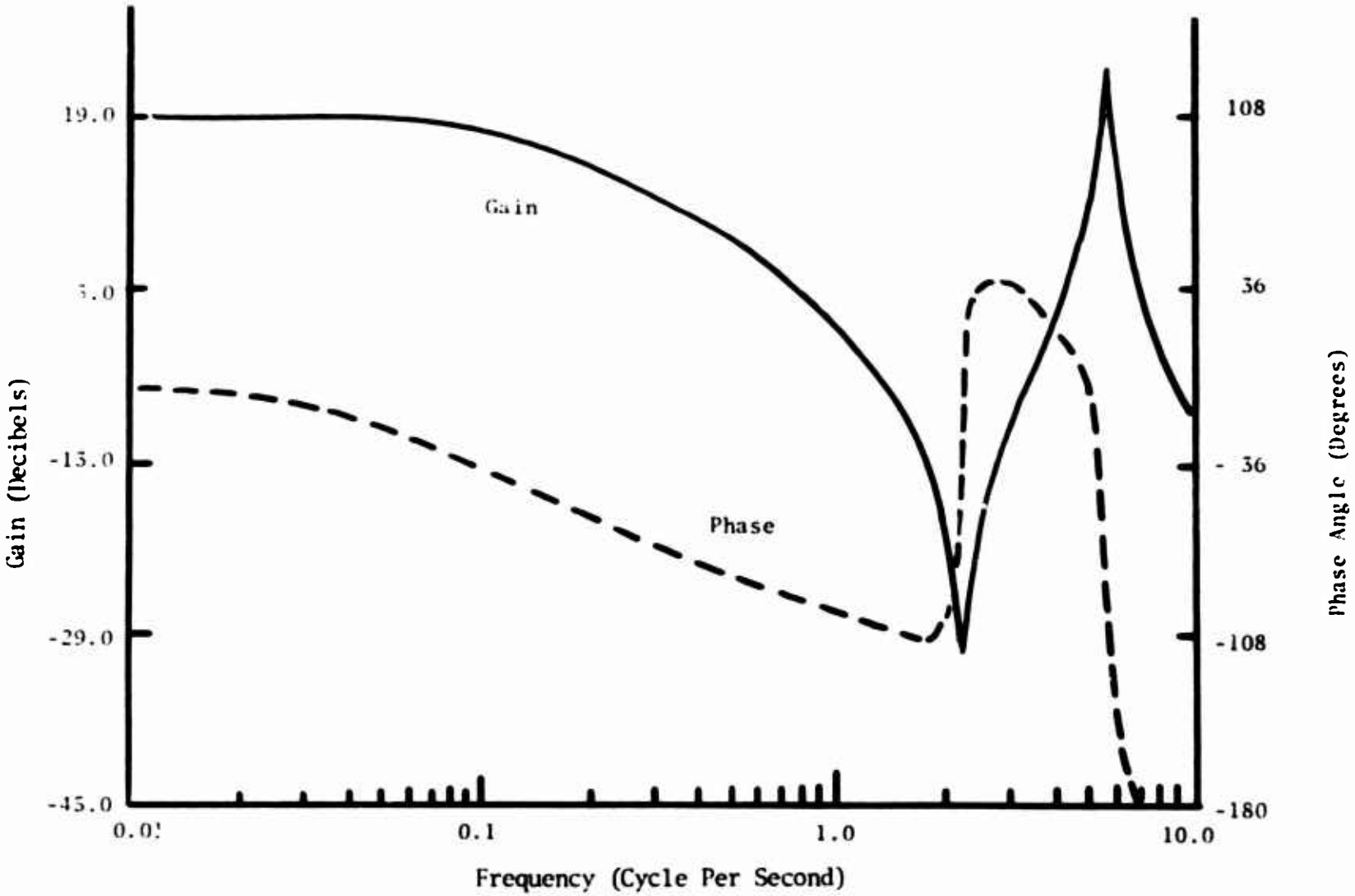

Figure 65. Bode Plots--Direct Fuel Flow Governor, One-Spool Turbine Engine, $C_s = 0.0 \frac{ft\text{-}lb}{rad/sec}$.

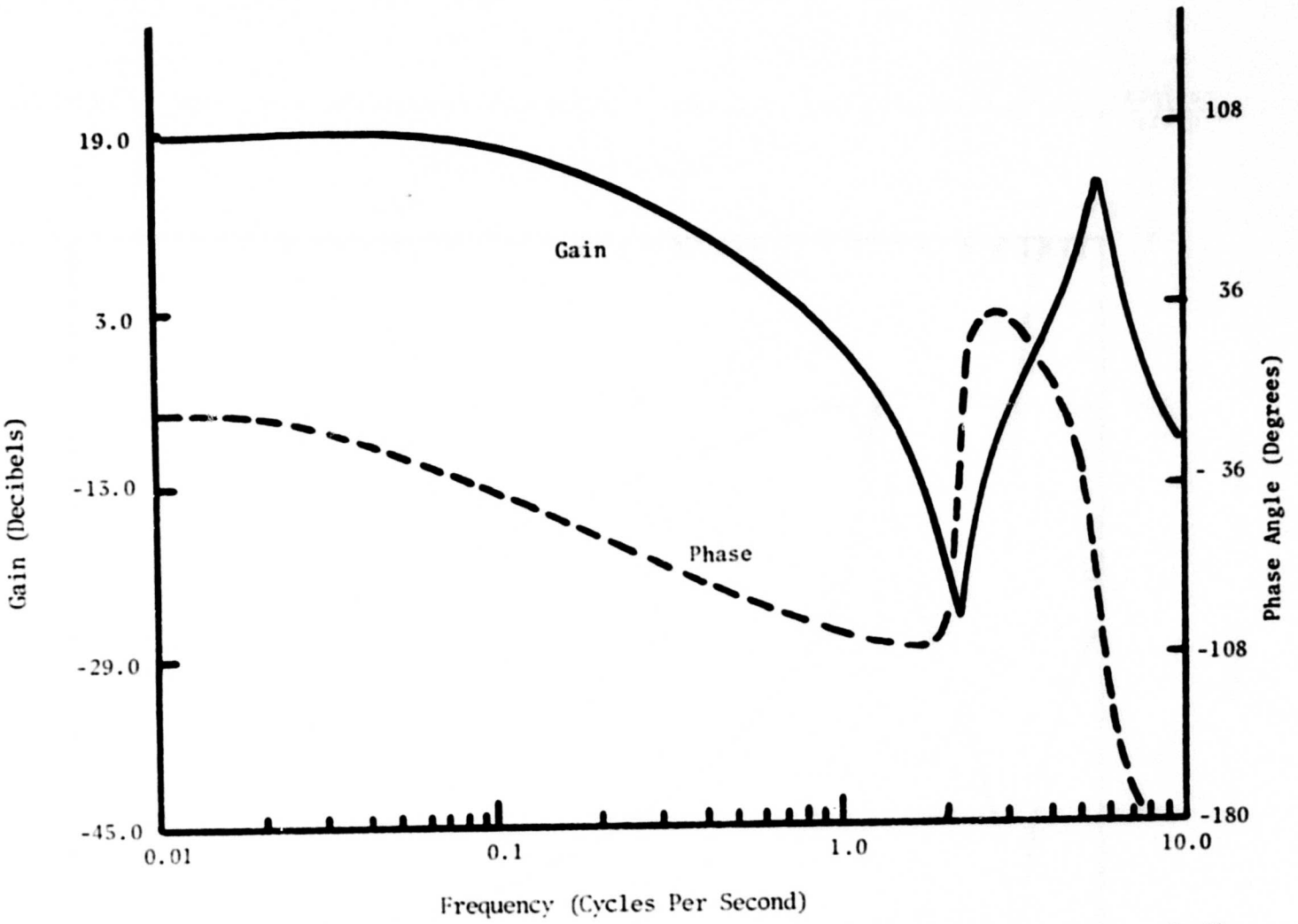

Figure 66. Bode Plots--Direct Fuel Flow Governor, Single-Spool Turbine Engine, $C_s = 2.24 \frac{\text{ft-lb}}{\text{rad/sec}}$.

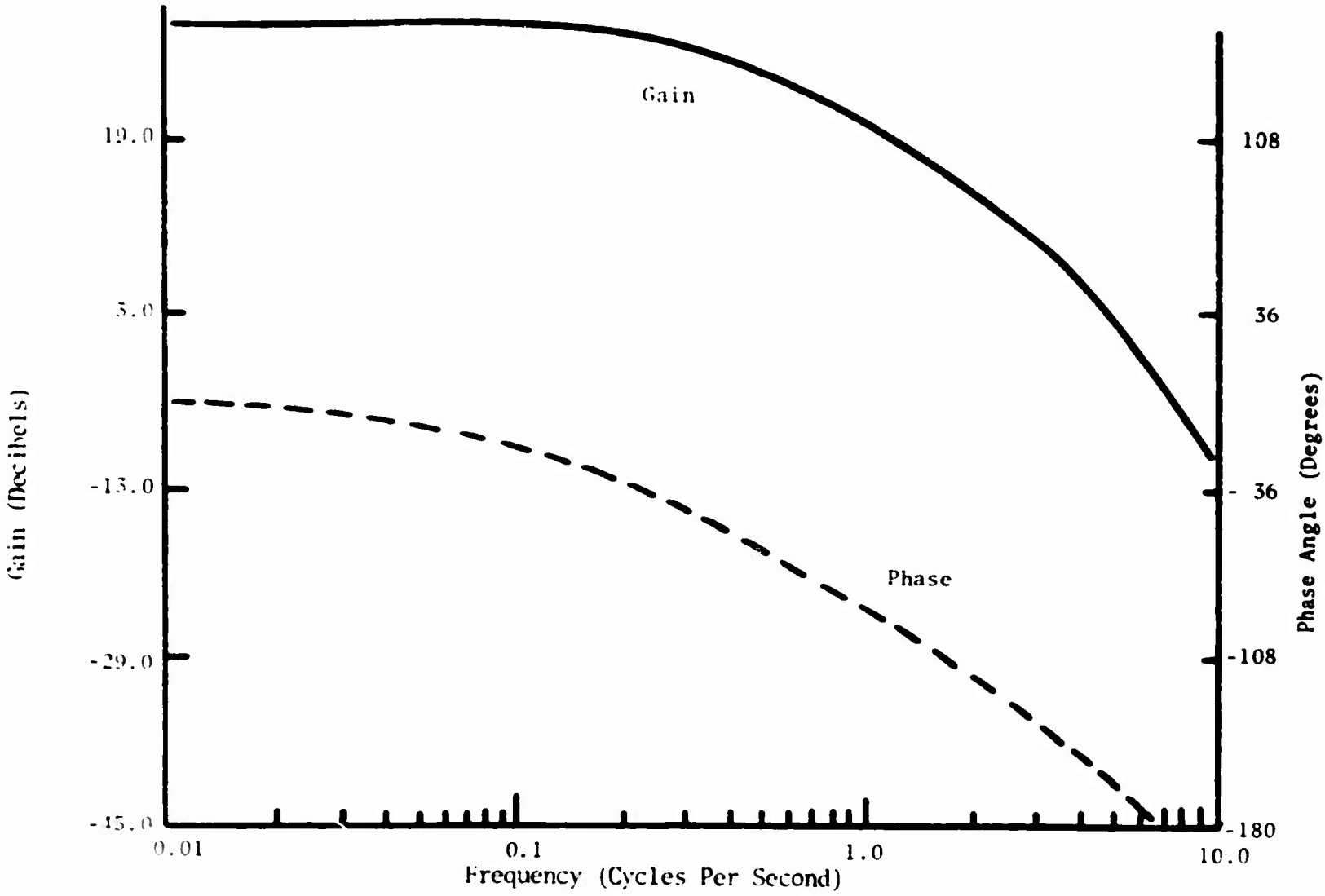

Figure 67. Bode Plots--Direct Fuel Flow Governor, Single-Spool Turbine Engine With ZTS Coupling (Decoupled Rotor Model).

$$\Delta W_e(s) = Y_c(s)\ \Delta\Omega(s) \tag{218}$$

The set speed is assumed to be a step function of magnitude Ω, making the variation of the set speed an impulse. Therefore, $\Delta\Omega(s)$ can be replaced by $\Delta\Omega$, giving the ratio of the variation of the engine speed from its steady-state value to the change in governor set speed as equation 219.

$$\frac{\Delta W_e(s)}{\Delta\Omega} = Y_c(s) \tag{219}$$

Since it is the variation of the engine speed from the steady-state value that is being solved for, rather than the engine speed itself, the solution will be harmonic about zero. In order to find the solution of $\Delta\omega_e$ in the time domain, it is necessary to take the inverse Laplace transform of the closed-loop transfer function. Equations 157 and 159 are combined to find the closed-loop transfer function for the system without a ZTS coupling, resulting in equation 220.

$$Y_c(s) = \frac{K_p K_B K_L (\tau_B S+1)(A_1 S^2+A_2 S+1)}{K_p K_B K_L (\tau_B S+1)(A_1 S^2+A_2 S+1)}$$

$$+ (\tau_1 S+1)(\tau_2 S+1)(\tau_e S+1)(B_1 S^3+B_2 S^2+B_3 S+1) \tag{220}$$

Using the substitutions in equations 219 and 221 through 227, this equation can be rewritten as equation 228.

$$D_1 = \tau_1\tau_2\tau_e B_1 \tag{221}$$

$$D_2 = \tau_1\tau_2\tau_e B_2+(\tau_1\tau_2+\tau_1\tau_e+\tau_2\tau_e)B_1 \tag{222}$$

$$D_3 = \tau_1\tau_2\tau_e B_3+(\tau_1\tau_2+\tau_1\tau_e+\tau_2\tau_e)B_2+(\tau_1+\tau_2+\tau_e)B_1 \tag{223}$$

$$D_4 = \tau_1\tau_2\tau_e+(\tau_1\tau_2+\tau_1\tau_e+\tau_2\tau_e)B_3+(\tau_1+\tau_2+\tau_e)B_2+B_1+K_p K_B K_L \tau_B A_1 \tag{224}$$

$$D_5 = (\tau_1\tau_2+\tau_1\tau_e+\tau_2\tau_e)+(\tau_1+\tau_2+\tau_e)B_3+B_2+K_p K_B K_L(\tau_B A_2+A_1) \tag{225}$$

$$D_6 = (\tau_1+\tau_2+\tau_e)+B_3+K_p K_B K_L(\tau_B+A_2) \tag{226}$$

$$D_7 = K_p K_B K_L+1 \tag{227}$$

$$\frac{\Delta W_e(s)}{\Delta\Omega} = \frac{K_p K_B K_L (\tau_B S+1)(A_1 S^2+A_2 S+1)}{(D_1 S^6+D_2 S^5+D_3 S^4+D_4 S^3+D_5 S^2+D_6 S+D_7)} \tag{228}$$

In order to find the inverse Laplace transform of this function, the denominator must first be factored and the function must be broken up by partial fraction expansion. This has been done, with the same system parameters used previously for the Bode plots, by the computer program in Appendix VII. This is done for both zero shaft damping and for the same nonzero value of shaft damping that was used for the Bode analyses. For zero shaft damping, equation 229 results and for nonzero shaft damping, equation 230 results.

$$\frac{\Delta W_e(S)}{\Delta \hat{\Omega}} = \left[\frac{0.138}{(S+68.1)} - \frac{(0.02 + j\ 0.082)}{(S-0.055-j\ 43.9)} - \frac{(0.02 - j\ 0.082)}{(S-0.055+j\ 43.9)}\right.$$

$$\left. - \frac{0.180}{(S+11.2)} + \frac{(0.041 - j\ 0.062)}{(S + 4.87 - j\ 4.66)} + \frac{(0.041 + j\ 0.062)}{(S+4.87 + j\ 4.66)}\right] \times 10^{-2} \qquad (229)$$

$$\frac{\Delta W_e(S)}{\Delta \hat{\Omega}} = \left[\frac{0.139}{(S+68.5)} - \frac{(0.022 + j\ 0.083)}{(S+1.73 - j\ 44.1)} - \frac{(0.022 - j\ 0.083)}{(S+1.73 + j\ 44.1)}\right.$$

$$\left. - \frac{0.175}{(S+11.1)} + \frac{(0.04 + j\ 0.062)}{(S+4.85 + j\ 4.66)} + \frac{(0.04 + j\ 0.062)}{(S+4.85 - j\ 4.66)}\right] \times 10^{-2} \qquad (230)$$

The inverse Laplace transform of equation 229 is given by equation 231, while the inverse Laplace transform of equation 230 is given by equation 232.

$$\frac{\hat{\Delta}_e(t)}{\hat{\Omega}} = 0.00138e^{-68.1t}$$

$$+ 0.00168e^{0.055t} \sin(43.9t - 0.24)$$

$$- 0.0018e^{-11.2t}$$

$$+ 0.00149e^{-4.87} \sin(4.66t + 0.58) \qquad (231)$$

$$\frac{\hat{\Delta}_e(t)}{\hat{\Omega}} = 0.00139e^{-68.5t}$$

$$+ 0.00172e^{-173t} \sin(44.1t - 0.26)$$

$$- 0.00175e^{-11.1t}$$

$$+ 0.00147e^{-4.85t} \sin(4.66t + 0.57) \qquad (232)$$

These functions are plotted in Figures 68 and 69. For the system with a ZTS coupling, the closed-loop transfer function is found to be represented by equation 233.

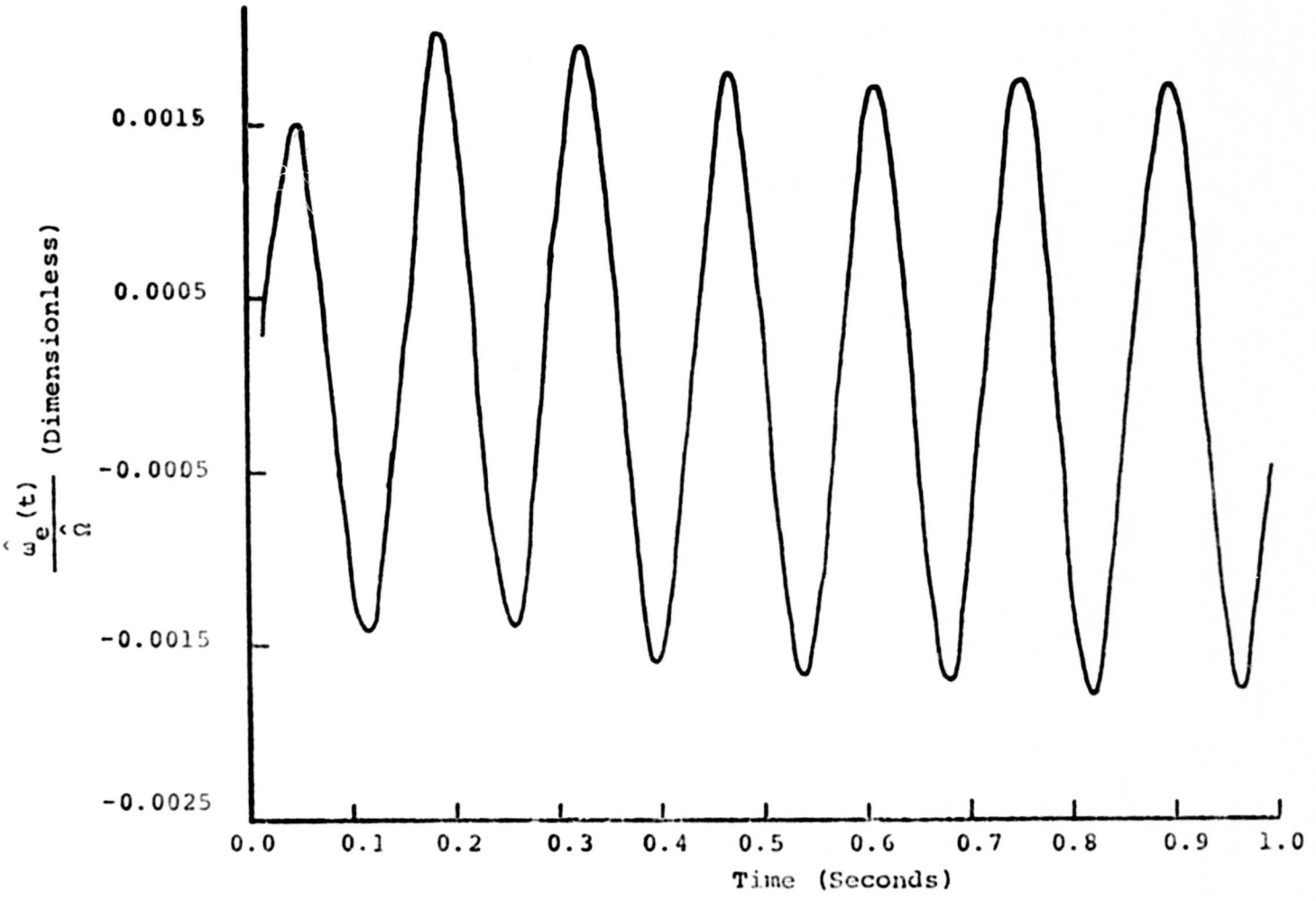

Figure 68. Linear Time Response, $C_s = 0.0$ $\frac{\text{ft-lb}}{\text{rad/sec}}$.

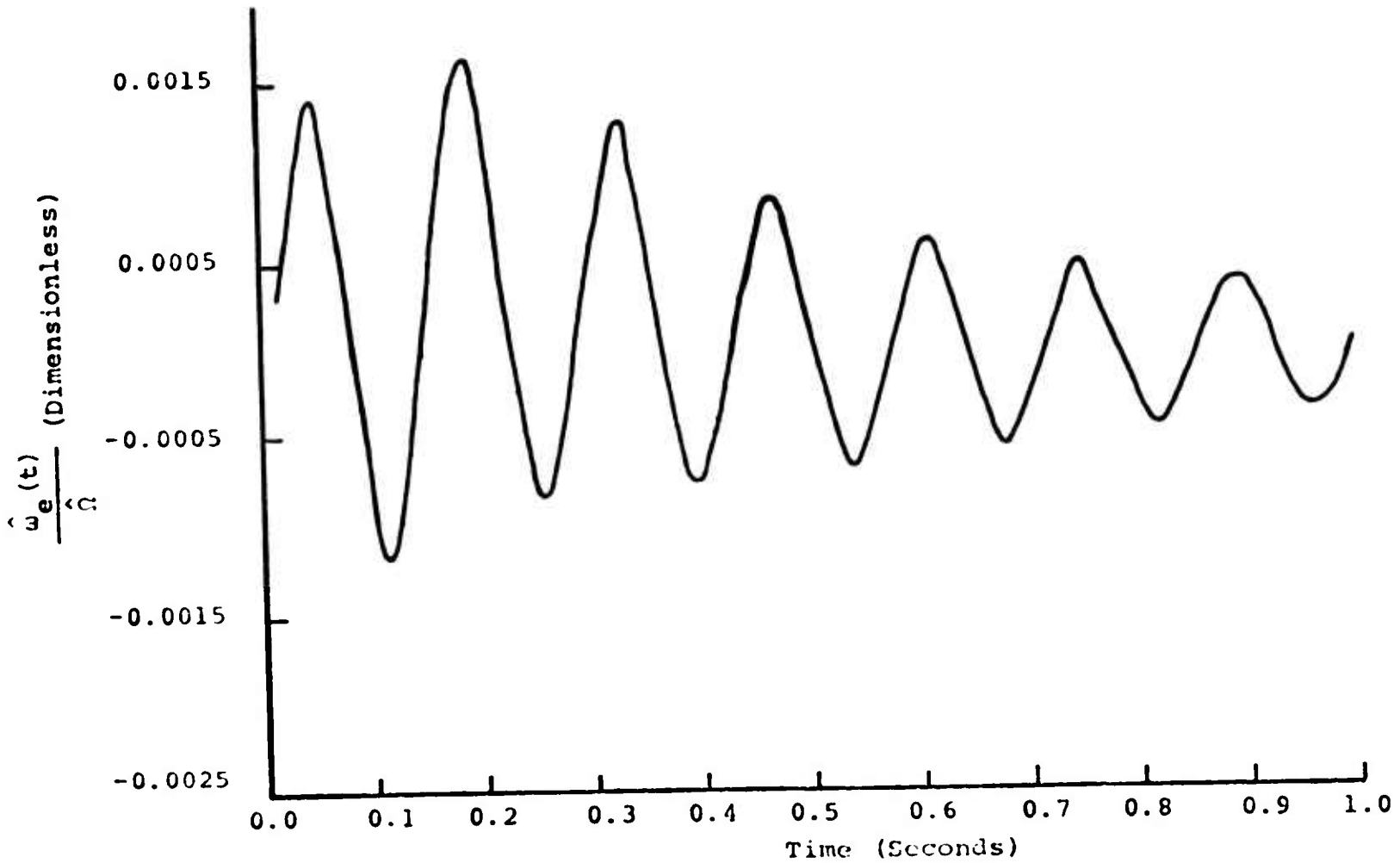

Figure 69. Linear Time Response, $C_s = 2.24 \frac{\text{ft-lb}}{\text{rad sec}}$.

$$Y_c(S) = \frac{K_p K_B K_{LC}(\tau_B S+1)}{K_p K_B K_{LC}(\tau_B S+1)+(\tau_1 S+1)(\tau_2 S+1)(\tau_e S+1)(B_4 S+1)} \quad (233)$$

The substitutions of equations 219 and 234 through 238 reduce the above equation down to equation 239.

$$E_1 = \tau_1\tau_2\tau_e B_4 \quad (234)$$

$$E_2 = \tau_1\tau_2\tau_e+\tau_1\tau_2 B_4+\tau_1\tau_e B_4+\tau_2\tau_e B_4 \quad (235)$$

$$E_3 = \tau_1\tau_2+\tau_1\tau_e+\tau_1 B_4+\tau_2\tau_e+\tau_2 B_4+\tau_e B_4 \quad (236)$$

$$E_4 = K_p K_B K_{LC}\tau_B+\tau_1+\tau_2+\tau_e+B_4 \quad (237)$$

$$E_5 = K_p K_B K_{LC}+1 \quad (238)$$

$$\frac{\Delta W_e(S)}{\Delta\Omega} = \frac{K_p K_B K_{LC}(\tau_B S+1)}{E_1 S^4+E_2 S^3+E_3 S^2+E_4 S+E_5} \quad (239)$$

Similar to the above situation, the denominator of this function must be factored, and the resulting equation must be broken up by partial fraction expansion. This has also been done by the computer program in Appendix VII, resulting in equation 240.

$$\frac{\Delta W_e(S)}{\Delta\Omega} = \left[\frac{0.115}{(S+74.7)}+\frac{(-0.137S+8.25)}{(S+4.34)^2+(31.8)^2}-\frac{0.0011}{(S+5.46)}\right] \times 10^{-2} \quad (240)$$

The inverse Laplace transform of the previous function is given by equation 241.

$$\frac{\hat{\Delta W}_e(t)}{\hat{\Omega}} = [0.145e^{-74.7t}+0.28e^{-4.3t}\sin(31.8t-0.421) - 0.00110e^{-5.46t}] \times 10^{-2} \quad (241)$$

This function is plotted in Figure 70.

The zero ordinate lines in Figures 68 through 70 represent the new values of steady-state engine speed after the change in set speed. Therefore, the initial peak of each curve represents the overshoot of the system. The entire curve shows the transient response of each system as it approaches

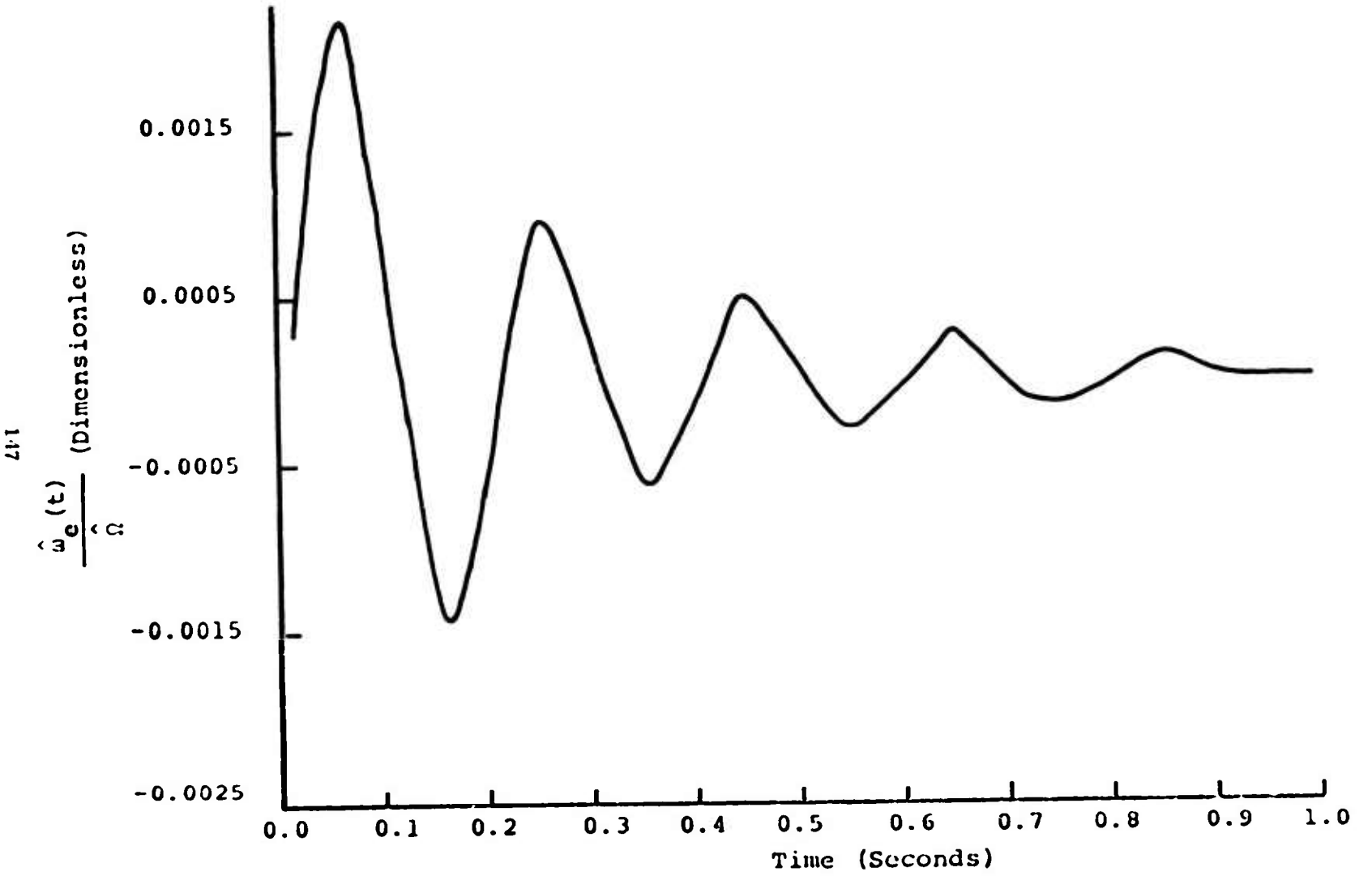

Figure 70. Linear Time Response With ZTS Coupling.

its steady-state values. From Figure 68 it can be seen that the engine speed for the case with zero shaft damping diverges, and is, therefore, completely unstable. However, from Figures 69 and 70, the other two cases are seen to have engine speeds which converge, and so are at least marginally stable. Comparing Figures 69 and 70, it is apparent that the helicopter system with a ZTS coupling has a greater overshoot, but also a shorter settling-down period, than the system without a ZTS coupling. The greater overshoot is reasonable since the inertia of the linearized system is reduced by the use of a ZTS coupling. That is, when the set speed is first changed, the initial change in the fuel flow will be the same, and the initial change in engine torque will be the same, whether or not the system has a ZTS coupling. Therefore, the system with the smaller inertia will have the greater initial acceleration, or deceleration, and will likely have the greater overshoot. The shorter settling-down period is also reasonable. This is because, for the linearized system with a ZTS coupling, only the oscillation of the engine inertia must be damped out. However, for the linearized system without a ZTS coupling, oscillation must be damped out of both the engine and rotor inertias, which are, in addition, out-of-phase oscillations. It would seem that a shorter settling time is a more important advantage, in considering transient response, than a smaller overshoot is. Therefore, according to the linearized analysis, adding a ZTS coupling to a helicopter drive system will improve the time response of the system.

For comparison, as was done with the Bode analysis, the time response of the engine speed can also be found for the helicopter drive system without speed governor dynamics, without gas generator dynamics, and without both.

First, for the helicopter drive system with an ideal governor and a one-spool turbine engine, the frequency transfer functions of equations 212 and 213 are converted to Laplace transfer functions by replacing each $j\omega$ with an S. Then the closed-loop transfer functions are derived, with the aid of equation 159, to become equations 242 and 243, respectively.

$$Y_c(s) = \frac{K_p K_B K_L (A_1 S^2 + A_2 S + 1)}{B_1 S^3 + (B_2 + A_1 K_p K_B K_L) S^2 + (B_3 + A_2 K_p K_B K_L) S + K_p K_B K_L + 1} \qquad (242)$$

$$Y_c(s) = \frac{K_p K_B K_{LC}}{B_4 S + K_p K_B K_{LC} + 1} \qquad (243)$$

The inverse Laplace transforms for these transfer functions for the same three cases considered above, again using the computer program in Appendix VII, are given by equations 244, 245, and 246.

$$\frac{\hat{\omega}_e(t)}{\hat{\Omega}} = (6.02 \times 10^{-9})e^{-19.9t} \sin(19.6g + 1.59) - (1.05 \times 10^{-8})e^{-15.4t} \quad (244)$$

$$\frac{\hat{\omega}_e(t)}{\hat{\Omega}} = (8.76 \times 10^{-9})e^{-21.2t} \sin(16.5t + 1.54) - (1.32 \times 10^{-8})e^{-16.7t} \quad (245)$$

$$\frac{\hat{\omega}_e(t)}{\hat{\Omega}} = -(1.08 \times 10^{-4})e^{-75.8t} \quad (246)$$

These functions are plotted in Figures 71, 72, and 73. All three plots illustrate a very quick response. It is much quicker than the response of the system with speed governor and gas producer dynamics. However, there is a marked similarity between the response of the two systems. That is, both of these systems, when including a ZTS coupling, have a larger initial variation from steady state, but converge to steady state much quicker.

The next model used includes gas producer dynamics, in the form of a two-spool turbine engine, and an ideal speed governor. The closed-loop Laplace transfer functions for this model are derived from the open-loop frequency transfer functions of equations 214 and 215 in the same manner as described above. The resulting equations, 247 and 248, are inverse transformed by the computer program in Appendix VII to give equations 249, 250, and 251 for the same three cases used previously.

$$Y_c(S) = \frac{K_p K_B K_L (\tau_B S+1)(A_1 S^2+A_2 S+1)}{K_p K_B K_L (\tau_B S+1)(A_1 S^2+A_2 S+1)+(\tau_e S+1)(B_1 S^3+B_2 S^2+B_3 S+1)} \quad (247)$$

$$Y_c(S) = \frac{K_p K_B K_{LC}(\tau_B+1)}{\tau_e B_4 S^2+(\tau_e+B_4+K_p K_B K_{LC}\tau_B)\ S+K_p K_B K_{LC}+1} \quad (248)$$

$$\frac{\hat{\omega}_e(t)}{\hat{\Omega}} = 0.0056e^{-14.7t} \sin(32.4t + 4.5) + 0.0418e^{-1.62t} \sin(3.24t + 2.39) \quad (249)$$

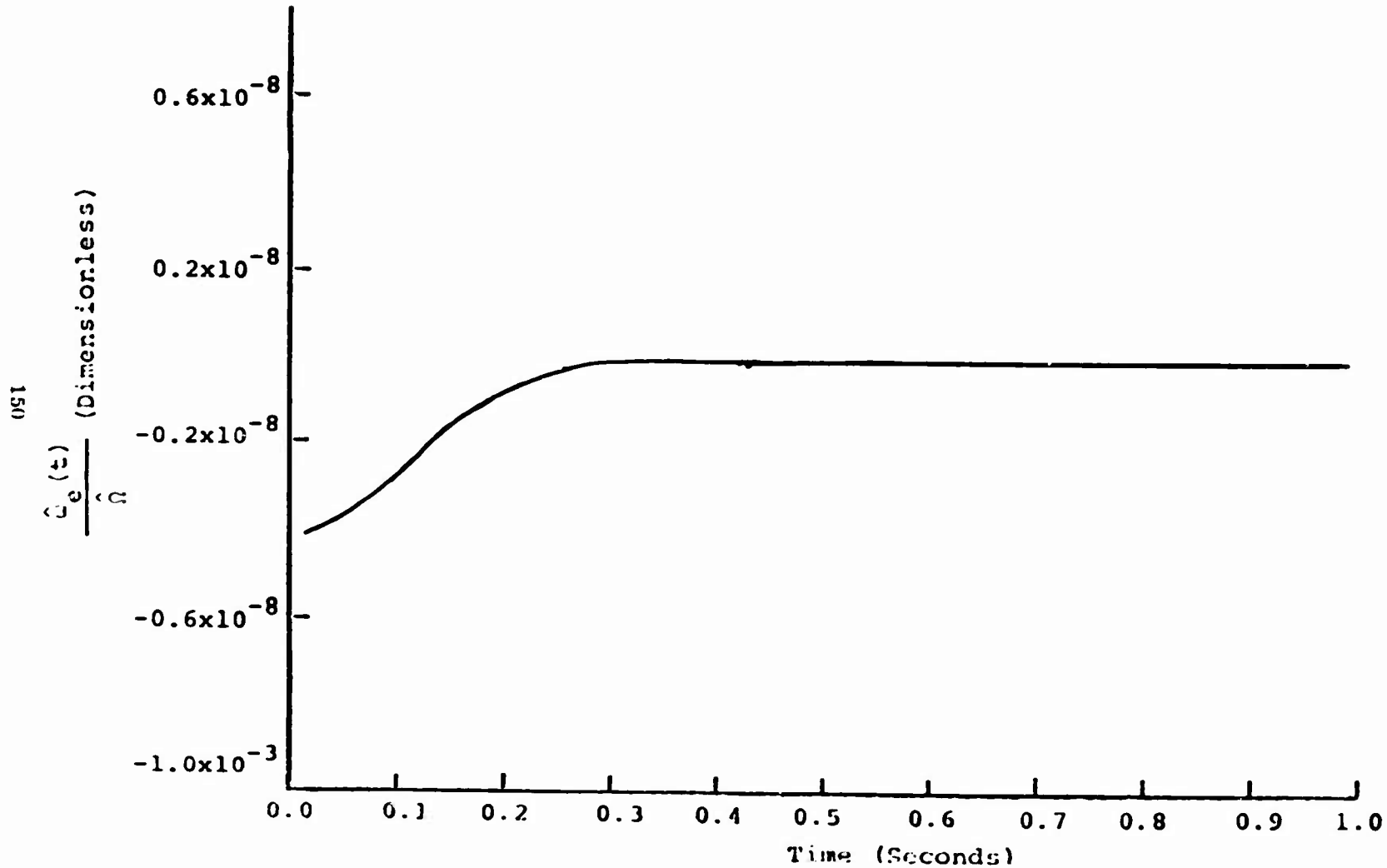

Figure 71. Linear Time Response--Ideal Governor, One-Spool Turbine Engine, $C_s = 0.0 \frac{\text{ft-lb}}{\text{rad/sec}}$.

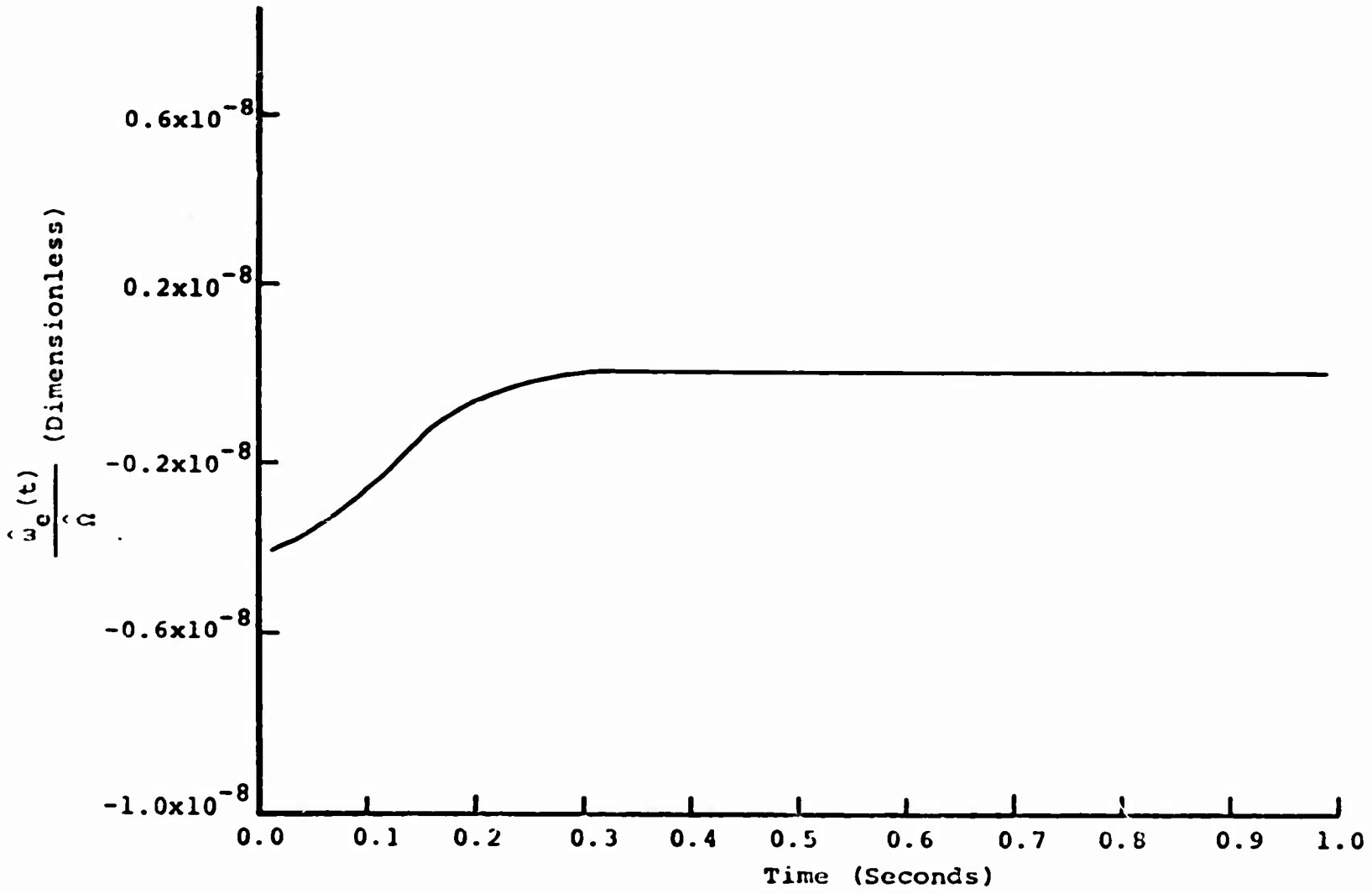

Figure 72. Linear Time Response--Ideal Governor, One-Spool Turbine Engine, $C_s = 2.24 \frac{\text{ft-lb}}{\text{rad/sec}}$.

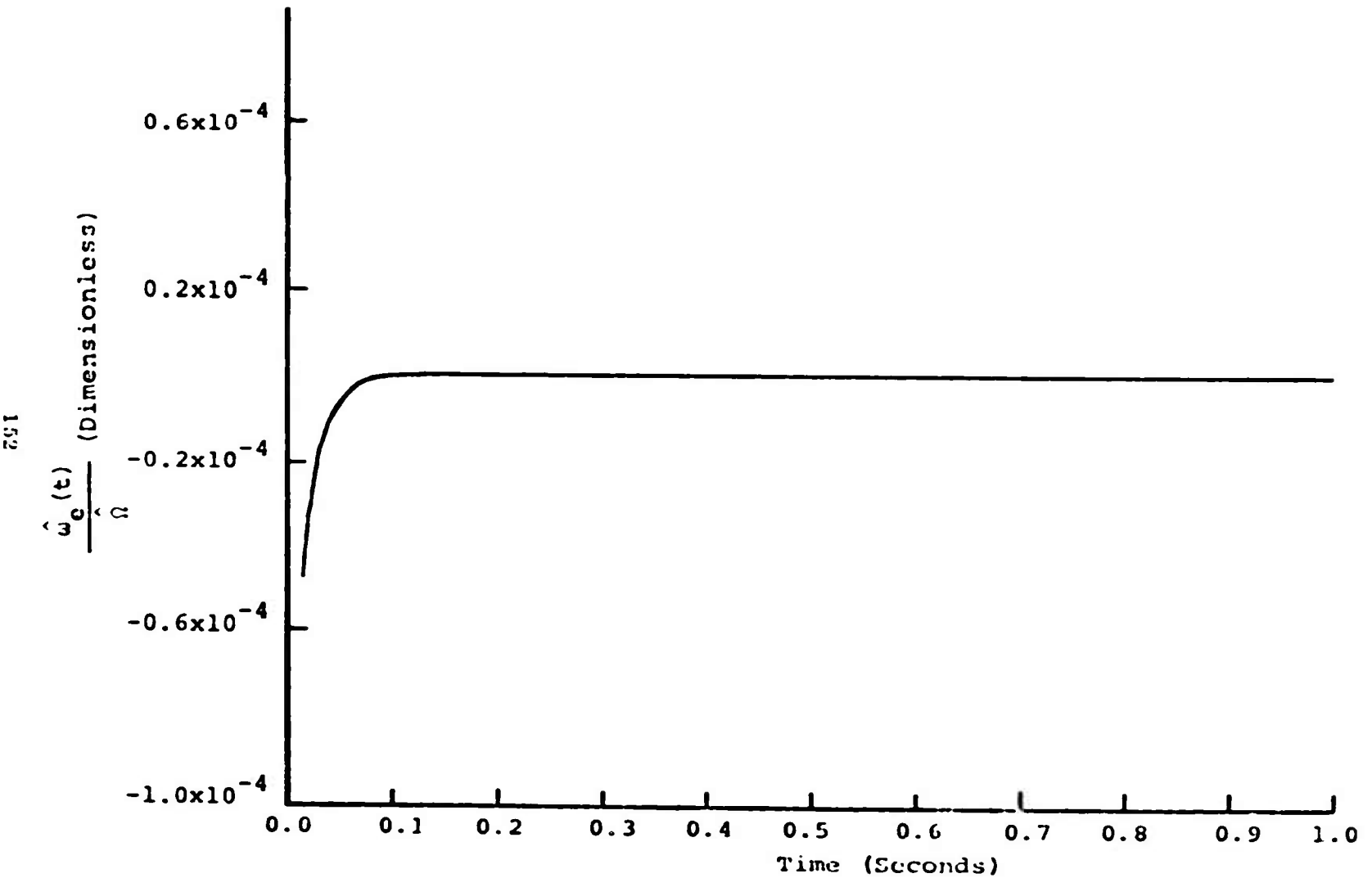

Figure 73. Linear Time Response--Ideal Governor, One-Spool Turbine Engine With ZTS Coupling.

$$\frac{\hat{\omega}_e(t)}{\hat{\Omega}} = 0.0058e^{-16.6t} \sin (31.4t + 4.44)$$

$$+ 0.0419e^{-4.61t} \sin (3.25t + 2.38) \quad (250)$$

$$\frac{\hat{\omega}_e(t)}{\hat{\Omega}} = 0.00362e^{-45.9t} - 0.00381e^{-5.5t} \quad (251)$$

These three functions are plotted in Figures 74, 75, and 76, respectively. It can be seen from the first two graphs that this system without a ZTS coupling has a rather large initial variation from steady state, but it converges very quickly. However, the time response of this system with a ZTS coupling, as shown in Figure 76, is much improved. Therefore, it appears that a ZTS coupling does help to significently reduce the transient oscillations in a helicopter drive system with gas producer dynamics, but with no speed governor dynamics.

The next model used includes speed governor dynamics, in the form of a direct fuel flow speed governor, but no gas producer dynamics, modeled as a one-spool turbine engine. The closed-loop Laplace transfer functions for this model are derived from the open-loop frequency transfer functions of equations 216 and 217 in the same manner as described above. The resulting equations, 252 and 253, are inverse transformed by the computer program in Appendix VII to give equations 254, 255, and 256.

$$Y_c(S) = \frac{K_p K_B K_L (A_1 S^2 + A_2 S + 1)}{K_p K_B K_L (A_1 S^2 + A_2 S + 1) + (\tau_1 S + 1)(\tau_2 S + 1)(B_1 S^3 + B_2 S^2 + B_3 S + 1)} \quad (252)$$

$$Y_c(S) = \frac{K_p K_B K_{LC}}{\tau_1 \tau_2 B_4 S^3 + (\tau_1 \tau_2 + \tau_1 B_4 + \tau_2 B_4) S^2 + (\tau_1 + \tau_2 + B_4) S + K_p K_B K_{LC} + 1} \quad (253)$$

This is for the same three cases used previously.

$$\frac{\hat{\omega}_e(t)}{\hat{\Omega}} = - (7.51 \times 10^{-5}) e^{-74.5t}$$

$$+ (1.66 \times 10^{-4}) e^{0.78t} \sin (47.8t + 4.42)$$

$$+ (4.84 \times 10^{-4}) e^{-6.36t} \sin (8.8t + 3.44) \quad (254)$$

$$\frac{\hat{\omega}_e(t)}{\hat{\Omega}} = - (7.55 \times 10^{-5}) e^{-74.9t}$$

$$+ (1.68 \times 10^{-4}) e^{-0.91t} \sin (48.1t + 4.36)$$

$$+ (4.75 \times 10^{-4}) e^{-6.34t} \sin (8.71t + 3.45) \quad (255)$$

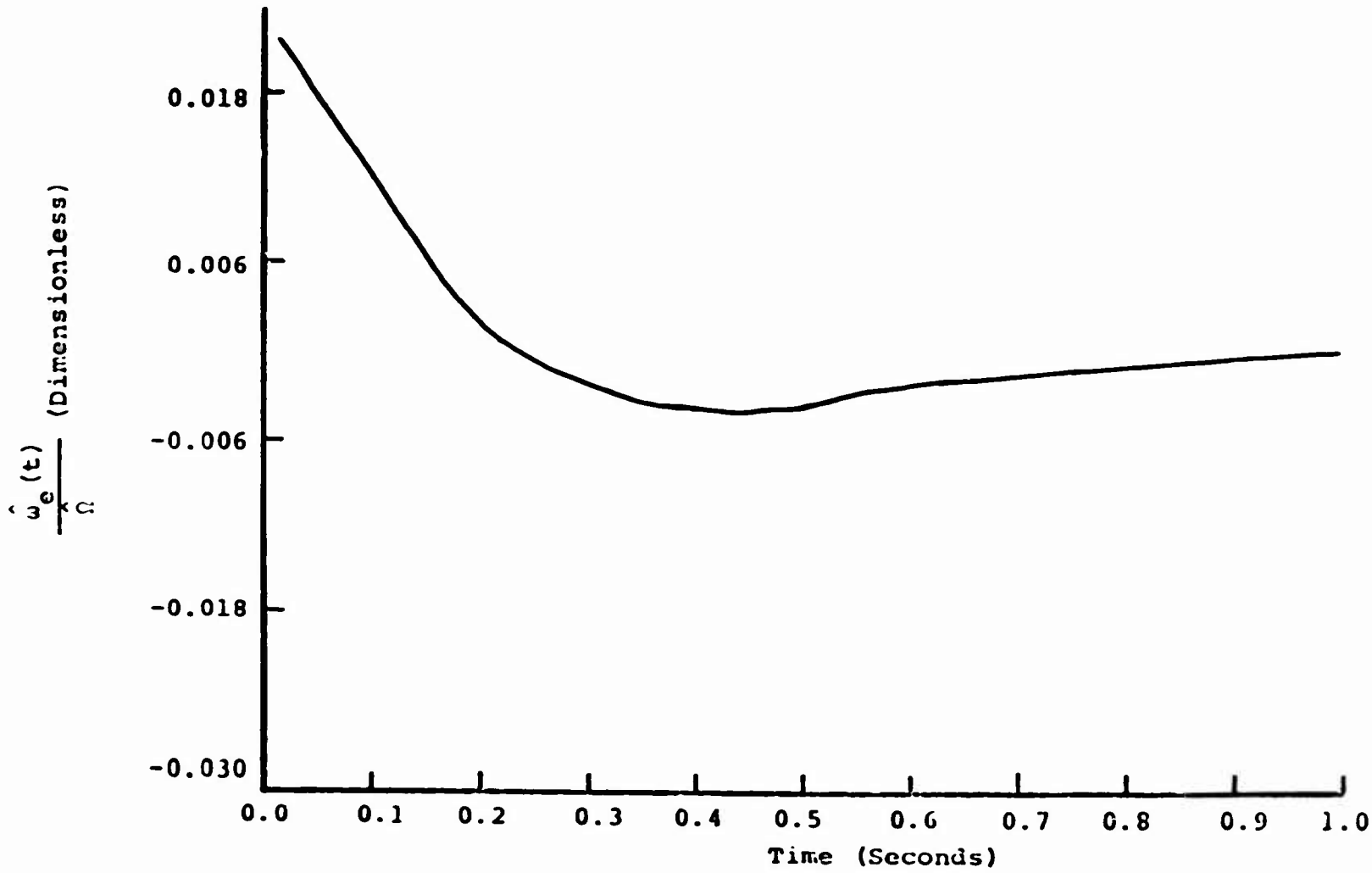

Figure 74. Linear Time Response--Ideal Governor, Two-Spool Turbine Engine, $C_s = 0.0 \frac{\text{ft-lb}}{\text{rad/sec}}$.

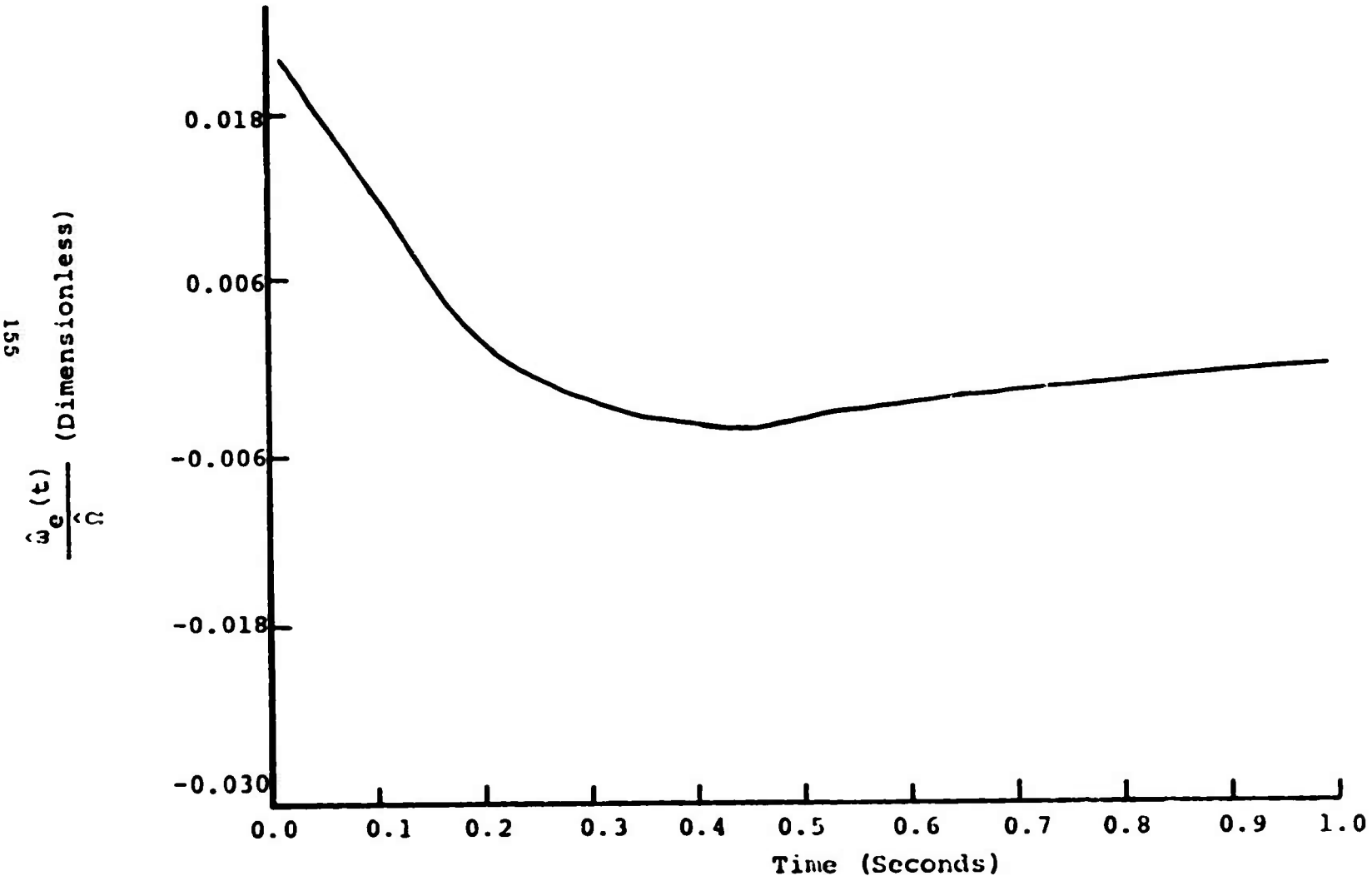

Figure 75. Linear Time Response--Ideal Governor, Two-Spool Turbine Engine, $C_s = 2.24 \frac{\text{ft-lb}}{\text{rad/sec}}$.

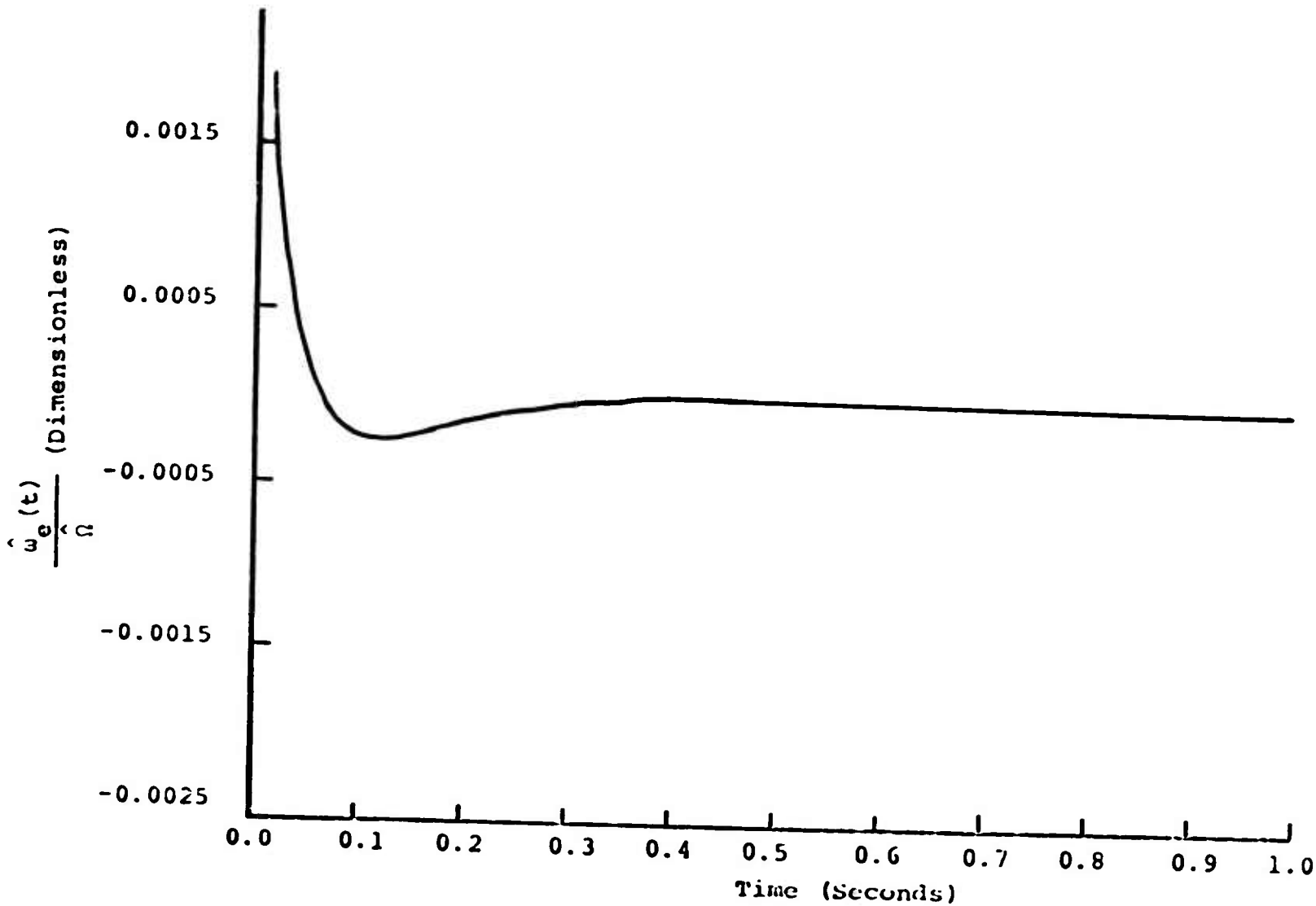

Figure 76. Linear Time Response--Ideal Governor, Two-Spool Turbine Engine, With ZTS Coupling.

$$\frac{\hat{\omega}_e(t)}{\hat{\Omega}} = -(5.67 \times 10^{-5})e^{-81.8t} + (2.68 \times 10^{-4})e^{-1.87t} \sin(39.3t + 4.21) \quad (256)$$

These three functions are plotted in Figures 77, 78, and 79. It can be seen from Figure 77 that this system with zero shaft damping diverges, and is, therefore, completely unstable. This system with nonzero shaft damping, from Figure 78, is stable, but it converges rather slowly. With a ZTS coupling, this system has both a smaller initial variation from the steady state and a more rapid convergence to the steady state. Therefore, it appears that a ZTS coupling certainly improves the time response of this system. As compared to the previously analyzed ideal governor, two-spool turbine engine drive system model, this system has a smaller initial variation from the steady state, but it also has a much slower convergence to the steady state.

In general, it appears that the results and comparisons of the several systems and cases, deduced from the time response analyses, agree very well with the stability information found from the Bode analyses.

STABILITY ANALYSIS WITH LINEARIZED ZTS COUPLING DYNAMICS AND DAMPING

In Part I, a ZTS coupling is designed for high speed, high power applications, such as a helicopter drive system. This ZTS coupling is illustrated in Figures 80 through 82. The drive train with the ZTS coupling is shown in Figure 83. The governing equations for this drive train are given by equations 257 through 262.

$$\dot{p}_c + C_c\dot{\theta}_c^2 + C_s(\dot{\theta}_e - \dot{\theta}_R - \dot{\theta}) + K_\theta(\theta_e - \theta_R - \theta) = T_e \quad (257)$$

$$p_c = (I_c + I_{fe})\dot{\theta}_e + I_{fR}(\dot{\theta}_e - \dot{\theta}) + \frac{N}{2}\left[M + \frac{m\ell}{2} + 2\frac{I_\ell}{\ell^2}\right]\left[2(\dot{\theta}_e - \frac{\dot{\theta}}{2})\left[r\cos\frac{\theta}{2} + (\ell^2 - r^2\sin^2\frac{\theta}{2})^{\frac{1}{2}}\right]^2\right] + \frac{N}{2}\left[\frac{m\ell}{2} - 2\frac{I_\ell}{\ell^2}\right]\left[4r\left[r\cos\frac{\theta}{2} + (\ell^2 - r^2\sin^2\frac{\theta}{2})^{\frac{1}{2}}\right](\dot{\theta}_e - \frac{\dot{\theta}}{2})\cos\frac{\dot{\theta}}{2}\right] + \frac{N}{2}\left[\frac{M_c}{2} + 2\frac{I_\ell}{\ell^2}\right]\left[r^2(2\dot{\theta}_e - \dot{\theta})\right] \quad (258)$$

$$\dot{p}_c - C_s(\dot{\theta}_e - \dot{\theta}_R - \dot{\theta}) - K_\theta(\theta_e - \theta_R - \theta) - C_c\dot{\theta} - \frac{N}{2}\left[M + \frac{m\ell}{2} + 2\frac{I_\ell}{\ell^2}\right]\left[\frac{\dot{\theta}}{2}\left[r\sin\frac{\theta}{2} + \frac{r^2}{2}\sin\theta(\ell^2 - r^2\sin^2\frac{\theta}{2})^{-\frac{1}{2}}\right]\right.$$

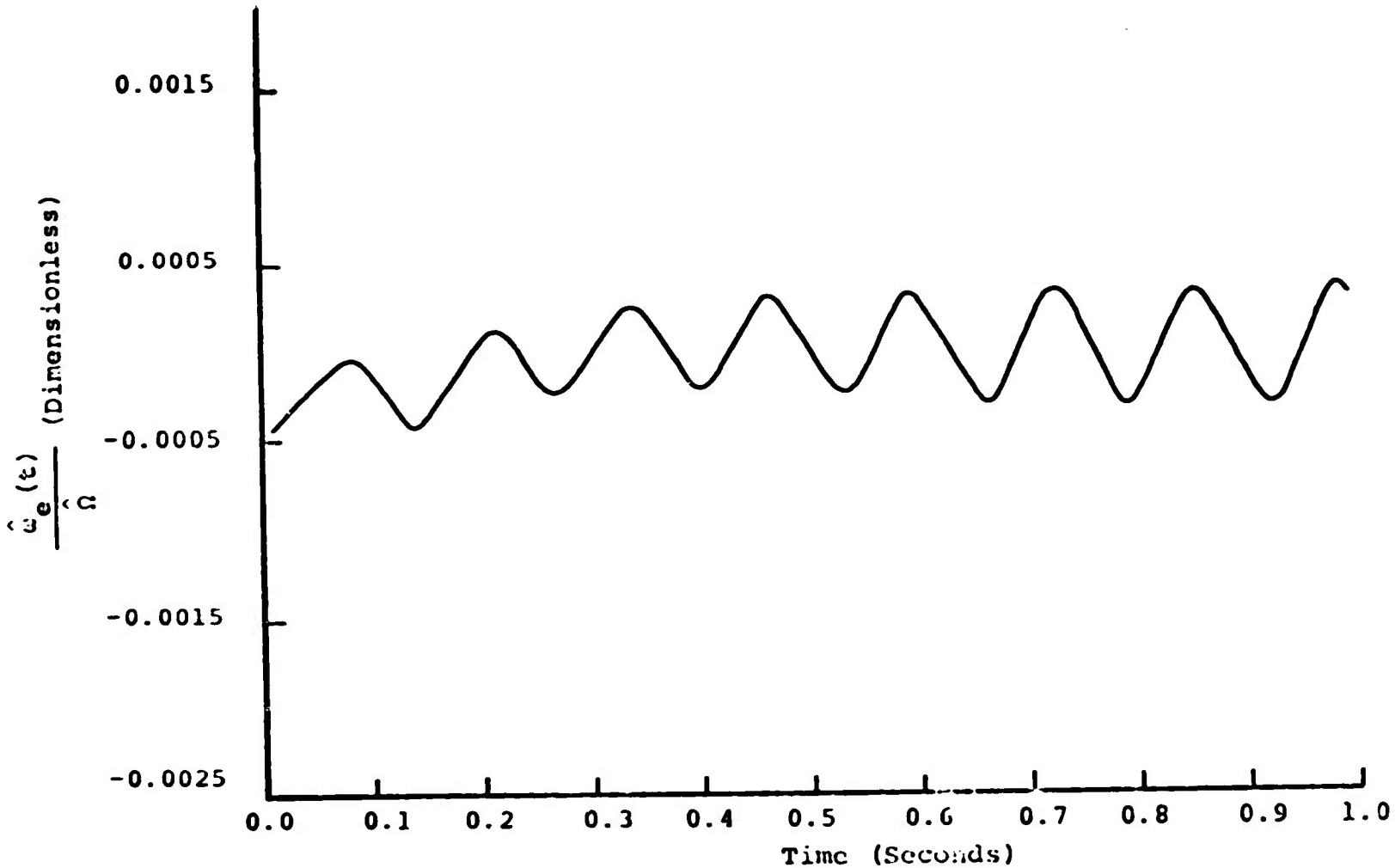

Figure 77. Linear Time Response--Direct Fuel Flow Governor, One-Spool Turbine Engine, $C_s = 0.0 \frac{\text{ft-lb}}{\text{rad sec}}$.

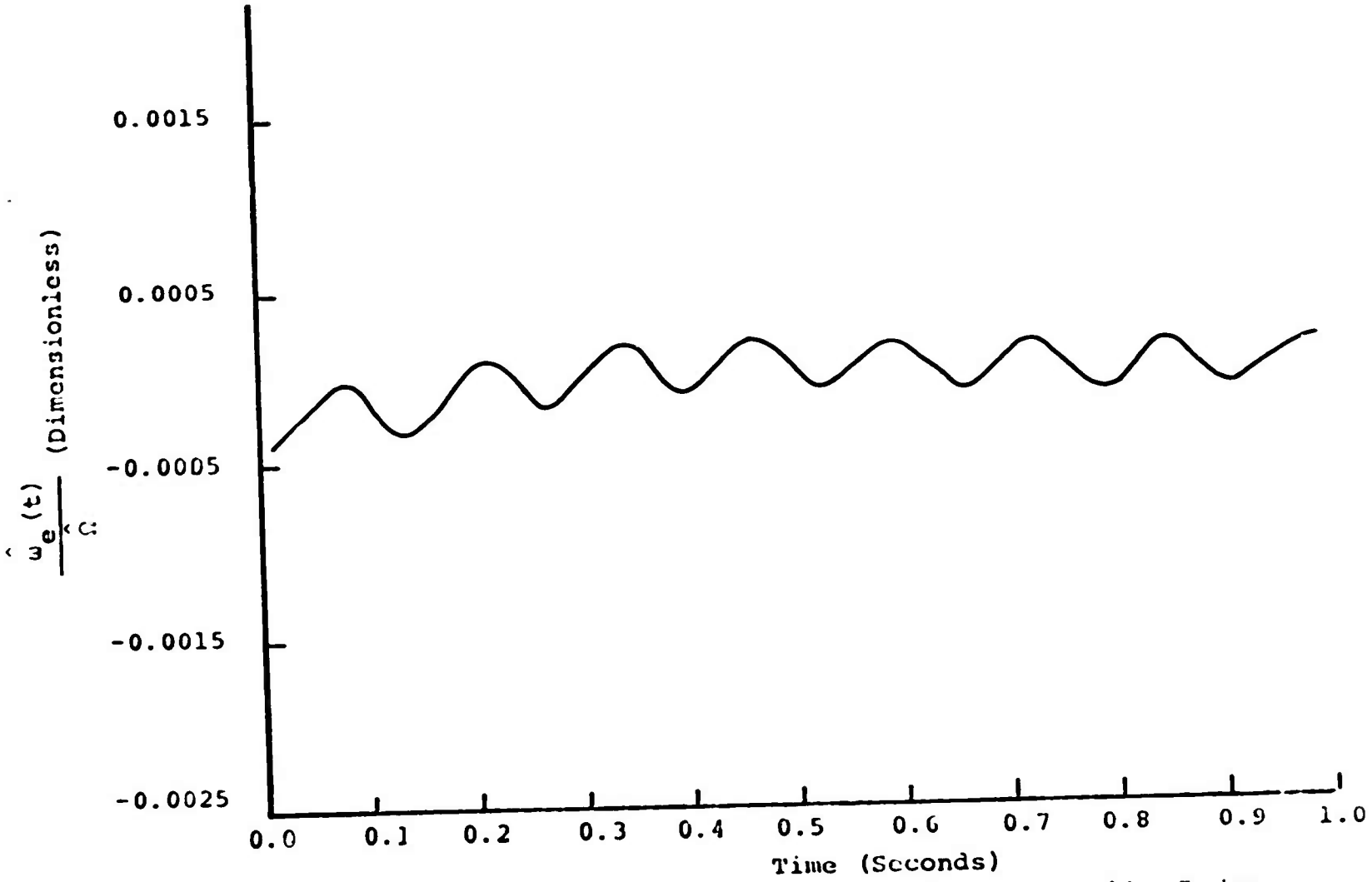

Figure 78. Linear Time Response--Direct Fuel Flow Governor, One-Spool Turbine Engine, $C_s = 2.24 \frac{\text{ft-lb}}{\text{rad/sec}}$.

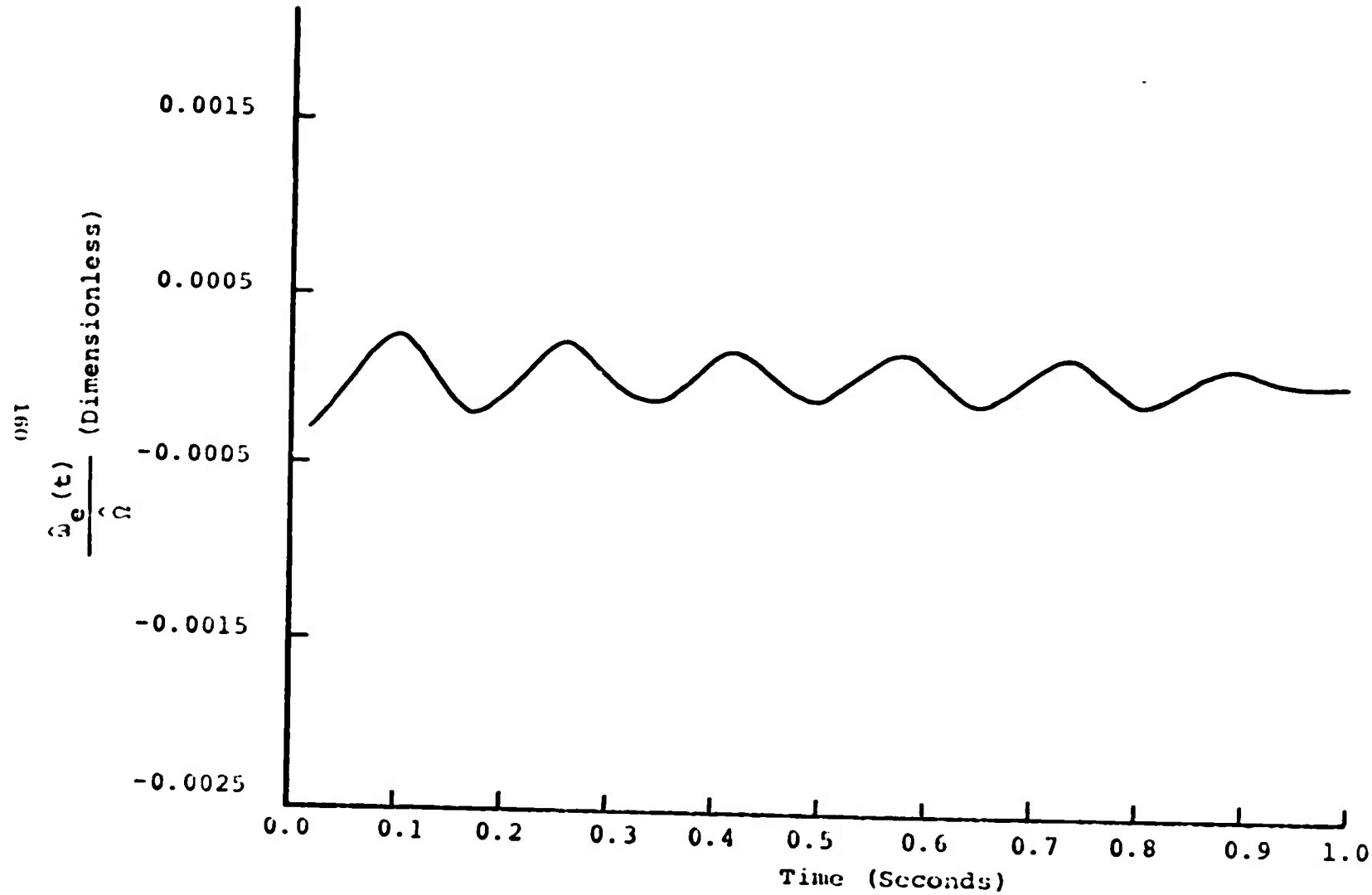

Figure 79. Linear Time Response--Direct Fuel Flow Governor, One-Spool Turbine Engine, With ZTS Coupling.

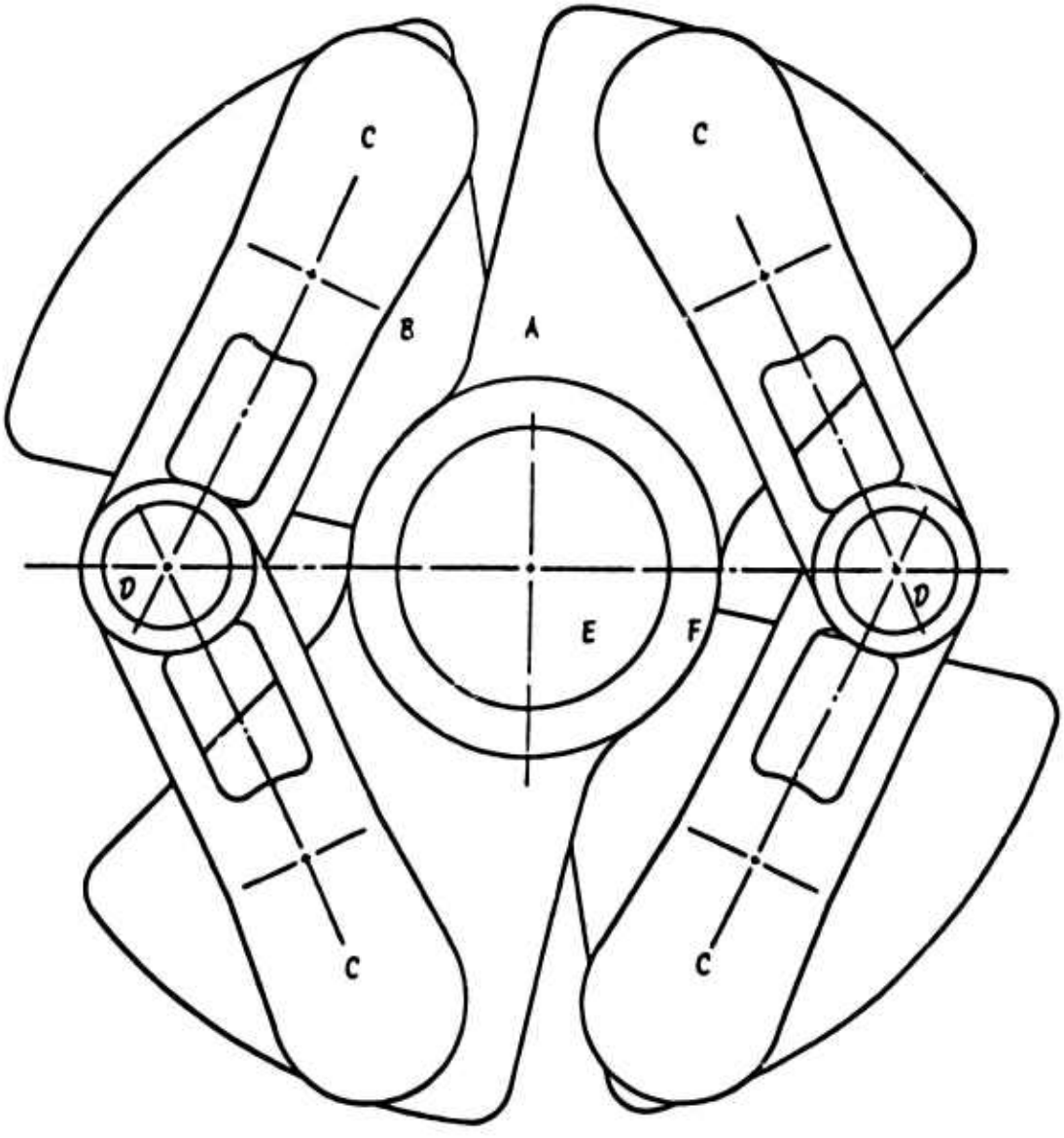

Figure 80. ZTS Coupling (Front).

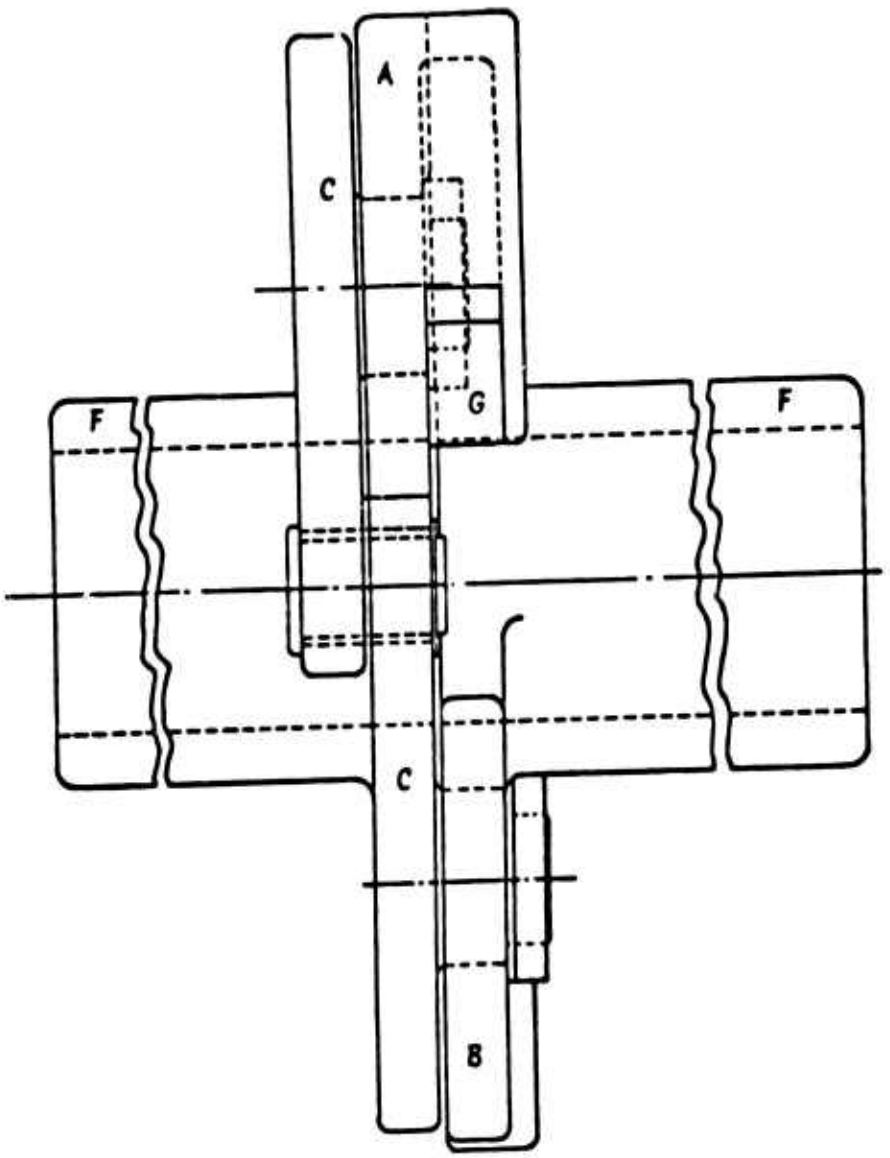

Figure 81. ZTS Coupling (Side).

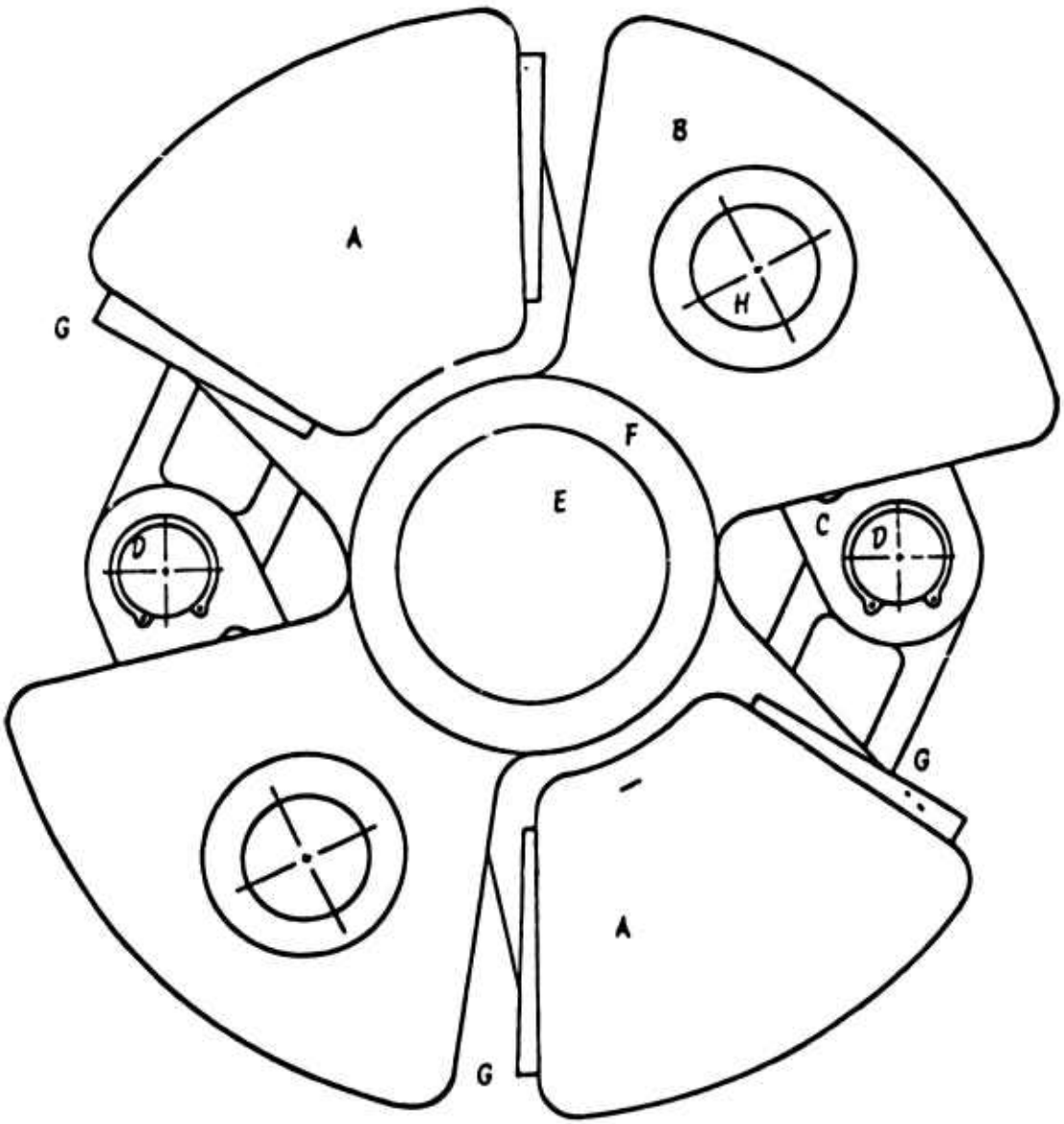

Figure 82. ZTS Coupling (Back).

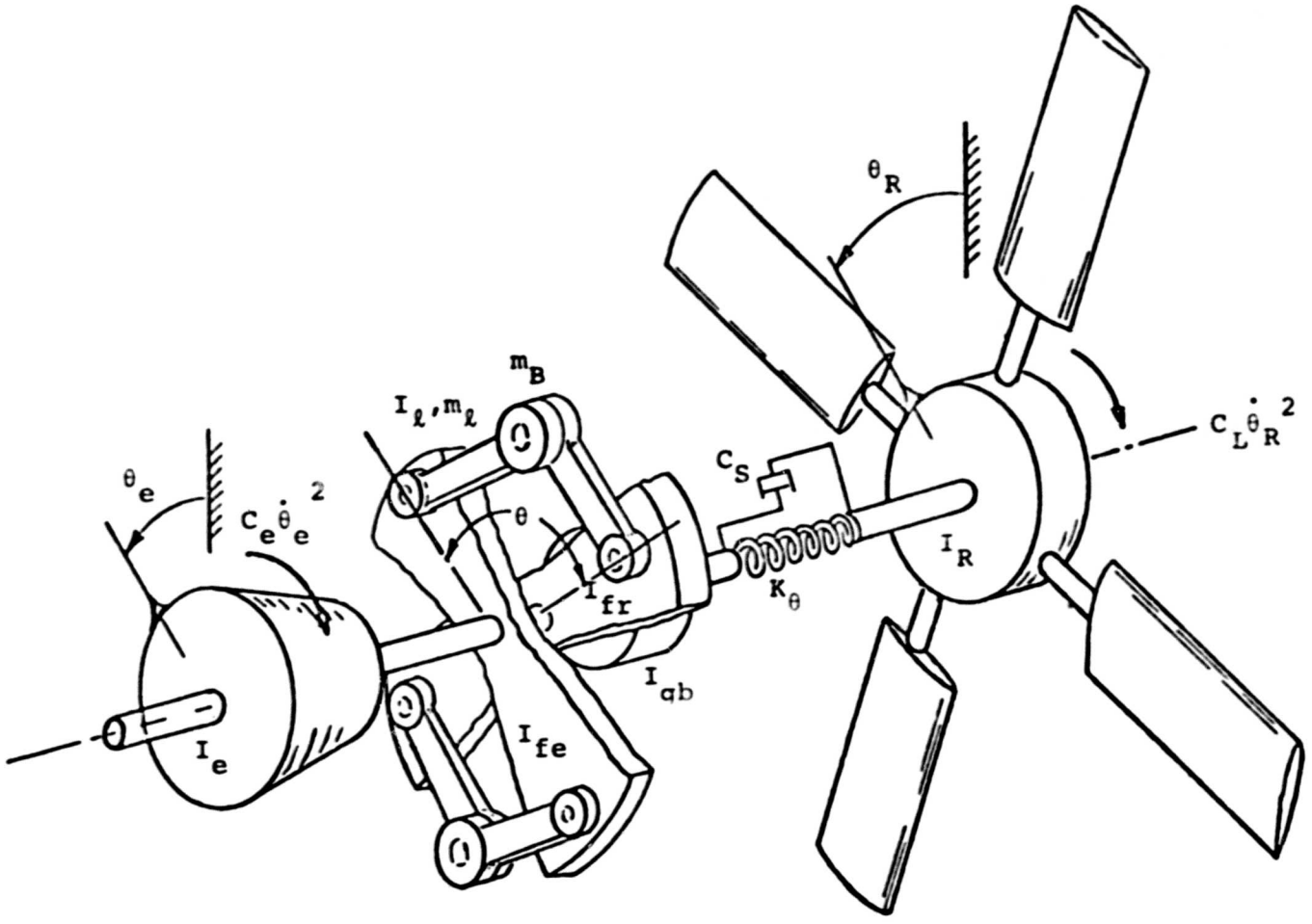

Figure 83. Helicopter Drive Train (With Coupling).

$$+\left[\frac{r}{2}\cos\frac{\theta}{2}+\frac{r^2}{2}\cos\theta(\ell^2-r^2\sin^2\frac{\theta}{2})^{-\frac{1}{2}}\right]+\frac{r^4}{8}\sin^2\theta(\ell^2-r^2\sin^2\frac{\theta}{2})^{-3/2}$$

$$+2(\dot\theta_e-\frac{\dot\theta}{2})^2\left[r\cos\frac{\theta}{2}+(\ell^2-r^2\sin^2\frac{\theta}{2})^{\frac{1}{2}}\right]\left[-\frac{r}{2}\sin\frac{\theta}{2}\right.$$

$$\left.-\frac{r^2}{4}\sin\theta\,(\ell^2-r^2\sin^2\frac{\theta}{2})^{-\frac{1}{2}}\right]+\frac{N}{2}\left[\frac{m_\ell}{2}-2\frac{I_\ell}{\ell^2}\right]\left[-\frac{r\dot\theta^2}{4}\cos\frac{\theta}{2}\left[r\sin\frac{\theta}{2}\right.\right.$$

$$+\frac{r^2}{2}\sin\theta\,(\ell^2-r^2\sin^2\frac{\theta}{2})^{-\frac{1}{2}}\Big]-\frac{r\dot\theta^2}{2}\sin\frac{\theta}{2}\left[r\cos\frac{\theta}{2}\right.$$

$$\left.+\frac{r^2}{2}\cos\theta\,(\ell^2-r^2\sin^2\frac{\theta}{2})^{-\frac{1}{2}}\right]+\frac{r^4}{8}\sin^2\theta\,(\ell^2-r^2\sin^2\frac{\theta}{2})^{-3/2}$$

$$\left.+(\dot\theta_e-\frac{\dot\theta}{2})^2\,r\cos\frac{\theta}{2}\left[r\sin\frac{\theta}{2}\sin\theta\,(\ell^2-r^2\sin^2\frac{\theta}{2})^{-\frac{1}{2}}\right]\right]=0 \qquad (259)$$

$$p_c - I_{fR}(\dot\theta_e-\dot\theta)+\frac{N}{2}\left[M+\frac{m_\ell}{2}+2\frac{I_\ell}{\ell^2}\right]\left[\frac{\dot\theta}{2}\left[r\sin\frac{\theta}{2}\right.\right.$$

$$+\frac{r^2}{2}\sin\theta\,(\ell^2-r^2\sin^2\frac{\theta}{2})^{-\frac{1}{2}}\Big]^2-(\theta_e-\frac{\dot\theta}{2})\left[r\cos\frac{\theta}{2}\right.$$

$$\left.\left.+(\ell^2-r^2\sin^2\frac{\theta}{2})^{\frac{1}{2}}\right]^2\right]+\frac{N}{2}\left[\frac{m_\ell}{2}-2\frac{I_\ell}{\ell^2}\right]\left[r\dot\theta\sin\frac{\theta}{2}\left[r\sin\frac{\theta}{2}\right.\right.$$

$$+\frac{r^2}{2}\sin\theta\,(\ell^2-r^2\sin^2\theta)^{-\frac{1}{2}}\Big]-2(\dot\theta_e-\frac{\dot\theta}{2})\,r\cos\frac{\theta}{2}\left[r\cos\frac{\theta}{2}\right.$$

$$\left.\left.+(\ell^2-r^2\sin^2\frac{\theta}{2})^{\frac{1}{2}}\right]\right]+\frac{N}{2}\left[\frac{m_\ell}{2}+2\frac{I_\ell}{\ell^2}\right]\left[r^2(\dot\theta-\dot\theta_e)\right] \qquad (260)$$

$$\dot p_r+C_2\dot\theta_R^2-C_s(\dot\theta_e-\dot\theta_R-\dot\theta)-K_\Delta(\theta_e-\theta_R-\theta)=0 \qquad (261)$$

$$p_R=I_R\dot\theta_R \qquad (262)$$

It has been shown that the mass M, located at point D of the coupling, can be made to include the link mass, m_ℓ. It has also been shown that the link inertia, I_ℓ, has a negligible effect on the dynamics of the ZTS coupling. Therefore, by setting m_ℓ and I_ℓ equal to zero, equations 258 through 260 can be reduced to give equations 263 through 265, respectively.

$$p_e=(I_e+I_{fe})\dot\theta_e+I_{fR}(\dot\theta_e-\dot\theta)+NM\left[(\dot\theta_e-\frac{\dot\theta}{2})\left[r\cos\frac{\theta}{2}+(\ell^2-r^2\sin^2\frac{\theta}{2})^{\frac{1}{2}}\right]^2\right] \qquad (263)$$

$$\dot{p}_c - C_s(\dot{\theta}_e-\dot{\theta}-\dot{\theta}_R) - K_\theta(\theta_e-\theta-\theta_R) + C_c\dot{\theta}$$

$$- \frac{NM}{2}\left[\frac{\dot{\theta}^2}{2}\left[r\sin\frac{\theta}{2} + \frac{r^2}{2}\sin\theta(\ell^2-r^2\sin^2\frac{\theta}{2})^{-\frac{1}{2}}\right]\left[\frac{r}{2}\cos\frac{\theta}{2}\right.\right.$$

$$\left.\left. + \frac{r^2}{2}\cos\theta\,(\ell^2-r^2\sin^2\frac{\theta}{2})^{-\frac{1}{2}} + \frac{r^4}{8}\sin^2\theta\,(\ell^2-r^2\sin^2\frac{\theta}{2})^{-3/2}\right]\right.$$

$$+ 2(\dot{\theta}_e-\frac{\dot{\theta}}{2})^2\left[r\cos\frac{\theta}{2} + (\ell^2-r^2\sin^2\frac{\theta}{2})^{\frac{1}{2}}\right]\left[-\frac{r}{2}\sin\frac{\theta}{2}\right.$$

$$\left.\left. - \frac{r^2}{4}\sin\theta\,(\ell^2-r^2\sin^2\frac{\theta}{2})^{-\frac{1}{2}}\right]\right] = 0 \qquad (264)$$

$$p_c = -I_{fR}(\dot{\theta}_e-\dot{\theta}) + \frac{NM}{2}\left[\frac{\dot{\theta}}{2}\left[r\sin\frac{\theta}{2} + \frac{r^2}{2}\sin\theta\,(\ell^2-r^2\sin^2\frac{\theta}{2})^{-\frac{1}{2}}\right]^2\right.$$

$$\left. - (\dot{\theta}_e-\frac{\dot{\theta}}{2})\left[r\cos\frac{\theta}{2} + (\ell^2-r^2\sin^2\frac{\theta}{2})^{\frac{1}{2}}\right]^2\right] \qquad (265)$$

A coordinate transformation is made, once again employing θ_s, the angle of twist in the shaft. For the helicopter drive train with a ZTS coupling, θ_s is given by

$$\theta_s = \theta_e - \theta_R - \theta.$$

Substituting θ_s into equations 257, 263 through 265, 261, and 262, eliminating θ_R and its derivatives, and replacing $\dot{\theta}_e$ by ω_e and $\ddot{\theta}_e$ by $\dot{\omega}_e$, results in equations 266 through 271.

$$\dot{p}_e + C_e\omega_e^2 + C_s\dot{\theta}_s + K_\theta\theta_s = T_e \qquad (266)$$

$$p_e = (I_e + I_{fe})\omega_e + I_{fR}(\omega_e-\dot{\theta})$$

$$+ NM\left[(\omega_e-\frac{\dot{\theta}}{2})\left[r\cos\frac{\theta}{2} + (\ell^2-r^2\sin^2\frac{\theta}{2})^{\frac{1}{2}}\right]^2\right] \qquad (267)$$

$$\dot{p}_c - C_s\dot{\theta}_s - K_\theta\theta_s + C_c\dot{\theta} - \frac{NM}{2}\left[\frac{\dot{\theta}^2}{2}\left[r\sin\frac{\theta}{2} + \frac{r^2}{2}\sin\theta(\ell^2-r^2\sin^2\frac{\theta}{2})^{-\frac{1}{2}}\right]\right.$$

$$\left. + \left[\frac{r}{2}\cos\frac{\theta}{2} + \frac{r^2}{2}\cos\theta(\ell^2-r^2\sin^2\frac{\theta}{2})^{-\frac{1}{2}} + \frac{r^4}{8}\sin^2\theta(\ell^2-r^2\sin^2\frac{\theta}{2})^{-3/2}\right]\right.$$

$$+ 2(\omega_e-\frac{\dot{\theta}}{2})^2\left[\cos\frac{\theta}{2} + (\ell^2-r^2\sin^2\frac{\theta}{2})^{\frac{1}{2}}\right]\left[-\frac{r}{2}\sin\frac{\theta}{2} - \frac{r^2}{4}\sin\theta\right.$$

$$\left.\left. + (\ell^2-r^2\sin^2\frac{\theta}{2})^{-\frac{1}{2}}\right]\right] = 0 \qquad (268)$$

$$p_c = -I_{fr}(\omega_e-\dot{\theta}) + \frac{NM}{2}\frac{\dot{\theta}}{2}\left[r\sin\frac{\theta}{2} + \frac{r^2}{2}\sin\theta\,(\ell^2-r^2\sin^2\frac{\theta}{2})^{-\frac{1}{2}}\right]^2$$

$$- (\omega_e-\frac{\dot{\theta}}{2})\left[r\cos\frac{\theta}{2} + (\ell^2-r^2\sin^2\frac{\theta}{2})^{\frac{1}{2}}\right]^2\Bigg] \qquad (269)$$

$$\dot{p}_R + C_L(\omega_e - \dot{\theta} - \dot{\theta}_s)^2 - C_s\dot{\theta}_s - K_\theta\theta_s = 0 \tag{270}$$

$$p_R = I_R(\omega_e - \dot{\theta} - \dot{\theta}_s) \tag{271}$$

Taking the time derivatives of equations 267, 269, and 271 and inserting them into equations 266, 268, and 270, respectively, results in equations 272 through 274.

$$(I_e+I_{fe})\dot{\omega}_e+I_{fR}(\dot{\omega}_e-\ddot{\theta}) + \frac{NM}{2}\left[(2\dot{\omega}_e-\ddot{\theta})\left[r\cos\frac{\theta}{2} + (\ell^2-r^2\sin^2\frac{\theta}{2})^{\frac{1}{2}}\right]^2\right.$$
$$+ (\frac{\dot{\theta}^2}{2}-\dot{\theta}\omega_e)\left[r^3\sin\theta\cos\frac{\theta}{2}(\ell^2-r^2\sin^2\frac{\theta}{2})^{-\frac{1}{2}} + 2r^2\sin\theta\right.$$
$$\left.\left. + 2r\sin\frac{\theta}{2}(\ell^2-r^2\sin^2\frac{\theta}{2})^{\frac{1}{2}}\right]\right] + C_e\omega_e^2 + C_s\dot{\theta}_s + K_\theta\theta_s = T_e \tag{272}$$

$$I_{fR}(\ddot{\theta}-\dot{\omega}_e) + \frac{NM}{2}\left[\frac{\ddot{\theta}}{2}\left[r\sin\frac{\theta}{2} + \frac{r^2}{2}\sin\theta(\ell^2-r^2\sin^2\frac{\theta}{2})^{-\frac{1}{2}}\right]^2\right.$$
$$+ (\frac{\dot{\theta}}{2}-\dot{\omega}_e)\left[r\cos\frac{\theta}{2} + (\ell^2-r^2\sin^2\frac{\theta}{2})^{\frac{1}{2}}\right]^2 + \frac{\dot{\theta}^2}{2}\left[-\frac{r^2}{4}\sin\theta\right.$$
$$- \frac{r}{2}\sin\frac{\theta}{2}(\ell^2-r^2\sin^2\frac{\theta}{2})^{\frac{1}{2}} + \frac{r^3}{2}\sin\frac{\theta}{2}\cos\theta(\ell^2-r^2\sin^2\frac{\theta}{2})^{-\frac{1}{2}}$$
$$+ \frac{r^4}{4}\sin\theta\cos\theta(\ell^2-r^2\sin^2\frac{\theta}{2})^{-1} + \frac{r^5}{8}\sin\frac{\theta}{2}\sin^2\theta(\ell^2-r^2\sin^2\frac{\theta}{2})^{-3/2}$$
$$\left.\left. + \frac{r^6}{16}\sin^3\theta(\ell^2-r^2\sin^2\frac{\theta}{2})^{-2}\right] + \omega_e^2\left[\frac{r^3}{2}\sin\theta\cos\frac{\theta}{2}(\ell^2-r^2\sin^2\frac{\theta}{2})^{-\frac{1}{2}}\right.\right.$$
$$\left.\left. + r^2\sin\theta + r\sin\frac{\theta}{2}(\ell^2-r^2\sin^2\frac{\theta}{2})^{\frac{1}{2}}\right]\right] - C_s\dot{\theta}_s - K_\theta\theta_s + C_e\dot{\theta} = 0 \tag{273}$$

$$I_R(\dot{\omega}_e-\ddot{\theta}-\ddot{\theta}_s) + C_L(\omega_e-\dot{\theta}-\dot{\theta}_s)^2 - C_s\dot{\theta}_s - K_s\theta_s = 0 \tag{274}$$

In order to linearize these equations, a Taylor's series expansion of each equation is taken about the steady-state values of engine speed, coupling angle, and shaft twist angle. Assuming that the variations of these parameters from their steady-state variables are relatively small, all terms of the Taylor's series above the first degree can be ignored. An ordinary Taylor's series expansion is given by equation 275.[15]

$$f(x) = f(a) + (x-a)f^{2}(a) + \ldots + \frac{(x-a)^{n}}{n!} f^{(n)}(a) + \ldots \qquad (275)$$

Expanding this to cover more than one variable and eliminating all terms above first order results in equation 276.

$$f(x,y,\ldots) = f(a,b,\ldots) + (x-a)\left(\frac{\partial f}{\partial x}\bigg|_{x=a}\right) + (y-b)\left(\frac{\partial f}{\partial y}\bigg|_{y=b}\right) + \ldots \qquad (276)$$

Using equation 276 with ω_e, θ and θ_s and their time derivatives as the variables and substituting

$$\omega_e - \bar{\omega}_e = \hat{\omega}_e \qquad \dot{\omega}_e \quad \dot{\omega}_e$$

$$\theta - \bar{\theta} = \hat{\theta} \qquad \dot{\theta} \quad \dot{\hat{\theta}} \qquad \ddot{\theta} \quad \ddot{\theta}$$

$$\theta_s - \bar{\theta}_s = \hat{\theta}_s, \qquad \dot{\theta}_s \quad \dot{\hat{\theta}}_s \qquad \ddot{\theta}_s \quad \ddot{\hat{\theta}}_s$$

where $\bar{\omega}_e$ is the steady-state engine speed and $\hat{\omega}_e$ is the variation of the engine speed from the steady state, the result is equation 277.

$$f(\omega_e,\theta,\theta_s,\dot{\omega}_e,\dot{\theta},\dot{\theta}_s,\ddot{\theta},\ddot{\theta}_s,T_e) = f(\bar{\omega}_e,\bar{\theta},\bar{\theta}_s,0,0,0,0,0,\bar{T}_e) + \omega_e\left(\frac{\partial f}{\partial \omega_e}\bigg|_{\omega_e=\bar{\omega}_e}\right)$$

$$+ \hat{\theta}\left(\frac{\partial f}{\partial \theta}\bigg|_{\theta=\bar{\theta}}\right) + \hat{\theta}_s\left(\frac{\partial f}{\partial \theta_s}\bigg|_{\theta_s=\bar{\theta}_s}\right) + \dot{\omega}_e\left(\frac{\partial f}{\partial \dot{\omega}_e}\bigg|_{\dot{\omega}_e=0}\right) + \dot{\theta}\left(\frac{\partial f}{\partial \dot{\theta}}\bigg|_{\dot{\theta}=0}\right)$$

$$+ \dot{\theta}_s\left(\frac{\partial f}{\partial \dot{\theta}_s}\bigg|_{\dot{\theta}_s=0}\right) + \ddot{\theta}\left(\frac{\partial f}{\partial \ddot{\theta}}\bigg|_{\ddot{\theta}=0}\right) + \ddot{\theta}\left(\frac{\partial f}{\partial \ddot{\theta}_s}\bigg|_{\ddot{\theta}_s=0}\right) \qquad (277)$$

Using equation 277 to linearize equations 272 through 274 results in equations 278 through 280.

$$(I_e + I_{fe})\dot{\omega}_e + I_{fR}(\dot{\omega}_e - \ddot{\theta}) + \frac{NM}{2}\left\{(2\omega_e - \dot{\theta})\left[r\cos\frac{\bar{\theta}}{2} + \left(L^2 - r^2\sin^2\frac{\bar{\theta}}{2}\right)^{\frac{1}{2}}\right]^2 + \right.$$

$$\left. + C_e\bar{\omega}_e^2 + 2C_e\bar{\omega}_e\omega_e + C_s\dot{\theta}_s + K_\theta\bar{\theta}_s + K_\theta\theta_s = \bar{T}_e + T_e \right. \qquad (278)$$

$$I_{fR}(\ddot{\bar{\theta}} - \dot{\omega}_e) + \frac{NM}{2}\left\{\frac{\ddot{\bar{\theta}}}{2}\left[r \sin\frac{\bar{\theta}}{2} + \frac{r^2}{2}\sin\bar{\theta}\left(\ell^2 - r^2\sin^2\frac{\bar{\theta}}{2}\right)^{-\frac{1}{2}}\right]^2\right.$$

$$+ \left(\frac{\ddot{\bar{\theta}}}{2} - \dot{\omega}_e\right)\left[r\cos\frac{\bar{\theta}}{2} + \left(\ell^2 - r^2\sin^2\frac{\bar{\theta}}{2}\right)^{\frac{1}{2}}\right]^2$$

$$+ (\bar{\omega}_e + 2\dot{\omega}_e)\bar{r}_e\left[\frac{r^3}{2}\sin\bar{\theta}\cos\frac{\bar{\theta}}{2}\left(\ell^2 - r^2\sin^2\frac{\bar{\theta}}{2}\right)^{-\frac{1}{2}}\right.$$

$$\left. + r^2\sin\bar{\theta} + r\sin\frac{\bar{\theta}}{2}\left(\ell^2 - r^2\sin^2\frac{\bar{\theta}}{2}\right)^{\frac{1}{2}}\right]$$

$$+ \dot{\theta}\,\bar{r}_e^2\left[\frac{r^3}{2}\cos\bar{\theta}\cos\frac{\bar{\theta}}{2}\left(\ell^2 - r^2\sin^2\frac{\bar{\theta}}{2}\right)^{-\frac{1}{2}}\right.$$

$$- \frac{r^3}{2}\sin\bar{\theta}\sin\frac{\bar{\theta}}{2}\left(\ell^2 - r^2\sin^2\frac{\bar{\theta}}{2}\right)^{-\frac{1}{2}}$$

$$+ \frac{r^5}{8}\sin^2\bar{\theta}\cos\frac{\bar{\theta}}{2}\left(\ell^2 - r^2\sin^2\frac{\bar{\theta}}{2}\right)^{-3/2} + r^2\cos\bar{\theta}$$

$$\left.\left. + \frac{r}{2}\cos\frac{\bar{\theta}}{2}\left(\ell^2 - r^2\sin^2\frac{\bar{\theta}}{2}\right)^{\frac{1}{2}}\right]\right\} - C_s\dot{\theta} - K_\theta\bar{\theta}_s$$

$$- K_\theta\theta_s + C_c\dot{\theta} = 0 \qquad (279)$$

$$I_R(\ddot{\bar{r}}_e - \ddot{\bar{\theta}} - \ddot{\theta}_s) + C_L\bar{r}_e^2 + 2C_L\bar{r}_e(\dot{\omega}_e - \dot{\bar{\theta}} - \dot{\theta}_s)$$

$$- C_s\dot{\bar{\theta}}_s - K_\theta\bar{\theta}_s - K_\theta\theta_s = 0 \qquad (280)$$

Equations 70 and 71 are substituted into equations 278 through 280. In addition, the following substitutions are made for constant coefficients:

$$E_1 \quad \frac{NM}{2}\left[r\cos\frac{\bar{\theta}}{2} + \left(\ell^2 - r^2\sin^2\frac{\bar{\theta}}{2}\right)^{\frac{1}{2}}\right]^2$$

$$E_2 \quad \frac{NM}{2}\left[r\sin\frac{\bar{\theta}}{2} + \frac{r^2}{2}\sin\bar{\theta}\left(\ell^2 - r^2\sin^2\frac{\bar{\theta}}{2}\right)^{-\frac{1}{2}}\right]^2$$

$$E_3 = \frac{NM}{2}\left[\frac{r^3}{2}\sin\bar{\theta}\cos\frac{\bar{\theta}}{2}\left(\ell^2 - r^2\sin^2\frac{\bar{\theta}}{2}\right)^{\frac{1}{2}} + r^2\sin\bar{\theta}\right.$$

$$\left. + r\sin\frac{\bar{\theta}}{2}\left(\ell^2 - r^2\sin^2\frac{\bar{\theta}}{2}\right)^{\frac{1}{2}}\right]$$

$$E_4 = \frac{NM}{2}\left[\frac{r^3}{2}\cos\bar{\theta}\cos\frac{\bar{\theta}}{2}\left(\ell^2 - r^2\sin^2\frac{\bar{\theta}}{2}\right)^{\frac{1}{2}}\right.$$

$$- \frac{r^3}{2}\sin\bar{\theta}\sin\frac{\bar{\theta}}{2}\left(\ell^2 - r^2\sin^2\frac{\bar{\theta}}{2}\right)^{-\frac{1}{2}} + \frac{r^5}{8}\sin^2\bar{\theta}\cos\frac{\bar{\theta}}{2}\left(\ell^2 - r^2\sin^2\frac{\bar{\theta}}{2}\right)^{-3/2}$$

$$\left. + r^2\cos\bar{\theta} + \frac{r}{2}\cos\frac{\bar{\theta}}{2}\left(\ell^2 - r^2\sin^2\frac{\bar{\theta}}{2}\right)^{\frac{1}{2}}\right]$$

The resulting differential equations are given by equations 281 through 283.

$$(I_e + I_{fe})\dot{\hat{\omega}}_e + I_{fR}(\dot{\hat{\omega}}_e - \ddot{\bar{\theta}}) + (2\dot{\bar{\omega}}_e - \ddot{\bar{\theta}})E_1 + C_e\bar{\omega}_e^2$$

$$+ C_T\hat{\omega}_e + C_s\dot{\hat{\theta}}_s + K_\theta\bar{\theta}_s + K_\theta\hat{\theta}_s = \bar{T}_e + \hat{T}_e \qquad (281)$$

$$I_{fR}(\ddot{\bar{\theta}} - \dot{\bar{\omega}}_e) + \frac{\ddot{\bar{\theta}}}{2}E_2 + (\frac{\ddot{\bar{\theta}}}{2} - \dot{\bar{\omega}}_e)E_1 + \bar{\omega}_e^2E_3 + 2\bar{\omega}_e\hat{\omega}_eE_3$$

$$+ \hat{\theta}\bar{\omega}_e^2E_4 - C_s\dot{\hat{\theta}}_s - K_\theta\bar{\theta}_s - K_\theta\hat{\theta}_s + C_c\dot{\hat{\theta}} = 0 \qquad (282)$$

$$I_R(\dot{\hat{\omega}}_e - \ddot{\hat{\theta}} - \ddot{\hat{\theta}}_s) + C_L\bar{\omega}_e^2 + C_D(\hat{\omega}_e - \dot{\hat{\theta}} - \dot{\hat{\theta}}_s) - C_s\dot{\hat{\theta}}_s$$

$$- K_\theta\bar{\theta}_s - K_\theta\hat{\theta}_s = 0 \qquad (283)$$

Setting all system variables and their time derivatives equal to zero yields equations 284 through 286.

$$C_e\bar{\omega}_e^2 + K_\theta\bar{\theta}_s = \bar{T}_e \qquad (284)$$

$$\bar{\omega}_e^2E_3 - K_\theta\bar{\theta}_s = 0 \qquad (285)$$

$$C_L\bar{\omega}_e^2 - K_\theta\bar{\theta}_s = 0 \qquad (286)$$

These equations represent the steady-state solutions of equations 281 through 283. It is the transient solutions that are of primary interest, since they determine stability. The steady-state solutions can be removed from equations 281 through 283 by subtracting equations 284 through 281 respectively, yielding equations 287 through 289.

$$(I_e + I_{fe})\dot{\hat{\omega}}_e + I_{fR}(\dot{\hat{\iota}}_e - \ddot{\hat{\theta}}) + (2\dot{\hat{\iota}}_e - \ddot{\hat{\theta}})E_1 + C_T\dot{\hat{\iota}}_e + C_s\dot{\hat{\theta}}_s + K_\theta\hat{\theta}_s = \hat{T}_e \tag{287}$$

$$I_{fR}(\ddot{\hat{\theta}} - \dot{\hat{\iota}}_e) + \frac{\ddot{\hat{\theta}}}{2}E_2 + (\frac{\ddot{\hat{\theta}}}{2} - \dot{\hat{\omega}}_e)E_1 + 2\bar{\iota}_e E_3\dot{\hat{\iota}}_e + \bar{\iota}_e^2 E_4\hat{\theta} - C_s\dot{\hat{\theta}}_s - K_\theta\hat{\theta}_s + C_c\dot{\hat{\theta}}_s = 0 \tag{288}$$

$$I_R(\dot{\hat{\iota}}_e - \ddot{\hat{\theta}} - \ddot{\hat{\theta}}_s) + C_D(\dot{\hat{\iota}}_e - \dot{\hat{\theta}} - \dot{\hat{\theta}}_s) - C_s\dot{\hat{\theta}}_s - K_\theta\hat{\theta}_s = 0 \tag{289}$$

These are the linearized equations for a helicopter drive train with the ZTS coupling designed in Part I.

A frequency transfer function is derived from these equations to be used in a Bode analysis. The Laplace transform is taken of equations 287 through 289 to give equations 290 through 292.

$$(I_e+I_{fe})S\Delta W_e(S) + I_{fR}(S\Delta W_e(S) - S^2\Delta\theta(S)) + (2S\Delta W_e(S) - S^2\Delta\theta(S))E_1 + C_T\Delta W_e(S) + C_sS\Delta\theta_s(S) + K_\theta\Delta\theta_s(S) = \Delta T_e(S)$$

$$I_{fR}(S^2\Delta\theta(S) - S\Delta W_e(S)) + \frac{E_2}{2}S^2\Delta\theta(S) + \left(\frac{S^2}{2}\Delta\theta(s) - S\Delta W_e(s)\right)E_1 + 2\bar{\iota}_e E_3\Delta W_e(S) + \bar{\iota}_e^2 E_4\Delta\theta(S) - C_sS\Delta\theta_s(S) - K_\theta\Delta\theta_s(S) + C_cS\Delta\theta(S) = 0 \tag{291}$$

$$I_R(S\Delta W_e(S) - S^2\Delta\theta(S) - S^2\Delta\theta_s(S)) + C_D(\Delta W_e(S) - S\Delta\theta(S) - S\Delta\theta_s(S)) - C_sS\Delta\theta_s(S) - K_\theta\Delta\theta_s(S) = 0 \tag{292}$$

Equation 292 is solved for $\Delta\Theta_s(S)$ giving

$$\Delta\Theta_s(S) = \frac{(I_R s + C_D)\,\Delta\omega_e(s) - S\Delta\Theta(S)}{I_R s^2 + (C_D + C_s)S + K_\theta}$$

which is substituted into equations 290 and 291 in order to eliminate $\Delta\Theta_s(s)$ from the equations. The resulting equations are given by equations 293 and 294.

$$\left[(I_e+I_{fe}+I_{fR}+2E_1)S + C\right]\Delta W_e(s) - (I_{fR}+E_1)S^2\Delta\Theta(s)$$

$$+\frac{(C_s S + K_\theta)(C_D+I_R s)(\Delta W_e(s) - S\Delta\Theta(s))}{\left[I_R s^2 + (C_s+C_D)S + K_\theta\right]} = \Delta T_e(s) \qquad (293)$$

$$-\left[(I_{fR}+E_1)S - 2\bar{\omega}_e E_3\right]\Delta W_e(s) + \left[\left(I_{fR}+\frac{E_2}{2}+\frac{E_1}{2}\right)S^2 + C_c S + \bar{\omega}_e^2 E_4\right]\Delta\Theta(s)$$

$$-\frac{(C_s S+K_\theta)(C_D+I_R s)(\Delta W_e(s) - S\Delta\Theta(s))}{\left[I_R s^2 + (C_s+C_D)S + K_\theta\right]} = 0 \qquad (294)$$

Equation 294 is solved for $\Delta\Theta(s)$ giving

$$\Delta\Theta(s) = \left\{\left[(I_{fR}+E_1)S - 2\bar{\omega}_e E_3\right]\left[I_R s^2 + (C_s+C_D)S + K_\theta\right] + (C_s S+K_\theta)(C_D+I_R s)\right\}\Delta W_e(s) \Big/ \left\{\left[\left(I_{fR}+\frac{E_2}{2}+\frac{E_1}{2}\right)S^2 + C_s S + \bar{\omega}_e^2 E_4\right]\left[I_R s^2 + (C_s+C_D)S + K_\theta\right] + S(C_s S+K_\theta)(C_D+I_R S)\right\},$$

which is substituted into equation 293 in order to eliminate $\Delta\Theta(S)$ from the equation. In addition, the following substitutions are made:

$$E_5 = I_e + I_{fe} + I_{fR} + 2E_1$$

$$E_6 = I_{fR} + E_1$$

$$E_7 = I_{fR} + \frac{E_2}{2} + \frac{E_1}{2}$$

$$E_8 = 2\bar{I}_c E_3$$

$$E_9 = \bar{I}_c^2 E_4$$

The resulting equation is given by equation 295.

$$(E_5S+C_T)\Delta W_c(S) + \left\{\left[\left[I_RS^2+(C_s+C_D)S+K_\theta\right]\left[(C_sS+K_\theta)(I_RS+C_L)(-2E_6S^2+E_7S^2\right.\right.\right.$$
$$\left.\left.\left.+C_cS+E_8S+E_9)\right] - \left[I_RS^2+(C_s+C_D)S+K_\theta\right]^2\left[E_6S^2(E_6S-E_8)\right]\right]\right\}$$
$$+ \Delta W_c(s)\Big/\left\{\left[\left[I_RS^2+(C_s+C_D)S+K_\theta\right](E_7S^2+C_cS+E_9)\right.\right.$$
$$\left.\left. + S(C_sS+K_\theta)(I_RS+C_L)\right]\right\} \quad \Delta T_c(s) \qquad (295)$$

This equation is converted into a Laplace transfer function with the aid of the following substitutions:

A_1 I_RE_7

A_2 $E_7(C_s+C_D) + (C_s+C_c)I_R$

A_3 $I_RE_9 + E_7K_\theta + I_RK_\theta + (C_s+C_D)C_c$

A_4 $E_9(C_s+C_D) + K_\theta(C_c+C_D)$

A_5 $K_\theta E_9$

B_1 $I_R(E_5E_7-E_6^2)$

B_2 $I_R\left[E_7C_T+E_5C_c+E_6I_8+C_s(E_7+E_5-2E_6)\right]$
$+ (C_s+C_D)(E_5E_7-E_6^2)$

B_3 $I_R\left[E_5E_9+C_cC_T+C_s(I_8+C_c+C_T)\right] + (C_s+C_D)(E_7C_T+E_5C_c+E_6I_8)$
$+ K_\theta(E_5E_7-E_6^2) + (K_\theta I_R+C_sC_D)(E_7-2E_6+E_5)$

$$B_4 = I_R E_9(C_s+C_T) + (C_s+C_D)(E_5E_9+C_cC_T)$$
$$+ K_\theta\left[E_7C_T + E_5C_c + E_6E_8 + C_D(E_7+2E_6+E_5)\right]$$
$$+ (C_sC_D + K_\theta I_R)(E_8+C_c+C_T)$$

$$B_5 = K_\theta\left[E_9(E_5+I_R) + C_cC_T + C_D(E_8+C_c+C_T)\right]$$
$$+ (C_s+C_D)E_9C_T + C_sC_DE_9$$

$$B_6 = K_\theta E_9(C_T+C_D)$$

The transfer function is given by equation 296.

$$\frac{\Delta W_e(s)}{\Delta T_e(s)} = \frac{A_1S^4 + A_2S^3 + A_3S^2 + A_4S + A_5}{B_1S^5 + B_2S^4 + B_3S^3 + B_4S^2 + B_5S + B_6} \qquad (296)$$

The corresponding frequency transfer function is found by substituting jw for s in equation 296.

In order to determine the values of the coefficients of equations 296, it is necessary to find the steady-state values for the system parameters. These are found by solving the differential equations of the system for the stationary solutions of the system parameters. This is done by setting the highest time derivatives in the system differential equations equal to zero, and solving for the stationary solutions. Equations 179 through 181 for steady-state fuel flow, gas producer speed and engine torque, respectively, can be applied to the nonlinear case, because the differential equations for the speed governor and gas producer are approximated by assuming that the average values of the coefficients in those differential equations are approximately equal to the values of those coefficients used for small changes about steady state. This does not compromise the major objective of determining the effect of the ZTS coupling on the closed-loop system. To find the stationary solutions for the engine and rotor speeds, equations 272 and 274 are reduced as described above to produce equations 297 and 298.

$$C_e\bar{\omega}_e^2 + K_\theta\bar{\theta}_s = \bar{T}_e \qquad (297)$$

$$C_L\bar{\omega}_e^2 - K_\theta\bar{\theta}_s = 0 \qquad (298)$$

Adding these equations and substituting equation 181 for T_e results in

$$(C_e+C_L)\bar{\omega}_e^2 = K_pK_B\bar{\epsilon}$$

Substituting into this equation for the speed error and rearranging the terms gives

$$\bar{\omega}_e^2 + \frac{K_p K_B}{C_e + C_L}\bar{\omega}_e - \frac{K_p K_B}{C_e + C_L}\Omega = 0$$

This equation is solved for $\bar{\omega}_e$ using the quadratic equation to obtain equation 299, the steady-state engine speed.

$$\bar{\omega}_e = -\frac{K_p K_B}{2(C_e + C_L)} + \sqrt{\left[\frac{K_p K_B}{2(C_e + C_L)}\right]^2 + \frac{K_p K_B}{C_e + C_L}\Omega} \qquad (299)$$

Using the value of K_p determined for a steady-state speed droop of 5 percent for the linearized system, and using the values given previously for the rest of the parameters in equation 299, $\bar{\omega}_e$ is solved for. The steady-state engine speed for the nonlinear case is equal to 1378 radians per second for a set speed of 1447 radians per second. Substituting these values into equation 65 gives a steady-state speed droop of about 4.8 percent for the nonlinear system with the same gain that gives the linear system a 5-percent steady-state speed droop. To find the stationary solution for the angle of the coupling, θ, equation 273 is reduced as described above to yield

$$\frac{NM\bar{\omega}_e^2}{2}\left[\frac{r^2}{2}\sin\bar{\theta}\cos\frac{\bar{\theta}}{2}\left(\ell^2 - r^2\sin^2\frac{\bar{\theta}}{2}\right)^{-\frac{1}{2}} + r^2\sin\bar{\theta} + r\sin\frac{\bar{\theta}}{2}\left(\ell^2 - r^2\sin^2\frac{\bar{\theta}}{2}\right)^{\frac{1}{2}}\right] - K_\theta\bar{\theta}_s = 0$$

Equation 298 is subtracted from this equation, and the result is divided by $\bar{\omega}_e^2$ to give equation 300.

$$\frac{r^3}{2}\sin\bar{\theta}\cos\frac{\bar{\theta}}{2}\left(\ell^2 - r^2\sin^2\frac{\bar{\theta}}{2}\right)^{-\frac{1}{2}} + r^2\sin\bar{\theta} + r\sin\frac{\bar{\theta}}{2}\left(\ell^2 - r^2\sin^2\frac{\bar{\theta}}{2}\right)^{\frac{1}{2}} = \frac{2C_L}{NM} \qquad (300)$$

The ZTS coupling is designed for this helicopter drive system, to give the following coupling parameters (see Pinned Link Design Analysis, Part I):

N	2	m	0.2385 lb-mass
r	3 in.	ℓ	2.61 in.

Using the previously introduced value of rotor damping, the stationary solution for the coupling angle is found from equation 300 to be 1.64 radians. The steady-state speed error is found from equation 117 and the values for $\bar{\Omega}$ and $\bar{\omega}_e$ calculated above. The steady-state fuel flow for this set speed is found from equation 179 to be approximately 2760 pounds per hour. Equation 180 gives the steady-state value of the gas producer speed as about 294 radians per second. From equation 181, the steady-state value for the torque applied to the power turbine is found to be about 2540 foot-pounds.

To find the steady-state values of engine and rotor speed for the same helicopter drive system model, but without a ZTS coupling, equations 68 and 69 are reduced as above to give

$$C_e \bar{\omega}_e^2 + K_\theta \bar{\theta}_s = \bar{T}_e$$

$$C_L \bar{\omega}_e^2 - K_\theta \bar{\theta}_s = 0$$

These equations are identical to equations 297 and 298. Therefore, the stationary solutions of engine and rotor speed for this helicopter drive system are the same whether or not it has a ZTS coupling. It follows that the steady-state values for engine torque, fuel flow, and gas producer speed are also independent of the use of this ZTS coupling.

Without a special damper, the viscous damping coefficient C_c would be negligible. However, in the hope of increasing the stability of the system, this damping coefficient may be artificially increased, through use of an elastomeric damper. Therefore, in further stability analyses of this ZTS coupling, C_c will be used as zero and as 50 percent of critical damping, for comparison. Since the helicopter system with the ZTS coupling is no longer a simple two-degree-of-freedom torsional spring-mass system, the determination of the critical damping is greatly complicated. However, it is assumed that the critical damping of this system is of the same order of magnitude as the critical damping of the helicopter system without a ZTS coupling. Previously, this was found to be about 45 foot-pounds per radian per second. Therefore, it is safe to use a value of 10 foot-pounds per radian per second for coupling damping without fear of exceeding 50 percent of critical damping. Since the coupling damping is produced by an elastomeric damper, the exact value of damping is arbitrary, because the damper can be designed to create whatever damping is desired. Part of the intention of this investigation is to determine the effect of coupling damping on the stability of the system, rather than to determine the effect of a specific amount of coupling damping on the stability of the system.

There is now sufficient information to determine the value of substitutions E_1 through E_9 and all of the coefficients of equation 296. The values of

E_1 and E_2 turn out to be much smaller than the values of the inertias I_e, I_{fe}, and I_{fR}. Based on this, equations 287 through 289 can be reduced to equations 301 through 303.

$$(I_e+I_{fe}+I_{fR})\dot{\omega}_e - I_{fR}\ddot{\theta} + C_T\hat{\omega}_e + C_s\dot{\theta}_s + K_\theta\hat{\theta}_s = \hat{T}_e \tag{301}$$

$$I_{fR}(\ddot{\theta}-\dot{\omega}_e) + 2\bar{\omega}_e E_3\hat{\omega}_e + C_c\dot{\theta} + \bar{\omega}_e^2 E_4\hat{\theta} - C_s\dot{\theta}_s - K_\theta\hat{\theta}_s = 0 \tag{302}$$

$$I_R(\dot{\omega}_e-\ddot{\theta}-\ddot{\theta}_s) + C_D(\hat{\omega}_e-\dot{\theta}-\dot{\theta}_s) - C_s\dot{\theta}_s - K_\theta\hat{\theta}_s = 0 \tag{303}$$

It can be seen from equation 302 that this coupling does not truly have zero torsional stiffness when deviated from the equilibrium solution, but rather has a low-torsional stiffness with a spring constant given by $\bar{\omega}_e^2 E_4$.

The frequency transfer function for the helicopter drive train with this ZTS coupling, derived from equation 296, is combined with the frequency transfer functions for the direct fuel flow speed governor and two-spool turbine engine, to give equation 304.

$$F(j\omega) = \left\{K_p K_B[\tau_B(j\omega)+1][A_1(j\omega)^4+A_2(j\omega)^2 + A_3(j\omega)^2 + A_4(j\omega) + A_5]\right\} \Big/ \left\{[\tau_1(j\omega)+1] \cdot[\tau_2(j\omega)+1][\tau_e(j\omega)+1][B_1(j\omega)^5 + B_2(j\omega)^4 + B_3(j\omega)^3 + B_4(j\omega)^2 + B_5(j\omega) + B_6\right\} \tag{304}$$

The coefficients A_5 and B_6 can be factored out of the numerator and denominator, respectively, resulting in equation 305, where K_L is the same as defined earlier.

$$F(j\omega) = \left\{K_p K_B K_L[\tau_B(j\omega)+1]\left[\frac{A_1}{A_5}(j\omega)^4 + \frac{A_2}{A_5}(j\omega)^3 + \frac{A_3}{A_5}(j\omega)^2 + \frac{A_4}{A_5}(j\omega)+1\right]\right\} \Big/ \left\{[\tau_1(j\omega)+1] \cdot[\tau_2(j\omega)+1][\tau_e(j\omega)+1]\left[\frac{B_1}{B_6}(j\omega)^5 + \frac{B_2}{B_6}(j\omega)^4 + \frac{B_3}{B_6}(j\omega)^3 + \frac{B_4}{B_6}(j\omega)^2 + \frac{B_5}{B_6}(j\omega)+1\right]\right\} \tag{305}$$

This transfer function results in the same steady-state speed droop as the similar transfer functions in previous sections. Therefore to achieve a 5-percent steady-state speed droop, the same value of speed governor gain is used as was used before

A Bode analysis of the frequency transfer function of equation 305 was conducted. This was done for values of zero and 2.24 for shaft damping, and

zero and 10.0 for coupling damping, all in units of foot-pounds per radian per second. All four combinations were analyzed and the resulting Bode plots are given in Figures 84 through 87. The gain and phase margins found from these Bode plots are given in Table II. It appears that all four of these cases are not only stable, but they even meet the minimum margin requirements for practical stability as given in Reference 5. Furthermore, it appears that, although shaft damping seems to have little effect on system stability, introduction of coupling damping makes the system even more stable. This is a very desirable situation, because the ZTS coupling can be designed with whatever amount of damping is necessary to meet realistic stability requirements. Therefore, from this linearized stability analysis, it appears that the ZTS coupling designed in Part I can be used to make the helicopter drive system stable enough, with a direct fuel flow speed governor, to be practically usable without necessitating redesigning the speed governor.

TABLE II. BODE RESULTS FOR LINEAR COUPLING DESIGN

Shaft Damping (ft-lb rad per sec)	Coupling Damping (ft-lb rad per sec)	Gain Margin (db)	Phase Margin (deg)
0.0	0.0	7.1	26.5
2.24	0.0	7.1	26.6
0.0	10.0	7.2	64.0
2.24	10.0	8.2	63.0

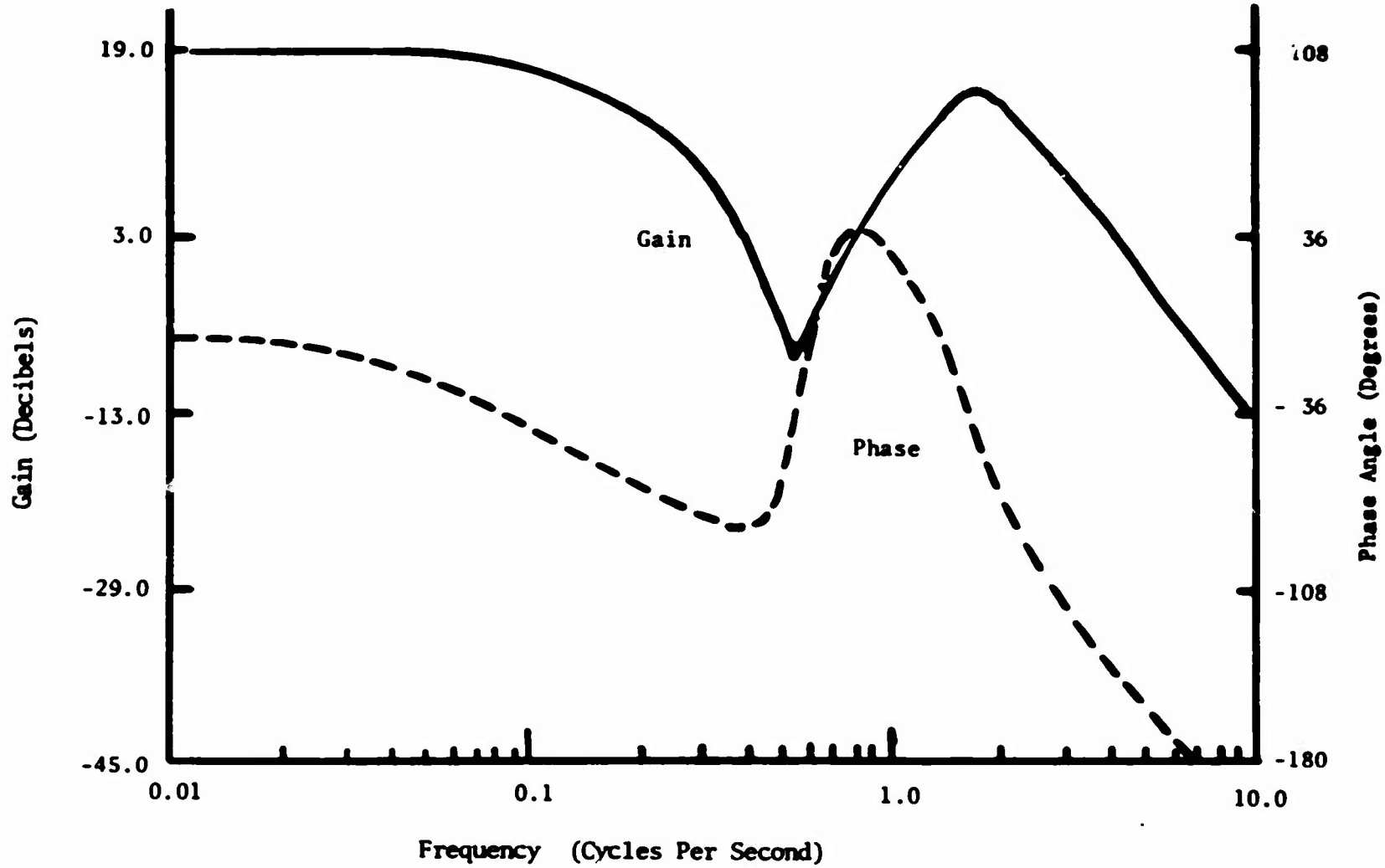

Figure 84. Bode Plots--Direct Fuel Flow Governor With ZTS Coupling (Linearized Design Model)

$C_s = 0.0 \frac{\text{ft-lb}}{\text{rad/sec}}$ $C_c = 0.0 \frac{\text{ft-lb}}{\text{rad/sec}}$.

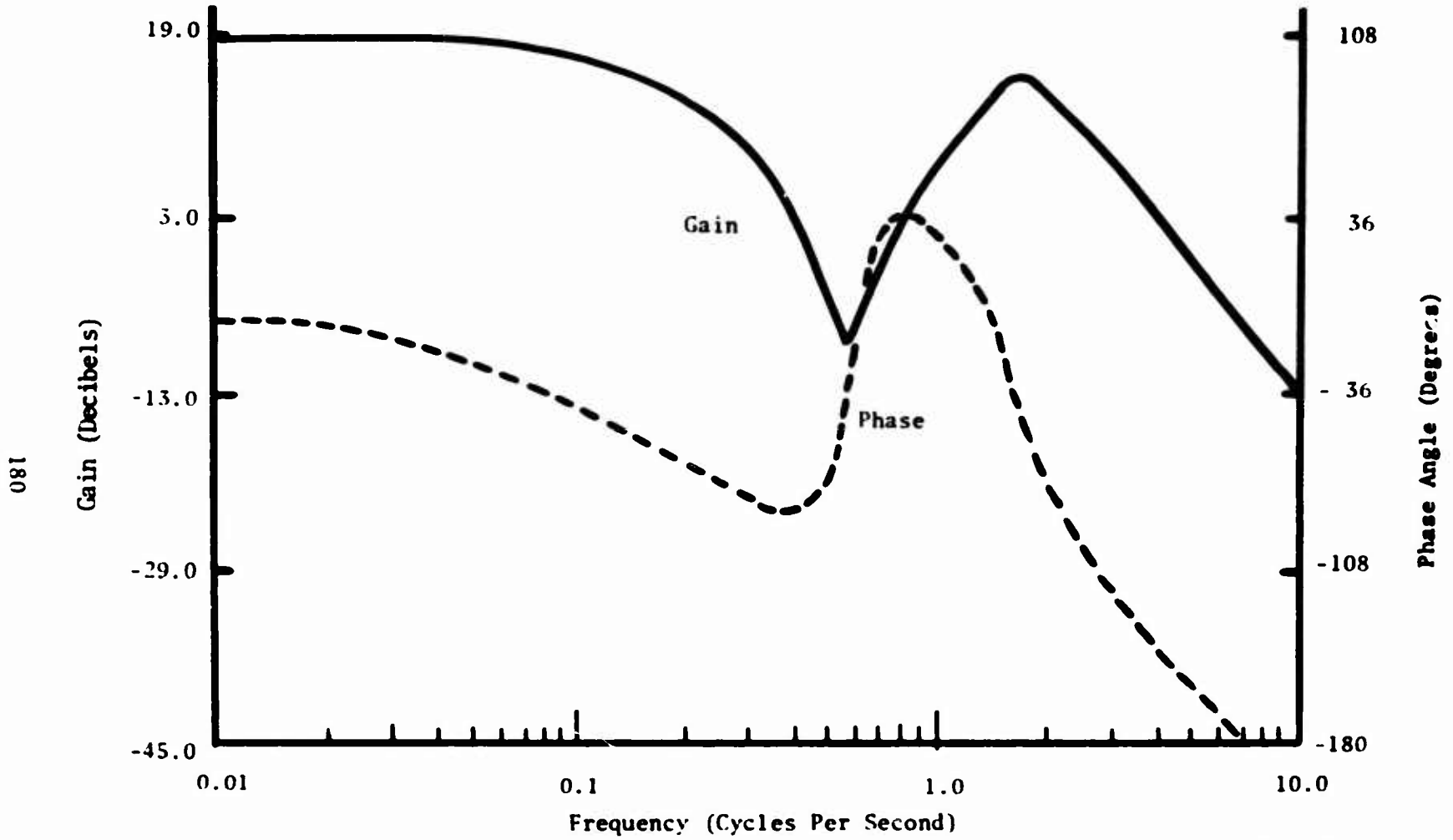

Figure 85. Bode Plots--Direct Fuel Flow Governor With ZTS Couplings (Linearized Desing Model)

$$C_s = 2.24 \frac{\text{ft/lb}}{\text{rad/sec}} \quad C_c = 0.0 \frac{\text{ft-lb}}{\text{rad-sec}} .$$

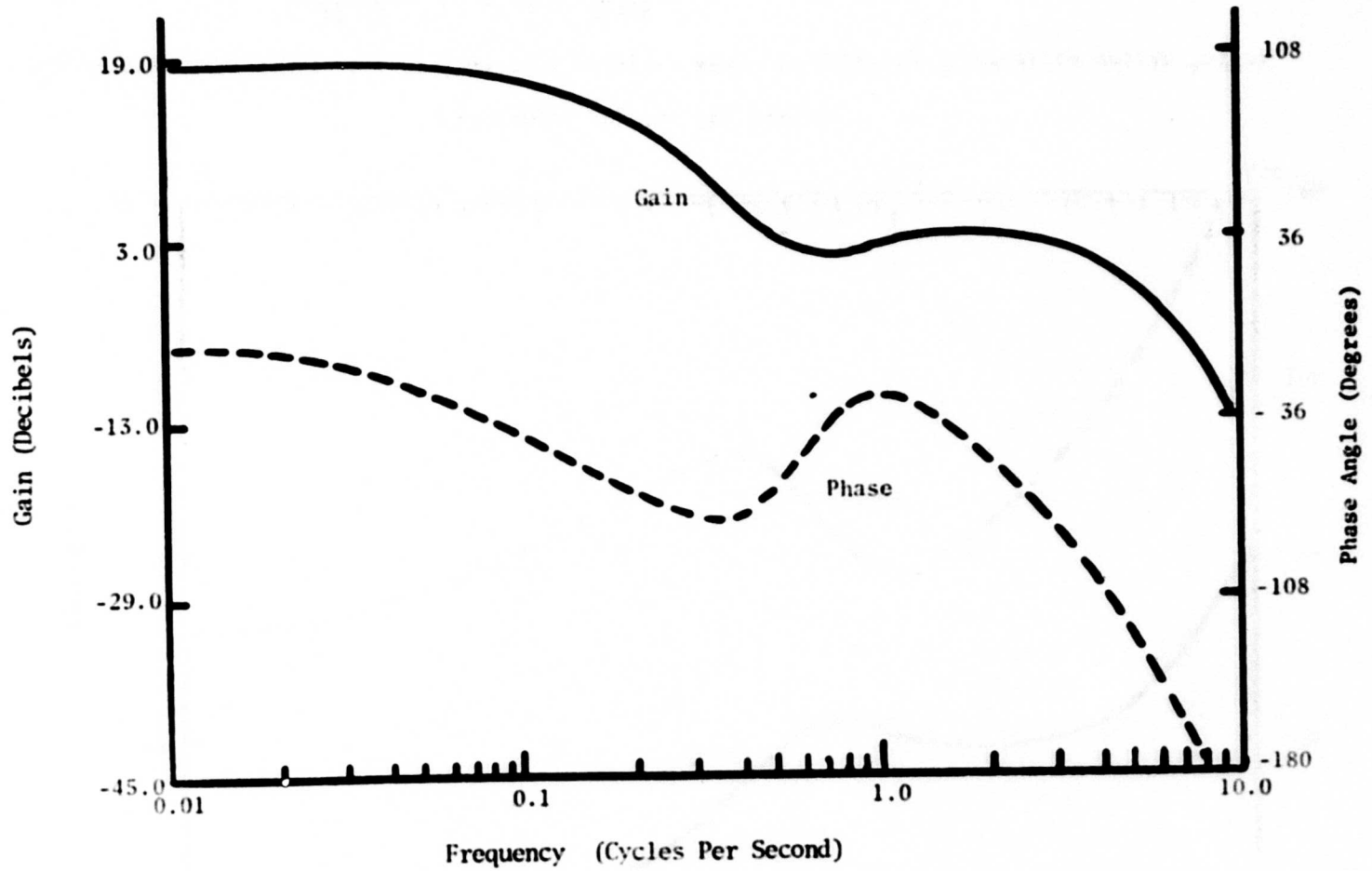

Figure 86. Bode Plots--Direct Fuel Flow Governor With ZTS Coupling (Linearized Design Model)

$C_s = 0.0 \frac{\text{ft-lb}}{\text{rad/sec}}$, $C_c = 10.0 \frac{\text{ft-lb}}{\text{rad/sec}}$.

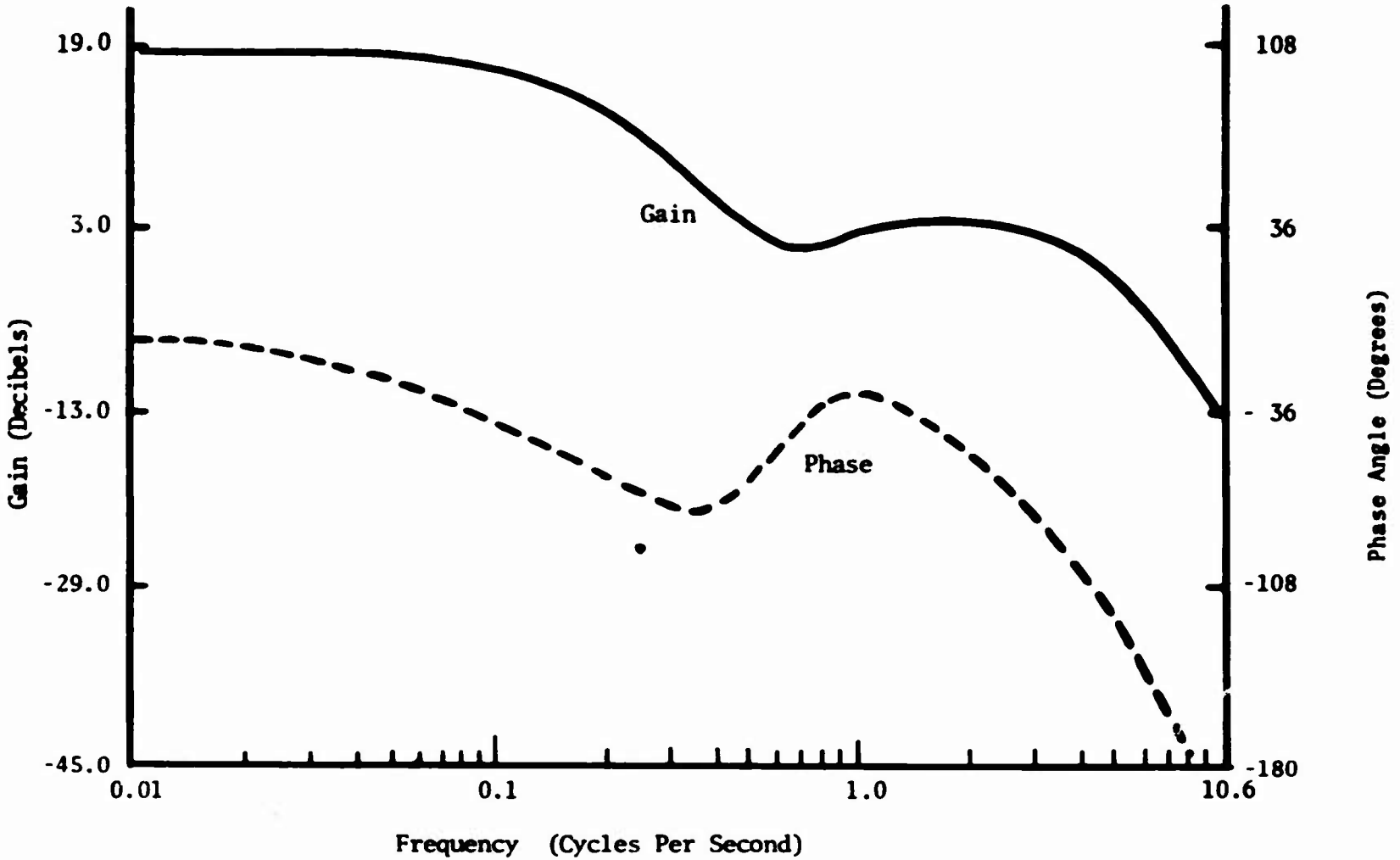

Figure 87. Bode Plots--Direct Fuel Flow Governor With ZTS Coupling (Linearized Design Model)

$c_s = 2.24 \frac{\text{ft-lb}}{\text{rad/sec}}$, $C_c = 10.0 \frac{\text{ft-lb}}{\text{rad/sec}}$.

NUMERICAL SIMULATION OF THE NONLINEAR CLOSED-LOOP SYSTEM

In general, there are no known methods to solve the differential equations of motion for the nonlinearized system analytically. It is possible to solve the differential equations numerically with the aid of a digital computer. This is also known as simulating the dynamic system. The numerical routine involves marching the differential equations through small increments in time. For the purposes of the numerical simulation, the differential equations of the drive train are used in their canonical form.

The drive train differential equations for the system without a ZTS coupling are converted to canonical form from equations 66 and 67 to form equations 306 through 309.

$$\dot{p}_e = -\frac{C_e}{I_{eg}} p_e^2 - C_s\left(\frac{p_e}{I_{eg}} - \frac{p_R}{I_R}\right) - K_\theta(\theta_e - \theta_R) + T_e \tag{306}$$

$$\omega_e = \frac{p_e}{I_{eg}} \tag{307}$$

$$\dot{p}_R = -\frac{C_L}{I_R} p_R^2 - C_S\left(\frac{p_R}{I_R} - \frac{p_e}{I_{eg}}\right) - K_\theta(\theta_R - \theta_e) \tag{308}$$

$$\omega_R = \frac{p_R}{I_R} \tag{309}$$

For the drive train with the ZTS coupling, shown in Figure 83, the governing differential equations are given by equations 257 through 262. The differential equation for a direct fuel flow speed governor is given by equation 112. After making the substitution of equation 121, the result is equation

$$M_g \ddot{W}_f + C_g \dot{W}_f + K_g W_f = K_g K_p(\omega_r - \omega_e) \tag{310}$$

The differential equations for a two-spool turbine engine are derived from equations 114 and 115, under the assumption that the average values of the partial derivatives are approximately equal to the values used under the small changes assumptions. The substitutions of equations 125 through 128 are made, resulting in equations 311 and 312.

$$I_g \dot{\omega}_g = K_1 W_f - C_1 \omega_g \tag{311}$$

$$T_e = K_2 W_f + K_3 \omega_g \tag{312}$$

A computer program is developed in Part I to numerically integrate equations 306 through 309 and another computer program is also developed to numerically integrate equations 257 through 262. These computer programs are modified here to include equations 310 through 312, thereby effectively closing the loop on the helicopter drive system. These modified computer programs are listed in Appendix VIII. These computer simulations are used to compare the stability of the helicopter drive systems with respect to both time response and frequency response.

The time response of each system is determined by running the system at steady state and then suddenly stepping the set speed from 1447 radians per second to 1500 radians per second. The time response of the engine speed is then observed and plotted. It is also determined what length of time is required for the system's engine speed oscillations to settle down to within 1 radian per second of its final value. For the helicopter drive system without a ZTS coupling, and with zero shaft damping, the time response is plotted in Figure 88. It can be seen that this system is divergent and is, therefore, completely unstable. Also, when operating at steady state, any slight perturbation in the system will cause the engine speed to diverge from its steady-state value. This is in complete agreement with the results of the linearized stability analyses.

Also, for the helicopter drive system with a ZTS coupling, and with zero shaft damping and zero coupling damping, any slight perturbation from steady state causes the engine speed to diverge. In addition, in attempting to find the time response of this system, the coupling numerically comes apart. Therefore, this system is, also, completely unstable. This does not agree with the linearized stability analyses, which shows that some accuracy may have been lost in the linearization of the ZTS coupling. However, if a coupling damping of 10 foot-pounds per radian per second is introduced to this system, it becomes convergent as shown in Figure 88. Also, from Table III, it takes only 1.27 seconds for the engine speed of this system to settle down to within 1 radian per second of its final value. Therefore, this system appears to be quite stable.

Next, the time response of the same three systems, but with a shaft damping of 2.24 foot-pounds per radian per second, is compared. The system without a ZTS coupling, whose time response is given in Figure 89, converges, but very slowly. From Table III, it takes 6.41 seconds to settle down to within 1 radian per second of its final value. Therefore, this system is stable, but it is not quick enough to be practical. The time response of the system with a ZTS coupling, but with zero coupling damping, is shown in Figure 89. Although its engine speed oscillations are rather large at first, it settles down quite rapidly. From Table III, the engine speed takes only 1.66 seconds to settle down to within 1 radian per second of its final value. Therefore, the time response of this system is a distinct improvement over that of the system without a ZTS coupling, despite the large initial oscillations. However, the time response of this system is not as good as the time response of the system with zero shaft damping and with a ZTS coupling with a coupling damping of 10 foot-pounds per

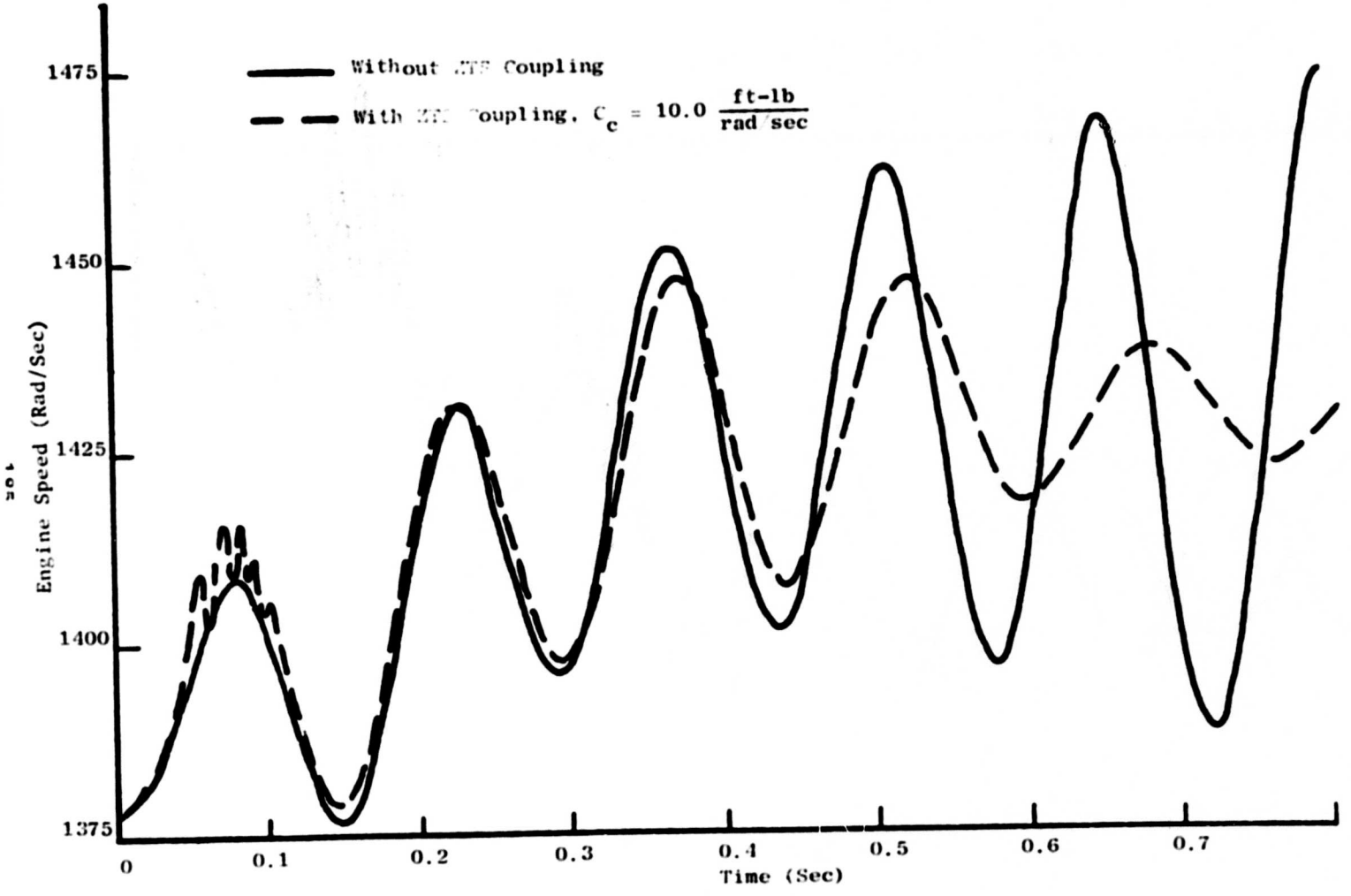

Figure 88. Time Response (C_s = 0.0).

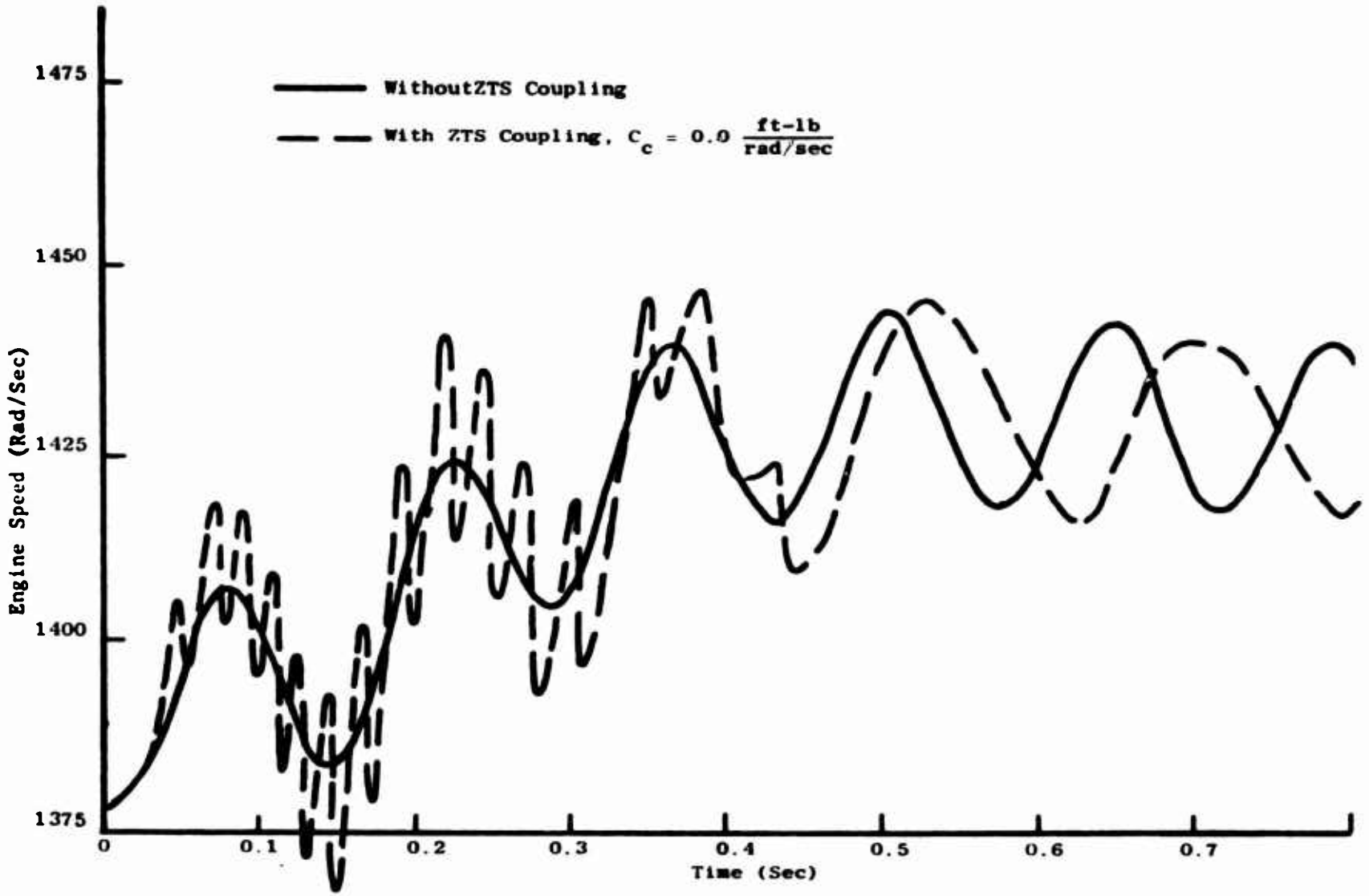

Figure 89. Time Response (C_s = 2.24, C_c = 0.0).

TABLE III. ENGINE SPEED SETTLING TIME

ZTS Coupling	C_2 $(\frac{ft\text{-}lb}{rad/sec})$	C_c $(\frac{ft\text{-}lb}{rad/sec})$	Time (sec)
Without	2.24	0.0	6.41
With	2.24	0.0	1.66
With	0.0	10.0	1.27
With	2.24	10.0	1.05
With	2.24	20.0	1.14
With	2.24	5.0	1.21
With	2.24	6.0	1.07
With	2.24	16.0	1.04
With	2.24	17.0	1.14
With	2.24	25.0	1.15

radian per second. Therefore, it appears that the ZTS coupling acts as a means for artificially increasing "shaft" damping, in order to improve the closed-loop system stability.

The system with a ZTS coupling and shaft damping, and with a coupling damping of 10 foot-pounds per radian per second, shows an even more improved time response, as illustrated in Figure 90. Also, from Table III the engine speed of this system takes only 1.05 seconds to settle down to within 1 radian per second of its final value. Therefore, this system is much more stable than the system with a ZTS coupling. It appears that increasing the coupling damping increases the stability of the system. However, this is only true to a point. This is demonstrated by determining the time response of the above system with an increase in coupling damping. A coupling damping of 20 foot-pounds per radian per second is used and the time response of the system is shown in Figure 90. From Table III, the engine speed of this system takes 1.14 seconds to settle down to within 1 radian per second of its final value. Looking at Figure 90, it doesn't appear that doubling the coupling damping has significantly improved the

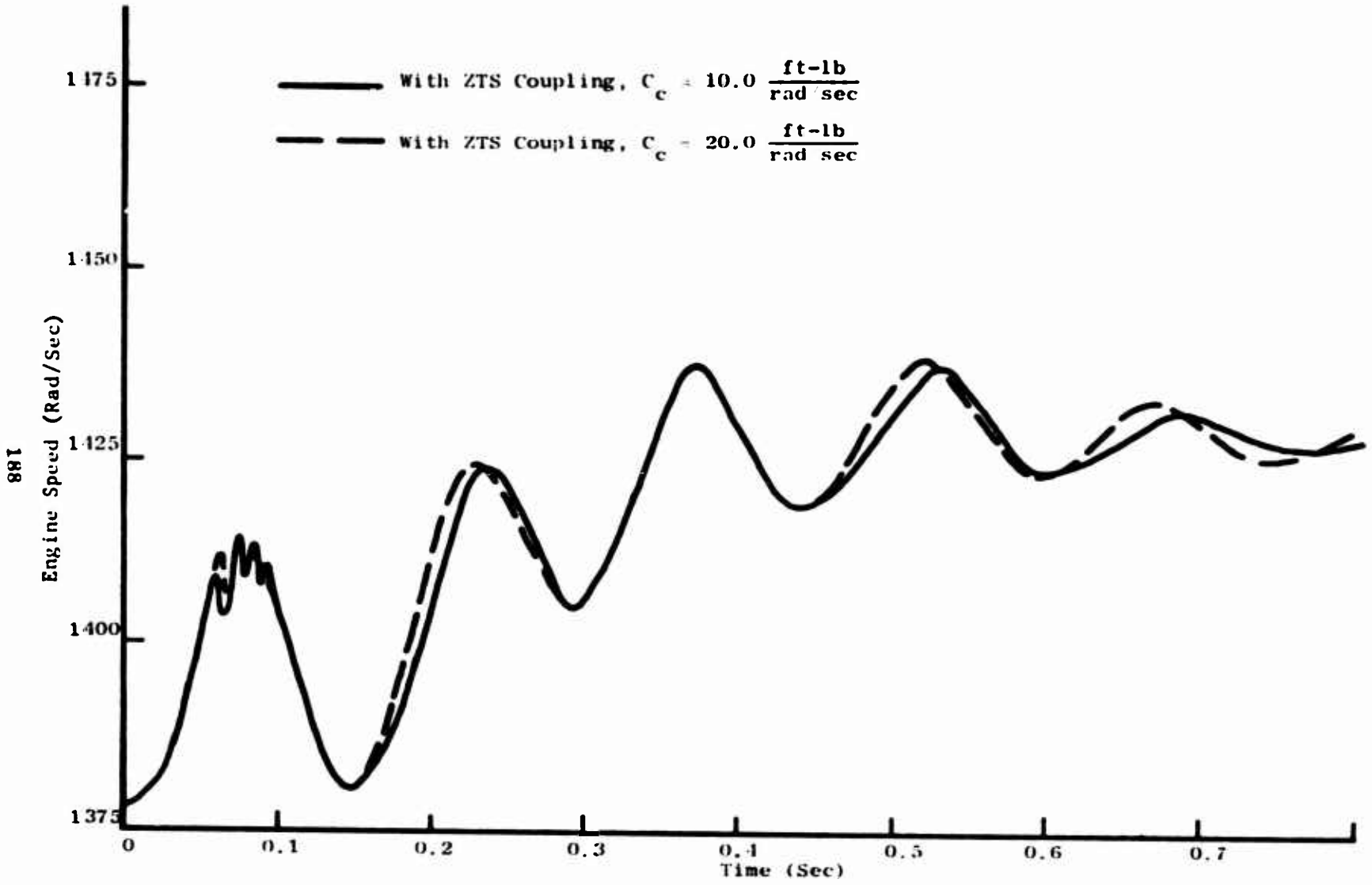

Figure 90. Time Response (C_s = 2.21, C_c = 0.0).

time response, and it has, in fact, slightly increased the settling time. This means not only that increasing the coupling damping beyond a certain value does not improve stability, but also, and more importantly, as long as the coupling damping is some minimum value, its exact value is relatively unimportant. This fact greatly simplifies the problem of designing and constructing the coupling damper. In order to determine the range of coupling damping that will give this system its optimum stability, the time response of the system is found for several different values of coupling damping. It is found that the time response of the system is virtually unchanged for values of coupling damping from 6 to 16 foot-pounds per radian per second. The time response of this system for each of these values for coupling damping is shown in Figure 91. Also, the length of the time required for the engine speed of this system to settle down to within 1 radian per second of its final value, for several different values of coupling damping, is given in Table III. It is of principal importance that the coupling damping be at least the minimum value in this range, because if it is below this range, the time response of this system gets perceptively worse. However, if the coupling damping exceeds the maximum value of this range, the time response of the system becomes only slightly worse. Therefore, it is necessary to design the ZTS coupling with a coupling damping of at least 6 foot-pounds per radian per second, and preferably, not more than 16 foot-pounds per radian per second, in order to optimize the time response of the system.

The frequency response of each system is determined by varying the rotor damping coefficient sinusoidally, as would occur in forward flight, at different frequencies. The variation in engine output speed is plotted as a function of the frequency of excitation. The frequency response is found for the helicopter drive system with a shaft damping of 2.24 foot-pounds per radian per second. For this system without a ZTS coupling, the frequency response, as plotted in Figure 92, displays two apparent critical frequencies. The first is found below 2 Hertz which is below the range of normal system excitation. The second critical frequency for this system is at about 7 Hertz. System excitation at, or near, this frequency would create engine speed oscillations that could be destructive. This critical frequency lies dangerously near the range of normal system excitation, which is about 8 to 10 Hertz.

When a ZTS coupling is inserted in this system, the frequency response changes drastically, as illustrated in Figure 92. The second, and more dangerous, critical frequency is completely eliminated. In addition, the engine speed variation is reduced for all excitation frequencies between 2 and 10 Hertz. There is virtually no change in the frequency response of this system with a ZTS coupling, if coupling damping is added, for excitation frequencies above 3 Hertz. However, for excitation frequencies below 3 Hertz, the existence of coupling damping tends to reduce the variation of engine speed. Therefore, it appears that the introduction of a ZTS coupling greatly improves the frequency response of this helicopter drive train system, and that adding coupling damping improves the frequency response even a little more.

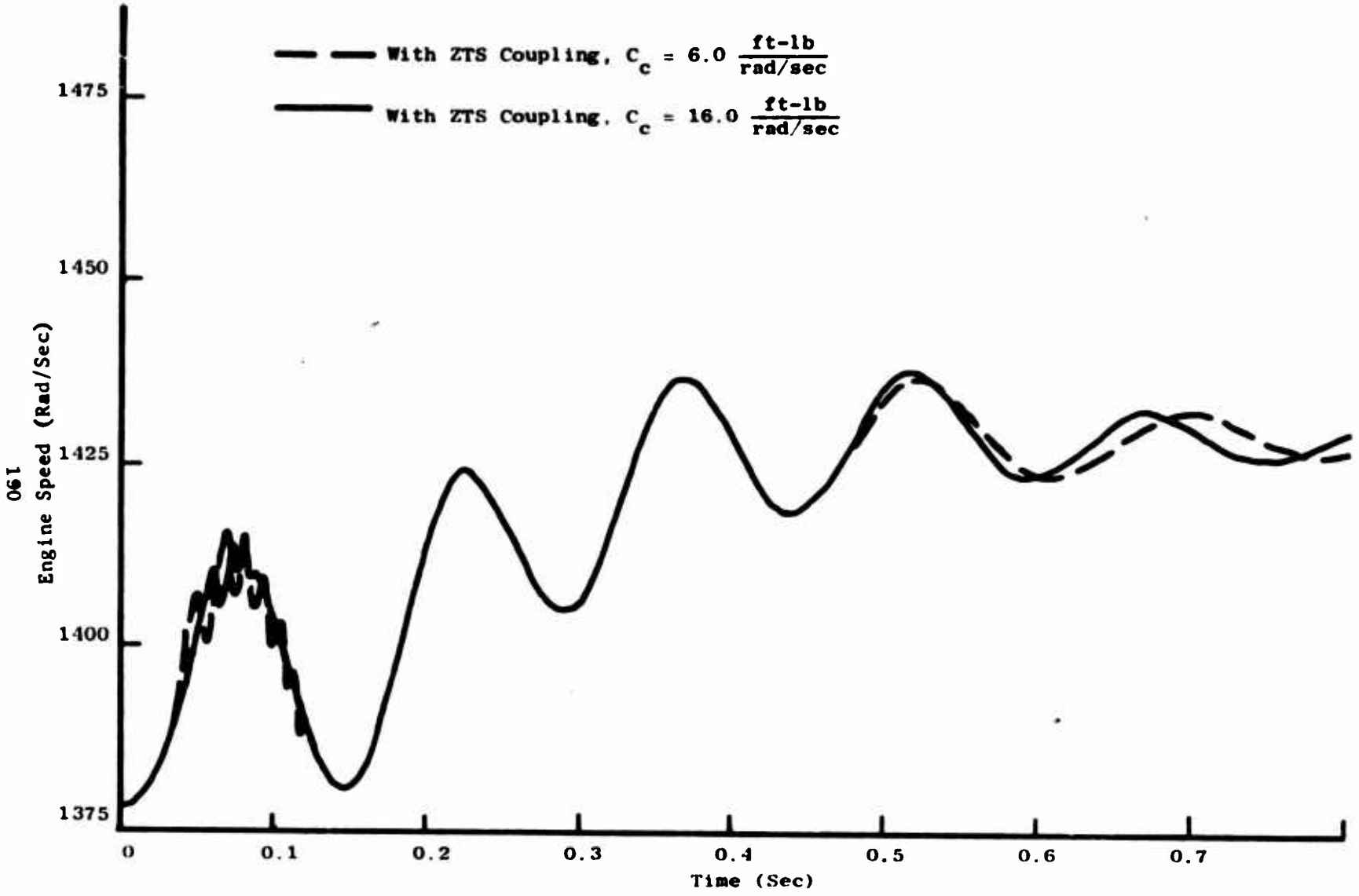

Figure 91. Time Response (Acceptable Extremes of C_c).

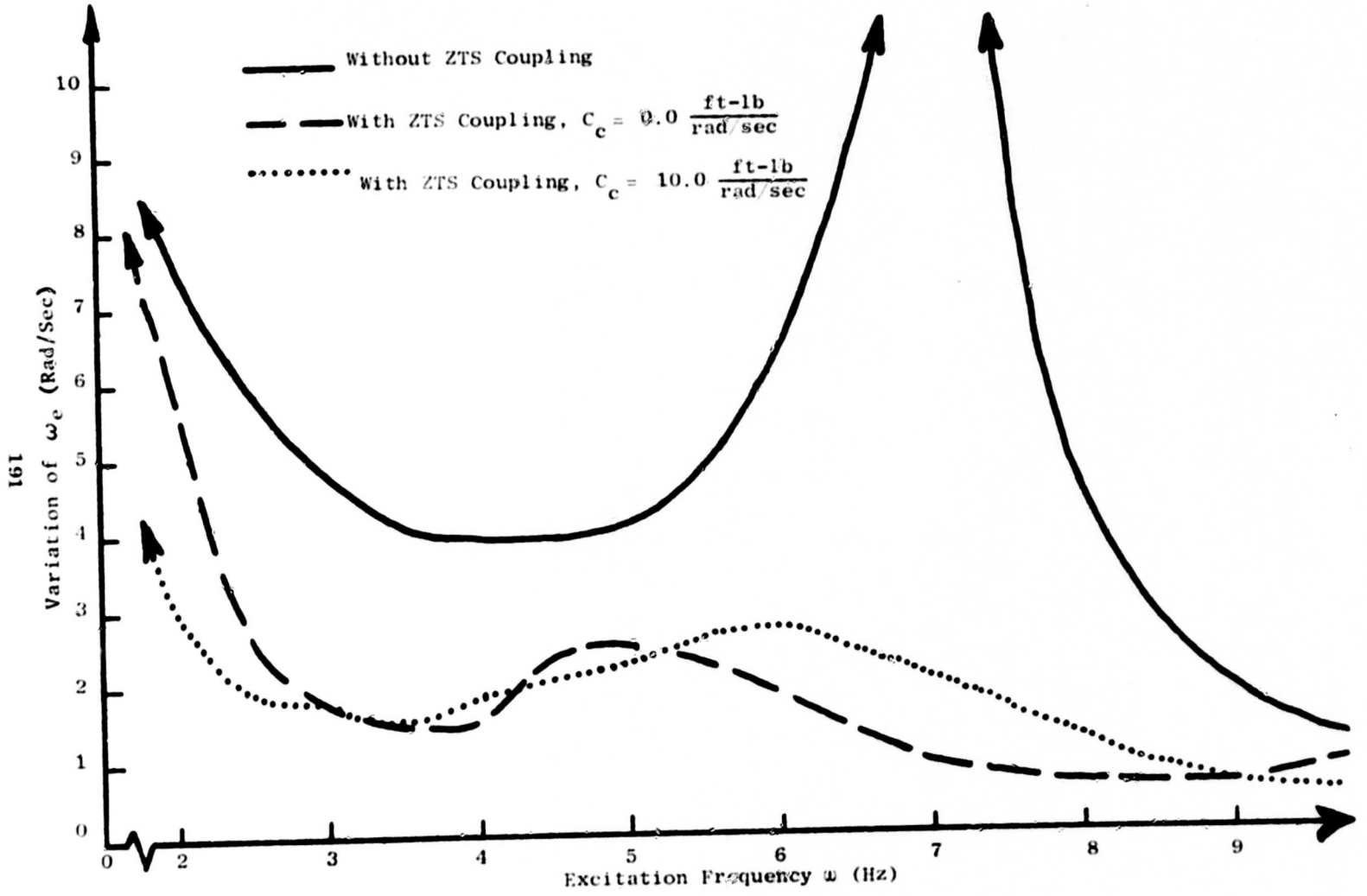

Figure 92. Frequency Response (Variation of C_L).

SUMMARY OF RESULTS

The helicopter drive system analyzed in Reference 5, with a direct fuel flow speed governor, is not, inherently, a very stable system. Although the instability is primarily due to the speed governor lags, the amount of shaft damping in the drive train has a critical effect on the stability of this system.

The ZTS coupling designed in Part I acts in two ways to improve the stability of this system. First, it provides a mode for artificially increasing the "shaft" damping of the drive train, in order to improve the closed-loop stability of the helicopter drive system. This is done by using an elastomeric damper as a torsional damper in the ZTS coupling. The closed-loop stability of this system is optimized by designing the coupling damping to be in the range of 6 to 16 foot-pounds per radian per second, although letting the coupling damping be greater than this will not significantly hurt the stability of this system.

Second, the ZTS coupling acts to isolate the rotor inertia of the helicopter drive system from the engine inertia. That is, it removes rotor-induced oscillations from the system before they reach the engine. In this respect, the ZTS coupling is very effective in that it completely eliminates one critical frequency from the system and reduces the amplitude of the engine speed oscillations over the entire range of excitation frequencies examined. The existence of coupling damping has little effect on the frequency response of the system.

Therefore, using the ZTS coupling designed in Part I with the coupling damping in the range discussed above is an effective way of stabilizing the helicopter drive system presented in Reference 5, with a direct fuel flow speed governor. In this way, the relative simplicity of this type of speed governor does not have to be sacrificed in order to stabilize the system.

CONCLUSIONS

The principal conclusions of this investigation and analysis are as follows:

1. A shaft coupling can be designed to meet the horsepower and speed requirements of modern U.S. Army helicopter drive trains with zero torsional stiffness at the design speed and horsepower. Specifically, two different types of zero torsional stiffness (ZTS) couplings were designed to transmit 5270 horsepower at 13,820 rpm. For one type of coupling, simple design equations were derived to size a coupling for any helicopter application.

2. Three significant design innovations for ZTS couplings were developed during this investigation:

   a. The counterbalanced link for the pinned-link coupling which allows applications at much higher shaft speeds than were heretofore possible.

   b. The ZTS coupling damper which allows the introduction of significant amounts of shaft damping into a drive train.

   c. The off-center elastic link which allows operation of an elastic-link ZTS coupling at high speed without the negative stiffness exhibited by the English "Half-Moon" design.

3. A ZTS coupling in a helicopter drive train acts as a torsional vibration isolator and can provide significant damping which is not otherwise available to the designer. Engine and control response to excitation at the rotary-wing can be reduced or completely eliminated with a ZTS coupling, depending on the amplitude and frequency of excitation. As an example, the engine response to a rotary-wing excitation of ± 10% full load torque was found to be almost totally eliminated at all frequencies above 4 Hz by the use of a ZTS coupling in the drive train of Reference 5.

4. The use of a ZTS coupling with damper greatly improves the torsional stability characteristics of a helicopter drive train with automatic speed control. For example, the drive train of Reference 5 with a simple direct fuel flow governor and sufficient gain to produce 5% droop was found to have negative stability margins (unstable) with no ZTS coupling, and large positive stability margins (stable) with a ZTS coupling. These stability predictions were verified by numerical simulations of closed-loop drive train dynamics on a digital computer.

LITERATURE CITED

1. Rumford, K., Fredrickson, C., and Stephenson, C., FACTORS AFFECTING FUEL CONTROL STABILITY OF A TURBINE ENGINE HELICOPTER ROTOR DRIVE SYSTEM, 27th Annual National V STOL Forum of the American Helicopter Society, Washington, D.C., May 1971.

2. Chapman, C. W., ZERO (OR LOW) TORSIONAL STIFFNESS COUPLINGS, Journal Mechanical Engineering Science, Vol. 11, No. 1, 1969.

3. Balzhi, M. F., and Esir, G. D., FLEXIBLE METALLIC COUPLINGS WITH DYNAMIC LINKS, The Engineer's Digest, April 1960.

4. Peczkowski, Joseph L., AUTOMATIC CONTROL OF FREE TURBINE ENGINES, ASME Paper No. 63-WA-159, August 1963.

5. Swick, R. M., and Skarvan, C. A., INVESTIGATION OF COORDINATED FREE TURBINE ENGINE CONTROL SYSTEMS FOR MULTIENGINE HELICOPTERS, USAAVLABS Technical Report 67-73, U.S. Army Aviation Materiel Laboratories, Fort Eustis, Virginia, December 1967, AD 666796.

6. Canale, Raymond P., and McCabe, Patrick R., THE FUEL FLOW RESET APPROACH TO GAS TURBINE GOVERNING, SAE Paper NO. 650530, May 1965.

7. Vance, John M., and Stichin, Ammon, NUMERICAL SOLUTION OF DYNAMICAL SYSTEMS BY DIRECT APPLICATION OF HAMILTON'S PRINCIPLE, International Journal for Numerical Methods in Engineering, Vol. 4, 207-216, 1972.

8. Lear Siegler-Transport Dynamics Division (catalog), 3131 West Segerstrom Avenue, Santa Ana, California 92702.

9. McClintock, Frank A., and Argon, Ali S., MECHANICAL BEHAVIOR OF MATERIALS, Addison-Wesley, Inc., pp. 258-259, 1966.

10. Saucedo, R., and Schiring, E. E., INTRODUCTION TO CONTINUOUS AND DIGITAL CONTROL SYSTEMS, New York, The Macmillan Company, 1968.

11. Pipes, Louis A., APPLIED MATHEMATICS FOR ENGINEERS AND PHYSICISTS, New York, McGraw-Hill Book Company, Inc., 1958.

12. Vance, J. M., INFLUENCE OF COUPLING PROPERTIES ON THE DYNAMICS OF HIGH SPEED POWER TRANSMISSION SHAFTS, ASME Paper No. 72-PTG-36, July 1972.

13. Baumeister, Theodore, Editor-in-Chief, MARKS' STANDARD HANDBOOK FOR MECHANICAL ENGINEERS, Seventh Edition, New York, McGraw-Hill Book Company, Inc., 1967.

14. Elgerd, Ollie I., CONTROL SYSTEMS THEORY, New York, McGraw-Hill Book Company, Inc., 1967.

15. Selby, Samuel M., Editor-in-Chief, HANDBOOK OF TABLES FOR MATHEMATICS, The Chemical Rubber Company, 1970.

16. Timoshenko, S., and Goodier, J. N., THEORY OF ELASTICITY, 2nd Ed., New York, McGraw-Hill Book Co., Inc., 1951, pp. 73078.

17. Seely, F. B., and Smith, J. O., ADVANCED MECHANICS OF MATERIALS, 2nd Ed., New York, John Wiley & Sons, Inc., 1966, p. 438.

APPENDIX I
ELASTICITY ANALYSIS OF CURVED LINK

The elasticity analysis of the elastic link shown in Figure 94 proceeds along a similar vein as for the curved bar shown in Figure 93 which has been analyzed by Timoshenko and Goodier.[16] The pin force P at A and B is replaced with the shear force shown in Figure 94 so that polar coordinates can be used to specify this force as a boundary condition. The total error caused by this assumption is small as a consequence of the principle of Saint Venant.

Considering the external force ρ only and treating this as a plane stress problem (no stress in Z direction), then

$$\sigma_z = \tau_{rz} = \tau_{z\theta} = 0 \tag{313}$$

The equations of equilibrium and compatibility must be satisfied in conjunction with the boundary conditions by some assumed stress distribution.

It has been shown for polar coordinates that if a stress function ϕ is defined such that

$$\sigma_r = \frac{1}{r}\frac{\partial}{\partial r}\left(r\frac{\partial \phi}{\partial r}\right) + \frac{1}{r^2}\frac{\partial^2 \phi}{\partial \theta^2}$$

$$\sigma_\rho = \frac{\partial^2 \phi}{\partial r^2}$$

and

$$\tau_{r\theta} = \frac{\partial}{\partial r}\left(\frac{1}{r}\frac{\partial \phi}{\partial \theta}\right) \tag{314}$$

the equations for equilibrium

$$\frac{\partial \sigma_r}{\partial r} + \frac{1}{r}\frac{\partial \tau_{r\theta}}{\partial \theta} + \frac{\sigma_r - \sigma_\theta}{r} = 0$$

$$\frac{1}{r}\frac{\partial \sigma_\theta}{\partial \theta} + \frac{\partial \tau_{r\theta}}{\partial r} + \frac{2\tau_{r\theta}}{r} = 0 \tag{315}$$

are satisfied for any function $\phi(r,\theta)$.

If

$$\phi = f(r) \sin \theta \tag{316}$$

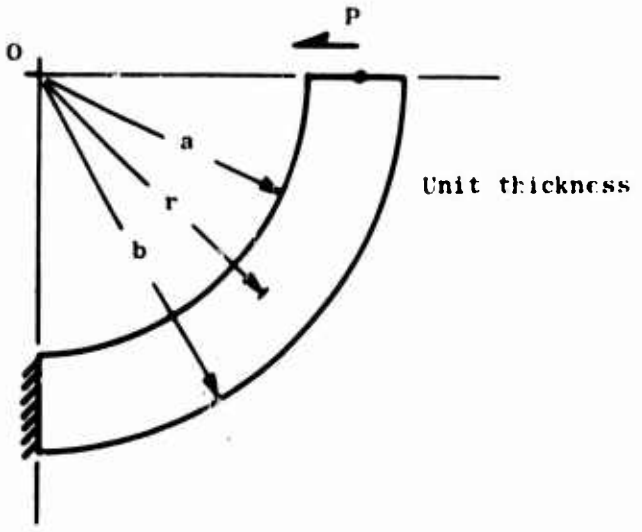

Figure 93. Curved Bar.

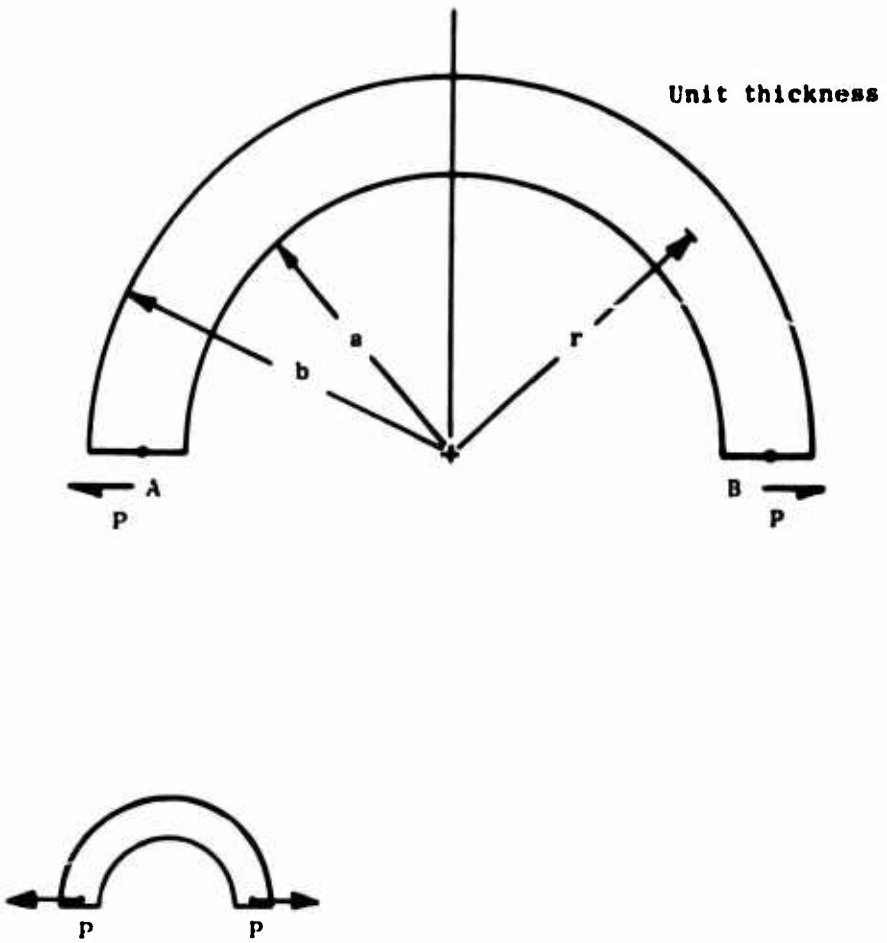

Figure 94. Elastic Link.

is substituted into the biharmonic equation in polar coordinates

$$\nabla^4\phi = 0 = \left(\frac{\partial}{\partial r^2} + \frac{1}{r}\frac{\partial\phi}{\partial r} + \frac{1}{r^2}\frac{\partial^2}{\partial\theta^2}\right)\left(\frac{\partial^2\phi}{\partial r^2} + \frac{1}{r}\frac{\partial\phi}{\partial r} + \frac{1}{r^2}\frac{\partial^2\phi}{\partial\theta^2}\right)$$

then compatibility is also satisfied by

$$f(r) = Ar^3 + B\frac{1}{r} + Cr + Dr \log r \tag{317}$$

It must be determined if all the boundary conditions

$$\sigma\,(r=a) = \sigma_r(r=b) = 0 \qquad \text{for all } \theta$$

$$\tau_{r\theta}(r=a) = \tau_{r\theta}(r=b) = 0 \qquad \text{for all } \theta \tag{318}$$

$$\int_a^b \tau_{r\theta}(\theta=\pi)\,dr = \int_a^b -\tau_{r\theta}(\theta=0)dr = P$$

can be satisfied by the stress function

$$\phi = (Ar^3 + B\frac{1}{r} + Cr + Dr \log r)\sin\theta \tag{319}$$

Substituting ϕ into the stress equations (314) and applying the B.C.

$\sigma(r=a) = 0$ gives

$$2Aa - \frac{2B}{a^3} + \frac{D}{a} = 0 \tag{320}$$

$\sigma(r=b) = 0$ gives

$$2Ab - \frac{2B}{b^3} + \frac{D}{b} = 0 \tag{321}$$

$\int_a^b \tau_{r\theta}(\theta=0) = -P$ gives

$$-\left[A(b^2 - a^2) + B\left(\frac{1}{b^2} - \frac{1}{a^2}\right) + D \log\frac{b}{a}\right] = P \tag{322}$$

Solving equations 320 through 322 for A, B, and D and letting

$$N = a^2 - b^2 + (a^2 + b^2) \log b/a$$

gives

$$A = -P/2N$$

$$B = (a^2 b^2 P/2N) \tag{323}$$

$$D = \frac{P(a^2+b^2)}{N}$$

The term coefficient C in equation (317) is not needed to satisfy the B.C. The stresses are now found from equations 314 to be

$$\sigma_r = -P/N\left[r + \frac{a^2b^2}{r^3} - \frac{(a^2+b^2)}{r}\right]\sin\theta$$

$$\sigma_\theta = -P/N\left[3r - \frac{a^2b^2}{r^3} - \frac{(a^2+b^2)}{r}\right]\sin\theta \tag{324}$$

$$\tau_{r\theta} = P/N\left[r + \frac{a^2b^2}{r^3} - \frac{(a^2+b^2)}{r}\right]\cos\theta$$

which are the same as the Timoshenko and Goodier's analysis for the curved bar in Figure 93.

To find the displacements u and v in the radial and tangential directions respectively, the strain-displacement relationships 325 are used.

$$\epsilon_r = \partial u/\partial r$$

$$\epsilon_\theta = u/r + 1/r(\partial v/\partial\theta) \tag{325}$$

$$\gamma_{r\theta} = 1/r(\partial u/\partial\theta) + \partial v/\partial r - v/r$$

In conjunction with Hooke's law,

$$\epsilon_r = 1/E(\sigma_r - \mu\sigma_\theta)$$

$$\epsilon_\theta = 1/E(\sigma_\theta - \mu\sigma_r) \tag{326}$$

$$\gamma_{r\theta} = 1/G(\tau_{r\theta})$$

where E is the modulus of elasticity, G is the modulus of rigidity, and μ is Poisson's ratio to give

$$\partial u/\partial r = 1/E[2Ar - 2B/r^3 + D/r - \mu GAr + 2B/r^3 + D/r)] \sin\theta \quad (327)$$

Integration of 327 gives

$$u = \sin\theta/E[(1-3\mu)Ar^2 + (1+\mu)B/r^2 + (1-\mu)D\ln r] + f(\theta) \quad (328)$$

From the second of equations 325,

$$\partial v/\partial\theta = r\epsilon_\theta - u$$

and substituting ϵ_θ from equation 326 and u from 327 gives

$$\partial v/\partial\theta = \sin\theta E[(5+\mu)Ar^2 + (1+\mu)B/r^2 + (1-\mu)D - (1-\mu)D\ln r] - f(\theta) \quad (329)$$

Integration of the above gives

$$v = -\cos\theta/E[(5+\mu)Ar^2 + (1+\mu)B/r^2 + (1-\mu)D - (1-\mu)D\ln r] - \int f(\theta)d\theta + g(r) \quad (330)$$

From the last of equations 325 and 326,

$$\gamma_{r\theta} = \frac{1}{r}\frac{\partial u}{\partial\theta} + \partial v/\partial r - v/r = \tau_{r\theta}/G \quad (331)$$

Replacing G with $E/2(1+\mu)$, differentiating u with respect to θ and v with respect to r and then substituting into equation 331 gives, after some rearrangement and canceling of terms,

$$-4D\cos\theta/E = f'(\theta) + rg'(r) - g(r) + \int f(\theta)d\theta$$

or

$$f'(\theta) + \int f(\theta)d\theta + (4D\cos\theta/E) = rg'(r) - g(r) \quad (332)$$

The left side of equation 332 is a function of θ only and the right is a function of r only. A solution to this equation can be found if both sides of equation 332 are set equal to zero which gives

$$\frac{dg(r)}{dr} = \frac{1}{r} g(r)$$

or

$$g(r) = Hr \tag{333}$$

Differentiating the left side of equation 332 with respect to θ gives

$$f''(\theta) + f(\theta) = 4D \sin \theta/E \tag{334}$$

with homogeneous solution

$$f(\theta)_H = K \sin \theta + L \cos \theta \tag{335}$$

To find the particular solution of 334, let $f(\theta)p = M\theta \cos \theta$, then

$$f'(\theta) = M \cos \theta - M\theta \sin \theta$$

$$f''(\theta) = -M \sin \theta - M \sin \theta - M \cos$$

and

$$f(\theta) + f''(\theta) = -2M \sin \theta = 4D \sin \theta/E$$

or

$$M = -2D/E$$

$$f(\theta)_p = (-2D/E)\ \theta \cos \theta$$

$$f(\theta) = (-2D/E)\theta \cos \theta + K \sin \theta + L \cos \theta \tag{336}$$

The integral of f(θ) is needed in equation 330 and is given in equation 337 after integrating 336 by parts.

$$\int f(\theta)d\theta = \int (-2D/E)\theta \cos \theta - K \cos \theta + L \sin \theta$$

$$p = \theta \quad dp = d\theta$$

$$dq = \cos \theta\, d\theta \qquad q = \sin \theta$$

$$\int f(\theta)d\theta = (-2D/E)[\theta \sin \theta - \int \sin \theta\, d\theta] - K \cos \theta + L \sin \theta$$

$$\int f(\theta)d\theta = (-2D/E)(\theta \sin \theta + \cos \theta) - K \cos \theta + L \sin \theta \tag{337}$$

After substitution of equations 333, 336, and 337 into equations 328 and 330, the expressions for u and v become

$$u = \sin\theta/E[(1-3\mu)Ar^2 + (1+\mu)B/r^2 + (1-\mu)D\,\ell n\, r]$$

$$- (2D\theta\ \cos\theta/E) + K\sin\theta + L\cos\theta \qquad (338)$$

$$v = -\cos\theta/E[(5+\mu)Ar^2 + 1 + \mu B/r^2 + (1-\mu)D - (1-\mu)D\,\ell n\, r]$$

$$\cdot \frac{-2D(\theta\sin\theta + \cos\theta)}{E} K\cos\theta + L\sin\theta + Hr \qquad (339)$$

The arbitrary constants H, K, and L must be evaluated from the boundary conditions for displacement, which are:

$$u(r,o) = 0$$

$$v(R,O) = 0 \quad \text{where } R = (a+b)/2 \qquad (340)$$

$$v(R,\pi) = 0$$

The first B_oC_o when applied to equation 338 gives $L = 0$, the second B_oC_o applied to equation 339 results in the following relationship between K and H:

$$K = HR + 1/E[D(\mu-3) - (\mu+5)AR^2 - (1+\mu)B/R^2 + (1-\mu)D\,\ell n\, R] \qquad (341)$$

Finally, applying the last B_oC_o to equation 339 gives

$$K = -HR - 1/E[-D(\mu-3) + (\mu+5)AR^2 + (1+\mu)B/R^2 - (1-\mu)D\,\ell n\, r] \qquad (342)$$

Adding 341 to 342 and rearranging terms gives

$$H = 0$$

$$K = \frac{(\mu-3)D}{E} - 1/E[(5+\mu)AR^2 + (1+\mu)B/R^2 - (1-\mu)D\,\ell n\, R]$$

Substituting the values of A, B, D, H, K, and L into equation 338 along with the coordinates of the position where the deflection is desired, $u(R,\pi)$, yields

$$u(R,\pi) = 2\pi D/E = \frac{-2\pi P(a^2+b^2)}{E[(b^2-a^2) + (a^2+b^2)\log a/b} \qquad (343)$$

Equation 343 gives for displacement Δ between points A and B, due to P:

$$\Delta = \frac{2\pi P(a^2+b^2)}{E[a^2-b^2) + (a^2+b^2) \log b/a]}$$

the spring constant K_p is P/Δ; thus,

$$Kp = \frac{E[(a^2-b^2) + (a^2+b^2) \ell n\, b/a]}{2\pi(a^2+b^2)} \qquad \text{(unit thickness)}$$

The deflection Δ is twice that of curved bar problem solved by Timoshenko and Goodier. This result might be expected if one considers the curved bar problem in Figure 93 as simply half of the symmetric elastic link. The analysis presented here with the details of each step should suggest a method of solution for other curved link problems.

APPENDIX II
REPRESENTATION OF SPEED REDUCERS

To simplify the dynamic analysis of systems with speed reducers, it is common practice to reference all spring constants and inertias to one side of the speed reducer. Figure 95a shows a three-degree-of-freedom system which has the following relationships between the dependent coordinates θ_2 and θ_3:

$$\theta_3 = N\theta_2 \tag{344}$$

$$\dot{\theta}_3 = N\dot{\theta}_2 \tag{345}$$

where N is the gear ratio.

If the coordinate θ_4 is referenced to the left side of the speed reducer, then the referenced position θ_4' and the referenced velocity $\dot{\theta}_4'$ are

$$\theta_4' = \theta_4 N \tag{346}$$

$$\dot{\theta}_4' = \dot{\theta}_4/N \tag{347}$$

The kinetic energy of the system is

$$KE = 1/2I_1\dot{\theta}_1^2 + 1/2I_2\dot{\theta}_4^2 + 1/2I_{G_1}\dot{\theta}_2^2 + 1/2I_{G_2}\dot{\theta}_3^2$$

or upon substitution of equations 345 and 347,

$$KE = 1/2I_1\dot{\theta}_1^2 + 1/2I_2N^2(\dot{\theta}_1)^2 + 1/2(I_{G_1} + I_{G_2}N^2)\dot{\theta}_2^2$$

The potential energy of the system is

$$PE = 1/2K_1(\theta_2-\theta_1)^2 + 1/2K_2N^2(\theta_2-\theta_4')^2$$

Letting

$$K_2' = K_2N^2$$

$$I_2' = I_2N^2$$

$$I_G = I_{G_1} + I_{G_2}N^2$$

the three-degree-of-freedom system takes the form shown in Figure 95b.

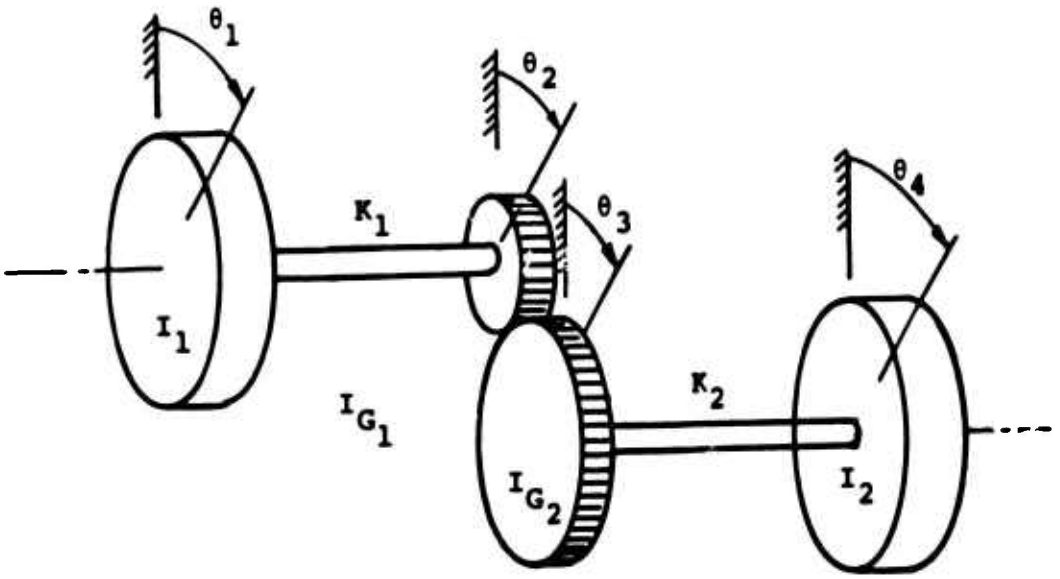

(a)

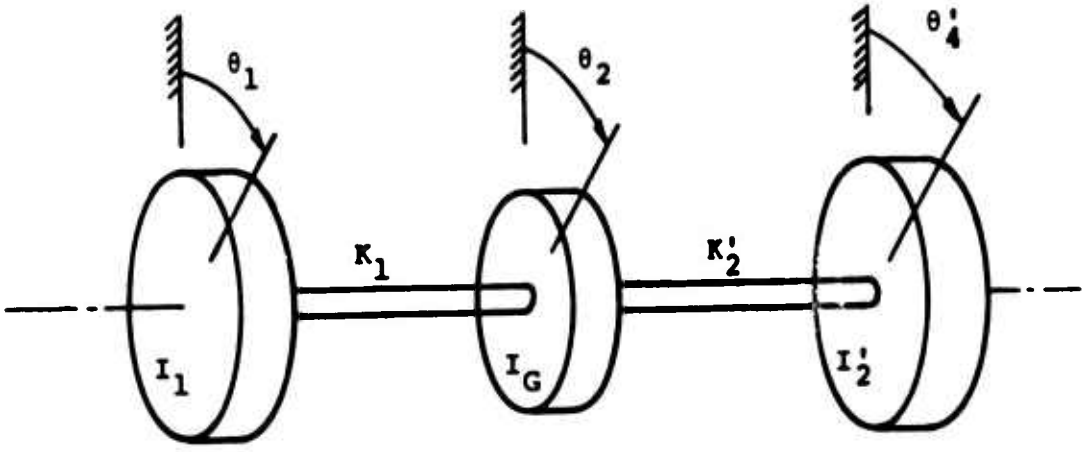

(b)

Figure 95. Representation of Speed Reducer.

APPENDIX III
FORMULATION OF LINK VELOCITIES

An expression for the angular velocity of each link as well as the linear velocity of the center of gravity of each link is determined by using velocity polygons.

The velocities shown in Figure 96 are

V_{ℓ_1} = velocity of cg of link 1

V_{ℓ_2} = velocity of cg of link 2

and

V_A, $V_{A'}$, and B = velocities of points A, A′, and B.

A velocity in the form $V_{i/j}$ is the velocity of point i relative to point j.

Velocities with subscripts x and y are component velocities in the x and y directions.

The equations representing the vectors in Figure 96 are

$$V_{\ell_1} = V_A + V_{\ell/A} \tag{348}$$

$$V_{\ell_{1x}} = V_{A_x} + V_{\ell/A_x} \tag{349}$$

$$V_{\ell_{1y}} = V_{A_y} + V_{\ell/A_y} \tag{350}$$

$$V_{\ell/A} = 1/2V_{B/A} \tag{351}$$

$$V_{B/A} = V_B - V_A \tag{352}$$

$$V_{B/A_x} = V_{B_x} - V_{A_x} \tag{353}$$

$$V_{B/A_y} = V_{B_y} - V_{A_y} \tag{354}$$

The magnitude of V_{ℓ_1} from equations 349 and 350 is

$$v^2_{\ell_1} = (v_{A_x} + v_{\ell/A_x})^2 + (v_{A_y} + v_{\ell/A_y})^2 \tag{355}$$

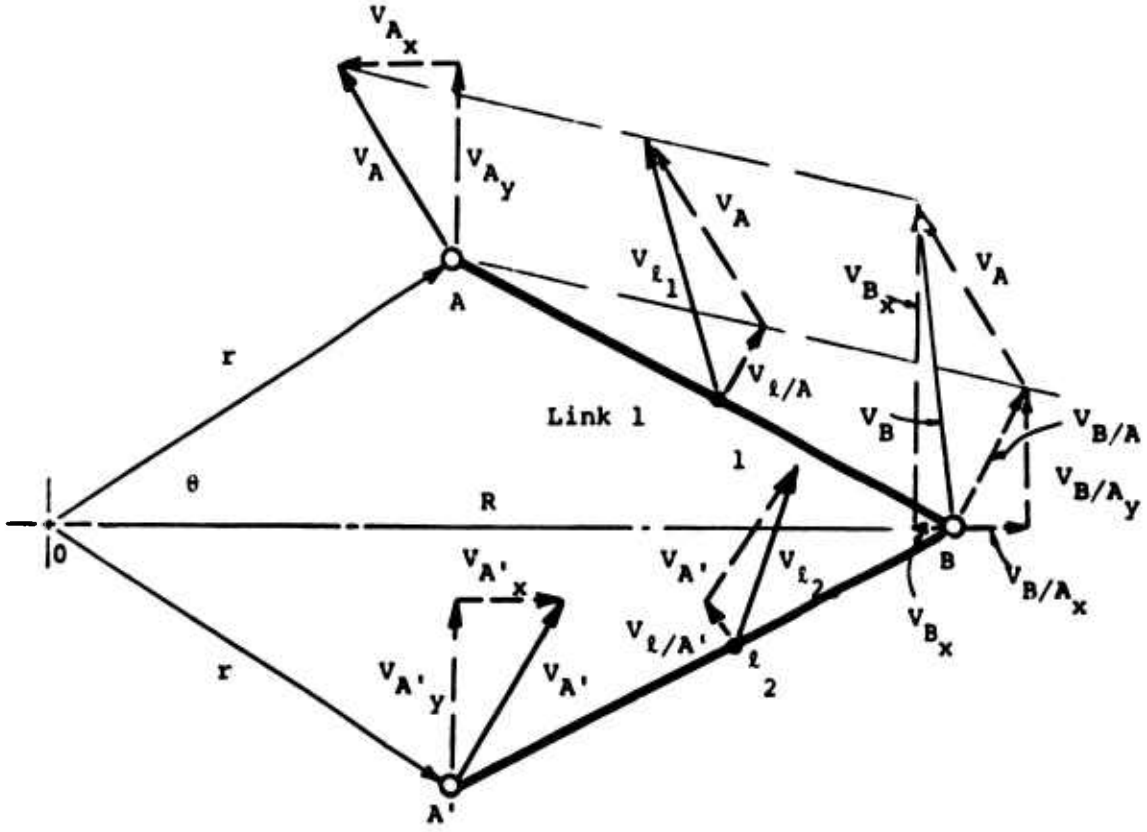

Figure 96. Velocity Diagram.

Using equations 351, 352, and 353, equation 355 takes the following form:

$$v_{\ell_1}^2 = \frac{(v_{A_x} + v_{B_x})^2 + (v_{A_y} + v_{B_y})^2}{4} \tag{356}$$

The expression for the magnitude of the velocity of link 2 is similar to equation 356 with A replaced with A′ giving

$$v_{\ell_2}^2 = \frac{(v_{A'_x} + v_{B_x})^2 + (v_{A'_y} + v_{B_y})^2}{4} \tag{357}$$

For point B,

$$v_{B_x} = \dot{R} \tag{358}$$

$$v_{B_y} = R(\dot{\theta}_e - \dot{\theta}/2) \tag{359}$$

thus

$$v_B^2 = \dot{R}^2 + R^2(\dot{\theta}_e - \dot{\theta}/2)^2 \tag{360}$$

For point A,

$$v_{A_x} = -r\dot{\theta}_e \sin \theta/2 \tag{361}$$

$$v_{A_y} = r\dot{\theta}_e \cos \theta/2 \tag{362}$$

For point A′,

$$v_{A'_x} = r(\dot{\theta}_e - \dot{\theta}) \sin \theta/2 \tag{363}$$

$$v_{A'_y} = r(\dot{\theta}_e - \dot{\theta}) \cos \theta/2 \tag{364}$$

Let $v_\ell^2 = v_{\ell_1}^2 + v_{\ell_2}^2$ (see equation 54) (365)

Substituting equations 358 through 364 into equations 356 and 357 gives the following equntion for v_ℓ^2 in terms of R, $\dot{R}$, θ, $\dot{\theta}$, and $\dot{\theta}_e$.

$$v_{\ell}^2 = 1/4\{(-r\dot{\theta}_e \sin \theta/2 + \dot{R})^2 + r\dot{\theta}_e \cos \theta/2 + R(\dot{\theta}_e - \dot{\theta}/2)\}^2$$

$$+ [r(\dot{\theta}_e - \dot{\theta}) \sin \theta/2 + \dot{R}]^2$$

$$+ [r(\dot{\theta}_e - \dot{\theta}) \cos \theta/2 + R(\dot{\theta}_e - \dot{\theta}/2)]^2 \qquad (366)$$

Squaring and combining terms in equation 366 gives

$$v_{\ell}^2 = 1/2\{r^2(\dot{\theta}_e^2 - \dot{\theta}_e\dot{\theta} + \dot{\theta}^2/2) - r\dot{R}\dot{\theta} \sin \theta/2$$

$$+ \dot{R}^2 + 2rR(\dot{\theta}_e - \dot{\theta}/2)^2 \cos \theta/2$$

$$+ R^2(\dot{\theta}_e - \dot{\theta}/2)^2\} \qquad (367)$$

The angular velocity of link 1 is

$$\omega_{\ell_1} = \frac{V_{B/A}}{\ell}$$

or

$$\omega_{\ell_1}^2 = \frac{1}{\ell^2} = \{(v_{B_x} - v_{A_x})^2 + (v_{B_y} - v_{A_y})^2\} \qquad (368)$$

and for link 2

$$\omega_{\ell_2} = \frac{V_{B/A'}}{\ell} \qquad \text{where } V_{B/A'} = V_B - V_{A'}$$

or

$$\omega_{\ell_2}^2 = 1/\ell^2\{(v_{B_x} - v_{A_x'})^2 + (v_{B_y} - v_{A_y'})^2\} \qquad (369)$$

Let $\omega_{\ell}^2 = \omega_{\ell_1}^2 + \omega_{\ell_2}^2$ (see equation 54)

Substituting equations 358 through 364 into 368 and 369 gives

$$\omega_{\ell}^2 = 2/\ell^2\{r^2(\dot{\theta}_e^2 - \dot{\theta}_e\dot{\theta} + \dot{\theta}^2/2) + r\dot{R}\dot{\theta} \sin \theta/2$$

$$+ \dot{R}^2 - 2rR(\dot{\theta}_e - \dot{\theta}/2)^2 \cos \theta/2 + R^2(\dot{\theta}_e - \dot{\theta}/2)^2\} \qquad (370)$$

APPENDIX IV
COMPUTER PROGRAMS

FOR COUPLING DESIGN

Design Equation I--$f(\beta,\theta)$

Input Data

Quantity	Value	Dimensions
N	2	none
m	.2385	lb_m
r	3.	in.
β	.87	none
ω	13820	rpm

```
C       DESIGN EQUATION I
        REAL M
        READ(5,5)N
      5 FORMAT(I1)
        READ(5,1)M,R,BETA,W
      1 FORMAT(F10.0)
        PRINT,N,M,R,BETA,W
        PI=3.14159
        M=M/32.17
        R=R/12.
        W=W*PI/30.
        TH=PI/180.
      2 S=SIN(TH/2.)
        C=COS(TH/2.)
        ST=SIN(TH)
        RAD=BETA*BETA-S*S
        IF(RAD.LT.0)GO TO 3
        Z=SQRT(RAD)
        T=N*M*R*R*W*W*.5*(ST*S*Z+C*ST/(2.*Z))
        RH=TH*180/PI
        WRITE(6,4)TH,RH,T
      4 FORMAT(' THETA-RADIANS=',F7.4,'     THETA-DEGREES=',F5.0,'      TORQ
     .UE=',E15.7)
        TH=TH+PI/180.
        IF(TH.LE.PI)GO TO 2
      3 STOP
        END
```

Stress and Force Analysis

Input Data

Quantity	Value	Dimensions
m	.2385	lb_m
m_ℓ	.130	lb_m
r_e	1.3	in.
ℓ	2.61	in.
ω	1447	rad/sec
r	3.0	in.
A_1	.375	$in.^2$
A_2	.6875	$in.^2$
A_3	.25	$in.^2$
A_4	.4418	$in.^2$
I/C	.143	$in.^3$
m_B	.416	lb_m
m_3	.416	lb_m

```
C       STRESS PROGRAM
        REAL M,ML,L,IC,MOM,ME,MC,MB,M3
        READ(5,1)M,ML,RE,L,W,R,A1,A2,A3,A4,IC,MB,M3
        PRINT,M,ML,RE,L,W,R,A1,A2,A3,A4,IC,MB,M3
      1 FORMAT(F15.0)
        WRITE(6,4)
      4 FORMAT('1',T8,'TH(DEG)',T16,'TH(RAD)',T26,'SA',T36,'SN',
     .T46,'SB',T56,'TB',T66,'MOM',T76,'FA',T86,'F5',T96,'F4',T106,'FB')
        PI=3.14159
        M=M/32.17
        ML=ML/32.17
        MB=MB/32.17
        M3=M3/32.17
        RE=RE/12.
        L=L/12.
        R=R/12.
        ME=ML+MB-M
        MC=ME*L/(2*RE)
        F1=(MC+(ME+ML)/2.)*R*W*W
        F2=M3*R*W*W
        T=56.
      2 T=T+1.
        TR=T*PI/180.
        S=SIN(TR/2.)
        C=COS(TR/2.)
        RR=R*C+SQRT(L*L-R*R*S*S)
        H=R*S
        ALPHA=ARSIN(H/L)
        F3=M*RR*W*W
        F4=F3/(2.*COS(ALPHA))
        FB=F4*SIN(ALPHA)
        F5=.5*(MB+ML)*RR*W*W/COS(ALPHA)
        FA=SQRT(((F1+F2)*C
     1                  +F4*COS(ALPHA))**2+((F1+F2)*S-F4*SIN(ALPHA))**2)
```

```
      MOM=ME*RR*W*W*H*12.*.74/2.
      SBEAR=FA/A2
      SLO2=MOM/IC+F5/A1
      SB=F4/A3
      TB=FB/A4
      WRITE(6,3)T,TR,SBEAR,SLO2,SB,TB,MOM,FA,F5,F4,FB
    3 FORMAT(' ',F10.0,F10.3,9F10.0)
      IF(T.LE.115)GO TO 2
      STOP
      END
```

Simulation of System 1

Input Data

Quantity	Value	Dimensions
Count (integration steps line of output)	10	none
I_e	.709	slug-ft^2
I_R	3.888	slug-ft^2
C_s	2.32	ft-lb-sec
K_s	212.1-1696.8	ft-lb rad
C_e	.000382	ft-lb-sec^2
C_L	.0009564	ft-lb-sec^2
T_e	2804.6	ft-lb
Start time	Variable	sec
End time	Variable	sec
ι	Variable	rad/sec

```
C       SIMULATION OF SYSTEM 1
        IMPLICIT REAL*8(A-Z)
        INTEGER NN,NNN,COUNT
        INTEGER JO
        COMMON CS2,IE,IR,K2,CL,CENG,ENGINE,W
        READ(5,1003)COUNT
 1003   FORMAT(I2)
        READ(5,1002)IE,IR,CS2,K2,CENG,CL,ENGINE,TSTART,TSTOP
        PRINT,      IE,IR,CS2,K2,CENG,CL,ENGINE,TSTART,TSTOP
 1001   READ(5,1002,END=444)EXTRA
        W=EXTRA
        PRINT,EXTRA
        JO=0
        TIME=TSTART
        NNN=COUNT
        NN=50
 1000   CONTINUE
        CALL OUT(E,R,PE,PR,TIME,ED,RD,PED,PRD,TE,FR,DEL,JO,EXTRA)
        DIFF=(E-R)
        MAG=DIFF*K2/2004.
        IF(NN.NE.50)GO TO 13
        PRINT,E,ED,R,RD,PE,PR,TIME
        WRITE(6,11)
        NN=0
   13   CONTINUE
        IF(NNN.EQ.COUNT)GO TO 55
        NNN=NNN+1
        GO TO 111
   55   WRITE(6,10)E,ED,R,RD,TE,FR,DEL,TIME,DIFF,MAG
        NNN=1
        NN=NN+1
  111   CONTINUE
        IF(DEL.LT..0009)GO TO 900
C  EULER INTEGRATION  START.....................................
```

```
      E=E+ED*DEL
      R=R+RD*DEL
      PE=PE+PED*DEL
      PR=PR+PRD*DEL
      TIME=TIME+DEL
      GO TO 901
C  EULER INTEGRATION  END.....................................
  900 CONTINUE
C  RUNGE-KUTTA  START.....................................
      HH=3*DEL/4
      EN=E+ED*HH
      RN=R+RD*HH
      PEN=PE+PED*HH
      PRN=PR+PRD*HH
      TIMEN=TIME+HH
      CALL DOT(EN,RN,PEN,PRN,TIMEN,EDN,RDN,PEDN,PRDN,TE,FR,DEL,JO,EXTRA)
      E=E+DEL*(ED/3.+(2./3.)*EDN)
      R=R+DEL*(RD/3.+(2./3.)*RDN)
      PE=PE+DEL*(PED/3.+(2./3.)*PEDN)
      PR=PR+DEL*(PRD/3.+(2./3.)*PRDN)
      TIME=TIME+DEL
C  RUNGE-KUTTA  END.....................................
  901 CONTINUE
      IF(TIME.LT.TSTOP)GO TO 1000
 1002 FORMAT(F20.1)
   10 FORMAT(' ',4F9.2,2F10.3,F10.7,F10.4,2F10.3)
   11 FORMAT('1',////
     .       T4,'THETA E',T12,'DTHETA E',T22,'THETA R',T31,'DTHETA R',
     . T40,'TORQUE E',T50,'TORQUE R',T60,'DEL',T70,'TIME',
     .  T80,'SHAFT',T90,'M.F.'/)
      GO TO 1001
  444 STOP
      END
```

```
      SUBROUTINE DOT(E,R,PE,PR,TIME,ED,RD,PED,PRD,TE,FR,DEL,JO,EXTRA)
C  TIME DERIVATIVES OF POSITION AND MOMENTUM.....
      IMPLICIT REAL*8(A-Z)
      INTEGER JO
      INTEGER NN,NNN,COUNT
      COMMON CS2,IE,IR,K2,CL,CENG,ENGINE,W
      IF(JC.GT.0)GO TO 1
      JO=1
C  INITIAL CONDITIONS--START UP.....
      E=0.
      R=0.
      ED=0.
      RD=0.
C  START SYSTEM AT STEADY STATE FOR TEST1 AND TEST2.....
C  NOTE THAT E CAN BE SET TO 0  R=-2004/K2  ED=RD=1447.56
      CELT=.001
      PE=IE*ED
      PR=IR*RD
C  DYNAMICS.....
    1 CONTINUE
      CEL=CELT
C  ANGULAR VELOCITIES.....
      ED=PE/IE
      RD=PR/IR
C  POTENTIAL FORCES.....
      DE=-K2*(E-R)
      DR=-DE
C  GENERALIZED FORCES.....
      FCE=-CS2*(ED-RD)
      FCR=-CS2*(RD-ED)
      TE=(ENGINE*TIME/3.)*(2.-TIME/3.)
      IF(TIME.GT.3)TE=ENGINE
      FE=TE-CENG*ED*DABS(ED)+FCE
      VL=CL
```

```
      IF(TIME.GT.15)VL=CL *(1+.10*DSIN(W*TIME))
      FR=-VL*DABS(RD)*RD+FCR
      PED=CE+FE
      PRD=CR+FR
      RETURN
      END
```

Simulation of System 2

Input Data

Quality	Value	Dimensions
N	2	none
Count (integration steps/ line of output	10	none
r	3	in.
ℓ	2.61	in.
m_B *	.2385	lb_m
m_ℓ *	0	lb_m
I_ℓ	.0003	$slug\text{-}ft^2$
C_D	0	ft-lb-sec
TT (reverse stop contact)	1	rad
K_L (reverse stop)	66,800	ft-lb/rad
TTT (forward stop contact)	1.97	rad
K_L (forward stop)	66,800	ft-lb/rad
RFL (free length of spring**)	0	in.
KE (linear spring constant**)	0	lb/in.
C_s	2.32	ft-lb-sec
K_s	212.1-1696.8	ft-lb/rad

*Any combination of m_B and m_ℓ which sums to m can be used.

**A coupling spring can be added between the link pins (B) and the center of the coupling (not used in analysis).

Quality	Value	Dimensions
I_e	.5	slug-ft^2
I_R	3.888	slug-ft^2
I_{fe}	.015	slug-ft^2
I_{fR}	.209	slug-ft^2
C_e	.000382	ft-lb-sec^2
C_L	.0009564	ft-lb-sec^2
T_e	2804	ft-lb
Start Time	Variable	sec
End Time	Variable	sec
ω	Variable	rad/sec

```
C      SIMULATION OF SYSTEM 2
       IMPLICIT REAL*8(A-Z)
       INTEGER NN,NNN,COUNT,NM
       INTEGER JO
       COMMON R1,L,    M,ML,CDAMP,CS2,TT,IE,IR,IFE,IFR,RFL,TTT,KE,K2,
      .CL,CENG,ENGINE,W,X,Y,IL,NM
       READ(5,1003)NM,COUNT
 1003  FORMAT(I2)
       READ(5,1002)R1,L,M,ML,IL,CDAMP,TT,X,TTT,Y,RFL,KE,CS2,
      .K2,IE,IR,IFE,IFR,CENG,CL,ENGINE,TSTART,TSTOP
       PRINT,      R1,L,M,ML,IL,CDAMP,TT,X,TTT,Y,RFL,KE,CS2,
      .K2,IE,IR,IFE,IFR,CENG,CL,ENGINE,TSTART,TSTOP
C    CONVERSION FACTORS
       R1=R1/12.
       L=L/12.
       M=M/32.17
       ML=ML/32.17
       KE=KE*12.
       RFL=RFL/12.
 1001  READ(5,1002,END=444)EXTRA
       PRINT,EXTRA
       W=EXTRA
 1002  FORMAT(F20.1)
       JO=0
       TIME=TSTART
       NNN=COUNT
       NN=50
 1000  CONTINUE
       CALL DGT(T,E,R,PT,PE,PR,TIME,TD,ED,RD,PTD,PED,PRD,DET,
      .DET1,DET2,TE,FR,DEL,JO)
       DIFF=(E-T-R)
       MAG=DIFF*K2/2004.
       IF(NN.NE.50)GO TO 13
       WRITE(6,11)
```

```
      NN=0
   13 CONTINUE
      IF(NNN.EQ.COUNT)GO TO 55
      NNN=NNN+1
      GO TO 111
   55 WRITE(6,10)E,EC,R,RC,T,TD,DET,DIFF,MAG,TE ,
     .FR,DEL,TIME
      NNN=1
      NN=NN+1
  111 CONTINUE
      IF(DEL.LT..0002)GO TO 900
C  EULER INTEGRATION  START.....................................
      T=T+TD*DEL
      E=E+EC*DEL
      R=R+RC*DEL
      PT=PT+PTC*DEL
      PE=PE+PEC*DEL
      PR=PR+PRC*DEL
      TIME=TIME+DEL
      GO TO 901
C  EULER INTEGRATION  END.....................................
  900 CONTINUE
C  RUNGE-KUTTA INTEGRATION  START.....................................
      HH=3*DEL/4
      TN=T+TD*HH
      EN=E+EC*HH
      RN=R+RC*HH
      PTN=PT+PTC*HH
      PEN=PE+PEC*HH
      PRN=PR+PRC*HH
      TIMEN=TIME+HH
      CALL OUT(TN,EN,RN,PTN,PEN,PRN,TIMEN,TDN,EDN,RDN,PTDN,PEDN,PRDN,DET
     . ,DET1,DET2,TE,FR,DEL,JO)
      T=T+DEL*(TD/3.+(2./3.)*TDN)
```

```
      E=E+DEL*(ED/3.+(2./3.)*EDN)
      R=R+DEL*(RD/3.+(2./3.)*RDN)
      PT=PT+DEL*(PTD/3.+(2./3.)*PTDN)
      PE=PE+DEL*(PED/3.+(2./3.)*PEDN)
      PR=PR+DEL*(PRD/3.+(2./3.)*PRDN)
      TIME=TIME+DEL
C  RUNGE-KUTTA INTEGRATION  END.............................
  901 CONTINUE
      IF(TIME.LT.TSTOP)GO TO 1000
   10 FORMAT(' ',4F9.2,F9.5,F10.5,F12.8,F8.3,F12.3,
     . F13.3,F10.3,F10.7,F10.4)
   11 FORMAT('1',////
     .       T4,'THETA E',T12,'DTHETA E',T22,'THETA R',T31,'DTHETA R',
     .T41,'THETA',T49,'DTHETA',T61,'DET',T72,'SHAFT',T84,'M.F. ',
     .T94,'TORQUE E',T104,'TORQUE R',T115,'DEL',T125,'TIME')
      GO TO 1001
  444 STOP
      END
```

```
      SUBROUTINE DOT(T,E,R,PT,PE,PR,TIME,TD,ED,RD,PTD,PED,PRD,DET,
     .DET1,DET2,TE,FR,DEL,JO)
C  TIME DERIVATIVES OF POSITION AND MOMENTUM.....
      IMPLICIT REAL*8(A-Z)
      INTEGER JO
      INTEGER NN,NNN,COUNT,NM
      COMMON R1,L,   M,ML,CDAMP,CS2,TT,IE,IR,IFE,IFR,RFL,TTT,KE,K2,
     .CL,CENG,ENGINE,W,X,Y,IL,NM
      IF(JC.GT.0)GO TO 1
      JO=1
      ILL=IL/(L*L)
      MASS1=M+ML/2.+2*ILL
      MASS2=ML/2.-2*ILL
      MASS3=ML/2.+2*ILL
C  INITIAL CONDITIONS--START UP.....
      T=1.466
      E=T/2
      R=-T/2
      TD=0
      ED=0
      RD=0
C  START SYSTEM AT STEADY STATE FOR TEST1 AND TEST2.....
C  NOTE THAT E CAN BE SET TO 0 AND T IS APPROX 1.65-1.75 AND
C  R=E-T-2004/K2     EC=RD=1447.56   TD=0
      DELT=.001
      CT=DCOS(T/2)
      ST=DSIN(T/2)
      ST2=DSIN(T)
      CT2=DCOS(T)
      RAD=RADR(T,R1,L,ST)
      RR=R1*CT+RAD
      RRDD=-(R1*ST+R1*R1*ST2/(2*RAD))/2.
      PRRDTD=RRDD
      PRRT=RRDD
```

```
      A1=(NM/2)*(MASS1*(2*RRDB*PRRDTD+RR*RR/2)
     .    +MASS2*(-R1*PRRDTD*ST-R1*RRDB*ST+R1*RR*CT)
     .    +MASS3*R1*R1) +IFR
      B1=(NM/2)*(-MASS1*RR*RR-2*MASS2*R1*RR*CT
     .    -MASS3*R1*R1) -IFR
      A2=B1
      B2=-2*B1+IE    +IFE-IFR
      PT=A1*TD+B1*ED
      PE=A2*TD+B2*ED
      PR=IR*RD
C  DYNAMICS.....
    1 CONTINUE
      DEL=DELT
      IF(TIME.LT.5)DEL=.0001
      IF(T.LT.TTT-.02.AND.T.GT.TT+.02)GO TO 777
      DEL=.0001
  777 CONTINUE
      ST=DSIN(T/2)
      CT=DCOS(T/2)
      ST2=DSIN(T)
      CT2=DCOS(T)
      RAD=RADR(T,R1,L,ST)
      RR=R1*CT+RAD
      RRDB=-(R1*ST+R1*R1*ST2/(2*RAD))/2.
      PRRDTD=RRDB
      PRRT=RRDB
C  ANGULAR VELOCITIES.....
      RD=PR/IR
      A1=(NM/2)*(MASS1*(2*RRDB*PRRDTD+RR*RR/2)
     .    +MASS2*(-R1*PRRDTD*ST-R1*RRDB*ST+R1*RR*CT)
     .    +MASS3*R1*R1)+IFR
      B1=(NM/2)*(-MASS1*RR*RR-2*MASS2*R1*RR*CT
     .    -MASS3*R1*R1)-IFR
      A2=B1
```

```
      B2=-2*B1+IE *IFE-IFR
      CET1=A1*B2
      CET2=A2*B1
      DET=DET1-DET2
      TD=(B2*PT-B1*PE)/DET
      ED=(A1*PE-A2*PT)/DET
C  POTENTIAL FORCES.....
      DE=-K2*(E-T-R)
      CR=-CE
      RRD=RRCB*TD
      PRRCT=-((R1*CT+R1*R1*CT2/RAD+
     .       (R1**4)*(ST2**2)/(4*RAD**3))/4)*TD
      CD=ED-TD/2
      CT=NM*MASS1*(RRD*PRRDT+CD*CD*RR*PRRT)
     .       +NM*MASS2*(CD*CD*R1*PRRT*CT
     .       -TD*PRRDT*ST*R1/2
     .       -TD*RRD*CT*R1/4-
     .   CD*CD*RR*ST*R1/2)+K2*(E-T-R)
C  GENERALIZED FORCES.....
      FCR=-CS2*(RD-ED+TD)
      FCE=-CS2*(ED-TD-RD)
      FCT=-CS2*(RD-ED+TD)
      TE=(ENGINE*TIME/3.)*(2.-TIME/3.)
      IF(TIME.GT.3)TE=ENGINE
      FE=TE-CENG*ED*DABS(ED)+FCE
      FST=KE*(RFL-RR)*PRRT*NM
      IF(RR.GT.RFL)FST=0
      FT=-CDAMP*TD-TLARGE(T,TT,TTT,X,Y)+FCT+FST
      VL=CL
      IF(TIME.GT.15)VL=CL *(1+.10*DSIN(W*TIME))
      FR=-VL*DABS(RD)*RD+FCR
      PTD=DT+FT
      PED=DE+FE
      PRD=DR+FR
      RETURN
      END
```

```
      FUNCTION RADR(T,R1,X,ST)
      IMPLICIT REAL*8(A-Z)
      RAD=X*X-R1*R1*ST*ST
      RADR=DSQRT(RAD)
      RETURN
      END
```

```
FUNCTION TLARGE(T,TT,TTT,X,Y)
IMPLICIT REAL*8(A-Z)
TLARGE=0
IF(T.GT.TTT)TLARGE=Y*(T-TTT)
IF(T.LT.TT)TLARGE=X*(T-TT)
RETURN
END
```

APPENDIX V
DERIVATION OF DRIVE TRAIN TRANSFER FUNCTION

The following is the derivation of the drive train transfer function used in References 1, 6, and 9, and given by equation 209. This derivation was adapted, in part, from a derivation by R. M. Swick and C. A. Skarvan.

Equations 144 through 149 are substituted into equation 150, and the shaft damping coefficient, C_s, is set equal to zero, to give equation 371.

$$\frac{\Delta W_e(s)}{\Delta T_e(s)} = \left\{ \frac{1}{C_T+C_D} \left[\frac{I_R}{K_\theta} S^2 + \frac{C_D}{K_\theta} S + 1 \right] \right\} \Bigg/ \left\{ \left[\frac{I_R I_{eg}}{K_\theta (C_D+C_T)} \right] S^3 + \left[\frac{C_D I_{eg} + C_T I_R}{K_\theta (C_D+C_T)} \right] S^2 + \left[\frac{K_\theta (I_R+I_{eg}) + C_D C_T}{K_\theta (C_D+C_T)} \right] S + 1 \right\} \tag{371}$$

The denominator of equation 371 is factored by long division as follows:

$$\frac{\left[\frac{I_R I_{eg}}{K_\theta (I_R+I_{eg})}\right] S^2 + \left[\frac{C_D I_{eg}^2 + C_T I_R^2}{K_\theta (I_{eg}+I_R)^2}\right] S + 1}{\frac{(I_{eg}+I_R)}{(C_T+C_D)} S + 1 \;\Big\overline{\left[\frac{I_R I_{eg}}{K_\theta (C_D+C_T)}\right] S^3 + \left[\frac{C_D I_{eg} + C_T I_R}{K_\theta (C_T+C_D)}\right] S^2 + \left[\frac{K_\theta (I_{eg}+I_R) + C_D C_T}{K_\theta (C_T+C_D)}\right] S + 1}}$$

$$\left[\frac{I_R I_{eg}}{K_\theta (C_T+C_D)}\right] S^3 + \left[\frac{I_{eg} I_R}{K_\theta (I_{eg}+I_R)}\right] S^2$$

$$0 + \left[\frac{C_D I_{eg}^2 + C_T I_R^2}{K_\theta (I_{eg}+I_R)(C_T+C_D)}\right] S^2 + \left[\frac{K_\theta (I_{eg}+I_R) + C_D C_T}{K_\theta (C_T+C_D)}\right] S$$

$$\left[\frac{C_D I_{eg}^2 + C_T I_R^2}{K_\theta (I_{eg}+I_R)(C_T+C_D)}\right] S^2 + \left[\frac{C_D I_{eg}^2 + C_T I_R^2}{K_\theta (I_{eg}+I_R)^2}\right] S$$

$$0 + \left[\frac{I_{eg}+I_R}{C_T+C_D}\right] S + 1$$

$$\left[\frac{I_{eg}+I_R}{C_T+C_D}\right] S + 1$$

$$0$$

The term with the asterisk is an approximation which is obtained in the following manner:

$$\left[\frac{K_\theta(I_{eg}+I_R)+C_DC_T}{K_\theta(C_T+C_D)}\right]S - \left[\frac{C_DI_{eg}^2+C_TI_R^2}{K_\theta(I_{eg}+I_R)^2}\right]S$$

$$= \left[\frac{K_\theta(I_{eg}+I_R)^3 + C_DC_T(I_{eg}+I_R)^2 - (C_DI_{eg}^2+C_TI_R^2)(C_T+C_D)}{K_\theta(C_T+C_D)(I_{eg}+I_R)^2}\right]S$$

$$= \left[\frac{K_\theta(I_{eg}+I_R)^3 + 2C_DC_TI_{eg}I_R - C_D^2I_{eg}^2 - C_T^2I_R^2}{K_\theta(C_T+C_D)(I_{eg}+I_R)^2}\right]S$$

$$= \left[\frac{K_\theta(I_{eg}+I_R)^3 - (C_DI_{eg} - C_TI_R)^2}{K_\theta(C_T+C_D)(I_{eg}+I_R)^2}\right]S$$

Under the assumption that

$$(C_DI_{eg} - C_TI_R)^2 \ll K_\theta(I_{eg}+I_R)^3$$

the above equation reduces to

$$\left[\frac{(I_{eg}+I_R)}{(C_T+C_D)}\right]S$$

For the values of the system parameter used in this report, the left side of the inequality becomes

$$[(2.768)(0.6944) - (1.106)(3.888)]^2 = 5.65$$

while the right side becomes

$$800.0(-0.6944 + 3.88)^2 = 7.68 \times 10^4$$

Therefore, the inequality is true and the assumption based on it is a reasonable one.

After the denominator is factored, the drive train transfer function is given by equation 372.

$$\frac{\Delta W_e(s)}{\Delta T_e(s)} = \frac{\left(\frac{1}{C_T+C_D}\right)\left[\frac{I_R}{K_\theta} s^2 + \frac{C_D}{K_\theta} s + 1\right]}{\left[\left(\frac{I_{eg}+I_R}{C_T+C_D}\right) s+1\right]\left[\left(\frac{I_R I_{eg}}{K_\theta(I_R+I_{eg})}\right) s^2 + \left(\frac{C_D I_{eg}^2 + C_T I_R^2}{K_\theta(I_{eg}+I_R)^2}\right) s + 1\right]} \qquad (372)$$

The following substitutions are made, leaving the drive train transfer function in its final form, given by equation 373.

$$K_L = \frac{1}{C_T+C_D}$$

$$\tau_L = \frac{I_{eg}+I_R}{C_T+C_D} \qquad \zeta_r = \frac{C_D}{2\sqrt{K_\theta I_R}}$$

$$\omega_r = \sqrt{\frac{K_\theta}{I_R}} \qquad \zeta_n = \frac{C_D I_{eg}^2 + C_T I_R^2}{2\sqrt{K_\theta I_R I_{eg}}\,(I_{ef}+I_R)^{3/2}}$$

$$\omega_R = \sqrt{\frac{K_\theta(I_{eg}+I_R)}{I_{eg} I_R}}$$

$$\frac{\Delta W_e(s)}{\Delta T_e(s)} = \frac{K_L\left[\left(\frac{1}{\omega_r}\right)^2 s^2 + \left(\frac{2\zeta_r}{\omega_r}\right) s + 1\right]}{\left[\tau_L s + 1\right]\left[\left(\frac{1}{\omega_n}\right)^2 s^2 + \left(\frac{2\zeta_n}{\omega_n}\right) s + 1\right]} \qquad (373)$$

APPENDIX VI
BODE ANALYSIS COMPUTER PROGRAM

The plotting subroutines used in this program are available on the FORTRAN IV G Compiler at the Northeast Florida Regional Data Center.

Input Data

Quantity	Value (and Meaning)	Units
SSD	5.0	percent
τ_B	0.1869	seconds
τ_1	0.02	seconds
τ_2	0.03	seconds
τ_e	0.3	seconds
τ_I	0.773	seconds
τ_r	0.2	seconds
K_B	0.941	$\frac{\text{ft-lb}}{\text{lb/hr}}$
K_θ	800.0	$\frac{\text{ft-lb}}{\text{rad}}$
I_R	3.888	$\frac{\text{ft-lb}}{\text{rad/sec}^2}$
I_e or (with ZTS)	0.5 or	$\frac{\text{ft-lb}}{\text{rad/sec}^2}$
I_{eg} (without ZTS)	0.6944	
C_D	2.768	$\frac{\text{ft-lb}}{\text{rad/sec}}$
C_T	1.106	$\frac{\text{ft-lb}}{\text{rad/sec}}$
K_R	0.5	none
C_s	variable	$\frac{\text{ft-lb}}{\text{rad/sec}}$

Quantity	Value (and Meaning)	Units
C_c	variable	$\frac{\text{ft-lb}}{\text{rad/sec}}$
I_{fe}	0.015	$\frac{\text{ft-lb}}{\text{rad/sec}^2}$
I_{fR}	0.2094	$\frac{\text{ft-lb}}{\text{rad/sec}^2}$
ITF1	1 = CDP/LGR speed governor 2 = FE/LGR speed governor 3 = DFF speed governor	none
ITF3	1 = Standard Drivetrain 2 = Decoupled Rotor Model of ZTS Coupling 3 = Linearized Design of ZTS Coupling	none
LPHP	1 = High Power 2 = Low Power	none
KREAD	1 = Use Same Drivetrain Parameters 2 = Read New Drivetrain Parameters	none
K_P	40.27	$\frac{\text{lb/hr}}{\text{rad/sec}}$

```
C  ..........................................................
C          THIS PROGRAM IS DESIGNED TO PRODUCE.....................
C          BODE PLOTS FOR A HELICOPTER DRIVE SYSTEM.................
C          GIVEN SPECIFIED SYSTEM PARAMETERS........................
C  ..........................................................
      COMPLEX J, G, JW, Y1, Y2, Y3, W
      COMPLEX   CSQRT
      REAL IE, KB, KP, KTH, KL, IR, K1, K2, KR
      DIMENSION GRAPH(1500) , XP(300) , YPG(300) , YPP(300)
    5 READ(5,50,END=9999) SSD,TAUB,TAU1,TAU2,TALE,TAUI,TAUR,KB,KTH,IR,
     + IE,CC,CT,KR,CS,CC,AIFE,AIFR
   50 FORMAT (F10.4)
    6 READ(5,60) ITF1,ITF3,LPHP,KREAD
   60 FORMAT (I4)
      READ (5,50) KP
      WEB = 1378.0
      E1 = 0.0006359
      E2 = 0.001434
      E3 = 0.00095464
      E4 = 0.00002968
      E5 = IE + AIFE + AIFR + 2.0*E1
      E6 = AIFR + E1
      E7 = AIFR + E2/2.0 + E1/2.0
      E8 = 2.0*WEB*E3
      E9 = E4*(WEB**2)
      E10 = E5*E7 - E6*E6
      E11 = E7*CT + E5*CC + E6*E8 + CS*(E7 + E5 - 2.0*E6)
      E12 = E7*CT + E5*CC + E6*E8
      E13 = E7 + E5 - 2.0*E6
      E14 = E5*E9 + CC*CT + CS*(E8 + CC + CT)
      E15 = E5*E9 + CC*CT
      E16 = E8 + CC + CT
      E17 = E7*CT + E5*CC + E6*E8 + CD*(E7 + E5 - 2.0*E6)
      E18 = E5*E9 + CC*CT + CC*(E8 + CC + CT)  + E9*IR
```

```
      A1 = IR*E7
      A2 = E7*(CS +CD) + (R*(CS + CC)
      A3 = IR*E9 + E7*KTH + IR*KTH + CS*CD + CC*(CS + CD)
      A4 = E9*(CS + CC) + KTH*(CC + CD)
      A5 = KTH*E9
      B1 = IR*E10
      B2 = IR*E11 + (CS + CD)*E10
      B3 = IR*E14 + (CS + CD)*E12 + KTH*E10 + (KTH*IR + CS*CD)*E13
      B4 = IR*E9*(CS + CT) + (CS + CD)*E15 + KTH*E17 + (CS*CD + KTH*IR)
     +    *E16                                                          B4
      B5 = KTH*E18 + (CS + CD)*E9*CT + CS*CD*E9
      B6 = KTH*E9*(CT + CD)
      KL = 1.0/(CT + CD)
      TAUL = (IE + IR)/(CT + CD)
      C = CD/IR
      CDB = CT/IE
      C1 = CS/IE
      C2 = CS/IR
      K1 = KTH/IE
      K2 = KTH/IR
      WRITE (6,70)          SSD,TAUB,TAU1,TAU2,TAUE,TAUI,TAUR,KB,KTH,IR,
     + IE,CD,CT,KR,TAUL,KL,KP,CS,CC,AIFE,AIFR
   70 FORMAT ('1',//T20,'STEADY STATE DROOP = ',F5.1,' PERCENT',/T20,
     $ 'TAUB = ',F7.4,' SEC',/T20,'TAU1 = ',F7.4,' SEC',/T20,'TAU2 = ',
     $ F7.4,' SEC',/T20,'TAUE = ',F7.4,' SEC',/T20,'TAUI = ',F7.4,
     $ ' SEC',/T20,'TAUR = ',F7.4,/T20,'KB = ',F7.4,/T20,'SHAFT STIFFNES
     $S = ',F10.4,' FT-LB/RAD',/T20,'ROTOR INERTIA = ',F10.6,' SLUG-FT**
     $2',/T20,'ENGINE INERTIA = ',F10.6,' SLUG-FT**2',/T20,'ROTOR DAMPIN
     $G = ',F10.6,' FT-LB-SEC/RAD',/T20,'TURBINE DAMPING = ',F10.6,
     $ ' FT-LB-SEC/RAD',/T20,'KR = ',F7.4,/T20,'TAUL = ',F10.6,' SEC',
     $ /T20,'KL = ',F10.6,/T20,'KP = ',F10.6,/T20,'SHAFT DAMPING = ',
     $F10.6,' FT-LB-SEC/RAD',/T20,'COUPLING DAMPING = ',F10.6,' FT-LB-SE
     $C/RAD',/T20,'ENGINE-SIDE FLANGE INERTIA =   ',F10.6,' SLUG-FT**2',
     $ /T20,'ROTOR-SIDE FLANGE INERTIA = ',F10.6,' SLUG-FT**2')
```

```
      IF (ITF1-2) 101,102,103
  101 WRITE(6,111)
  111 FORMAT (T20,'FUEL FLOW/COMPRESSOR DISCHARGE PRESSURE GOVERNOR WITH
     + LAGGED GAIN RESET')
      GO TO 150
  102 WRITE(6,112)
  112 FORMAT (T20,'FUEL FLOW GOVERNOR WITH LAGGED GAIN RESET')
      GO TO 150
  103 WRITE(6,113)
  113 FORMAT (T20,'DIRECT FUEL FLOW GOVERNOR')
  150 IF (ITF3-2) 121,122,123
  121 WRITE(6,131)
  131 FORMAT (T30,'WITH ROTOR AND DRIVE TRAIN')
      GO TO 160
  122 WRITE(6,132)
  132 FORMAT (T30,'WITH DECOUPLED ROTOR MODEL OF ZTS COUPLING')
      GO TO 160
  123 WRITE(6,133)
  133 FORMAT (T30,'WITH LINEARIZED ZTS COUPLING DESIGN')
  160 IF (LPHP.GE.2) GO TO 141
      WRITE(6,139)
  139 FORMAT (T35,'AT HIGH POWER'///)
      GO TO 170
  141 WRITE(6,142)
  142 FORMAT (T35,'AT LOW POWER'///)
  170 CONTINUE
C  BEGIN CALCULATION OF POINTS FOR BODE PLOT.....................
      COM = 0.001
      OMEGA = 0.01
      K = 3
      IP = 1
      W = -1.0
      J = CSQRT(W)
      WRITE(6,20)
```

```
   20 FORMAT (T25,'OMEGA (CPS)'
     +                    ,T45,'GAIN (DB)',T60,'PHASE ANGLE (DEGREES)'/)
    1 DO 2 I=1,90
      OMEGAR = OMEGA*2.0*3.141592
      JW = J*OMEGAR
      GO TO(11,12,13),ITF1
   11 Y1 = KP*(TAUR*JW + 1.0)*(TAUE*JW + 1.0)/((TAUI*JW + 1.0)*((TAUR/(
     + 1.0-KR))*JW + 1.0)*(TAU1*JW + 1.0)*(TAU2*JW + 1.0))
      GO TO 200
   12 Y1 = KP*(TAUR*JW + 1.0)/((TAU1*JW + 1.0)*(0.1*TAUR*(JW**2) +
     + (0.1 + 2.0*TAUR)*JW + 1.0))
      GO TO 200
   13 Y1 = KP/((TAU1*JW+1.0)*(TAU2*JW+1.0))
  200 CONTINUE
      Y2 =(KB*(TAUB*JW+1.0)/(TAUE*JW+1.0))
      GO TO(31,32,33),ITF3
   31 Y3 =(JW*(JW + C + C2) + K2)/(IE*((JW**3) + (CBB + C + C1 + C2)*
     + (JW**2) + (CBB*C + C*C1 + K1 + K2 + CBB*C2)*JW + K1*C + K2*CBB))
      GO TO 250
   32 Y3 = 1.0/(IE*JW+CT)
      GO TO 250
   33 Y3 = ( A1*(JW**4) + A2*(JW**3) + A3*(JW**2) + A4*JW + A5)/(B1*(JW
     + **5) + B2*(JW**4) + B3*(JW**3) + B4*(JW**2) + B5*JW + B6)          Y3
  250 CONTINUE
      G = Y1*Y2*Y3
C     GAIN IS THE MAGNITUDE OF G.....
      GMAG = CABS(G)
C     CONVERT GAIN TO DECIBELS.....
      GMAGL = 20.0*ALOG10(GMAG)
C     PHASE IS THE ANGLE OF G.....
      GANG = ATAN2(AIMAG(G),REAL(G))
C     CONVERT PHASE ANGLE TO DEGREES.....
      GANGD = GANG*180.0/3.141592
      YPG(I) = GMAGL
```

```
      YPP(IP) = GANGD
      WRITE(6,30) OMEGA, GMAGL, GANGD
   30 FORMAT (T20,F12.6,10X,F12.6,10X,F12.6)
      IP = IP + 1
    2 OMEGA = OMEGA + DOM
      IF ( K.GE.5 ) GO TO 999
      K = K+1
      DOM = DOM*10.0
      GO TO 1
  999 CONTINUE
      IP = 0
C  CONVERT POINTS FOR PLOTTING.....................................
      DO 8 J2 = 1,3
      DO 8 I2 = 10,99
      IP = IP + 1
      XP(IP) = ALOG10((I2)*(10.**(J2-4)))
    8 YPP(IP) = (YPP(IP)/4.5) - 5.0
      WRITE (6,302)
  302 FORMAT ('1')
C  CALL PLOT SUBROUTINES.....................................................
      CALLPLOT2(GRAPH,1.0,-2.0,35.0,-45.0)
      CALLPLOT3(1HM,XP(1),YPG(1),270)
      CALLPLOT3(1HP,XP(1),YPP(1),270)
      CALLPLOT4(51,51H180        108        36         -36       -108     -18
     +0)
      WRITE (6,301)
  301 FORMAT (/T50,'FREQUENCY  10**X CPS',/T30 , 'M = GAIN IN DB', T60,
     +  'P = PHASE ANGLE IN DEGREES')
      IF (KREAD.GE.2) GO TO 5
      READ(5,50,END=9999) SSD,TAUB,TAU1,TAU2,TAUE,TAUI,TAUR
      GO TO 6
 9999 STOP
      END
```

```
      SUBROUTINE PLOT1 (NTEST,NHL,NSHL,NVL,NSVL)
      LOGICAL*1 FLAG1
      DATA FLAG1/.FALSE.    /
      IF (NTEST.NE.0) FLAG1=.TRUE.
      RETURN
      ENTRY PLOT2(GRAPH,XMAX,XMIN,YMAX,YMIN)
      DIMENSION GRAPH(1)
      IF (FLAG1) GO TO  100
      NHL=51
      NSHL=10
      NVL=101
      NSVL=10
  100 CALL PRPLOT (GRAPH,NHL,NSHL,NVL,NSVL,XMAX,XMIN,YMAX,YMIN)
      RETURN
      END
      SUBROUTINE PRPLOT (LGRAPH,NHL,NSHL,NVL,NSVL,XMAX,XMIN,YMAX,YMIN)
      IMPLICIT LOGICAL*1 (L)
      DIMENSION LGRAPH (NVL,NHL)
      DATA LBK,LPLUS,LDASH,LBAR/' ','+','-','I' /
      DATA LBK,LPLUS,LDASH,LBAR/' ','+','-','I' /
C     NHL---NUMBER OF CHARACTERS IN THE Y DIRECTION (51)
C     NVL---NUMBER OF CHARACTERS IN THE X DIRECTION (101)
C     NSHL---
C     A HORIZONTAL LINE WILL BE PLACED IN THE FIRST AND EVERY NSHL*TH
C               CHARACTER POSITION THEREAFTER (10)
C     NSVL---
C     A VERTICAL LINE WILL BE PLACED IN THE LEFTMOST AND EVERY NSVL*TH
C               CHARACTER POSITION THEREAFTER (10)
      I=NHL+1
      DO 101 IL=1,NHL
      I=I-1
      LPUT=LBK
      ITEST=MOD(I,NSHL)
      IF(ITEST.EQ.1)LPUT=LDASH
```

```
      J=NVL+1
      DO 101 JL=1,NVL
      J=J-1
      LGRAPH(J,I)=LPUT
      JTEST=MOD(J,NSVL)
      IF(JTEST.NE.1) GO TO 101
      LGRAPH(J,I)=LBAR
      IF(ITEST.EQ.1)LGRAPH(J,I)=LPLUS
  101 CONTINUE
      NERROR=0
      SCALEX=NVL -1
      SCALEX=SCALEX/(XMAX-XMIN)
      SCALEY=NHL -1
      SCALEY=SCALEY/(YMAX-YMIN)
    5 FORMAT (1X,F10.5,2X,F10.5)
      RETURN
      ENTRY PLOT3 (LCHAR,RX,RY,NPTS)
      DIMENSION RX(1),RY(1)
      DO 200 IU=1,NPTS
      IF(RX(IU).GT.XMAX.OR.RX(IU).LT.XMIN) GO TO 199
      IF(RY(IU).GT.YMAX.OR.RY(IU).LT.YMIN) GO TO 199
      X=RX(IU)-XMIN
      Y=RY(IU)-YMIN
      IX=X*SCALEX+1.5
      IY=Y*SCALEY+1.5
      LGRAPH(IX,IY)=LCHAR
      GO TO 200
  199 NERROR=NERROR+1
      IF (NERROR .GT. 20) GO TO 200
      WRITE (6,198) RX(IU),RY(IU)
  198 FORMAT (1X,'ERROR***(',F8.3,',',F8.3,') IS OUT OF PLOTTING RANGE')
  200 CONTINUE
      RETURN
      ENTRY PLOT4(NCHAR,LYNAME)
```

```
      ENTRY FPLOT4(NCHAR,LYNAME)
      DIMENSION LYNAME(1),LYNAMI(108),XVALUE(26)
      IF (NCHAR.GT.108) NCHAR=108
      J=NCHAR+1
      DO 400 I=1,NCHAR
      J=J-1
  400 LYNAMI(I)=LYNAME(J)
      J=NCHAR+1
      DO 401 I=J,103
  401 LYNAMI(I)=LBK
      YVALUE=YMAX
      DELY=YMAX-YMIN
      YN=NSML
      DELY=DELY*YN
      YN=NML-1
      DELY=DELY/YN
      I=NML+1
      DO 444 IL=1,NML
      I=I-1
      ITEST=MOD(I,NSML)
      IF(ITEST.EQ.1)GO TO 402
      WRITE(6,1000)LYNAMI(I),(LGRAPH(J,I),J=1,NVL)
 1000 FORMAT(1X,A1,8X,1X,120A1)
      GO TO 444
  402 WRITE(6,1001) LYNAMI(I),YVALUE,(LGRAPH(J,I),J=1,NVL)
 1001 FORMAT (1X,A1,F8.3,1X,120A1)
      YVALUE=YVALUE-DELY
  444 CONTINUE
      N=NVL/NSVL+1
      XVALUE(1)=XMIN
      DELX=NVL/NSVL
      DELX=(XMAX-XMIN)/DELX
      IF(N.GT.26) RETURN
      DO 403 I=2,N
```

```
403 XVALUE(I)=XVALUE(I-1)+DELX
    LOGICAL*1 FMTX (30)
    DATA FMTX/' (/   X,F  . ,50F    . ) '/
    NYFMT=8
    NXDEC=3
    NSVLF1= NSVL
500 NXSKIP=4+NYFMT+NXDEC-NSVLF1
    IF(NXSKIP.LT.1.AND.NXSKIP.GT. -3) NXSKIP=1
    IF(NXSKIP.GT.0) GO TO 501
    NSVLF1=NSVLF1/2
    GO TO 500
501 IF(NXDEC.LT.NSVLF1) GO TO 502
    NXDEC=NXDEC-1
    GO TO 500
502 CALL IN4TAF(NXSKIP,FMTX(4),3)
    CALL IN4TAF(NSVLF1,FMTX(10),2)
      CALL IN4TAF(NXDEC,FMTX(13),1)
    CALL IN4TAF(NSVL  ,FMTX(18),3)
    CALL IN4TAF (NXDEC,FMTX(22),1)
    WRITE(6,FMTX) (XVALUE(I),I=1,N)
    RETURN
    END

    SUBROUTINE IN4TAF (I4,A, N)
    IMPLICIT LOGICAL*1(A ),INTEGER*2(L)
    DIMENSION A( N),ACH(2)
    EQUIVALENCE (ACH(1),LCH)
    DATA LO,ABLK,AMINUS/Z00F0,Z40,Z60 /
200 CONTINUE
    LN=N
    LBF=1
    DO 100 I=1,LN
100 A(I)=ABLK
    JI4=I4
```

```
      IF(JI4 .GE.0) GO TO 101
      A(LBF)=ARINUS
      JI4=-JI4
      LBF=LBF+1
      IF (LBF.GT.LN) RETURN
  101 I=0
      J=JI4
  102 I=I+1
      J=J/10
      IF(J.GT.0) GO TO 102
  103 J=JI4
      I=I-1
      NTENS=10**I
      J=J/NTENS
      LCH=J+LO
      A(LBF)=ACH(2)
      LBF=LBF+1
      IF (LBF.GT.LN) RETURN
      IF(I.LE.0) RETURN
      JI4=JI4-J*NTENS
      GO TO 103
      ENTRY IN2TAF (L2,A,N)
      I4=L2
      GO TO 200
      END
```

APPENDIX VII
LINEAR TIME RESPONSE COMPUTER PROGRAM

The subroutine DPRQD is available in the IBM Scientific Subroutine Package. The plotting subroutines used in this program are the same as those listed in Appendix VI. The units for all input data in this program may be found in the data list in Appendix VI.

Input Data

Quantity	Value (or meaning)
I_e	0.6944
I_{eg}	0.5
I_R	3.888
K_θ	800.0
C_s	variable
C_T	1.106
C_D	2.768
τ_1	0.02
τ_2	0.03
τ_B	0.1869
τ_e	0.3
K_B	0.941
K_P	40.27

```
C  ..........................................................
C  THIS COMPUTER PROGRAM IS DESIGNED TO CALCULATE.............
C  AND PLOT THE TIME RESPONSE OF A LINEARIZED HELICOPTER.......
C  DRIVE SYSTEM WIT AND WITHOUT A DECOUPLED ROTOR..............
C  MODEL OF A ZTS COUPLING.....................................
C  ..........................................................
      IMPLICIT REAL*8(A-Z)
      COMPLEX*16   SOL,  FACT
      COMPLEX*16   DCMPLX
      REAL*4  TIMS, RESS, BIG
      DIMENSION  TIMS(100), RESS(100)
      DIMENSION  C( 7), G( 7), E( 7), POL( 7)
      DIMENSION  SOL(7), FACT(7)
      DIMENSION  TIME(100), RESP(100), GRAPH(1500)
      DATA  TIME, RESP / 200*0.0 /
      INTEGER   IC, IER, JR, I, J, KEY, DOFR
      KEY = 0
      TIMEI = 0.02
      TIMEI = 0.01
      DO 550 I = 1,100
      TIME(I) = TIMEI*I
  550 CONTINUE
      TIMEL = 0.0
      TIMEH = TIME(100)
      PI = 3.14159265359
      READ(5,300)IE,IEG,IR,KTH,CS,CT,CD,TAU1,TAU2,TAUB,TAUE,KB,KP
  300 FORMAT(F10.6)
      READ(5,311)DOFR
  311 FORMAT(I2)
      CB= CD/IR
      C1 = CS/IE
      C2 = CS/IR
      K1 = KTH/IE
      K2 = KTH/IR
```

```
      CBB = CT/IE
      A1 = CB+ C2
      A2 = CBB + C1
      A3 = A1 + A2
      A4 = CBB*CB+ CBB*C2 +CB*C1 + K1 + K2
      A5 = K1*CB+ K2*CBB
      A6 = KB*KP
      A7 = TAU1*TAU2 + TAU1*TAUE + TAU2*TAUE
      A8 = TAU1 + TAU2 + TAUE
      A9 = TAU1*TAU2*TAUE
      A10 = A7 + A9*A3
      A11 = A8 + A7*A3 + A9*A4
      A12 = A1*TAUB + 1.0
      A13 = TAUB*K2 + A1
      A14 = 1.0 + A8*A3 + A7*A4 + A9
      A15 = A3 + A8*A4 + A7*A5
      A16 = A4 + A8*A5
C     FOR THE SYSTEM WITHOUT A ZTS COUPLING.....
      IC = 7 - DOFR
      JR = 6 - DOFR
C     COEFFICIENTS OF THE DENOMINATOR OF THE CLOSED-LOOP TRANSFER FUNCTION
      C(1) = IE*A5 + A6*K2
      C(2) = IE*A16 + A6*A13
      C(3) = IE*A15 + A6*A12
      C(4) = IE*A14 + A6*TAUB
      C(5) = IE*A11
      C(6) = IE*A10
      C(7) = IE*A9
C     FACTORING THE DENOMINATOR OF THE CLOSED-LOOP TRANSFER FUNCTION
      CALL CPRCD(C,IC,C,E,POL,JR,IER)
      WRITE(6,140)
  140 FORMAT ('1',T30,'HELICOPTER SYSTEM WITHOUT A ZTS COUPLING'//)
      WRITE(6,305)
  305 FORMAT ( T30,'ROOTS OF THE DENOMINATOR',T65,'COEFFICIENTS OF THE DEN
```

```
     $OMINATOR',/T30,'REAL',T50,'IMAGINARY',T70,'ORIGINAL', T90,'FROM RO
     $OTS'/)
      DO 102 I = 1,7
      WRITE(6,101) C(I), E(I), C(I), POL(I)
  101 FORMAT (T20,4D20.5)
  102 CONTINUE
      SOL(7) = 0.0
C   BREAKING UP THE CLOSED-LOOP TRANSFER FUNCTION.................
C   BY PARTIAL FRACTION EXPANSION.................................
      DO 111 I = 1,6
      SOL(I) =DCMPLX(C(I),E(I))
      FACT(I) = A6*(TAU3*(SOL(I)**3) + A12*(SOL(I)**2) + A13*SOL(I)+K2)
  111 CONTINUE
      DO 112 I = 1,6
      DO 112 J = 1,6
      IF( I.NE.J ) FACT(I) = FACT(I)/(SOL(I) - SOL(J))
  112 CONTINUE
      WRITE(6,306)
  306 FORMAT(//T35,'NUMERATORS AFTER PARTIAL FRACTION EXPANSION',/T40,
     $ 'REAL',T60,'IMAGINARY'/)
      DO 114 I = 1,6
      WRITE(6,113)FACT(I)
  113 FORMAT (T30,2D20.5)
  114 CONTINUE
      GO TO 601
  444 CONTINUE
      KEY = 2
      DO 150 J = 1,100
  150 RES(J) = 0.0
C   FOR THE SYSTEM WITH A ZTS COUPLING.............................
      IC = 5 - DOFR
      JR = 4 - DOFR
C   COEFFICIENTS OF THE DENOMINATOR OF THE CLOSED-LOOP TRANSFER FUNCTION
      C(1) = A6 + CT
```

```
      C(2) = A8*CT + IEG+ A6*TAUB
      C(3) = A7*CT + A8*IEG
      C(4) = A9*CT + A7*IEG
      C(5) = A9*IEC
C     FACTORING THE DENOMINATOR OF THE CLOSED-LOOP TRANSFER FUNCTION
      CALL DPRGDI(C,IC,C,E,POL,JR,IER)
      WRITE(6,240)
  240 FORMAT ('1',T30,'HELICOPTER SYSTEM WITH A ZTS COUPLING'//)
      WRITE(6,305)
      DO 202 I = 1,5
      WRITE(6,201) C(I), E(I), C(I), POL(I)
  201 FORMAT (T20,4D20.5)
  202 CONTINUE
      SOL(5) = 0.0
C     BREAKING UP THE CLOSED-LOOP TRANSFER FUNCTION.................
C     BY PARTIAL FRACTION EXPANSION.................................
      DO 211 I = 1,4
      SOL(I) =DCMPLX(C(I),E(I))
      FACT(I) = A6*(TAUB*SOL(I) + 1.0)
  211 CONTINUE
      DO 212 I = 1,4
      DO 212 J = 1,4
      IF( I.NE.J ) FACT(I) = FACT(I)/(SOL(I) - SOL(J))
  212 CONTINUE
      WRITE(6,306)
      DO 214 I = 1,4
      WRITE(6,113)FACT(I)
  214 CONTINUE
  601 CONTINUE
      I = 1
      WRITE(6,501)
  501 FORMAT( //T10,'TIME RESPONSE  =')
  900 CONTINUE
      IF ( I.GE.IC ) GO TO 999
```

```
C  TAKING THE INVERSE LAPLACE TRANSFORM OF EACH TERM.............
C  OF THE CLOSED-LOOP TRANSFER FUNCTION.........................
C  CALCULATING  POINTS FOR THE PLOT.............................
      IF (DABS(E(I)).LE.0.0000001 ) GO TO 1000
      MAG = CDABS(FACT(I))
      ANG = DATAN2(DAIMAG(FACT(I)),DREAL(FACT(I)))
      PSI = ANG + PI/2.0
      DO 301 J = 1,100
      RESP(J) = RESP(J) + 2.0*MAG*DEXP(Q(I)*TIME(J))*DSIN(E(I)*TIME(J)
     + + PSI)
  301 CONTINUE
      WRITE(6,503)MAG,Q(I),E(I),PSI
  503 FORMAT( T25,'+ ( 2.0* ',D14.5,' * EXP( ',D14.5,' * TIME) * SIN( ',
     + D14.5,' * TIME + ',D14.5,' RAD.))')
      I = I + 1
      GO TO 998
 1000 CONTINUE
      REF =DREAL(FACT(I))
      DO 401 J = 1,100
      RESP(J) = RESP(J) +   REF     *  DEXP(Q(I)*TIME(J))
  401 CONTINUE
      WRITE(6,502)REF,Q(I)
  502 FORMAT( T30,'+ ( ',D14.5,' * EXP( ',D14.5,' * TIME))')
  998 I = I + 1
      GO TO 900
  999 CONTINUE
      WRITE(6,504)
  504 FORMAT( '1',T30,'TIME',T60,'TIME RESPONSE'/)
      DO 530 J = 1,100
      WRITE(6,505)TIME(J),RESP(J)
  505 FORMAT( T25,D14.5,T60,D14.5)
  530 CONTINUE
      BIG = 0.0
      DO 430 J = 1,100
```

```
      TIMS(J) = TIME(J)
      RESS(J) = RESP(J)
C  FINDING THE LARGEST NUMBER TO BE PLOTTED FOR DETERMINING THE SCALE
      IF ( RESS(J).GE.BIG ) BIG = RESS(J)
  430 CONTINUE
      WRITE(6,506)
  506 FORMAT(  '1')
      RESPH = BIG*1.3
      RESPL = - RESPH
C  CALL PLOTTING SUBROUTINES.....................................
      CALLPLOT2(GRAPH,TIMEH,TIMEL,RESPH,RESPL)
      CALLPLOT3(1H*,TIMS(1),RESS(1),100)
      CALLPLOT4(49,49H                                                    )
      WRITE(6,510)
  510 FORMAT ( /T50,'TIME IN SECONDS',/T30,'TIME RESPONSE OF LINEARIZED
     +HELICOPTER DRIVE SYSTEM')
      IF ( KEY.GE.1 ) GO TO 777
      GO TO 444
  777 CONTINUE
      STOP
      END
```

```
C                                                                       DPRQ  10
C     .....................................................b.....b..DPRQ  20
C                                                                       DPRQ  30
C        SUBROUTINE DPRQD                                               DPRQ  40
C                                                                       DPRQ  50
C        PURPOSE                                                        DPRQ  60
C           CALCULATE ALL REAL AND COMPLEX ROOTS OF A GIVEN POLYNOMIAL  DPRQ  70
C           WITH REAL COEFFICIENTS.                                     DPRQ  80
C                                                                       DPRQ  90
C        USAGE                                                          DPRQ 100
C           CALL DPRQD(C,IC,Q,E,POL,IR,IER)                             DPRQ 110
C                                                                       DPRQ 120
C        DESCRIPTION OF PARAMETERS                                      DPRQ 130
C           C      - COEFFICIENT VECTOR OF GIVEN POLYNOMIAL             DPRQ 140
C                    COEFFICIENTS ARE ORDERED FROM LOW TO HIGH          DPRQ 150
C                    THE GIVEN COEFFICIENT VECTOR GETS DIVIDED BY THE   DPRQ 160
C                    LAST NONZERO TERM                                  DPRQ 170
C                    DOUBLE PRECISION ARRAY                             DPRQ 180
C           IC     - DIMENSION OF VECTOR C                              DPRQ 190
C           Q      - WORKING STORAGE OF DIMENSION IC                    DPRQ 200
C                    ON RETURN Q CONTAINS REAL PARTS OF ROOTS           DPRQ 210
C                    DOUBLE PRECISION ARRAY                             DPRQ 220
C           E      - WORKING STORAGE OF DIMENSION IC                    DPRQ 230
C                    ON RETURN E CONTAINS COMPLEX PARTS OF ROOTS        DPRQ 240
C                    DOUBLE PRECISION ARRAY                             DPRQ 250
C           POL    - WORKING STORAGE OF DIMENSION IC                    DPRQ 260
C                    ON RETURN POL CONTAINS THE COEFFICIENTS OF THE     DPRQ 270
C                    POLYNOMIAL WITH CALCULATED ROOTS                   DPRQ 280
C                    THIS RESULTING COEFFICIENT VECTOR HAS DIMENSION IR+1DPRQ 290
C                    COEFFICIENTS ARE ORDERED FROM LOW TO HIGH          DPRQ 300
C                    DOUBLE PRECISION ARRAY                             DPRQ 310
C           IR     - NUMBER OF CALCULATED ROOTS                         DPRQ 320
C                    NORMALLY IR IS EQUAL TO DIMENSION IC MINUS ONE     DPRQ 330
C           IER    - RESULTING ERROR PARAMETER. SEE REMARKS             DPRQ 340
```

```
C                                                                       DPRQ 350
C       REMARKS                                                         DPRQ 360
C          THE REAL PART OF THE ROOTS IS STORED IN Q(1) UP TO Q(IR)     DPRQ 370
C          CORRESPONDING COMPLEX PARTS ARE STORED IN E(1) UP TO E(IR).  DPRQ 380
C          IER = 0 MEANS NO ERRORS                                      DPRQ 390
C          IER = 1 MEANS NO CONVERGENCE WITH FEASIBLE TOLERANCE         DPRQ 400
C          IER = 2 MEANS POLYNOMIAL IS DEGENERATE (CONSTANT OR ZERO)    DPRQ 410
C          IER = 3 MEANS SUBROUTINE WAS ABANDONED DUE TO ZERO DIVISOR   DPRQ 420
C          IER = 4 MEANS THERE EXISTS NO S-FRACTION                     DPRQ 430
C          IER =-1 MEANS CALCULATED COEFFICIENT VECTOR REVEALS POOR      DPRQ 440
C                  ACCURACY OF THE CALCULATED ROOTS.                    DPRQ 450
C                  THE CALCULATED COEFFICIENT VECTOR HAS LESS THAN      DPRQ 460
C                  6 CORRECT DIGITS.                                    DPRQ 470
C          THE FINAL COMPARISON BETWEEN GIVEN AND CALCULATED            DPRQ 480
C          COEFFICIENT VECTOR IS PERFORMED ONLY IF ALL ROOTS HAVE BEEN  DPRQ 490
C          CALCULATED.                                                  DPRQ 500
C          THE MAXIMAL RELATIVE ERROR OF THE COEFFICIENT VECTOR IS      DPRQ 510
C          RECORDED IN Q(IR+1).                                         DPRQ 520
C                                                                       DPRQ 530
C       SUBROUTINES AND FUNCTION SUBPROGRAMS REQUIRED                   DPRQ 540
C          NONE                                                         DPRQ 550
C                                                                       DPRQ 560
C       METHOD                                                          DPRQ 570
C          THE ROOTS OF THE POLYNOMIAL ARE CALCULATED BY MEANS OF       DPRQ 580
C          THE QUOTIENT-DIFFERENCE ALGORITHM WITH DISPLACEMENT.         DPRQ 590
C          REFERENCE                                                    DPRQ 600
C          H.RUTISHAUSER, DER QUOTIENTEN-DIFFERENZEN-ALGORITHMUS,       DPRQ 610
C          BIRKHAEUSER, BASEL/STUTTGART, 1957.                          DPRQ 620
C                                                                       DPRQ 630
C     ..................................................................DPRQ 640
C                                                                       DPRQ 650
      SUBROUTINE DPRQCIC,IC,Q,E,POL,IR,IER)                             DPRQ 660
C                                                                       DPRQ 670
C      DIMENSIONED DUMMY VARIABLES                                      DPRQ 680
```

```
      DIMENSION  E(IC), Q(IC), C(IC), POL(IC)
      DOUBLE PRECISION Q,E,O,P,T,EXPT,E$AV,U,V,W,C,POL,EPS                DPRQ 700
      DOUBLE PRECISION  DABS, DSQRT
C                                                                        DPRQ 710
C        NORMALIZATION OF GIVEN POLYNOMIAL                               DPRQ 720
C           TEST OF DIMENSION                                            DPRQ 730
C        IR CONTAINS INDEX OF HIGHEST COEFFICIENT                        DPRQ 740
      IR=IC                                                              DPRQ 750
      IER=0                                                              DPRQ 760
      EPS=1.D-16                                                         DPRQ 770
      TOL=1.E-6                                                          DPRQ 780
      LIMIT=10*IC                                                        DPRQ 790
      KOUNT=0                                                            DPRQ 800
    1 IF(IR-1)79,79,2                                                    DPRQ 810
C                                                                        DPRQ 820
C        DROP TRAILING ZERO COEFFICIENTS                                 DPRQ 830
    2 IF(C(IR))4,3,4                                                     DPRQ 840
    3 IR=IR-1                                                            DPRQ 850
      GOTO 1                                                             DPRQ 860
C                                                                        DPRQ 870
C           REARRANGEMENT OF GIVEN POLYNOMIAL                            DPRQ 880
C        EXTRACTION OF ZERO ROOTS                                        DPRQ 890
    4 C=1.0D0/C(IR)                                                      DPRQ 900
      IEND=IR-1                                                          DPRQ 910
      ISTA=1                                                             DPRQ 920
      NSAV=IR+1                                                          DPRQ 930
      JBEG=1                                                             DPRQ 940
C                                                                        DPRQ 950
C        Q(J)=1.                                                         DPRQ 960
C        C(J+I)=C(IR-I)/C(IR)                                            DPRQ 970
C        C(IR)=C(J)/C(IR)                                                DPRQ 980
C        WHERE J IS THE INDEX OF THE LOWEST NONZERO COEFFICIENT          DPRQ 990
      DO 9 I=1,IR                                                        DPRQ1000
      J=NSAV-I                                                           DPRQ1010
```

```
      IF(C(I))7,5,7                                                     DPRC1020
    5 CCTO(6,8);JBEG                                                    DPRQ1030
    6 NSAV=NSAV+1                                                       DPRQ1040
      C(ISTA)=0.DO                                                      DPRC1050
      E(ISTA)=0.DO                                                      DPRC1060
      ISTA=ISTA+1                                                       DPRQ1070
      GOTO 9                                                            DPRQ1080
    7 JBEG=2                                                            DPRC1090
    8 C(J)=C(I)*D                                                       DPRC1100
      C(I)=C(J)                                                         DPRQ1110
    9 CONTINUE                                                          DPRQ1120
C                                                                       DPRQ1130
C           INITIALIZATION                                              DPRQ1140
      ESAV=0.DO                                                         DPRQ1150
      C(ISTA)=0.DO                                                      DPRQ1160
   10 NSAV=IR                                                           DPRC1170
C                                                                       DPRQ1180
C        COMPUTATION OF DERIVATIVE                                      DPRQ1190
      EXPT=IR-ISTA                                                      DPRQ1200
      E(ISTA)=EXPT                                                      DPRQ1210
      DO 11 I=ISTA,IEND                                                 DPRQ1220
      EXPT=EXPT-1.0DO                                                   DPRQ1230
      PCL(I+1)=EPS*DABS(Q(I+1))+EPS                                     DPRQ1240
   11 E(I+1)=Q(I+1)*EXPT                                                DPRQ1250
C                                                                       DPRC1260
C        TEST OF REMAINING DIMENSION                                    DPRQ1270
      IF(ISTA-IEND)12,20,60                                             DPRQ1280
   12 JEND=IEND-1                                                       DPRQ1290
C                                                                       DPRC1300
C        COMPUTATION OF S-FRACTION                                      DPRQ1310
      DO 19 I=ISTA,JEND                                                 DPRQ1320
      IF(I-ISTA)13,16,13                                                DPRC1330
   13 IF(DABS(E(I))-PCL(I+1))14,14,16                                   DPRC1340
C                                                                       DPRQ1350
```

```
C        THE GIVEN POLYNOMIAL HAS MULTIPLE ROOTS, THE COEFFICIENTS OF    DPRQ1360
C        THE COMMON FACTOR ARE STORED FROM Q(NSAV) UP TO Q(IR)           DPRQ1370
   14 NSAV=I                                                             DPRQ1380
      DO 15 K=I,JEND                                                     DPRQ1390
      IF(DABS(E(K))-POL(K+1))15,15,80                                    DPRQ1400
   15 CONTINUE                                                           DPRQ1410
      GOTO 21                                                            DPRQ1420
C                                                                        DPRQ1430
C           EUCLIDEAN ALGORITHM                                          DPRQ1440
   16 DO 19 K=I,IEND                                                     DPRQ1450
      E(K+1)=E(K+1)/E(I)                                                 DPRQ1460
      Q(K+1)=E(K+1)-Q(K+1)                                               DPRQ1470
      IF(K-I)18,17,18                                                    DPRQ1480
C                                                                        DPRQ1490
C        TEST FOR SMALL DIVISOR                                          DPRQ1500
   17 IF(DABS(Q(I+1))-POL(I+1))80,80,19                                  DPRQ1510
   18 Q(K+1)=Q(K+1)/Q(I+1)                                               DPRQ1520
      POL(K+1)=POL(K+1)/DABS(Q(I+1))                                     DPRQ1530
      E(K)=Q(K+1)-E(K)                                                   DPRQ1540
   19 CONTINUE                                                           DPRQ1550
   20 Q(IR)=-Q(IR)                                                       DPRQ1560
C                                                                        DPRQ1570
C           THE DISPLACEMENT EXPT IS SET TO 0 AUTOMATICALLY.             DPRQ1580
C           E(ISTA)=0.,Q(ISTA+1),....,E(NSAV-1),Q(NSAV),E(NSAV)=0.,      DPRQ1590
C           FORM A DIAGONAL OF THE QD-ARRAY.                             DPRQ1600
C        INITIALIZATION OF BOUNDARY VALUES                               DPRQ1610
   21 E(ISTA)=0.D0                                                       DPRQ1620
      NRAN=NSAV-1                                                        DPRQ1630
   22 E(NRAN+1)=0.D0                                                     DPRQ1640
C                                                                        DPRC1650
C           TEST FOR LINEAR OR CONSTANT FACTOR                           DPRC1660
C        NRAN-ISTA IS DEGREE-1                                           DPRQ1670
      IF(NRAN-ISTA)24,23,31                                              DPRQ1680
C                                                                        DPRC1690
```

```
C          LINEAR FACTOR                                                DPRQ1700
   23 C(ISTA+1)=Q(ISTA+1)+EXPT                                          DPRQ1710
      E(ISTA+1)=0.CO                                                    DPRQ1720
C                                                                       DPRQ1730
C          TEST FOR UNFACTOREC COMMON DIVISOR                           DPRQ1740
   24 E(ISTA)=ESAV                                                      DPRQ1750
      IF(IR-NSAV)60,60,25                                               DPRQ1760
C                                                                       DPRQ1770
C          INITIALIZE QC-ALGORITHM FOR COMMON DIVISOR                   DPRQ1780
   25 ISTA=NSAV                                                         DPRQ1790
      ESAV=E(ISTA)                                                      DPRQ1800
      GOTO 10                                                           DPRQ1810
C                                                                       DPRQ1820
C          COMPUTATION OF ROOT PAIR                                     DPRQ1830
   26 P=P+EXPT                                                          DPRQ1840
C                                                                       DPRQ1850
C          TEST FOR REALITY                                             DPRQ1860
      IF(Q)27,28,28                                                     DPRQ1870
C                                                                       DPRQ1880
C          COMPLEX ROOT PAIR                                            DPRQ1890
   27 C(NRAN)=P                                                         DPRQ1900
      C(NRAN+1)=P                                                       DPRQ1910
      E(NRAN)=T                                                         DPRQ1920
      E(NRAN+1)=-T                                                      DPRQ1930
      GOTO 29                                                           DPRQ1940
C                                                                       DPRQ1950
C          REAL ROOT PAIR                                               DPRQ1960
   28 C(NRAN)=P-T                                                       DPRQ1970
      C(NRAN+1)=P+T                                                     DPRQ1980
      E(NRAN)=0.00                                                      DPRQ1990
C                                                                       DPRQ2000
C          REDUCTION OF DEGREE BY 2 (DEFLATION)                         DPRQ2010
   29 NRAN=NRAN-2                                                       DPRQ2020
      GOTO 22                                                           DPRQ2030
```

```
C                                                                       DPRC2040
C       COMPUTATION OF REAL ROOT                                        DPRC2050
   30 C(NRAN+1)=EXPT+P                                                  DPRQ2060
C                                                                       DPRC2070
C          REDUCTION OF DEGREE BY 1 (DEFLATION)                         DPRC2080
      NRAN=NRAN-1                                                       DPRC2090
      GOTO 22                                                           DPRQ2100
C                                                                       DPRQ2110
C       START GO-ITERATION                                              DPRQ2120
   31 JBEG=ISTA+1                                                       DPRC2130
      JEND=NRAN-1                                                       DPRQ2140
      TEPS=EPS                                                          DPRC2150
      TDELT=1.E-2                                                       DPRQ2160
   32 KOUNT=KOUNT+1                                                     DPRC2170
      P=C(NRAN+1)                                                       DPRQ2180
      R=ABS(SNGL(E(NRAN)))                                              DPRC2190
C                                                                       DPRC2200
C          TEST FOR CONVERGENCE                                         DPRC2210
      IF(R-TEPS)30,30,33                                                DPRQ2220
   33 S=ABS(SNGL(E(JEND)))                                              DPRQ2230
C                                                                       DPRC2240
C       IS THERE A REAL ROOT NEXT                                       DPRC2250
      IF(S-R)38,38,34                                                   DPRQ2260
C                                                                       DPRC2270
C       IS DISPLACEMENT SMALL ENOUGH                                    DPRC2280
   34 IF(R-TDELT)36,35,35                                               DPRC2290
   35 P=0.D0                                                            DPRC2300
   36 C=P                                                               DPRC2310
      DO 37 J=JBEG,NRAN                                                 DPRC2320
      C(J)=C(J)+E(J)-E(J-1)-D                                           DPRC2330
C                                                                       DPRQ2340
C          TEST FOR SMALL DIVISOR                                       DPRQ2350
      IF(DABS(C(J))-PCL(J))81,81,37                                     DPRQ2360
   37 E(J)=C(J+1)*E(J)/C(J)                                             DPRC2370
```

```
      C(NRAN+1)=-E(NRAN)+C(NRAN+1)-D                                          DPRC2380
      GOTO 54                                                                DPRC2390
C                                                                            DPRC2400
C        CALCULATE DISPLACEMENT FOR DOUBLE ROOTS                             DPRC2410
C           QUADRATIC EQUATION FOR DOUBLE ROOTS                              DPRC2420
C           X**2-(C(NRAN)+Q(NRAN+1)+E(NRAN))*X+Q(NRAN)*Q(NRAN+1)=0           DPRC2430
   38 P=0.500*(C(NRAN)+E(NRAN)+Q(NRAN+1))                                    DPRC2440
      C=P*P-C(NRAN)*Q(NRAN+1)                                                DPRC2450
      T=DSQRT(DABS(D))                                                       DPRC2460
C                                                                            DPRC2470
C        TEST FOR CONVERGENCE                                                DPRC2480
      IF(S-TOPS)26,26,39                                                     DPRC2490
C                                                                            DPRC2500
C        ARE THERE COMPLEX ROOTS                                             DPRC2510
   39 IF(C)43,40,40                                                          DPRC2520
   40 IF(P)42,41,41                                                          DPRC2530
   41 T=-T                                                                   DPRC2540
   42 P=P+T                                                                  DPRC2550
      K=S                                                                    DPRC2560
      GOTO 34                                                                DPRC2570
C                                                                            DPRC2580
C        MODIFICATION FOR COMPLEX ROOTS                                      DPRC2590
C        IS DISPLACEMENT SMALL ENOUGH                                        DPRC2600
   43 IF(S-TDELT)44,35,35                                                    DPRC2610
C                                                                            DPRC2620
C           INITIALIZATION                                                   DPRC2630
   44 C=C(JBEG)+E(JBEG)-P                                                    DPRC2640
C                                                                            DPRC2650
C           TEST FOR SMALL DIVISOR                                           DPRC2660
      IF(DABS(C)-POL(JBEG))81,81,45                                          DPRC2670
   45 T=(T/C)**2                                                             DPRC2680
      D=E(JBEG)*Q(JBEG+1)/(C*(1.0D0+T))                                      DPRC2690
      V=C+D                                                                  DPRC2700
C                                                                            DPRC2710
```

```
C        THREEFOLD LOOP FOR COMPLEX DISPLACEMENT                        DPRC2720
      KOUNT=KOUNT+2                                                     DPRC2730
      DO 53 J=JBEG,NRAN                                                 DPRC2740
      C=C(J+1)*E(J+1)-U-P                                               DPRC2750
C                                                                       DPRC2760
C           TEST FOR SMALL DIVISOR                                      DPRC2770
      IF(DABS(V)-POL(J))46,46,49                                        DPRC2780
   46 IF(J-NRAN)81,47,81                                                DPRC2790
   47 EXPT=EXPT+P                                                       DPRC2800
      IF(ABS(SNGL(E(JEND)))-TOL)48,48,81                                DPRC2810
   48 P=0.5D0*(V+D-E(JEND))                                             DPRC2820
      C=P*P-(V-U)*(D-L*T-U*W*(1.D0+T)/Q(JEND))                          DPRC2830
      T=DSQRT(DABS(D))                                                  DPRC2840
      GOTO 26                                                           DPRC2850
C                                                                       DPRC2860
C           TEST FOR SMALL DIVISOR                                      DPRC2870
   49 IF(DABS(D)-POL(J+1))46,46,50                                      DPRC2880
   50 R=U*C/J                                                           DPRC2890
      T=T*(V/D)**2                                                      DPRC2900
      C(J)=V+W-E(J-1)                                                   DPRC2910
      U=0.D0                                                            DPRC2920
      IF(J-NRAN)51,52,52                                                DPRC2930
   51 U=C(J+2)*E(J+1)/(D*(1.D0+T))                                      DPRC2940
   52 V=C+U-W                                                           DPRC2950
C                                                                       DPRC2960
C           TEST FOR SMALL DIVISOR                                      DPRC2970
      IF(DABS(C(J))-POL(J))81,81,53                                     DPRC2980
   53 E(J)=W*V*(1.0D0+T)/C(J)                                           DPRC2990
      C(NRAN+1)=V-E(NRAN)                                               DPRC3000
   54 EXPT=EXPT+P                                                       DPRC3010
      TEPS=TEPS*1.1                                                     DPRC3020
      TDELT=TDELT*1.1                                                   DPRC3030
      IF(KOUNT-LIMIT)32,55,55                                           DPRC3040
C                                                                       DPRC3050
```

```
C        NO CONVERGENCE WITH FEASIBLE TOLERANCE                          DPRG3060
C           ERROR RETURN IN CASE OF UNSATISFACTORY CONVERGENCE           DPRG3070
                                                                         DPRG3080
   55 IER=1                                                              DPRG3090
C                                                                        DPRG3100
C        REARRANGE CALCULATED ROOTS                                      DPRG3110
   56 IEND=NSAV-NRAN-1                                                   DPRG3120
      E(ISTA)=ESAV                                                       DPRG3130
      IF(IEND)59,59,57                                                   DPRG3140
   57 DO 58 I=1,IEND                                                     DPRG3150
      J=ISTA+I                                                           DPRG3160
      K=NRAN+1+I                                                         DPRG3170
      E(J)=E(K)                                                          DPRG3180
   58 C(J)=C(K)                                                          DPRG3190
   59 IR=ISTA+IEND                                                       DPRG3200
C                                                                        DPRG3210
C        NORMAL RETURN                                                   DPRG3220
   60 IR=IR-1                                                            DPRG3230
      IF(IR)78,78,61                                                     DPRG3240
C                                                                        DPRG3250
C        REARRANGE CALCULATED ROOTS                                      DPRG3260
   61 DO 62 I=1,IR                                                       DPRG3270
      C(I)=C(I+1)                                                        DPRG3280
   62 E(I)=E(I+1)                                                        DPRG3290
C                                                                        DPRG3300
C        CALCULATE COEFFICIENT VECTOR FROM ROOTS                         DPRG3310
      FCL(IR+1)=1.D0                                                     DPRG3320
      IEND=IR-1                                                          DPRG3330
      JBEG=1                                                             DPRG3340
      DO 69 J=1,IR                                                       DPRG3350
      ISTA=IR+1-J                                                        DPRG3360
      C=0.D0                                                             DPRG3370
      P=C(ISTA)                                                          DPRG3380
      T=E(ISTA)                                                          DPRG3390
      IF(T)65,63,65
```

```
C                                                                       DPRC3400
C          MULTIPLY WITH LINEAR FACTOR                                  DPRC3410
   63 DO 64 I=ISTA,IR                                                   DPRC3420
      PCL(I)=0-P*PCL(I+1)                                               DPRC3430
   64 C=PCL(I+1)                                                        DPRC3440
      GOTO 69                                                           DPRC3450
   65 GOTO(66,67),JBEG                                                  DPRC3460
   66 JBEG=2                                                            DPRC3470
      PCL(ISTA)=0.D0                                                    DPRC3480
      GOTO 69                                                           DPRC3490
C                                                                       DPRC3500
C          MULTIPLY WITH QUADRATIC FACTOR                               DPRC3510
   67 JBEG=1                                                            DPRC3520
      U=P*P+T*T                                                         DPRC3530
      P=P+P                                                             DPRC3540
      DO 68 I=ISTA,IEND                                                 DPRC3550
      PCL(I)=0-P*PCL(I+1)+U*PCL(I+2)                                    DPRC3560
   68 C=PCL(I+1)                                                        DPRC3570
      PCL(IR)=C-P                                                       DPRC3580
   69 CONTINUE                                                          DPRC3590
      IF(IER)78,70,78                                                   DPRC3600
C                                                                       DPRC3610
C          COMPARISON OF COEFFICIENT VECTORS, IE. TEST OF ACCURACY      DPRC3620
   70 P=0.D0                                                            DPRC3630
      DO 75 I=1,IR                                                      DPRC3640
      IF(C(I))72,71,72                                                  DPRC3650
   71 C=DABS(POL(I))                                                    DPRC3660
      GOTO 73                                                           DPRC3670
   72 C=DABS((POL(I)-C(I))/C(I))                                        DPRC3680
   73 IF(P-C)74,75,75                                                   DPRC3690
   74 P=C                                                               DPRC3700
   75 CONTINUE                                                          DPRC3710
      IF(SNGL(P)-TOL)77,76,76                                           DPRC3720
   76 IER=-1                                                            DPRC3730
```

```
   77 C(IR+1)=P                                                          DPRC3740
      E(IR+1)=0.D0                                                       DPRC3750
   78 RETURN                                                             DPRC3760
C                                                                        DPRC3770
C        ERROR RETURNS                                                   DPRC3780
C           ERROR RETURN FOR POLYNOMIALS OF DEGREE LESS THAN 1           DPRC3790
   79 IER=2                                                              DPRC3800
      IR=0                                                               DPRC3810
      RETURN                                                             DPRC3820
C                                                                        DPRC3830
C           ERROR RETURN IF THERE EXISTS NO S-FRACTION                   DPRC3840
   80 IER=4                                                              DPRC3850
      IR=ISTA                                                            DPRC3860
      GOTO 60                                                            DPRC3870
C                                                                        DPRC3880
C           ERROR RETURN IN CASE OF INSTABLE QD-ALGORITHM                DPRC3890
   81 IER=3                                                              DPRC3900
      GOTO 56                                                            DPRC3910
      END                                                                DPRC3920
```

APPENDIX VIII
COMPUTER SIMULATION OF NONLINEAR SYSTEMS

Any input data whose dimensions are omitted below may be found in Appendix VI.

I. Simulation of System Without ZTS Coupling

Input Data

Quantity	Value (or Meaning)	Units
Count (integration steps per line of output)	10	none
I_{eg}	0.6944	-
I_R	3.888	-
K_θ	800.0	-
C_s	2.24	-
C_e	0.000382	$\frac{\text{ft-lb}}{\text{rad/sec}^2}$
C_L	0.0009564	$\frac{\text{ft-lb}}{\text{rad/sec}^2}$
Start time	variable	seconds
End time	variable	seconds
τ_1	0.02	-
τ_2	0.03	-
K_ρ	40.27	-
$\frac{\partial T_g}{\partial \omega_g}$	-3.3333	$\frac{\text{ft-lb}}{\text{rad/sec}}$
$\frac{\partial T_g}{\partial W_f}$	0.3523	$\frac{\text{ft-lb}}{\text{lb/hr}}$

Quantity	Value (or Meaning)	Units
$\frac{\partial T_e}{\partial W_f}$	0.57	$\frac{\text{ft-lb}}{\text{lb/hr}}$
$\frac{\partial T_e}{\partial \omega_g}$	3.2563	$\frac{\text{ft-lb}}{\text{rad/sec}}$
KEY1	0 for frequency response 1 for time response	none
ω	variable	rad/sec

```
C  ..........................................................
C  THIS COMPUTER PROGRAM IS DESIGNED TO GIVE A.....................
C  NUMERICAL SIMULATION OF A HELICOPTER DRIVE SYSTEM...............
C  WITHOUT A ZTS COUPLING..........................................
C  ..........................................................
      IMPLICIT REAL*8(A-Z)
      INTEGER NN,NAN,COUNT ,JO,KEY1
      COMMON CS2,IE,IR,K2,CL,CENG,TAU1,TAU2,KP,EDSET,CNG1,CNG2,CTE1,CTE2
      COMMON  W
      READ(5,1003)COUNT
 1003 FORMAT(I2)
      READ(5,1002)IE,IR,K2,CS2,CENG,CL,TSTART,TSTOP,TAU1,TAU2,KP,CNG1,
     $ CNG2,CTE1,CTE2
      PRINT,      IE,IR,K2,CS2,CENG,CL,TSTART,TSTOP,TAU1,TAU2,KP,CNG1,
     $ CNG2,CTE1,CTE2
      READ(5,1003)KEY1
 1001 READ(5,1002,END=444)EXTRA
      W=EXTRA
      PRINT,EXTRA
      JO=0
      TIME=TSTART
      NAN=COUNT
      NN=50
      SET    = 1447.56
      EDSET2 = 1500.0
 1000 CONTINUE
      EDSET = SET
      IF ( TIME.GE.10.0 ) EDSET = EDSET2
C  SET KEY1 = 1  FOR TIME RESPONSE.................................
C  SET KEY1 = 0  FOR FREQUENCY RESPONSE............................
      IF( KEY1.LT.1 ) EDSET = SET
      CALL GCV (WF,WFC,WFCC,TE,NG,NGD,ED,JO)
      CALL CCT(E,R,PE,PR,TIME,ED,RD,PED,PRD,TE,FR,DEL,JO,EXTRA)
      DIFF=(E-R)
```

```
      MAG = DIFF*K2/1817.35
      IF(NN.NE.50)GO TO 13
      PRINT,E,ED,R,RD,PE,PR,TIME,WF,WFD,TE,NG ,WFDD
      WRITE(6,11)
      NN=0
   13 CONTINUE
      IF(NNN.EQ.COUNT)GO TO 55
      NNN=NNN+1
      GO TO 111
   55 WRITE(6,10)E,ED,R,RC,TE,FR,DEL,TIME,DIFF,MAG,WF,WFD,NG
      NNN=1
      NN=NN+1
  111 CONTINUE
      IF(DEL.LT..0009)GO TO 900
C  EULER INTEGRATION START.....
      E=E+EC*DEL
      R=R+RC*DEL
      PE=PE+PEC*DEL
      PR=PR+PRC*DEL
      WF = WF + WFC*DEL
      WFC = WFC + WFDC*DEL
      NG = NG + NGC*DEL
      TIME=TIME+DEL
      GO TO 901
C  EULER INTEGRATION END.....
  900 CONTINUE
C  RUNGE-KUTTA START.....
      HH=3*DEL/4
      EN=E+EC*HH
      RN=R+RC*HH
      PEN=PE+PEC*HH
      PRN=PR+PRC*HH
      WFN = WF + WFD*HH
      WFCN = WFC + WFDC*HH
```

```
      NGN = NG + NGD*HH
      TIMEN=TIME+HH
      CALL GOV (WFN,WFDN,WFDDN,TEN,NGN,NGDN,ED,JO)
      CALL DOT(EN,RN,PEN,PRN,TIMEN,EDN,RDN,PEDN,PRDN,TEN,FR,DEL,JO,
     . EXTRA)
      E=E+DEL*(ED/3.+(2./3.)*EDN)
      R=R+DEL*(RD/3.+(2./3.)*RDN)
      PE=PE+DEL*(PED/3.+(2./3.)*PEDN)
      PR=PR+DEL*(PRD/3.+(2./3.)*PRDN)
      WF = WF + DEL*(WFD/3.0 + (2.0/3.0)*WFDN)
      WFD = WFD + DEL*(WFDD/3.0 + (2.0/3.0)*WFDDN)
      NG = NG + DEL*(NGD/3.0 + (2.0/3.0)*NGDN)
      TIME=TIME+DEL
C  RUNGE-KUTTA END.....................................................
  901 CONTINUE
C  NEITHER FUEL FLOW NOR ENGINE TORQUE CAN BE LESS THAN ZERO.....
      IF ( WF.LE.0.0 ) WF = 0.0
      IF ( TE.LE.0.0 ) TE = 0.0
      IF(TIME.LT.TSTOP)GO TO 1000
 1002 FORMAT(F20.1)
C   10 FORMAT(' ',4F9.2,2F10.3,F10.7,F10.4,2F10.3)
   10 FORMAT(' ',4F9.2,2F10.3,F10.7,F10.4,5F10.3)
   11 FORMAT('1',////
     .       T4,'THETA E',T12,'DTHETA E',T22,'THETA R',T31,'DTHETA R',
     . T40,'TORQUE E',T50,'TORQUE R',T62,'DEL',T70,'TIME',
     .  T82,'SHAFT',T93,'M.F.',T102,'FUEL',T113,'DFUEL',T121,'GP SPEED'/
     $)
      GO TO 1001
  444 STOP
      END
```

```
      SUBROUTINE DOT(E,R,PE,PR,TIME,ED,RD,PED,PRD,TE,FR,DEL,JO,EXTRA)
C  TIME DERIVATIVES OF POSITION AND MOMENTUM.....................
      IMPLICIT REAL*8(A-Z)
      INTEGER AN,NNN,COUNT,JO
      COMMON CS2,IE,IR,K2,CL,CENG,TAU1,TAU2,KP,EDSET,CNG1,CNG2,CTE1,CTE2
      COMMON  W
      IF(JC.GT.0)GO TO 1
      JC=1
C  INITIAL CONDITIONS FOR STEADY STATE OPERATION.................
      ED = 1378.48
      RD = 1378.48
      E = 8.568
      E = 2.272
      R = 0.0
      DELT=.001
      PE=IE*ED
      PR=IR*RD
C  DYNAMICS.....................................................
    1 CONTINUE
      DEL=DELT
C  ANGULAR VELOCITIES...........................................
      ED=PE/IE
      RD=PR/IR
C  POTENTIAL FORCES.............................................
      DE=-K2*(E-R)
      DR=-DE
C  GENERALIZED FORCES...........................................
      FCE=-CS2*(ED-RD)
      FCR=-CS2*(RD-ED)
      FE=TE-CENG*ED*DABS(ED)+FCE
      VL=CL
      IF(TIME.GT.15)VL=CL *(1+.10*DSIN(W*TIME))
      FR=-VL*CABS(RD)*RD+FCR
      PED=DE+FE
```

```
PRC=CR+FR
RETURN
END
```

```
      SUBROUTINE GOV (WF,WFD,WFDD,TE,NG,NGD,ED,JO)
C  TIME DERIVATIVES OF FUEL FLOW AND GAS PRODUCER SPEED.....
      IMPLICIT REAL*8(A-Z)
      INTEGER JO
      COMMON CS2,IE,IR,K2,CL,CENG,TAU1,TAU2,KP,EDSET,CNG1,CNG2,CTE1,CTE2
      COMMON  W
      IF(JC.GT.0)GO TO 1
C  INITIAL CONDITIONS FOR STEADY STATE OPERATION.............
      WF = 2782.035
      WFD = 0.0
      WFDD = 0.0
      TE = 2543.22
      ED = 1378.48
      NG = 294.033
      NGD = 0.0
    1 CONTINUE
      EDERR = EDSET - ED
C  DIFFERENTIAL EQUATION FOR DIRECT FUEL FLOW SPEED GOVERNOR.....
      WFDD = (KP*EDERR - (TAU1 + TAU2)*WFD - WF)/(TAU1*TAU2)
C  DIFFERENTIAL EQUATIONS FOR A TWO-SPOOL TURBINE ENGINE.....
      NGD = CNG1*NG + CNG2*WF
      TE = CTE1*WF + CTE2*NG
      RETURN
      END
```

II. Simulation of System With ZTS Coupling

Quality	Value (or Meaning)	Units
N	2	none
Count (integration steps per line of output)	10	none
r	3	inches
ℓ	2.61	inches
M	0.2385	lb-mass
m_{ℓ}	0.0	lb-mass
C_c	variable	-
C_s	variable	-
TT (reverse stop contact)	1.0	radians
I_e	0.5	-
I_R	3.888	-
I_{fe}	0.015	-
I_{fR}	0.2094	-
RFL (free length of coupling spring; not used)	0.0	inches
TTT (forward stop contact)	1.97	radians
K_e (coupling spring; not used)	0.0	lb in.
K_θ	800.0	-
C_L	0.0009564	-
C_e	0.000382	-

Quality	Value (or Meaning)	Units
X (spring constant of reverse stop)	66,800	$\frac{\text{ft-lb}}{\text{rad}}$
Y (spring constant of forward stop)	66,800	$\frac{\text{ft-lb}}{\text{rad}}$
Start time	variable	seconds
End time	variable	seconds
τ_1	0.02	-
τ_2	0.03	-
K_p	40.27	-
$\frac{\partial T_g}{\partial \omega_g}$	-3.3333	$\frac{\text{ft-lb}}{\text{rad/sec}}$
$\frac{\partial T_g}{\partial W_f}$	0.3523	$\frac{\text{ft-lb}}{\text{lb/hr}}$
$\frac{\partial T_e}{\partial W_f}$	0.57	$\frac{\text{ft-lb}}{\text{lb/hr}}$
$\frac{\partial T_e}{\omega_g}$	3.2563	$\frac{\text{ft-lb}}{\text{rad/sec}}$
KEY1	0 for frequency response 1 for time response	none
ω	variable	rad/sec

```
C  .....
C  THIS COMPUTER PROGRAM IS DESIGNED TO GIVE A.....
C  NUMERICAL SIMULATION OF A HELICOPTER DRIVE SYSTEM.....
C  WITH A ZTS COUPLING.....
C  .....
      IMPLICIT REAL*8(A-Z)
      INTEGER NN,NNN,COUNT,NM,JO,KEY1
      COMMON  CNG1, CNG2,  CTE1, CTE2, TAU1, TAU2, EDSET, CL, CENG,
     .KP,W,X,R1,L, Y,M,ML,CDAMP,CS2,TT,IE,IR,IFE,IFR,RFL,TTT,KS,K2,NM
      READ(5,1003)NM,COUNT
 1003 FORMAT(I2)
      READ(5,1002)R1,L,M, ML,CDAMP,CS2,TT,IE,IR,IFE,IFR,RFL,TTT,KS,K2,
     .CL,CENG,X,Y,TSTART,TSTOP,TAU1,TAU2,KP,CNG1,CNG2,CTE1,CTE2
      PRINT,   NM,R1,L,   ML,CDAMP,CS2,TT,IE,IR,IFE,IFR,RFL,TTT,KS,K2,
     .CL,CENG,X,Y,TSTART,TSTOP,TAU1,TAU2,KP,CNG1,CNG2,CTE1,CTE2
C  CONVERSION FACTORS.....
      R1=R1/12.
      L=L/12.
      M=M/32.17
      ML=ML/32.17
      KS=KS*12.
      RFL=RFL/12.
      READ(5,1003)KEY1
 1001 READ(5,1002,END=444)EXTRA
      PRINT,EXTRA
      W=EXTRA
 1002 FORMAT(F20.1)
      JC=0
      TIME=TSTART
      NNN=COUNT
      NN=50
      SET    = 1447.56
      EDSET2 = 1500.0
 1000 CONTINUE
```

```
      EDSET = SET
      IF ( TIME.GE.10.0 ) EDSET = EDSET2
C  SET KEY1 = 0  FOR FREQUENCY RESPONSE.....
C  SET KEY1 = 1  FOR TIME RESPONSE.....
      IF( KEY1.LT.1 ) EDSET = SET
      CALL GOV (WF,WFC,WFCC,TE,NG,NGD,ED,JO)
      CALL DOT(T,E,R,PT,PE,PR,TIME,TD,ED,RD,PTD,PED,PRD,DET,
     .DET1,DET2,TE,FR,DEL,JO)
      DIFF=(E-T-R)
      MAG = DIFF*K2/1817.35
      IF(NN.NE.50)GO TO 13
      PRINT,E,ED,R,RD,T,TD,PE,PR,PT,TIME,WF,WFD,TE,NG ,WFDD
      WRITE(6,11)
      NN=0
   13 CONTINUE
      IF(NNN.EQ.COUNT)GO TO 55
      NNN=NNN+1
      GO TO 111
   55 WRITE(6,10)E,ED,R,RD,T,TD,WF ,DIFF,MAG,TE ,
     .FR,DEL,TIME
      NNN=1
      NN=NN+1
  111 CONTINUE
      IF(DEL.LT..0002)GO TO 900
C  EULER INTEGRATION START.....
      T=T+TD*DEL
      E=E+ED*DEL
      R=R+RD*DEL
      PT=PT+PTD*DEL
      PE=PE+PED*DEL
      PR=PR+PRD*DEL
      WF = WF + WFD*DEL
      WFC = WFC + WFCC*DEL
      NG = NG + NGD*DEL
```

```
      TIME=TIME+DEL
      GO TO 901
C  EULER INTEGRATION END.....................................
  900 CONTINUE
C  RUNGE-KUTTA START..........................................
      HH=3*DEL/4
      TN=T+TD*HH
      EN=E+ED*HH
      RN=R+RD*HH
      PTN=PT+PTD*HH
      PEN=PE+PED*HH
      PRN=PR+PRD*HH
      WFN = WF + WFD*HH
      WFDN = WFD + WFDD*HH
      NGN = NG + NGD*HH
      TIMEN=TIME+HH
      CALL GOV (WFN,WFDN,WFDDN,TEN,NGN,NGDN,ED,JO)
      CALL DDT(TN,EN,RN,PTN,PEN,PRN,TIMEN,TDN,EDN,RDN,PTDN,PEDN,PRDN,DET
     . ,DET1,DET2,TEN,ER,DEL,JO)
C     . ,DET1,DET2,TEN,ER,DEL,JO)
      T=T+DEL*(TD/3.+(2./3.)*TDN)
      E=E+DEL*(ED/3.+(2./3.)*EDN)
      R=R+DEL*(RD/3.+(2./3.)*RDN)
      PT=PT+DEL*(PTD/3.+(2./3.)*PTDN)
      PE=PE+DEL*(PED/3.+(2./3.)*PEDN)
      PR=PR+DEL*(PRD/3.+(2./3.)*PRDN)
      WF = WF + DEL*(WFD/3.0 + (2.0/3.0)*WFDN)
      WFD = WFD + DEL*(WFDD/3.0 + (2.0/3.0)*WFDDN)
      NG = NG + DEL*(NGD/3.0 + (2.0/3.0)*NGDN)
      TIME=TIME+DEL
C  RUNGE-KUTTA END............................................
  901 CONTINUE
C  NEITHER FUEL FLOW NOR ENGINE TORQUE CAN BE LESS THAN ZERO.....
      IF ( WF.LE.0.0 ) WF = 0.0
```

```
      IF ( TE.LE.0.0 ) TE = 0.0
      IF(T.GT.2.5)GO TO 444
      IF(TIME.LT.TSTOP)GO TO 1000
C  10 FORMAT(' ',4F9.2,F9.5,F10.5,F12.8,F8.3,F12.3,
   10 FORMAT(' ',4F9.2,F9.5,F10.5,F12.2,F8.3,F12.3,
     . F13.3,F10.3,F10.7,F10.4)
   11 FORMAT('1',////
     .       T4,'THETA E',T12,'DTHETA E',T22,'THETA R',T31,'DTHETA R',
     .T41,'THETA',T49,'DTHETA',T61,'FUEL FLO',T72,'SHAFT',T84,'M.F. ',
     .T94,'TORQUE E',T104,'TORQUE R',T115,'DEL',T125,'TIME'/)
      GO TO 1001
  444 STOP
      END
```

```
      SUBROUTINE DOT(T,E,R,PT,PE,PR,TIME,TD,ED,RD,PTD,PED,PRD,DET,
     .DET1,DET2,TE,FR,DEL,JC)
C  TIME DERIVATIVES OF POSITION AND MOMENTUM.....................
      IMPLICIT REAL*8(A-Z)
      INTEGER NN,NNN,COUNT,NM,JC
      COMMON  CNG1, CNG2,  CTE1, CTE2, TAU1, TAU2, EDSET, CL, CENG,
     .KP,W,X,R1,L, Y,P,ML,CCAMP,CS2,TT,IE,IR,IFE,IFR,RFL,TTT,KS,K2,NM
      IF(JC.GT.0)GO TO 1
      JC=1
C  INITIAL CONDITIONS FOR STEADY STATE OPERATION.................
      ILL=ML/12
      MASS1=P+ML/2.+2*ILL
      MASS2=ML/2.-2*ILL
      MASS3=ML/2.+2*ILL
      EC = 1378.48
      RC = 1378.48
      TD = 0.0
      T = 1.64
      E = 2.272 + T
      R = 0.0
      DELT=.001
      CT=DCOS(T/2)
      ST=DSIN(T/2)
      ST2=DSIN(T)
      CT2=DCOS(T)
      RAD=RADR(T,R1,L,ST)
      RR=R1*CT+RAD
      RRDB=-(R1*ST        +R1*R1*ST2    /(2*RAD))/2.
      PRRDTD=RRDB
      PRRT=RRDB
      A1=(NM/2)*(MASS1*(2*RRDB*PRRDTD+RR*RR/2)
     .    +MASS2*(-R1*PRRDTD*ST-R1*RRDB*ST+R1*RR*CT)
     .    +MASS3*R1*R1) *IFR
      B1=(NM/2)*(-MASS1*RR*RR-2*MASS2*R1*RR*CT
```

```
     .    -MASS3*R1*R1) -IFR
          A2=B1
          B2=-2*B1*IE    *IFE-IFR
          PT=A1*TD+B1*ED
          PE=A2*TD+B2*ED
          PR=IR*RD
C   DYNAMICS.....................................................
      1   CONTINUE
          DEL=DELT
          IF(TIME.LT.5)DEL=.0001
          IF(T.LT.TTT-.02.AND.T.GT.TT+.02)GO TO 777
          DEL=.0001
    777   CONTINUE
          ST=DSIN(T/2)
          CT=DCOS(T/2)
          ST2=DSIN(T)
          CT2=DCOS(T)
          RAD=RADR(T,R1,L,ST)
          RR=R1*CT+RAD
          RRDB=-(R1*ST        +R1*R1*ST2    /(2*RAD))/2.
          PRRDTD=RRDB
          PRRT=RRDB
C   ANGULAR VELOCITIES.....................................
          RD=PR/IR
          A1=(AM/2)*(MASS1*(2*RRDB*PRRDTD+RR*RR/2)
     .    +MASS2*(-R1*PRRDTD*ST-R1*RRDB*ST+R1*RR*CT)
     .    +MASS3*R1*R1)+IFR
          B1=(AM/2)*(-MASS1*RR*RR-2*MASS2*R1*RR*CT
     .    -MASS3*R1*R1)-IFR
          A2=B1
          B2=-2*B1+IE +IFE-IFR
          DET1=A1*B2
          DET2=A2*B1
          DET=DET1-DET2
```

```
      TC=(B2*PT-B1*PE)/DET
      EC=(A1*PE-A2*PT)/DET
C  POTENTIAL FORCES.....
      CE=-K2*(E-T-R)
      CR=-CE
      RRC=RRDB*TC
      PRRCT=-((R1*CT+R1*R1*CT2/RAD+
     .       (R1**4)*(ST2**2)/(4*RAD**3))/4)*TD
      CC=EC-TD/2
      CT=NM*MASS1*(RRC*PRRCT+CC*CC*RR*PRRT)
     .       +NM*MASS2*(CC*CC*R1*PRRT*CT
     .       -TC*PRRDT*ST*R1/2
     .       -TC*RRC*CT*R1/4-
     .    CC*CD*RR*ST*R1/2)+K2*(E-T-R)
C  GENERALIZED FORCES.....
      FCR=-CS2*(RD-ED+TD)
      FCE=-CS2*(EC-TC-RD)
      FCT=-CS2*(RD-EC+TD)
C        TORQUE DETERMINED BY ENGINE OUTPUT
C      TE=(ENGINE*TIME/3.)+(2.-TIME/3.)
C      IF(TIME.GT.3)TE=ENGINE
      FE=TE-CENG*EC*DABS(ED)+FCE
      FST=KS*(RFL-RR)*FRRT*NM
      IF(RR.GT.RFL)FST=0
      FT=-CDAMP*TC-TLARGE(T,TT,TTT,X,Y)+FCT+FST
      VL=CL
      IF(TIME.GT.15)VL=CL *(1+.10*DSIN(W*TIME))
      FR=-VL*DABS(RD)*RD+FCR
      FTC=CT+FT
      FEC=CE+FE
      FRC=CR+FR
      RETURN
      END
```

```
      FUNCTION RADR(T,R1,X,ST)
      IMPLICIT REAL*8(A-Z)
      RAD=X*X-R1*R1*ST*ST
      RADR=DSQRT(RAD)
      RETURN
      END
```

```
      FUNCTION TLARGE(T,TT,TTT,X,Y)
      IMPLICIT REAL*8(A-Z)
      TLARGE=0
      IF(T.GT.TTT)TLARGE=Y*(T-TTT)
      IF(T.LT.TT)TLARGE=X*(T-TT)
      RETURN
      END
```

```
      SUBROUTINE GOV (WF,WFD,WFDD,TE,NG,NGD,ED,JO)
C  TIME DERIVATIVES OF FUEL FLOW AND GAS PRODUCER SPEED.....
      IMPLICIT REAL*8(A-Z)
      INTEGER JO
      COMMON  CNG1, CNG2,  CTE1, CTE2, TAU1, TAU2, EDSET, CL, CENG,
     .KP,W,X,R1,L, Y,M,ML,CDAMP,CS2,TT,IE,IR,IFE,IFR,RFL,TTT,KS,K2,NH
      IF(JC.GT.0)GO TO 1
C  INITIAL CONDITIONS FOR STEADY STATE OPERATION.....
      WF = 2782.035
      WFD = 0.0
      WFDD = 0.0
      TE = 2543.22
      ED = 1378.48
      NG = 294.033
      NGD = 0.0
    1 CONTINUE
      EDERR = EDSET - ED
C  DIFFERENTIAL EQUATION FOR DIRECT FUEL FLOW SPEED GOVERNOR.....
      WFDD = (KP*EDERR - (TAU1 + TAU2)*WFD - WF)/(TAU1*TAU2)
C  DIFFERENTIAL EQUATIONS FOR A TWO-SPOOL TURBINE ENGINE.....
      NGD = CNG1*NG + CNG2*WF
      TE = CTE1*WF + CTE2*NG
      RETURN
      END
```

LIST OF SYMBOLS

a	mechanical advantage of set speed control
A_p	cross-sectional area of speed governor fuel regulating piston
C_c	viscous ZTS coupling damping coefficient
C_D	linearized aerodynamic rotor damping coefficient
C_e	aerodynamic power turbine damping coefficient
C_g	speed governor fuel regulating piston viscous damping coefficient
C_L	aerodynamic rotor damping coefficient
C_s	viscous shaft damping coefficient
C_T	linearized aerodynamic power turbine damping coefficient
$E(s)$	speed error Laplace function
hp	shaft horsepower
I_e	mass polar moment of inertia of power turbine
I_{eg}	mass polar moment of inertia of power turbine and transmission
I_g	mass polar moment of inertia of gas producer
I_{gb}	mass polar moment of inertia of transmission
I_l	mass polar moment of inertia of a ZTS coupling link about its center of gravity
I_R	mass polar moment of inertia of helicopter rotor
K_B	engine transfer function gain torque to fuel flow
K_g	speed governor piston spring stiffness
K_L	helicopter load gain
K_p	governor proportional gain, fuel flow to speed
K_r	power turbine governor reset gain, speed request to actual speed

LIST OF SYMBOLS (Continued)

K_t	governor proportional gain, fuel flow to speed
K_{TM}	engine torquemeter shaft stiffness
K_θ	helicopter mast shaft stiffness
ℓ	length of ZTS coupling link
M,m	concentrated mass at end of ZTS coupling link
M_g	mass of speed governor fuel regulating piston
m_ℓ	distributed mass of ZTS coupling link
P_c	compressor discharge pressure
p	pressure proportional to engine power turbine speed
r	distance from center of ZTS coupling to interior link pin
s,S	Laplace operator
SSD	steady-state speed droop
T	torque
T_c	torque across ZTS coupling
T_e	engine torque applied to power turbine
$T_e(s)$	Laplace function for engine torque applied to power turbine
T_g	torque applied to gas producer
T_L	load torque on turbine engine
T_T	power turbine drag torque
$W_e(s)$	Laplace function for power turbine speed
W_f	fuel flow
$W_f(s)$	Laplace function for fuel flow
$W_g(s)$	Laplace function for gas producer speed
X_g	speed governor fuel regulating piston displacement
ϵ	power turbine speed error

LIST OF SYMBOLS (Continued)

ζ_r	helicopter rotor damping ratio
ζ_n	power turbine damping ratio
θ	ZTS coupling angle
$\theta(s)$	Laplace function for ZTS coupling angle
θ_e	power turbine angle of rotation
θ_R	helicopter rotor angle of rotation
θ_s	angle of twist in shaft
$\theta_s(s)$	Laplace function for angle of twist in shaft
τ_B	engine gas producer lead time constant
τ_e	engine gas producer lag time constant
τ_L	load lag time constant
τ_r	power turbine governor reset lag time constant
τ_2	speed governor lag time constant
τ_1	speed governor lag time constant
ω_e	power turbine speed
ω_g	gas producer speed
ω_n	undamped natural frequency of power turbine and rotor on flexible shaft
ω_r	natural frequency of rotor drive system
ω_R	helicopter rotor speed
Ω	speed governor set speed
$\Omega(s)$	Laplace function for speed governor set speed
$\Delta F(s)$	incremental change in a Laplace function
$\hat{f}(t)$	incremental change in a time domain function
$\bar{f}(t)$	steady-state value of a time domain function
$\dot{f}(t)$	time derivative of a time domain function